Temperature Dependent Size Exclusion Chromatography for Investigating Thermoreversibly Bonding Polymer Systems

D I S S E R T A T I O N

zur Erlangung des akademischen Grades
Doctor rerum naturalium
(Dr. rer. nat.)

vorgelegt

der Fakultät Mathematik und Naturwissenschaften
der Technischen Universität Dresden

von

M.Sc. Josef Brandt

geboren am 07.11.1988 in Großenhain

Eingereicht am 18.03.2016

Die Dissertation wurde in der Zeit von 01 / 2013 bis 02 / 2016
im Leibniz-Institut für Polymerforschung Dresden e.V. angefertigt.

This dissertation was done under the scientific supervision of:

Prof. Dr. Brigitte Voit and PD Dr. Albena Lederer.

1st reviewer: Prof. Dr. Brigitte Voit
2nd reviewer: Prof. Dr. Peter Schoenmakers

Submitted: 18.03.2016
Defended: 11.07.2016

TABLE OF CONTENTS

ABBREVIATIONS

ACN	Acetonitrile
ANU	Australian National University
ATR-FTIR	Attenuated total reflection – Fourier transform infrared
ATRP	Atom transfer radical polymerization
b_p	Boiling point
BHT	Butylated hydroxytoluene
CAD	Charged aerosol detector
CDTE	Cyanodithioester
Da	Dalton (= 1 g/mol)
DA	Diels Alder
DMAc	*N,N*-Dimethylacetamide
DMF	*N,N*-Dimethylformamide
DMSO	*N,N*-Dimethylsulfoxide
DLS	Dynamic light scattering
DP	Differential pressure
DPn	Degree of polymerization
DSC	Differential scanning calorimetry
ε	Absorption coefficient
ELSD	Evaporative light scattering detector
EtOAc	Ethyl acetate
HDA	Hetero Diels Alder
HPLC	High performance liquid chromatography
IC	Interaction chromatography
KIT	Karlsruhe Institute of Technology
KMH	Kuhn-Mark-Houwink
LC	Liquid chromatography
LAC	Liquid adsorption chromatography
LIC	Liquid interaction chromatogramy
LCCC	Liquid chromatography at critical conditions
log k_{OW}	Octanol water partition coefficient
LS	Light scattering

MMD	Molar mass distribution
MS	Mass spectrometry
NMR	Nuclear magnetic resonance
PBMA	Poly(butyl methacrylate)
PEG	Polyethylene glycol
PMMA	Poly(methyl methacrylate)
PS	Polystyrene
PVP	Poly(2-vinyl pyridine)
RAFT	Reversible Addition-Fragmentation Chain Transfer
SEC	Size exclusion chromatography
SEM	Scanning electron microscopy
SI	Supporting Information
SLS	Static light scattering
TD DLS	Temperature dependent dynamic light scattering
TD SEC	Temperature dependent size exclusion chromatography
THF	Tetrahydrofuran
TGA	Thermogravimetric analysis
UHPLC	Ultra-high performance liquid chromatography

1 Introduction

The increasing complexity of our modern life style comes along with numerous *high tech* applications in the fields of life science, health care and material science. Developing adequate smart and functional materials is key for bringing new concepts into reality. In the past decades polymers have developed into a versatile platform for the flexible design of a manifold of functional materials. Functional groups can be integrated easily, which opens the doors for a variety of different applications.

One particularly interesting concept is the application of reversibly bonding polymers. These polymers feature particular binding motifs of either supramolecular or covalent nature that respond to changes in their ambient conditions by the fraction of opened and closed bonds.[1–5] Hence, the equilibrium position between open and closed bonds can be controlled by manipulating the respective ambient conditions, such as temperature, pH or concentration, as shown schematically in Figure 1.

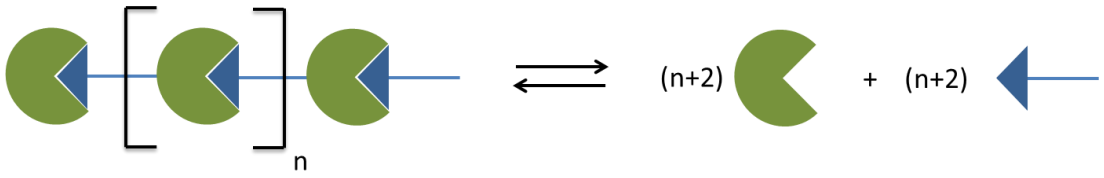

Figure 1: Scheme of a dynamic covalent polymer. The ratio of products to educts can be controlled by the ambient conditions (*e.g.*, temperature, pH, concentration).

The development of reversibly bonding polymer systems for various applications has made noticeable progress, as reflected in the number of corresponding publications and the increasing performance of the prepared materials. Their intrinsically stimulus responsive behavior renders reversibly bonding polymers promising candidates for self-healing materials[6–8] or drug-delivery systems[9–11]. Reversibly crosslinked polymers are furthermore highly desired for processing polymer networks easily by injection molding or 3D printing.[12] Employing reversibly crosslinked polymers as matrix material for fiber reinforced materials allows reshaping, healing and recycling the finished parts, which is impossible with a permanently crosslinked fiber reinforced material. Notable examples of reversibly bonding polymers are the upon ballistic impacts autonomously self-healing poly(ethylene-*co*-methacrylic acid) copolymers and ionomers[13–15], redox-responsive dynamic covalent miktoarm stars[16], polyesters that reorganize on the molecular level upon irradiation through disulfide exchange reactions[17] or temperature and redox responsive hydrogels formed by triblock copolymers.[18]

Besides developing more and more sophisticated structures it is equally important to keep on improving the analytical tools that are necessary for assessing the polymer's performance correctly. Deducing the reaction influencing parameters is crucial for the rational design of a material for any

particular application. The analytical assessment of reversibly bonding polymers is a particularly challenging endeavor, because not only the polymers themselves but also the bonding reactions must be understood correctly. As the polymers are intrinsically sensitive to changes in ambient conditions care has to be taken that the analyses are performed under *in situ* conditions.[19] Any changes of conditions during sample preparation could bias the outcome of the reactions and, thus, falsify the analysis result. Accordingly the effort of developing adequate analysis methods is not to be underestimated. Pushing forward the development of more advanced analysis techniques is important for not staying behind the developments in synthetic chemistry.

Different analysis techniques for information on the molecular or macroscopic level are available and can be evaluated according to their applicability for *in situ* analyses of dynamic bonding polymer systems.[19] All techniques follow specific principles that come along with particular benefits and disadvantages. If the progress of bonding and debonding reactions is of interest one interesting parameter that can be measured is the size of the polymers. The polymer's size is inherently going to change during the course of any bonding or debonding reaction and, thus, should allow for a precise monitoring of the progress of the respective reactions.

1.1 Objectives of the work

This work focuses on the in-depth analysis of Diels-Alder (DA) polymers that undergo depolymerization through the retro Diels-Alder (rDA) reaction at elevated temperatures. Novel pathways for controlling the thermoresponsive behavior by exploiting entropy effects are investigated. In detail the following objectives are aimed to be fulfilled:

(1) Develop new analysis procedures for monitoring the size of polymers during thermoreversible bonding reactions: Temperature dependent size exclusion chromatography (TD SEC) and temperature dependent dynamic light scattering (TD DLS).
(2) Establish reliable evaluation strategies and test them on versatile examples.
(3) Analyze the effect of size and flexibility of polymer building blocks on the rDA reactions by analyzing representative DA polymer samples.
(4) Investigate the kinetics of the thermoresponsive bonding behavior of the DA polymers by measuring the hydrodynamic size of the DA polymers in real time.
(5) Assess the reversibility of the rDA/DA reactions.

TD SEC allows monitoring the size distribution of polymers at different temperatures and, thus, evaluating the thermally controlled reactions quantitatively. A quantitative analysis method is necessary for deducing reaction influencing parameters. The TD SEC approach is expected to work universally for a variety of different polymer systems, irrespective of the actual nature of the dynamic bonds as only the change in polymer size is monitored. In contrast, a spectroscopic approach would require the presence of distinct functional groups that can be detected via their specific absorption or resonance characteristics. The only SEC prerequisites are that the polymers dissolve well in an applicable solvent and that their chemical bonds are stable enough to prevent the polymers from degradation from the relatively high shear force during the separation. The latter should be given for most polymers.[20] In order to obtain reliable results the evaluation of the acquired chromatograms has to be discussed in depth. Reliable evaluation protocols have to be developed that enable analyzing a broad variety of different polymer samples. The obtained results are expected to provide more information about possibilities for directing the reversible bonding reactions.

TD DLS is exploited as a valuable supplementary analysis technique. DLS allows determining the hydrodynamic radius of a dissolved polymer and, thus, essentially displays the same characteristic as SEC but from a different perspective. With TD DLS the rDA reactions can be monitored in real time. Furthermore the size of the DA polymers can be measured easily during multiple heating/cooling cycles, which allows investigating the reversibility of the reactions. The analyses procedures have to be optimized for these scopes in order to obtain robust and trustworthy results.

2 Scientific Background

2.1 Reversibly bonding polymers

One of the most important driving forces in sciences is to mimic nature. During billions of years of evolution nature developed highly complex systems with amazing capabilities. Many of those would be desirable in synthetic materials as well as our world evolves into more and more complexity and the demand for adequate materials is rising continuously. Applications in the field of medical therapeutics, sensor and actuator materials or self-healing materials require specifically designed structures that perform specific tasks autonomously.[8,21–25] The strategies for achieving the desired effects often require that the materials "sense" changes in their environment and act accordingly by varying their properties, thus giving them a responsive character. These often "smart" denoted materials can work by many different chemical mechanisms. Polymer materials have been exploited intensively during the past decades because of their versatility regarding their mechanical and chemical behavior and their possibility to integrate various functional moieties.

One concept frequently used for smart materials is the concept of reversible bonding where molecules associate or dissociate in dependence of ambient parameters, such as temperature, pH or mechanical stress.[1,3–5,26–28] Figure 2 shows the concept schematically: At first a conventional polymer is shown where the repeating units are linked by covalent bonds that do not allow any dynamic behavior. In the middle a supramolecular structure is shown where the repeating units are held together by non-covalent forces whose strength is inherently dependent on the ambient conditions. Depending on the ambient conditions the polymer is stable or collapses into its monomer units. The same behavior can be achieved with covalent bonds too, if suitable bonding reactions are used (third schematic).

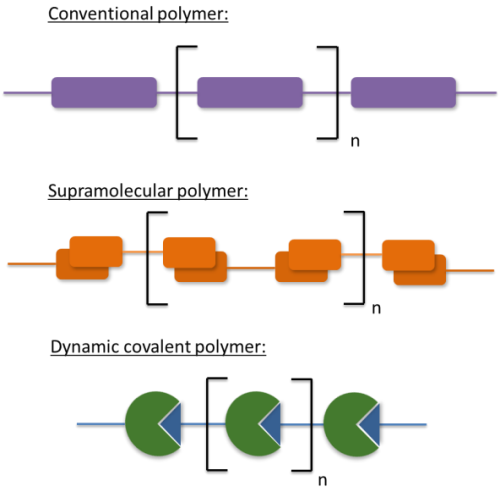

Figure 2: Schematic representation of a conventional, a supramolecular and a dynamic covalent polymer.

The advantage of this concept is that bonding or debonding of parts of the material result in relatively strong changes in the corresponding properties of the material. This can impact mechanical or optical properties or attributes related to permeability or hydrophilicity. The reactions that are used for the responsive bonding and debonding reactions can be of different nature and covalent and supramolecular types can be exploited. Non-covalent reactions are intrinsically dependent on their ambient conditions and can be controlled by temperature, salt concentrations or pH, but feature less stable bonds than covalent ones. If stronger associations are required covalent bonds have to be used. Reversible bonding reactions are for instance alkoxyamine reactions[29,30], the disulfide reactions[17,31,32], the Diels-Alder (DA) reaction[33–38] or the photo-dimerization of anthracene[39]. Further noticeable reaction types can be found in literature, for instance in the publications of Jean-Marie Lehn, who introduced the concept of "dynamers" as building blocks for reversibly bonding systems.[1,40] Figure 3 shows exemplary reversible reactions that can be controlled by temperature or light exposition.

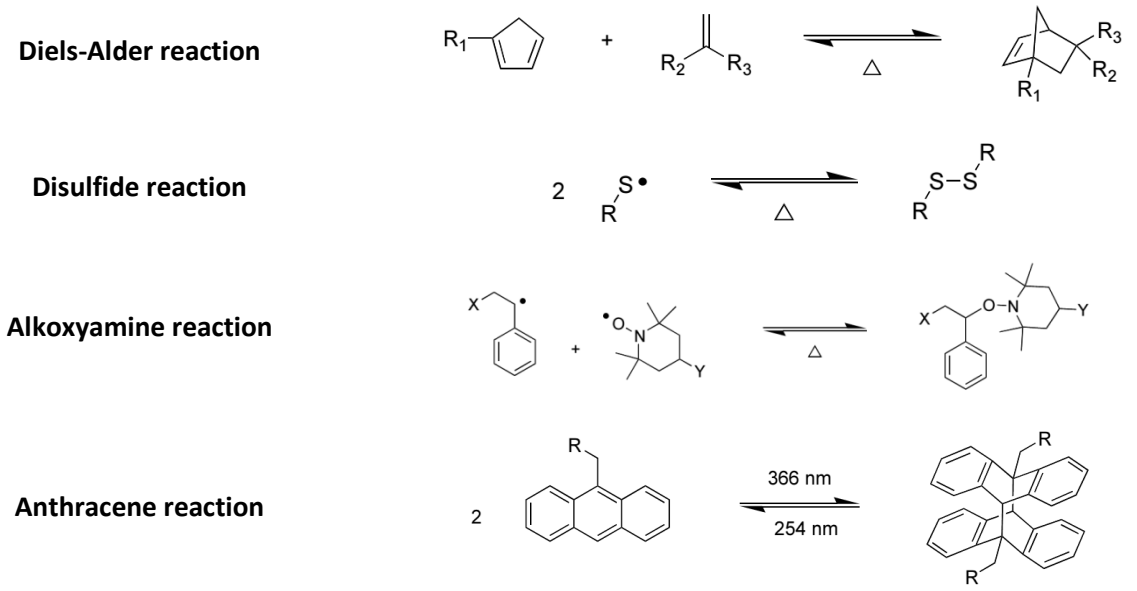

Figure 3: Examples of reactions forming reversible covalent bonds.

The mentioned reactions and processes can be used for various practical applications. One application that received increasing attention in the past years is the development of self-healing materials. Self-healing is a fundamental and often occurring principle in nature although the extent of healing can be quite different. Usually more advanced organism can only heal less complex structures, *i.e.* highly developed mammals usually can heal only minor damages like wounds in the skin. Other animals, like the axolotl or the zebrafish however possess astonishing self-healing abilities and are capable of regenerating entire organs, like arms, fins or parts of even more complex organs as their heart or eyes.[41–43] The autonomous regeneration of such complex structures fascinated researchers for

decades and until now the exact mechanisms remain still a mystery. It is needless to say that our synthetic materials are far, far away from the magnificent capabilities of natural systems (see Figure 4 for comparison) but still some decent progress has been achieved in the past decades.[7,44,45]

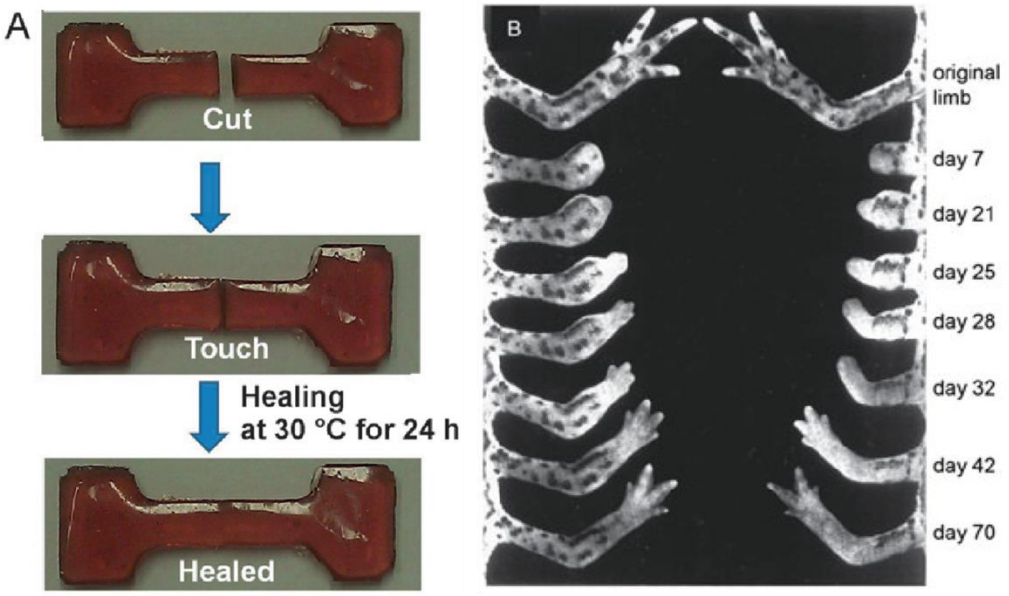

Figure 4: A: Self-healing of a synthetic supramolecular polymer assembly (reproduced with permission from Ref.[46], Copyright 2015, Wiley-VCH) and B: progress of limb regeneration of a red-spotted newt after different times after amputation. (From Ref[43]. Reprinted with permission from AAAS)

Two general concepts can be distinguished in the field of synthetic self-healing materials. The first is the concept of extrinsic self-healing and the second one is the intrinsic self-healing. Extrinsic self-healing is based on the incorporation of capsules or vascular channels that contain a healing agent that can be either a superglue or a monomer (solution). Upon mechanical stress and/or damage the healing agent flows out of the breaking capsules or channels, gets distributed in the cracked material and reconnects the separated parts. The advantage of the extrinsic healing concept is that it can be integrated quite easily in a variety of different matrix materials and that it allows for autonomous healing upon damage without the need of a separate external trigger. Disadvantageous is, however, that a particular spot of the material can be healed only once and that the material itself is getting less homogeneous by the introduction of the healing capsules, which can impact the material's mechanical properties.

Intrinsic self-healing on the other hand works by internal reorganization through reversible bonding reactions. As no healing agents (and their capsules) have to be added the material is more homogeneous and multiple healing of a particular spot is possible. Usually the healing does not occur autonomously but needs a dedicated trigger. Up to now a comprehensive library of concepts for polymer materials that can be healed by various triggers is reported and reviewed, demonstrating the general interest in this kind of

materials.[4,7,37,39–41,47] Upon the corresponding stimulus particular bonds in the polymer material are cleaved, which leads to a significant increase in polymer mobility. Consequently the polymers can flow in cracks and close and reconnect damaged parts of the material. Thermally self-healing materials were realized through the DA reaction of furan and maleimide[35,48,49] and offer easy control of the polymer mobility by the applied temperature. Öhlenschläger et al. demonstrated the transition of their DA network from a brittle rubber state into a liquid melt when heating from ambient temperature to 150 °C.[36] The photo-dimerization of anthracene was employed by Froimowicz et al. for generating films that self-heal after firstly cleaving the anthracene dimers by irradiation with light of 254 nm and then reconnecting the building blocks at 366 nm.[39] Chemical stimuli can be used for introducing reversible bonding reactions, as demonstrated by Vogt et al.[18] and Kowalski et al.[50]

A particular focus of this work lies on thermoresponsive materials. Temperature is a parameter that can be controlled relatively easily and can be applied to materials in solution or in bulk. It is furthermore possible to transfer heat locally constricted to distinguished parts of a material, thus allowing for spatial control. For the application as intrinsically self-healing materials temperature is consequently an attractive stimulus. But also further applications can be exploited through thermoreversibly bonding materials, as for instance printable polymer networks. When heated up the material behaves like a thermoplast and can be 3D printed or injection-molded. While cooling down, however, the polymers crosslink autonomously and form very robust materials that otherwise could not be realized with such processing techniques.

2.2 The Diels-Alder Reaction

The Diels-Alder (DA) reaction is probably one of the most famous and widely used reactions in the synthesis for the precise modification of organic molecules or polymers. In 1928 Otto Diels and Kurt Alder reported about a reaction that earned them the Nobel Prize in chemistry 22 years later.[51] The DA is a [4+2] cycloaddition reaction between a conjugated diene and an electron deficient dienophile that yields a 6-membered ring, as shown in Figure 5. The right part of the figure shows the DA dimerization of Cyclopentadiene (Cp), one of the most fundamental DA reactions. At elevated temperatures the reaction can be inverted to the retro Dies-Alder (rDA) reaction[33], making it very interesting for dynamic bonding materials. Furthermore, the reaction forms predominantly the endo product, works well with hetero atoms (hetero Diels-Alder reaction, HDA) and occurs in reasonable time frames (hours) at mild conditions. Because of the stability of the reacting groups against many functionalities (-COOH, -OH, -

NH_2) and as no byproducts are formed the reaction has drawn a lot of attention as an option in click chemistry.[35,38,52–55]

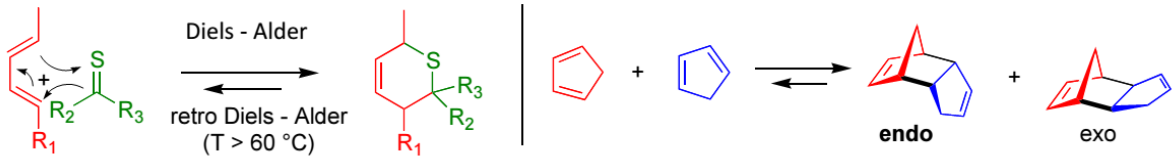

Figure 5: Scheme of the HDA and rDA reaction (left) and dimerization reaction of cyclopentadiene, forming the exo and the favored endo product (right).

The reactivity of the DA pairing can be tuned by introducing electron-withdrawing substituents to the dienophile, such as phosphonates, sulfonyl, cyano or pyridyl groups that lower the LUMO level of the dienophile.[35,56] The need of a catalyst (*e.g.*, a Lewis acid, such as $ZnCl_2$) and the temperature at which the reaction becomes reversible is specific for any particular DA pairing.[38] The versatility of the reaction made it popular for synthesizing and modifying polymeric materials. Especially the reaction between furan and maleimide derivatives was exploited intensively. Using bismaleimides for crosslinking polymers thermoreversibly is an often used approach and allows developing intrinsically self-healing materials, as described in the previous chapter.[57–59] Furthermore the DA reaction between furan and maleimide was used for effectively preparing thermoresponsive dendrimers[60,61]. The mild conditions of the DA reaction make it interesting even in biological applications, such as bioconjugation of oligonucleotides, RNA or DNA, modification of proteins or for live cell imaging.[62–67]

The HDA reaction of dithioesters is particularly interesting, because of the common use of dithioesters as RAFT agents. Hence, an accordingly designed RAFT agent can serve a double purpose: Besides its function in mediating the radical polymerization it can act as HDA agent for polymer analogue reactions.[35,68] Figure 6 shows an exemplary reaction pathway for a P-di-Linker that polymerizes isobornyl acrylate (^{i}BoA) and then undergoes HDA reaction with isophorone bis(sorbic carbamate) (IPDI-SA):[35,69]

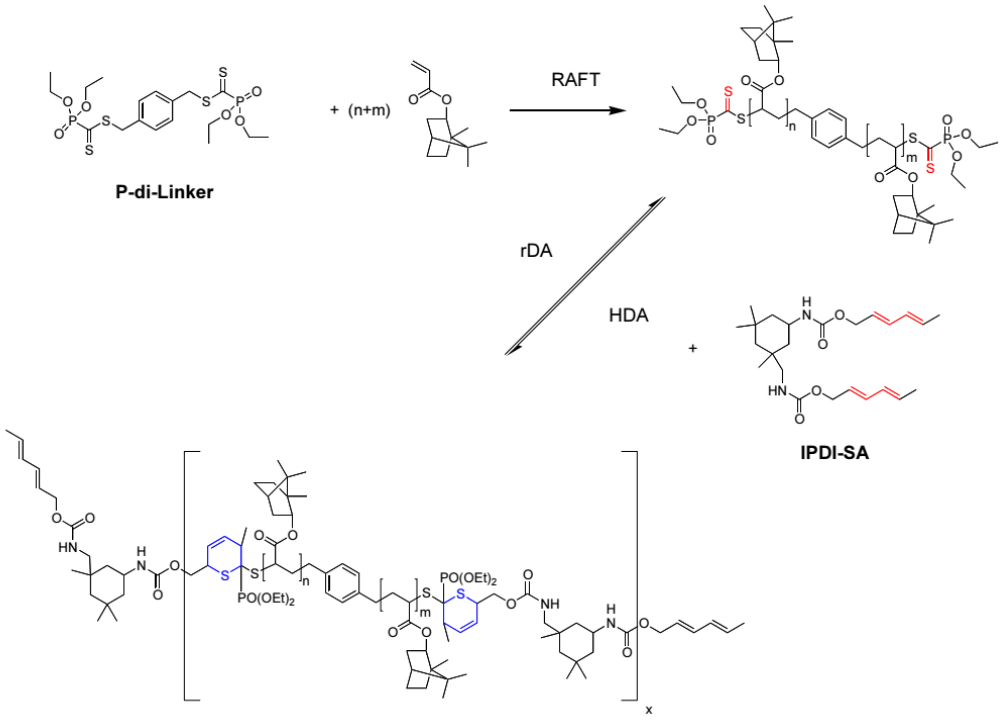

Figure 6: Reaction of P-di-Linker with ^{i}BoA in a RAFT polymerization and the subsequent HDA reaction with IPDI-SA.[35,69]

2.3 *In situ* Analyses

When a new material is developed it is important to know under what condition the material is supposed to perform. Otherwise it would not be possible to design the material adequately so that the optimal performance can be achieved. To be able to control the properties of a material it is consequently necessary to know the property influencing parameters that can be used to control its behavior. Hence, detailed analyses of the molecular properties and processes are required. The investigation of stimulus responsive materials is a particular challenge because the analysis procedures have to be carried out under precisely controlled conditions. For instance, when an rDA reaction that occurs at 120 °C is about to be investigated, all necessary steps have to be done at 120 °C because changes in temperature could influence the outcome of the investigated reaction. Or, in other words, the analysis has to be done *in situ* at exactly the same conditions that are required for the reaction of interest. Since the focus of this work lies on temperature sensitive DA materials, the further considerations shall be specific for temperature dependent analyses. It should be noted that the considerations could be done in a similar fashion for the investigation of processes that respond to changes in pH-value, salt concentrations or other parameters.

The following statements for an effective *in situ* analysis can be asserted:[19]

(1) The analysis has to be done at the same conditions at which the reactions are proceeding. If a change of conditions (*e.g.* solvent, temperature) for performing the analysis would be required the outcome of the respective bonding reactions could be falsified. In the ideal case the reactions can be done directly in the analysis instrument at the corresponding conditions.
(2) In order to obtain the highest possible amount of information it should be possible to perform the analyses at many different conditions. Being able to simply change solvents and adjust the temperature in a broad range increases the applicability of a given method for *in situ* analytics.
(3) The time necessary for a single measurement should be short compared to the timescale of the bonding reactions. If the analysis is too slow the course of the reactions cannot be captured. In such a case it is only possible to evaluate the equilibrium state of the reactions.
(4) The methodology should allow quantifying the results in order to compare the results across measurements obtained for different samples and at different conditions.
(5) Developing an analytical technique is always time consuming and requires optimizing many parameters. It is, consequently, advantageous if the developed methodology is not highly specific for a particular polymer system, so that the technique can be used more universally for various analytical tasks.

After having figured out what characteristics are beneficial for an effective *in situ* analysis tool different techniques can be evaluated with respect to these characteristics. An often used group of techniques in molecular science is the group of spectroscopic techniques. The concept is to expose the sample to light of a particular wavelength or to a magnetic field and to search for resonance phenomena that are correlated to the presence of very particular molecular features. Mostly used techniques are UV/Vis-, infrared (IR)-, and nuclear magnetic resonance (NMR)-spectroscopy. They all give direct information over present structural elements and can be used to monitor reactions of all kinds. The concept has proven its enormous power in countless examples. Monitoring the concentration of specific functional groups over the course of a reaction allows determining the conversion of the respective reactions. The advantages of spectroscopy lie in their applicability for many different systems because most functional groups can be detected with one of the techniques and their quantitative results (peak areas can be correlated to concentrations). Two major drawbacks shall be noted however: The techniques become difficult if the relevant signals of interest are overlapping with other signals, or if their intensity is too low to integrate the respective peaks. Both aspects can become an issue in polymer

analyses if the polymers exhibit a great number of different functional groups or if polymer endgroups at correspondingly low concentrations are to be detected.

Spectroscopy can, generally spoken, easily be performed in various solvents and at different temperatures. In the case of NMR it shall be noted that a high temperature instrument can be an issue because of its high cost and not trivial operation. If the requirements are met, NMR offers very detailed information about reversible bonding/debonding reactions, however. A thermally self-healing polymer based on the furan-maleimide DA reaction was analyzed by Syrett et al. by NMR. They could identify characteristic NMR signals of the educts and the DA cycloadduct that allowed monitoring the state of the reaction at different stages (Figure 7). The signals of the cycloadduct that are visible at ambient temperature (i) vanish completely when heating the DA polymer to 110 °C and the signals of the furan and the maleimide appear (ii). Cooling the sample down to 60 °C again yields a mixture of both, the signals of the educts and the cycloadduct, indicating a partial rebonding of the furan and the maleimide (iii).[70] Similar studies can be found in literature that demonstrate the power of NMR for following reversible reactions and determining their conversion[9,71–74] (even for supramolecular assemblies[75]).

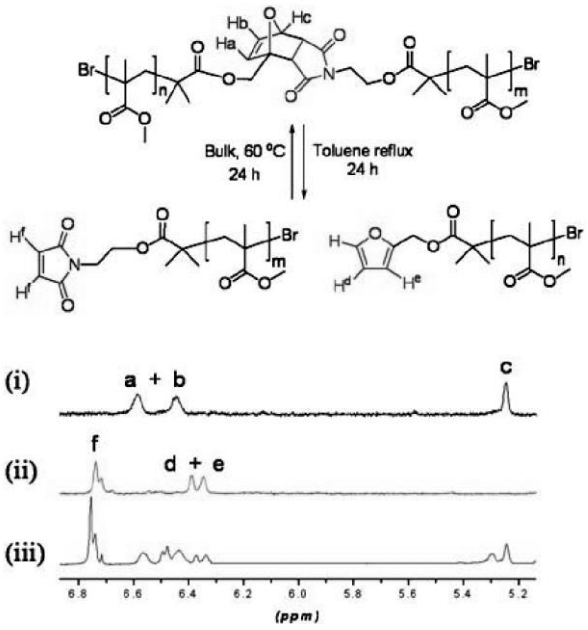

Figure 7: ^{1}H-NMR of a furan-maleimide DA polymer: (i) The spectrum of the polymer at ambient temperature, (ii) cleaved polymer after heating to 110 °C for 24 hours and (iii) after cooling to 60 °C again for further 24 hours. Reproduced from Ref[70] with permission of The Royal Society of Chemistry.

UV/Vis spectroscopy can be a powerful addition because of its very high analysis speed, as demonstrated in Figure 8. Kim Öhlenschläger exploited the characteristic absorption of a C=S double bond at 347 nm ($\pi \rightarrow \pi^*$ transition) for tracking the kinetics of the deprotection of a HDA-Dilinker at

100 °C (C=S formation), its DA reaction with a building block carrying Cp endgroups (C=S consumption) and once more the rDA reaction at 100 °C (C=S formation). The experiments validated the very quick bonding and debonding reactions that occur in the time frame of only few minutes.

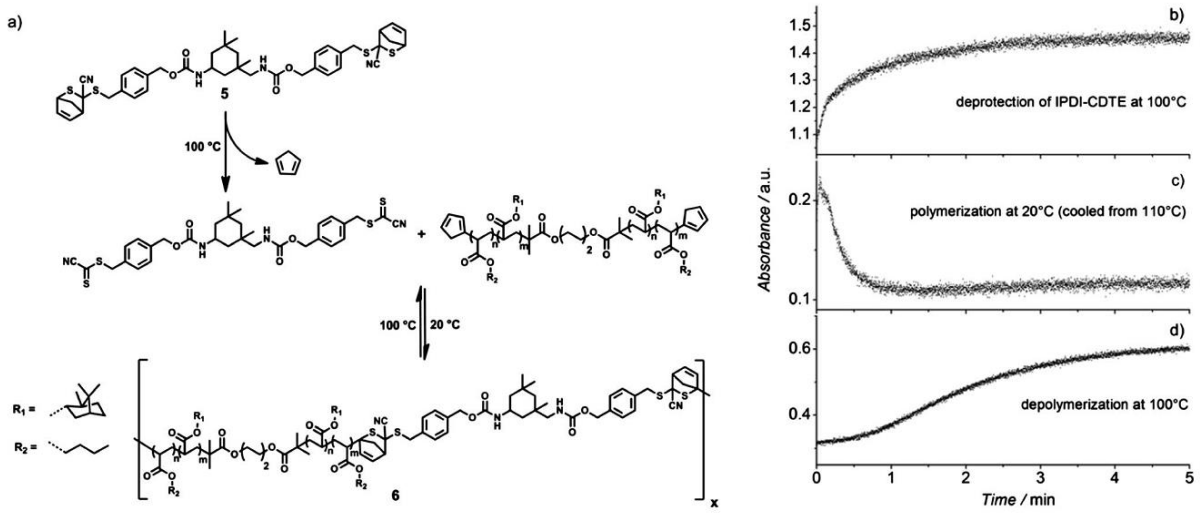

Figure 8: Application of UV/Vis spectroscopy for monitoring the formation and consumption of C=S double bonds during different bonding/debonding reactions in real time. Reproduced from Ref[72] with permission of The Royal Society of Chemistry.

Another concept that is useful for the investigation of dynamic bonding/debonding reactions is the determination of the mass and/or size of the reacting polymers. As the mass (or the size) of a polymer is a parameter that inherently has to change during a bonding/debonding reaction both can be exploited for evaluating the respective reactions. Popular techniques for the determination of molar masses are mass spectrometry, light scattering and size exclusion chromatography. Further techniques like viscometry, ultracentrifugation or osmometry are less frequently used.

Mass spectrometry (MS) is by far the most precise method. With accuracies well below 1 Da it is possible to monitor chemical reactions, if the conversion of functional groups is associated with distinct changes in molar mass. Unfortunately, mass spectrometry is dependent on the analysis of ionized molecules in the gas phase. Which may not be a problem for the investigation of small molecules is getting an issue in the world of polymers. The larger the molecule is the lower is its tendency to move into the gas phase. Additional difficulties arise from the ionization step, since very gentle techniques have to be applied in order to avoid fractionation of the macromolecules. Matrix assisted light desorption ionization (MALDI) in conjunction with a time-of-flight (TOF) mass analyzer has become a quite well working solution for mass spectrometry with polymers and in literature many examples can be

found were interesting investigations were performed.[76–80] However, the applicability of MS for a particular polymer system has to be tested for every individual case and the detailed procedures have to be optimized. Often the analysis itself cannot really be performed *in situ*, since the sample is analyzed in ultra-high vacuum. Although examples for ambient condition MS can be found in literature their applicability for analysis in a broad variety of different conditions seem limited.[81–86] And even if satisfying conditions can be found a further drawback is that the results of MS are, despite their extremely high accuracy with respect to mass, not quantitative. It cannot be guaranteed that all fractions of the sample have the same ionization tendency and that no fractionation occurs. In other words, the acquired mass distributions can be skewed or shifted and calculating representative molar mass averages is not really possible. Therefore separate concentration determinations are required.[87]

Light scattering (LS) is a method for determining the absolute molar mass of polymers and is based upon the fact that the scattered light intensity of a polymer is proportional to its molar mass. The exact mechanism are described in chapter 2.5; at this part it shall be enough to state that LS allows determining molar mass, radius of gyration, and/or hydrodynamic radius. The experiments are carried out in solution which makes them applicable for many polymers. However, if the polymers are too small and the corresponding light scattering intensity is too low, the measurements can become inaccurate or even impossible. If carried out in batch only weight average values are obtained that are representative only in the case of very narrow distributions. For broader distributions it is necessary to couple LS to a chromatographic system and to perform the LS experiment at each individual slice of the chromatogram. In most cases LS is coupled to size exclusion chromatography (SEC), because this technique separates according to size.

SEC is one of the most frequently employed analysis methods for polymers and separates dissolved polymers according to their hydrodynamic volume. Calculating molar masses is possible by either coupling an LS detector or establishing an adequate calibration with polymer standards of known molar masses. SEC is a very robust methodology for determining molar mass distributions (MMD) of many different polymers. The only prerequisites that have to be met are solubility in an SEC solvent, a molar mass between a few hundred and several million Da and stability at elevated pressures and shear rates.[88–90] If the last two criteria occur to be an issue other techniques, such as asymmetrical flow field flow fractionation have to be used. This flow field based technique is a lot more gentle, can separate particles up to µm size and allows investigating supramolecular assemblies; at the cost of a significantly more complex method development and optimization.[91–95]

With respect to the aforementioned criteria for an *in situ* analysis method, SEC appears to be a promising choice, due to its non-specificity and relatively easy method development. The instrumental

equipment can be found in virtually any polymer laboratory and is not associated with high costs. These considerations led to the development of the temperature dependent SEC (TD SEC) method that is mainly used in this work for investigating thermoreversibly bonding DA polymers.

The mentioned techniques are for analyses on the molecular level. In the later step of the development the molecular information is less important and the macroscopic material properties are of interest. Then it is necessary to extend the field of analysis techniques towards rheology and dynamic mechanical analyses, tensile testing or microscopy. Their importance is not to be underestimated and their potential for corresponding *in situ* analyses is summarized in literature[19]. In this work, however, the focus lies on analyses on the molecular level so that the material tests are of minor relevance.

2.4 Size Exclusion Chromatography

2.4.1 The separation in SEC

Size exclusion chromatography (SEC) is the most intensively used type of separation methodologies in polymer science. In contrast to interaction liquid chromatography the separation does not occur according to the chemical composition but to the size of the dissolved compounds. Or, in other words, rather than being sensitive to interactions between the dissolved analytes and the stationary phase, SEC is based on the distribution of dissolved molecules in a stationary phase with defined porous structure.

The elution volume of an analyte of a particular size depends on its accessible pore volume of the stationary phase. Equation 1 displays how the elution volume of an analyte can be calculated:

$$V_{elution} = V_0 + K_{SEC} \cdot V_p \qquad \text{Equation 1}$$

In here, $V_{elution}$ is the elution volume of the analyte, V_0 the interstitial volume of the column (volume of moving solvent), V_p the pore volume and K_{SEC} the fraction of pore volume that is accessible for the respective analyte molecule. K_{SEC} ranges between 0 (analyte is too large for all of the pores, “exclusion limit”) and 1 (analyte fits in all pores, “total permeation”) and is dependent on the size and flexibility of the polymers. Larger polymers have a lower pore volume accessible than smaller ones and, thus, are getting eluted earlier.

Having stated that, we notice that the size of a polymer is the most important property for describing its behavior in SEC. Unfortunately, the size of a polymer in solution can be interpreted in different ways and deserves some closer considerations. If a macromolecule is transferred in a solvent all of its segments start to experience interactions with the surrounding solvent. If these interactions are thermodynamically more favorable than the interactions between the polymer segments themselves, the macromolecule will tend to accumulate solvent molecules and, consequently, swell to a coil of a

certain size. In the contrary case the polymer coil displaces solvent molecules and shrinks to a more globular structure, thus minimizing the polymer-solvent-interface. In the case of equal interactions between polymer segments themselves and between polymer segments and solvent (Θ-state) the polymer coil will adapt unperturbed dimensions.

There are multiple ways for characterizing the size of a polymer coil, regardless of its thermodynamic situation. Figure 9 shows three common characteristics: The end-to-end distance, which is simply the distance between the endgroups of a linear polymer, the hydrodynamic radius (R_h) as the radius of a solid sphere with identical hydrodynamic friction as the respective polymer coil and the radius of gyration (R_g) as the average distance of each polymer segment to the molecule's center of gravity. Putting into relation R_g and R_h gives information about the conformation of the polymer coil: In the case of a very compact globular structure the molecule resembles a solid sphere and the ratio R_g/R_h, the so called ρ-factor, approximates 0.778. In less compact structures the R_g gets larger than the R_h and ratios of 1.5 - 1.7 are be reached.[96] As a consequence, both radii are dependent on the thermodynamic quality of the solvent.

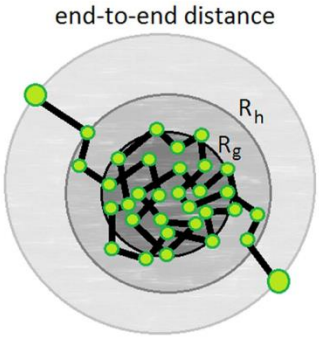

Figure 9: Dimensions of a polymer coil in solution: The end-to-end distance, the hydrodynamic radius (R_h), and the radius of gyration (R_g).

With regard to SEC the hydrodynamic radius is the most important dimension, as the separation in SEC is usually according to hydrodynamic size.[88] Since a polymer coil is a rather flexible structure, there is a chance that the coil can enter a pore that is somewhat smaller than the coil. A polymer can fit into a smaller pore if it adapts more compact conformations, which decreases its entropy because of the decreasing number of possible conformations inside the pore. Therefore the polymer experiences an unfavored entropy decrease when entering smaller pores. Hence, the driving force of the separation process is entropy. In contrary this means that enthalpic interactions between solute and stationary phase have to be avoided in order to achieve ideal SEC behavior. When enthalpic interactions are observed it is worth testing if a different solvent might be more suitable of if another stationary phase should be used.

Having described how the separation in SEC works we want to take a closer look on how the eluted polymers are being detected.

2.4.2 Detectors used in SEC

The first and most essential detector in SEC is the **differential refractive index (dRI) detector**. It is constructed by a flow cell with two chambers: One containing the pure solvent (reference cell) and one that is flushed by the eluent (sample cell). A laser beam passes through both cells and is being deflected according to the difference in the refractive index between sample and reference cell. The resulting voltage of the signal can be calculated according to

$$dRI\ Signal = K_{dRI} \cdot c \cdot \frac{dn}{dc} \qquad \text{Equation 2}$$

where K_{dRI} is the specific device constant, c the weight concentration of the analyte and dn/dc its specific refractive index increment. The concentration of the analyte can be calculated if K_{dRI} and dn/dc are known (both constants can also be merged into one, if dn/dc does not change). But for most standard applications it is not even necessary to determine the constants, because only the relative concentrations are required and the constants would cancel out anyways.

The great advantage of the dRI detector lies in its simple and robust construction, its non-specificity (virtually every substance can be detected, as long as its refractive index is different from the solvent's refractive index), its high sensitivity, and its signal proportionality to concentration. Disadvantageous is its high sensitivity towards solvent composition and temperature, often leading to unstable baselines and pronounced solvent peaks.

Another type of concentration sensitive detector is the **UV/Vis absorption detector**, which is composed of a flow cell that is passed by polychromatic light (typically a deuterium lamp for the UV and a halogen lamp for the visible light range) and photodiodes that allow to acquire the complete spectrum of the eluent at each slice of the chromatogram or that allow to selectively collect the absorption at one or two particular wavelengths. The absorption can be evaluated according to Lambert-Beer's law:

$$E_\lambda = \lg\frac{I_0}{I_t} = \varepsilon_\lambda \cdot c \cdot d \qquad \text{Equation 3}$$

where E_λ is the extinction at the wavelength λ, I_0 the incident light intensity , I_t the intensity of the transmitted light, ε_λ the coefficient of extinction at the wavelength λ, c the molar concentration and d the length of the pathway that the light passes through the eluent. Measuring the extinction at each slice allows calculating the corresponding molar concentrations, if an adequate calibration (determination of ε_λ) was performed.

The UV/Vis detector is less frequently used in SEC, since most polymers are transparent in the relevant wavelength range. Even if absorbing endgroups are present they need to be in sufficiently high concentrations. However, in the case of absorbing polymers a more specific (and probably sensitive) concentration determination than with the dRI detector can be achieved, with less vulnerability to drifting baselines and solvent impurities. The UV/Vis detector is particularly useful if samples with chemical composition distributions are to be analyzed. In such cases it is necessary to collect multiple independent concentration signals.[97]

In a similar way it is possible to couple **infrared (IR)** or **nuclear magnetic resonance (NMR)** spectroscopy detectors to SEC in order to gain even more information about the chemical composition of the eluting analytes. Dealing with the low sample concentrations of the SEC effluents is a difficulty, however, and the optimization of all parameters not trivial. Kok et al. reviewed the topic in detail and worked out advantages and disadvantages of the use of *online* flow cells vs. the use of a solvent-evaporation interface.[98] Other studies demonstrate the effort of developing the practical setup and handling the produced data.[99,100] Hyphenating NMR to LC is even more complicated but rewards with an otherwise unreached level of information about the samples. In Figure 10 the analysis of a blend of PS, PI and PMMA of similar molar masses is shown. All three components elute at virtually the same time but can be distinguished by their NMR spectra. Integrating the peak areas allows determining the concentration of all three components quantitatively, which is a huge advantage of the hyphenation.[101–105] Although the hyphenation of SEC with spectroscopic techniques is possible the complexity of the system optimization prevented these methods from ascending into the class of routine analytical tools until now.

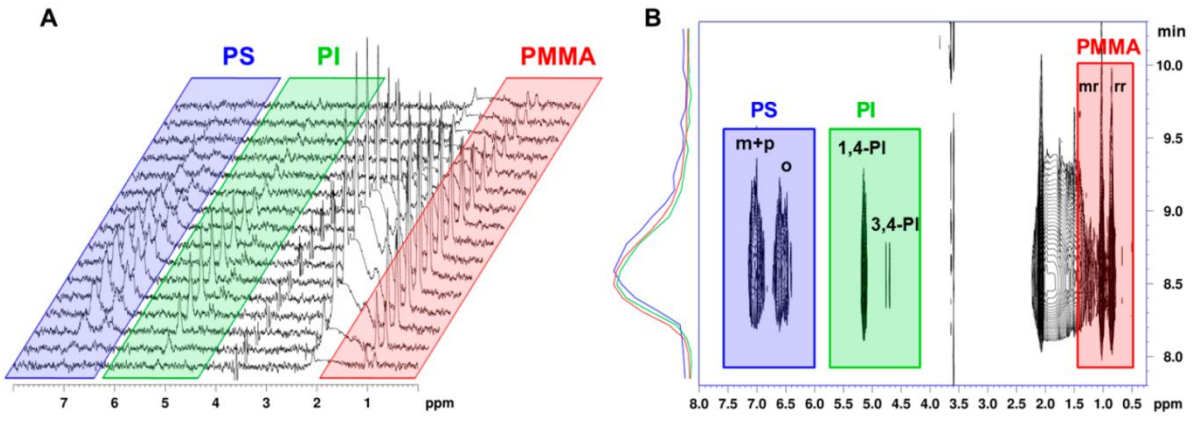

Figure 10: Stack of ^{1}H NMR spectra that were acquired in an SEC-NMR analysis of a PS-PI-PMMA blend (A) and the accordingly derived chromatograms and contour plots of the coeluting different polymer species (B). Reprinted with permission from Ref.[101]. Copyright 2014 American Chemical Society.

Further widely used detectors for SEC are the **light scattering detectors**. Light scattering allows the absolute determination of the molar masses and the radius of gyration of the eluting analytes, without being dependent on their elution time or the availability of adequate standards (the details are discussed in chapter 2.5). This makes SLS detectors very powerful and popular; their high price and technical complexity has to be considered as a drawback. SLS is especially expensive for high temperature applications and not trivial for temperature dependent analyses. A further fact has to be kept in mind: SLS works fine for rather large polymers that scatter enough light for getting strong signals. For polymers with molar masses lower than 10 kDa SLS is applicable only with limitations, as the scattered light intensity is getting low.

If an absolute molar mass determination via light scattering is not feasible or possible, the traditional approach of relative molar mass determination with respect to polymer standards has to be applied. The following chapter highlights different important strategies and aspects.

2.4.3 Relative Molar Mass Determination

As described in chapter 2.4.1, SEC separates according to hydrodynamic size and not to molar mass. Usually molar masses are of interest so that either a calibration of the SEC methodology relative to known polymer standards or a separate absolute determination of molar mass is required.

The most common concept for the calculation of molar mass (averages) is the calibration to polymer standards of known molar masses. The concept is to inject samples of polymer standards of narrow molar mass distribution, to collect their chromatograms and to plot their logarithm of their molar mass ($lg\ M$) over the elution volume (V), as shown in Figure 11. Around its center the curve can be approximated with a linear function. At the end, at high elution volumes, the curve decays more rapidly, indicating the limit of total permeation. There, the polymer coils can penetrate all pores and no further separation is observed ($K_{SEC} = 1$). Towards lower elution volumes a steep increase of the slope can be seen, which indicates the exclusion limit. Above a certain polymer size no SEC separation is observed because the polymers are larger than all of the pores and, thus, $K_{SEC} = 0$. However, separation of polymers larger than that critical size can still be achieved by exploiting the different flow velocities in between the packing material particles. Close to the walls of the particles the flow velocity is practically zero and increases towards the center of the “channels” between the particles. Larger polymers have lower probability of being close to the walls than smaller ones and, as a consequence, are predominantly

found in regimes of higher flow velocities and are eluted earlier. This concept of hydrodynamic chromatography shall not be considered in detail in this work, but many descriptions and examples can be found in the literature.[106,107]

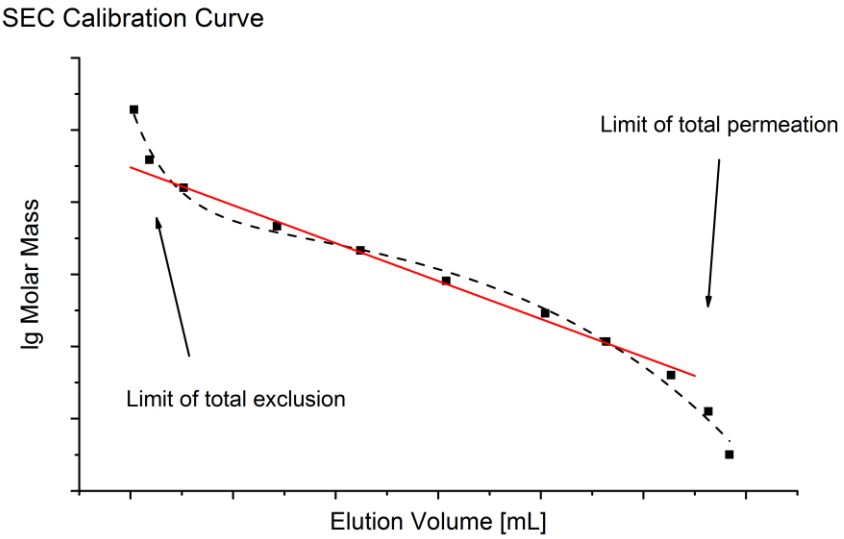

Figure 11: General appearance of a calibration curve in SEC, plotted as *lg M* as a function of the elution volume.

Having established a calibration curve it is possible to evaluate the chromatogram of an unknown sample by converting elution times into molar mass. In conjunction with a concentration sensitive detector the well-known molar mass averages can be calculated:

$$M_n = \frac{\sum_i c_i \cdot M_i}{\sum_i c_i} \qquad \text{Equation 4}$$

$$M_w = \frac{\sum_i c_i \cdot {M_i}^2}{\sum_i c_i \cdot M_i} \qquad \text{Equation 5}$$

$$Đ_m = \frac{M_w}{M_n} \qquad \text{Equation 6}$$

In these equations, M_n is the number average molar mass, M_w the weight average molar mass, $Đ_m$ the molar mass dispersity, c_i the molar concentration at each slice and M_i the corresponding molar mass at slice *i*. The concept of relative molar mass calibration works fine, if the standards that are used for the calibration are of the same type of polymer as the analytes that are to be measured. If molar mass averages of a sample are calculated by using the calibration curve of another type of polymer, substantial errors can occur, because the correlation between hydrodynamic radius and molar mass is strongly dependent on polymer type, architecture and solvent quality.

If no adequate standards are available, the concept of universal calibration can become very useful. Instead of taking the molar mass as the size for calibration, the product of molar mass and intrinsic viscosity (*[η]*) is used. This product is a direct measure of the hydrodynamic size of a particle, which makes it applicable for SEC calibration.[108] Grubisic et al. demonstrated the potential of this concept by measuring polymers of different chemical nature and different architectures and showing that the logarithm of *[η]*M* for all samples fall into one calibration curve (Figure 12).

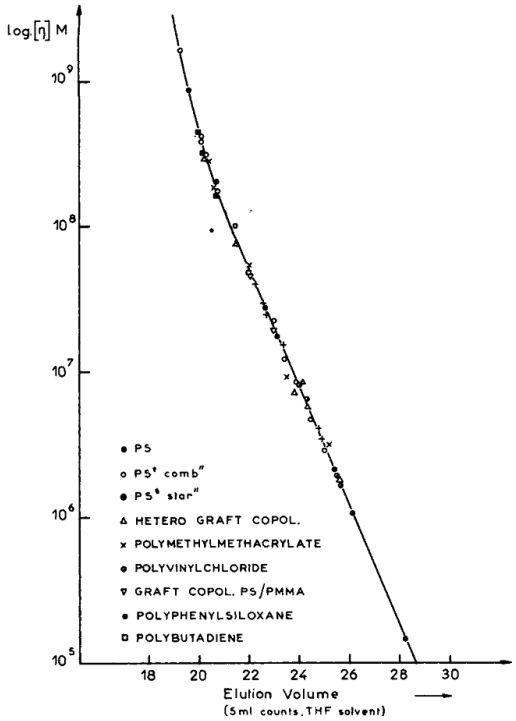

Figure 12: Universal calibration data for different polymer types and architectures. Reproduced with permission from Ref. [108], Copyright 2003, Wiley-VCH.

As a disadvantage, the universal calibration requires an additional viscosity detector in order to directly measure the viscosity of the sample at each slice of the chromatogram. If a viscometer is not available, the intrinsic viscosities of both, standard and sample, can be calculated according to the Mark-Houwink equation:

$$[\eta] = K \cdot M^{\alpha} \qquad \text{Equation 7}$$

Where *[η]* is the intrinsic viscosity, *M* the molar mass and *K* and *α* are the Mark-Houwink parameters that have to be known. With *K* and *α* known for the standard and the analyte, Equation 8 and, after substitution with the Mark-Houwink equation, Equation 9 can be set up:

$$[\eta]_1 \cdot M_1 = [\eta]_2 \cdot M_2 \qquad \text{Equation 8}$$

$$K_1 \cdot {M_1}^{\alpha_1} = K_2 \cdot {M_2}^{\alpha_2} \qquad \text{Equation 9}$$

In these equations the index 1 designates the standard and the index 2 the analyte. Equation 9 can be solved for M_2 and then the "true" molar masses can be calculated. The Mark-Houwink parameters have to be determined separately or can be found in literature. Using literature values is tempting but the validity of the employed values should be questioned, since they can be sensitive to changes in solvent composition, temperature or variations in the exact chemical structure or architecture. Even determining the Mark-Houwink parameters of the employed polymers can lead to imprecise results, as averaged values are obtained that do not account for differing values if the sample is not of a uniform architecture but is characterized by a morphological distribution.

In conclusion, universal calibration can be a very powerful improvement of the relative standard calibration, if the intrinsic viscosities are directly measured by a dedicated online viscometer. Calibrations done with the Mark-Houwink parameters are possible in principle but should be considered carefully, since they assume that the parameters in the SEC conditions are identical to the conditions where they were determined, and, that they are constant over the entire range of the samples distribution.

At last it shall be noted that both, the regular relative calibration and the universal calibration, are absolutely dependent on an ideal SEC behavior, where no enthalpic interactions between analyte and stationary phase are observed. If this cannot be guaranteed or if the interactions are unknown, additional absolute molar mass determination by LS is necessary

2.4.4 Chemical Composition Determination

Characterizing synthetic polymers comprehensively is a challenging endeavor, because of their dispersity in not only molar mass but often also chemical composition, architecture or end group constitution.[97,109] Especially in the case of copolymers or, more generally spoken, polymer systems with multiple chemically different components, the overlaying distributions render the situation complicated.

For the precise evaluation of an SEC experiment it is important to know the chemical composition at every position in the chromatogram. Otherwise the application of the previously described evaluation concepts cannot be used, as they require knowledge of the exact concentrations at each position of the chromatogram. Coeluting components of different chemical nature lead to detector signals in that the individual responses are superimposed. In such cases special treatment of the data becomes necessary.

The most common approach is to work with multiple concentration sensitive detectors (*e.g.*, dRI-, UV/Vis or IR-detectors). In general, the detector response signal of an arbitrary concentration signal of a mixture of *n* components can be described as follows:[101]

$$Signal = \sum_{i=1}^{i=n} ResponseFactor_i \cdot c_i \qquad \text{Equation 10}$$

Every component contributes to the final signal with its concentration c_i weighted by its characteristic response factor. This response factor is the *dn/dc* in the case of a dRI detector or the specific absorption coefficient in the case of spectroscopy of absorption detectors. The characteristic response factors have to be determined for every component, leaving the concentrations as the only unknowns. In order to resolve *n* unknowns at least *n* equations are required, meaning that at least *n* (independent) detectors have to be used. For example, if two different components are mixed and a dRI and a UV/Vis detector are used the problem can be solved for each point of the chromatogram by solving the following system of equations with two unknowns, namely c_1 and c_2:

$$dRI\ Signal = \frac{dn}{dc}_1 \cdot c_1 + \frac{dn}{dc}_2 \cdot c_2 \qquad \text{Equation 11}$$

$$UV\ Signal = \varepsilon_1 \cdot c_1 + \varepsilon_2 \cdot c_2 \qquad \text{Equation 12}$$

Although this concept seams relatively easy in theory, it can lead to imprecise results in practice, as shown in complex studies.[101] In general the procedure increases in accuracy if the individual response factors for each detector, so in our example dn/dc_1 and dn/dc_2, are as different as possible. The accuracy can be increased further if more detectors than components are accessible, for instance a further wavelength for the UV absorbance. In that case three equations describe two unknowns and an optimization process can be done for finding the best solutions for each slice of the chromatogram.

Having determined the chemical composition eventually allows deriving the absolute concentration of the analytes that is required for the correct evaluation of light scattering intensities, for instance.

2.5 Interaction Chromatography

Although SEC may be the most important LC technique in polymer science there are further methodologies that can be beneficial in particular applications; methodologies that are based on enthalpic interactions between the analytes and column materials. The importance of interaction chromatography in polymer science is underlined by numerous studies that can be found in literature.[110–115] For instance, already in 1978 Maeden et al. used the advantages of interaction

chromatography for detailed investigations of oligomers with respect to their size and functionality in order to study the kinetics of early stages of the respective polymerization processes.[116] This chapter highlights some of the theoretical fundamentals that are required for understanding and performing interaction chromatography with polymers.

The general driving force for analytes to move from the mobile phase to the stationary phase in an LC setup is given by the gain in free energy *ΔG*, as described in Equation 13:

$$\Delta G = \Delta H - T \cdot \Delta S \qquad \text{Equation 13}$$

where *ΔH* is the enthalpic, *ΔS* the entropic contribution to the process and *T* the temperature. In general three different categories of processes can be defined: At first the ideal SEC category where *ΔH* is zero so that the separation process is entirely driven by entropic effects and, thus, polymer size. In the second case *ΔH* is different from zero and enthalpic interactions of the polymer with the stationary phase occur, leading to additional retention. As a consequence, both, the size and the chemical nature of the polymer contribute to the retention mechanism. In a third case, under so called "critical conditions" *ΔH* and *ΔS* are equal and balance each other out. All three cases can be adjusted by variation of mobile and stationary phase. Even with the same stationary phase all three cases can be generated by mixing different solvents in the right ratios. If the thermodynamic quality of the solvent is very good the enthalpic interactions are going to be minimized, thus leading to SEC behavior. With decreasing quality of the solvent enthalpic interactions are getting more probable and the analytes start to adsorb to the stationary phase; the range of liquid adsorption chromatography (LAC) or high performance liquid chromatography (HPLC) is reached.

The strength of retention in LC is characterized by the so called retention factor *k* as shown in Equation 14:

$$k = f(\varphi, T, M) = \frac{t_r - t_0}{t_0} \qquad \text{Equation 14}$$

where t_r is the retention time of the analyte and t_0 the retention time of a non-retained molecule (*e.g.*, the solvent peak). The retention factor *k* is dependent on the thermodynamic quality of the mobile phase and, thus, on its composition *φ* (= fraction of strong solvent) and temperature *T*. A negative *k* would mean that the respective analyte elutes before any non-retained species, as it is the case in SEC where the polymers are effectively accelerated due to the exclusion effect. A *k* of zero signifies no retention at all; as it is in the case of the critical conditions where enthalpic and entropic contributions balance each other out. If *k* is larger than zero the analytes are effectively retained, where the retention time increases with increasing *k*.

The left graph in Figure 13 shows the retention times of three PEG standards with different molar masses as a function of the solvent composition (acetonitrile (ACN) in tetryhydrofuran (THF)). In the present example the higher ACN content renders the solvent more polar and, thus, stronger for the polar PEG polymers. Consequently, up to 55 % ACN (the strong solvent) we can observe SEC behavior where the highest molar masses elute first. Decreasing the fraction of ACN to 46 % leads to increasing enthalpic interactions so that the critical conditions are met and all molar masses coelute at the position of the solvent peak. Further decreasing of the ACN fraction to 40 % promotes the enthalpic interactions to the stationary phase even more because of the equally decreasing quality of the solvent mixture. In this case all polymers are retained and are eluted after the solvent peak and larger molar masses are retained stronger.

An often used application for LCCC is the investigation of block copolymers of two different monomers A and B. In order to determine the block size of monomer A and of B two SEC experiments are performed. At first critical conditions for monomer A are established so that it is getting virtually invisible in the experiment and only monomer B contributes to the retention. Vice versa, if then the critical conditions for monomer B are established the size of the block of monomer A can be analyzed.[97,110]

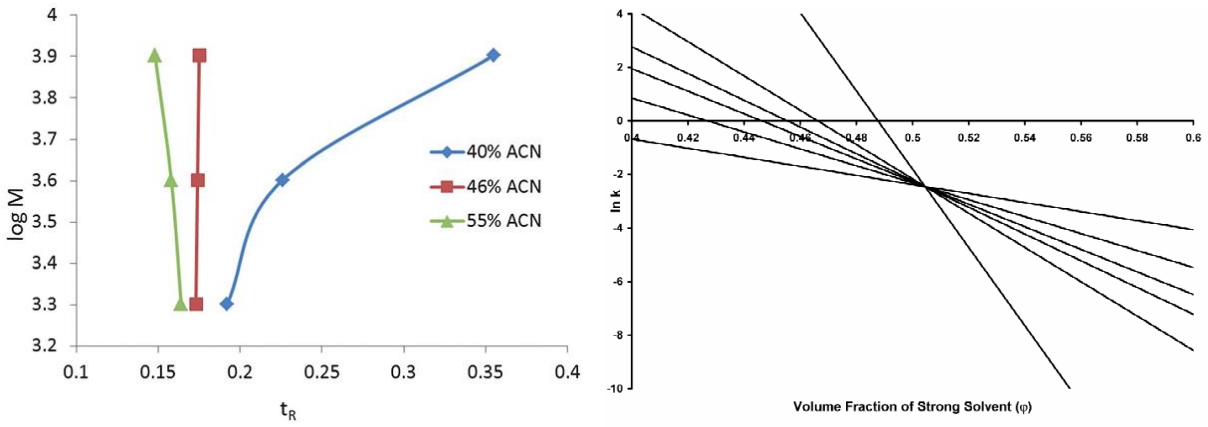

Figure 13: Left: Illustration of molar mass calibration curves of PEG standards for SEC (triangles), LCCC (squares) and HPLC (diamonds) in an UHPLC system. The legend indicates the respective solvent composition (ACN in THF). Note that the less polar solvent mixture leads to more enthalpic interactions. (Reproduced from Ref.[117] with permission of The Royal Society of Chemistry) Right: Logarithm of simulated retention factor (k) as a function of the mobile phase composition (φ) for a series of polystyrene polymers with increasing molar mass, where the steeper curves represent higher molar masses. (Reprinted from Ref[118], Copyright (2003), with permission from Elsevier)

Although the concept seems very powerful it is not very frequently used as the critical conditions are very sensitive and have to be established very precisely. In order to maintain the critical conditions the solvent composition has to be very stable with deviations of less than 1 %.[119] The reason for the high sensitivity can be found in the theory of adsorption or interaction chromatography. The dependency of the retention factor *k* on the mobile phase composition *φ* in a reverse phase system (unpolar stationary phase, relatively polar mobile phase) is given in Equation 15:

$$\ln k = \ln k_0 - S \cdot \varphi \qquad \text{Equation 15}$$

The logarithm of *k* follows a linear dependency on *φ*, where the intercept is given by *ln* k_0 and the slope by a value *S.* In this equation k_0 is the retention factor at 0 % strong solvent. Both parameters are specific for each substance and the respective separation conditions. In the right graph of Figure 13 simulated curves are presented for polystyrene polymers with different molar masses, where the steeper lines represent higher molar masses. At first we see that the retention factors are decreasing with *φ*, meaning that the polymers are less retained when the fraction of strong solvent increases. As the molar mass increases the lines are getting steeper and the system adapts an "on-off" type behavior: At low *φ* the retention factors are very high so that the polymers effectively "stick" on the columns. When a certain threshold composition of the solvent is passed the retention factors are getting very low and the polymers are virtually not retained at all. The consequence of that behavior is that small variations in *φ* result in significantly different retention factors, which makes it difficult to reproduce separations with high accuracy. One last message that can be derived from the *ln k* vs *φ* graph is the intercept of all lines in a certain point. The corresponding composition represents the critical conditions where all molar masses of the polymer behave identically. In praxis, however, the point is usually less well defined as in the shown simulation.[118]

Since the solvent composition (*i.e.*, its thermodynamic quality) influences the retention behavior substantially it can be used for separating mixtures according the chemical composition of their components. If the composition of the solvent is kept constant in the course of the separation it is called an isocratic experiment. In contrast to that it is also possible to change the composition of the solvent during the separation experiment and to perform a gradient elution. What is frequently used in HPLC for small organic molecules can also be applied for polymer separations. In a gradient experiment the analytes are injected in a solvent mixture of low elution strength (poor thermodynamic quality) and the solvent strength is increased continuously in order to elute the individual analytes successively.[115,118,120,121] The advantage over the isocratic experiment is that a whole range of *k* values can be accessed, which increases the separation power significantly. As a disadvantage the experimental

time is increased through the respective solvent gradient and after each experiment the column has to be conditioned again with the initial solvent composition before the next injection can be performed. Furthermore the application of certain detectors as the dRI detector is not possible, since they are too sensitive to changes in solvent composition. Frequently used detectors are UV/Vis absorption detectors and detectors that eliminate the solvent, *e.g.* the evaporative light scattering detector (ELSD) or the charged aerosol detector (CAD). The ELSD has become almost a standard detector for gradient elution experiments, as polymers usually yield good light scattering signals and the solvent composition is completely invisible in the chromatogram. It shall be kept in mind that the ELSD's response does not follow a simple concentration correlation and, hence, cannot be used for straight-forward quantitative evaluations.[122]

2.6 Light and Neutron Scattering

In light scattering, the sample is irradiated by a laser beam that hits the macromolecules. The electrons of the atoms in the molecules will start to move according to the alternating electric field of the laser. This motion makes them act as a Hertz dipole, thus letting them emit light at the same frequency as the incident light, but in a random direction. As a consequence, the light is being scattered in a random direction without changing its energy (Rayleigh scattering). The more electrons are present in a molecule (i.e., the larger a molecule is), the more light will be scattered and different information about the size of the molecules can be derived. In general, two different types of analysis can be distinguished: Static light scattering (SLS) and dynamic light scattering (DLS). Both types are reviewed shortly in this chapter.

2.6.1 Static Light Scattering

Static light scattering is about the absolute intensity of the scattered light coming from the sample. As already introduced, the more electrons are available in a molecule, the more light can be scattered. The precise relations are described in Equation 16, containing the optical constant *K'* (defined in Equation 17) and the Rayleigh ratio (reduced scattering intensity, defined in Equation 18).

$$\frac{Kc_B}{R_\theta} = \frac{1}{M_w P(\theta)} + 2A_2 c_B \qquad \text{Equation 16}$$

$$K = \frac{4\pi^2 {n_A}^2}{N_A \lambda_0^4} \left(\frac{dn}{dc_B}\right)^2$$ Equation 17

$$R_\theta = \frac{I}{I_0}\frac{r^2}{V}$$ Equation 18

K	… optical constant	n_a	… refractive index (solvent)
c_B	… polymer concentration	N_A	… Avogadro's number
R_Θ	… Rayleigh Ratio	λ_0	… vacuum wavelength
$P(\Theta)$	… Form factor	(dn/dc_B)	… refractive index increment (polymer)
Θ	… scattering angle	I, I_0	… intensity of scattered and incident light
M_w	… weight averaged molar mass	r	… distance of detector to scattering volume
A_2	… second virial coefficient	V	… volume observed by detector

The main message of Equation 16 is that SLS allows directly calculating the weight averaged molar mass M_w and the second virial coefficient A_2, if all other parameters are known. A_2 is a parameter that describes the interactions between the polymer and the solvent. In the case of a good solvent A_2 is positive, for a poor solvent A_2 is negative and in an Θ-solvent A_2 is zero.

Another important parameter is the form factor $P(\Theta)$. It describes the angular dependency of the scattered light intensity as the ratio of the light intensity at any angle Θ relative to the intensity at the angle Θ = 0. Speaking of angle dependency seams contra intuitive as we have seen that the scattered light from a molecule is emitted in a random direction and consequently the scattering intensity should be equal at all angles. If, however, a molecule is large enough for being hit by two (or more) incident photons, two (or more) scattered photons will be emitted. Since they are in close proximity they will start to interfere with each other. That case usually appears if the size of the particle is larger than λ/20. The interference of photons coming from two scattering centers in the same molecule is dependent on the angle from which it is observed, because of the angle dependent differences in the pathway that the photons have travel. This behavior leads to full scattering intensity in the forward direction (0 °) and decreasing scattering intensity with increasing angle because of destructive interference. The form factor describes the angular dependency as a function of the averaged radius of gyration R_g and can be simplified according to the Guinier approximation as shown in Equation 19[123]:

$$P(\theta) = \frac{I(\theta)}{I(\theta = 0)} \approx 1 - \frac{16\pi^2 n_0^2}{3\lambda_0^2} sin^2\left(\frac{\theta}{2}\right) R_g \qquad \text{Equation 19}$$

A common way for performing the experiment is to irradiate samples of different concentrations with a laser beam and to collect the intensity of the scattered light at multiple angles simultaneously (Figure 14)[124]. The by Zimm proposed procedure is a frequently used evaluation protocol where both, the scattering angle and the concentration, are extrapolated to zero in the respective plot, which is derived from Equation 16. In that way, two extrapolated lines are obtained: One at zero concentration and at all angles and one at angle zero for all concentrations. They both have the same intercept, which gives the reciprocal weight averaged molar mass M_w. The slope of the zero concentration extrapolation corresponds to the second virial coefficient A_2.[125] Finally, the angular dependency can be evaluated according to Equation 19 for calculating the radius of gyration.

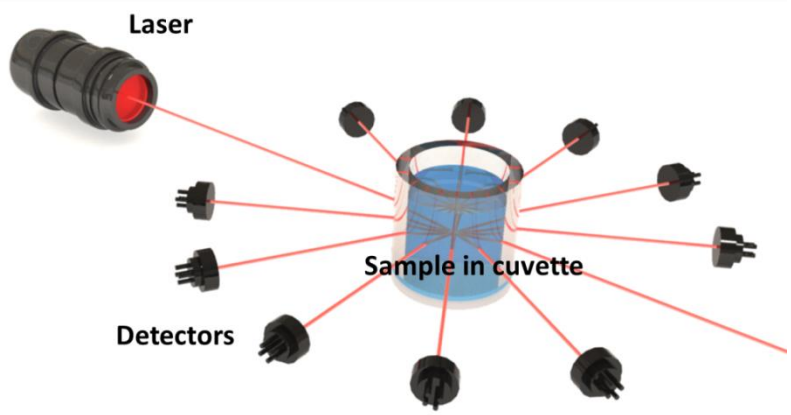

Figure 14: Instrumental setup for measuring SLS at multiple angles.

SLS can be performed both, in a cuvette and in a flow cell and is, thus, can be integrated in a chromatographic system relatively easy. Coupled to SEC it does not only allow to get absolute information about the molar mass of the investigated polymers, but also to get information about their shape in solution by measuring the radius of gyration simultaneously and plotting *lg* R_g over *lg M*. How the radius of gyration scales with molar mass is characteristic for different morphologies, *e.g.* globular, random-coil-like or elongated structures.[89,96,126]

The amount of information that can be derived from SLS is impressive but the experiment itself is not trivial since a variety of parameters have to be determined (see Equation 16 to Equation 18) accurately, which makes it challenging to perform SLS temperature dependently. Furthermore, the cost of the

required equipment is rather high and the flow cells are very sensitive to temperature changes. That is why online SLS was not performed in this work.

2.6.2 Dynamic Light Scattering

Dynamic light scattering, or quasi elastic light scattering (QUELS) evaluates the time dependent fluctuations in the light scattering intensity on a short time scale. DLS or QUELS exploit the random diffusion of the dissolved molecules (Brownian motion). Their motion leads to a broadening of the frequency spectrum of the incident light (that is ideally as narrow as possible), due to the Doppler effect. Quickly moving scattering centers lead to a larger shift in frequency than slower moving ones. The magnitude of the frequency shifts is relatively small in any case for the diffusion of molecules, and especially macromolecules in common solvents: it is to be expected in the range of 10^2 to 10^6 Hz of an incident frequency of approx. $5x10^{14}$ Hz (visible light)[123] and, as a consequence, cannot be measured directly. It is, however, possible to measure an indirect effect: the fluctuation of the light scattering intensity with time. The frequency distribution function of the light is the FOURIER transformation of the time correlation function of the light intensity, as shown in Figure 15. The figure shows that minor changes in the frequency are represented by long times in the autocorrelation function.

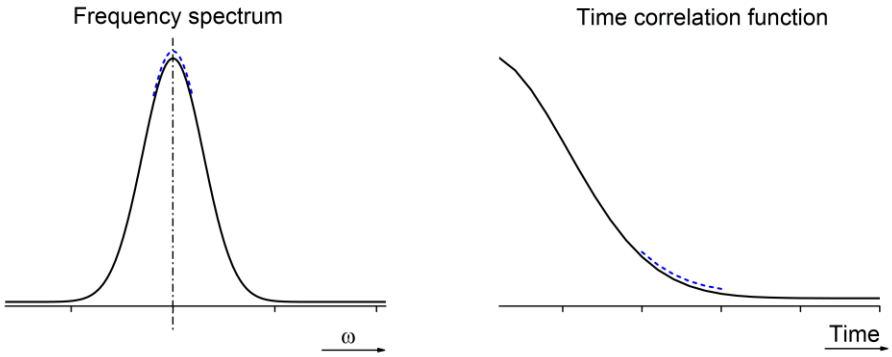

Figure 15: Spectrum of frequencies (left) and according FOURIER transformed time correlation function. The dashed areas represent corresponding regions. Adapted from Ref.[123]

The autocorrelation function in turn can be measured experimentally by a special hardware correlator. Its purpose is to measure the light scattering intensity at small time intervals and processes the recorded starting value *I(t=0)* with the intensity after time intervals *I(τ)*, with *τ* being the respective interval (*e.g.*, 100 ns). If the two values are close to each other, the correlation value is high and the more they differ from each other, the lower the correlation value will be. The time-averaged intensity autocorrelation function (ICF) $g_T^{(2)}(q, \tau)$ is calculated according to Equation 20:

$$g_T{}^{(2)}(q,\tau) = \frac{\langle I(q,0) \cdot I(q,\tau)\rangle_T}{\langle I(q,0)\rangle_T{}^2} \qquad \text{Equation 20}$$

, where τ is the time interval, q the scattering vector (= $4\pi n/\lambda \sin(\vartheta/2)$) and $\langle\ldots\rangle_T$ denotes the time average.[127,128] The acquired correlation function is then fitted by different models that describe the correlation theoretically and link it to the diffusion coefficient (Equation 21 and Equation 22). Making use of the Stokes-Einstein equation (Equation 23) allows in the last step to convert the diffusion coefficient D_t into the hydrodynamic radius R_h, if the solvent viscosity η_A and the temperature T are known:[123]

$$g_T{}^{(2)}(q,\tau) = 1 + e^{-\Gamma\tau} \qquad \text{Equation 21}$$

$$\Gamma = D_t q^2 \qquad \text{Equation 22}$$

$$\mathrm{D}_t = \frac{k_B T}{6\pi\eta_A R_h} \qquad \text{Equation 23}$$

D_t … translational diffusion coefficient
k_B … Boltzmann's constant
T … Temperature
η_A … viscosity of solvent
R_h … hydrodynamic radius

Since Equation 21 is valid for a strictly monodisperse functions, it needs to be substituted by the sum of multiple exponential decay functions that are weighed by their respective normalized intensities. A further expansion can be included for taking into account the width of the size distribution. If multiple size distributions are contributing to the scattering simultaneously, more complex calculations have to be done, which are usually carried out by the instrument's software. The accuracy of the results, however, decreases slightly, as it can be seen in Figure 16. In a simple experiment two narrowly distributed PS standards were measured firstly as individual samples. Then a mixture of the same standards was measured and processed according to the more complex evaluation procedure that takes into account multiple size distributions simultaneously. The results of both experiments should be identical but in practice slightly differing values are obtained. Furthermore the standard deviation of the measurements increases. One conclusion of this finding is that DLS works very well when being coupled to a separation technique, such as SEC or AF4. Then the analytes are already fractionated according to their size and the sample portions that reach the detector can be considered monodisperse and the results become most accurate.[129]

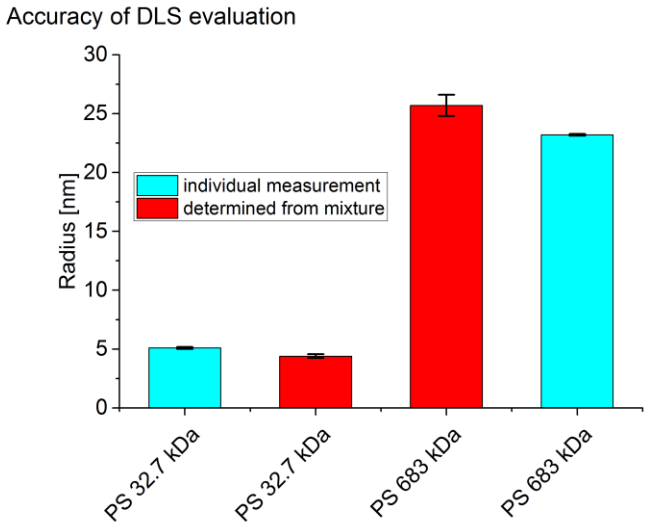

Figure 16: Two PS standards measured in toluene as individual samples (blue) and in a mixture (red). Each column represents the average of five individual measurements of each 15 single acquisitions. The experiments were carried out with the DynaPro NanoStar (Wyatt Technologies, US), see chapter 3.5 for details.

In contrast to SLS the angular dependency of the scattered light intensity is less important in DLS. Performing the experiment at a different angle usually does not impact the calculated sizes. However, the calculated abundancy of a particular species in a mixture is dependent on the angle dependent scattering profiles and, thus, different size distributions can be obtained at different angles.[130,131] Special care has to be taken when the samples are prepared. At first a concentration has to be used that guarantees a sufficiently strong light scattering signal in the respective solvent (consider the specific *dn/dc*). Especially in aromatic solvents concentrations higher than 10 mg/mL can be necessary if the analyzed polymers are not of high molar masses. But increasing the concentration can cause problems, too. The DLS analysis protocols rely on single scattering events, *i.e.* that every photon that reaches the detector was scattered only once in the observed scattering volume. If the polymer concentration is increased too far multiple scattering can play a role. Various techniques were developed for analyzing strongly scattering and opaque systems but they require more sophisticated equipment and analysis procedures.[132–134]

A second problem associated with higher concentration is the state of dissolution of the polymers. For the correct interpretation of the acquired data it is necessary to be assured to measure individually dissolved molecules rather than their aggregates. Although the common DLS algorithms are capable of calculating size distributions with multiple peaks out of the autocorrelation functions the “separation efficiency” is rather low and the accuracy of the results is decreasing with increasing complexity of the sample distribution.[135,136] For highest precision of the measurement it is consequently advisable to have

the sample as monodisperse as possible or, in other words, to provide a state of very good dissolution. In contrast to small molecules that dissolve mostly instantaneously polymers take more time to dissolve. Their dissolution is driven by diffusion of solvent molecules into the coils and eventually disentanglement of the chains.[137] The time for the whole process should not be underestimated and in case of doubt more time or stirring should be applied, whereas ultrasonication can lead to unwanted polymer degradation and, thus, should be avoided.[138,139]

Another issue coming at high polymer concentrations is that the viscosity of the solution can significantly differ from the solvent's viscosity. In that case it is necessary to separately determine the solution's viscosity (*e.g.*, with a capillary viscometer) and to use it for the calculations according to Equation 23.

This chapter demonstrated that DLS offers an easy and convenient way for determining the size distribution of a polymer solution. If the cuvette can be temperature controlled it is furthermore a promising methodology for following temperature dependent bonding reactions. The only parameters that have to be known are, as explained above, the precise temperature and the viscosity of the solvent at this respective temperature. But the fact that the hydrodynamic radius cannot be directly related with a molar mass or degree of polymerization of the polymers is critical to consider. On the contrary, the R_h is dependent on the thermodynamic quality of the solvent (and, thus, temperature), topology (*e.g.*, branching) of the polymer and its flexibility. Therefore measuring reference substances is required for the correct interpretation of the data.

2.6.3 Neutron Scattering

Obtaining structural information from multi angle scattering experiments relies on interference phenomena of the scattered waves, as described above. This fact limits the applicability of light scattering for relatively large structures. A rough estimation shows that even with a blue laser of 400 nm wavelength dimensions of approx. $\lambda/20$ = 20 nm can be assessed. If smaller structures are to be analyzed the wavelength of the incident radiation has to be decreased. Local structures inside the polymers are of the size of a few nanometers, so that significantly lower wavelengths than accessible by laser light are required. X-ray radiation would offer suitable wavelengths, but comes with two major disadvantages: At first the energy of an X-ray photon with λ=0.15 nm is approx. 8.2 keV, which is orders of magnitudes *higher* than the energy of a carbon-carbon bond (≈4 eV), so that serious degradations can occur in the material. And secondly, the scattering cross-section of X-rays as electromagnetic radiation is

proportional to the number of electrons surrounding an atomic nucleus. In other words, good scattering contrast is achieved by heavy elements, which are usually not present in polymers.[140]

At this point the advantages of particle radiation, especially neutron radiation, come into focus. Neutron radiation can be produced in a wavelength range of approx. 0.01 – 3 nm. In the case of radiation of particles with a finite mass the kinetic energy is determining the wavelength and for the relevant wavelength area relatively low energies are required. For example, the energy of a 0.15 nm neutron would be approx. 36.4 meV, and, thus, orders of magnitudes *lower* than the energy of a covalent bond. A second advantage of neutron radiation over X-ray radiation comes from the nature of the scattering mechanism. Neutrons interact directly with the nuclei and the scattering cross-section does not follow the nucleus size in a regular pattern. Especially the big difference in the neutron scattering cross-section with hydrogen and deuterium makes neutron scattering interesting for polymer analysis, as a good contrast can be achieved by dissolving the polymers in deuterated solvents.[140] The big disadvantage of neutron scattering, however, lies in the generation of the neutron radiation, the collimation of the neutron beams and finally the detection, as the interaction of neutron beams with matter is generally very weak. This is why neutron scattering, especially small angle neutron scattering (SANS) can only be performed at dedicated research facilities.

One application for SANS is the characterization of the flexibility of a polymer through its persistence length l_p.[141] The persistence length represents a characteristic length over which the spatial orientation of polymer segments cease to be in correlation. In other words, at scales smaller than l_p the polymer can be described as a flexible rod, whereas at scales larger than l_p only statistical statements can be done about the position of the polymer segments (*e.g.*, via random walk models). A smaller l_p indicates a more flexible, a larger l_p a stiffer polymer.

For determining l_p the measured scattering intensity *I(q)* is plotted as a function of the scattering vector q (or, more precisely the momentum transfer, which is the absolute value of the scattering vector). Through Equation 24 and Equation 25 q is related to the scattering angle Θ and consequently the size d of the scattering elements (Equation 26), taking into account the wavelength λ:

$$q = 4\pi \frac{\sin(\theta)}{\lambda} \qquad \text{Equation 24}$$

$$n\lambda = 2d \cdot sin(\theta) \qquad \text{Equation 25}$$

$$d = \frac{2\pi}{q} \qquad \text{Equation 26}$$

According to these relations large structures are represented at low *q* and small structures at high *q*. In other words, the scattering curves show the entire polymer molecule as a coil in the low *q* regime and "zoom in" the coil until individual rod like chains parts of the polymer chains at high *q* values. The angle dependent scattering behavior, described by the form factor *P(q)*, is different for a coil or a rod. It starts with a power law behavior of -2 (ideal Gaussian coil) and converts to a power law behavior of -1 (rod like) in a gradual transition around a characteristic *q**, which can be converted to l_p. Two different plot types for effectively finding *q** are shown in Figure 17. In this work the Casassa-Holtzer plot was chosen for the SANS evaluation.

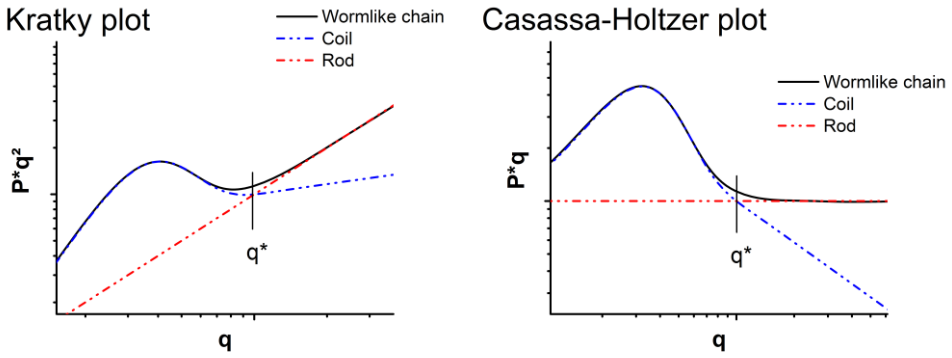

Figure 17: The double-log Kratky and Casassa-Holtzer plot for determining l_p. In these graphs, l_p would correspond to the indicated coil-to-rod-transition at *q**. Adapted from Ref.[142]

Furthermore it is possible to apply physical models for describing the scattering curves theoretically, whereby certain parameters, such as the persistence length is obtained in a fitting procedure. Several procedures are described in literature that can be used for that purpose.[143,144] In this work two relatively simple approaches were used that were discussed by Beaucage et al.[143] and that appear suitable for determining the persistence length of random coil polymers in good solvents without overcomplicating the fitting procedures with too many parameters. In both, the "Sharp and Bloomfield Global Function" and the "Unified Function", only three parameters need to be fitted, each. Together with the graphical evaluation according to the Casassa-Holtzer procedure a robust set of data should be obtained that allows discussing the difference in flexibility of the polymers.

The Casassa-Holtzer evaluation requires plotting $I_{norm}(q)*q$ over *q*, where the normalized scattering intensity $I_{norm}(q) = P(q)*M_w$, with *P(q)* being the true form factor at zero concentration. Also the evaluation by fitting the entire scattering functions requires deriving the true form factor *P(q)*. The procedure for deriving *P(q)* was proposed by Prof. Walther Burchard (University of Freiburg) and is based on the general form of the scattering function of macromolecules.[145]

$$\frac{Kc}{R_\theta} = \frac{1}{M_w P(q)} + 2A_2 c + 3A_3 c^2 + \cdots \qquad \text{Equation 27}$$

, where *K* is the optical constant and R_Θ the Rayleigh ratio (see chapter 2.6.1), M_w is the weight averaged molar mass, *P(q)* the form factor at the scattering vector *q* and the concentration *c=0* and A_2 and A_3 are the respective virial coefficients.

Firstly all experimentally acquired scattering curves are extrapolated to *q=0 Å*$^{-1}$ so that an apparent molar mass $M_{app}(c)$ can be calculated for each concentration according to Equation 28:

$$\frac{Kc}{R_{\theta=0}} = \frac{1}{M_w} + 2A_2 c + 3A_3 c^2 + \cdots = \frac{1}{M_{app}(c)} \qquad \text{Equation 28}$$

The apparent molar mass is the weight averaged molar mass, modified by the virial coefficients. Extrapolated to zero concentration it would equal M_w. For the next step Equation 27 is rearranged to give Equation 29

$$\frac{1}{M_w P(q)} + 2A_2 c + 3A_3 c^2 + \cdots = \frac{1}{M_{app}(c) \cdot P_{app}(q,c)} \qquad \text{Equation 29}$$

, where the apparent form factor $P_{app}(q,c)$ describes the angular dependency of the scattered light at finite concentration. Both, $1/M_{app(c)}$ and $1/P_{app}(q,c)$ can be measured directly without any assumptions. At *q=0 Å*$^{-1}$ we again obtain the apparent molar mass $M_{app}(c)$.

Subtracting and adding $1/M_w$ in Equation 29 and applying Equation 28 gives:

$$\frac{1}{M_w P(q)} - \frac{1}{M_w} + \frac{1}{M_w} + 2A_2 c + 3A_3 c^2 + \cdots = \frac{1}{M_{app}(c) \cdot P_{app}(q,c)} \qquad \text{Equation 30}$$

$$\frac{1}{M_w P(q)} - \frac{1}{M_w} = \frac{1}{M_{app}(c) \cdot P_{app}(q,c)} - \frac{1}{M_{app}(c)} \qquad \text{Equation 31}$$

Multiplying with M_w leads to:

$$\frac{1}{P(q)} - 1 = \frac{M_w}{M_{app}(c)} \left(\frac{1}{P_{app}(q,c)} - 1 \right) \qquad \text{Equation 32}$$

$$P(q) = \left[1 + \frac{M_w}{M_{app}(c)} \left(\frac{1}{P_{app}(q,c)} - 1 \right) \right]^{-1} \qquad \text{Equation 33}$$

With Equation 33 it is possible to calculate the form factor *P(q)* out of the *q* dependency of a scattering curve that was acquired at a finite concentration *c*. The equation requires knowledge of the ratio M_w/M_{app}. If *K* was determined M_{app} can be calculated directly according to Equation 28 and M_w can

be determined separately (*e.g.*, by SLS). If the optical constant could not be determined it is necessary to measure a series of different polymer concentrations. Each scattering curve is then extrapolated to *Θ=0* and the results can be extrapolated to *c=0*. As shown in Equation 34 and Equation 35 these scattering intensities can be used for deriving M_w/M_{app}, while *K* is cancelled out:

$$\frac{\left(\frac{K \cdot c}{I(\theta = 0)}\right)_{c=0}}{\left(\frac{K \cdot c}{I(\theta = 0)}\right)_{c}} = \frac{\frac{1}{M_w}}{\frac{1}{M_{app}(c)}} \qquad \text{Equation 34}$$

$$\frac{M_w}{M_{app}(c)} = \frac{\left(\frac{c}{I(\theta = 0)}\right)_{c}}{\left(\frac{c}{I(\theta = 0)}\right)_{c=0}} \qquad \text{Equation 35}$$

The advantage of the described procedure is that the true form factors can be derived from either a series of dilution if the optical constant could not be determined, of from a single measurement at finite concentration if *K* is known.

When *P(q)* is derived the Casassa-Holtzer plot can be constructed by multiplying *P(q)* with M_w and *q*, dividing it by π and plotting the result over *q* in a double log plot.

2.7 Temperature effects on polymers

At this point it is necessary to discuss the effect of temperature on the size of a polymer. The size of a polymer can be described in different terms, as we have seen in chapter 2.4.1. For SEC and DLS the most important radius is the hydrodynamic radius R_h. The dimensions of a polymer coil in a solvent are strongly dependent on the quality of the respective solvent. A thermodynamically good solvent will increase the concentration of solvent molecules inside the polymer coil, *i.e.* the polymer swells in the solvent. In the opposite case the coil will collapse, when polymer-solvent interactions are being minimized by pushing out the solvent molecules.[137] In the Θ-state the interactions between polymer segments themselves and polymer segments and the solvent molecules are identical and the polymer coil adapts unpertubed dimensions. The thermodynamic quality of the dissolution can be characterized in terms of the excluded volume *v*. The excluded volume *v* expresses the effective volume of each monomer unit as the volume that cannot be interpenetrated by any other monomer unit. In the unpertubed Θ –state *v = 0* and the each monomer occupies its own volume. In the case of a poor solvent the monomer units start to attract each other more strongly and the effective monomer volume decreases, hence *v < 0*. If the solvent is thermodynamically strong *v > 0* and the coil swells, as each monomer's effective volume increases.

The thermodynamic quality of a solvent is of course strongly related to its chemical structure and the structure of the monomer units, respectively. If both are more similar to each other the quality of the solvent usually increases, which has become known as the "like dissolves like" principle.[137] Besides the chemical nature of polymer and solvent the temperature is an important parameter as well. The temperature dependency of the excluded volume can be derived from simple considerations and can be approximated as shown in Equation 36

$$\nu \approx \frac{T-\theta}{T} \cdot b^3 \qquad \text{Equation 36}$$

, where T is the temperature, Θ the Θ-temperature and b^3 the volume of a monomer unit.[146] If the temperature is lower than the Θ-temperature the excluded volume becomes negative and if the temperature is higher than the Θ-temperature it becomes positive. How these effects scale on polymer dimensions can be derived from further calculations. Monte-Carlo simulations allow estimating the radius of gyration of polymers that consist of N monomers connected by Lennard-Jones potential. In Figure 18 the size of polymers with degree of polymerization from 20 to 320 are shown in a range of different temperatures:

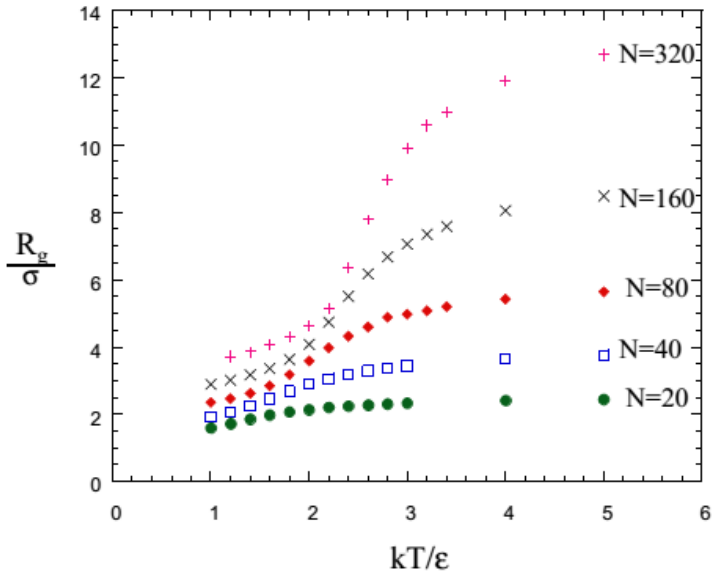

Figure 18: Polymer size as a function of temperature, calculated from Lennard-Jones chains of *N* monomers. The size is given as the ratio of radius of gyration R_g over the Lennard-Jones length σ. The temperature is given as the product of Boltzmann's constant k times the temperature T divided by the Lennard-Jones energy ε. Reproduced with permission from Ref. [146], Copyright 2004, Wiley-VCH.

The graph shows that, as expected, the polymer size increases with temperature, as the solvent's thermodynamic quality increases. When performing SEC or DLS temperature dependently it is important to keep these findings in mind. In the case of SEC the differently swelling polymers will result in different elution times, as the separation is mainly according to their hydrodynamic size. The effect can be taken into account by collecting chromatograms of polymers of known size at the respective temperatures. Analogously it is necessary to determine the hydrodynamic radius of reference polymers in DLS experiments when temperature dependent measurements are performed.

2.8 Entropy Effects

This chapter introduces an often overseen fact when reactions are evaluated thermodynamically: The effect of entropy. But let us start from the beginning. The energy gain (or loss) of a particular reaction is given by the Gibbs free energy:

$$\Delta G_0 = \Delta H_0 - T \cdot \Delta S_0 \qquad \text{Equation 37}$$

Which is determined by the reaction enthalpy (*ΔH*), the temperature (*T*) and the reaction entropy (*ΔS*). A negative ΔG signifies a loss in energy, making the reaction favorable and a positive *ΔG* means a gain in free energy which renders the reaction thermodynamically unfavorable.

The usual method for tuning the thermodynamics of a reaction is to modify the chemical structure of the reaction components, thus influencing *ΔH*. Although this concept is not inherently wrong it does not take into account the *ΔS* term of Equation 37. The effect of entropy on the reactions thermodynamics might be less intuitively tangible but theoretical considerations clearly show its potential. Calculating reaction enthalpies and entropies for debonding reactions of representative model compounds allows to estimate the impact of changing functional groups (*ΔH*) vs the effect of changing size, mass and flexibility (*ΔS*).[69] Guimard et al. found distinct entropy effects and pointed out their particular importance when dealing with temperature dependent reactions, since the entropy is multiplied with temperature in the Gibbs equation and, thus, gets more pronounced at higher temperatures.

The observations lead to an important question: In contrast to make functional groups more electron withdrawing or electron rich for impacting reaction enthalpies, what pathways are accessible for influencing the reaction entropies? An answer can be found by breaking down the reaction entropy in its contributions, namely translational, vibrational and rotational entropy. Considerations of different model compounds demonstrated interesting trends: The translational entropy is mainly affected by the mass and the rotational entropy depends on both, mass and geometry of the molecules. The vibrational

entropy, even though resembling qualitatively the flexibility of a given structure, does not seem to follow a distinct trend but appears dependent on the interplay of various factors.[147]

In conclusion, the variable factors for tuning the entropic contributions are the polymer mass, chain length, and flexibility. When a polymer is accordingly designed to gain more entropy during debonding, the debonding temperature can be decreased significantly.

3 Experimental Details

3.1 The investigated polymers

In the following list all employed substances are summarized with their main characteristics. Further details about the synthesis can be found in the cited publications. The syntheses of all compounds were done at the Karlsruhe Institute of Technology.

Structure 1: **Furan monomer**

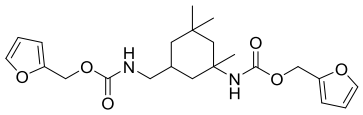

M = 418 g/mol

Structure 2: **Maleimide monomer**

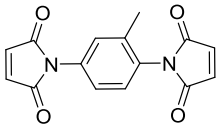

M = 282 g/mol

Structure 3: **DA Furan-Maleimide**

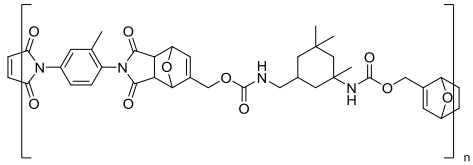

M_n = 7000 g/mol, M_w = 19000 g/mol, $Đ_m$ = 2.84

(from SEC-SLS in DMAc at 25 °C)

Structure 4: **$Cp_2P(^{i}BoA\text{-}^{n}BuA)$**[69]

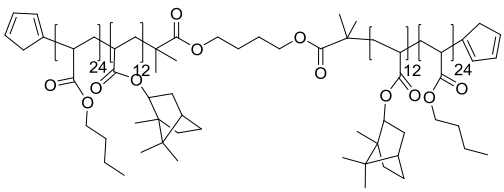

M_n = 13000 g/mol, M_w = 16700 g/mol, $Đ_m$ = 1.29

(from SEC-SLS in THF at 25 °C)

Structure 5: **P^{i}BoA 4**[69]

Structure 6: **P^{i}BoA 6**[69]

Structure 7: **P^{i}BoA 7**[69]

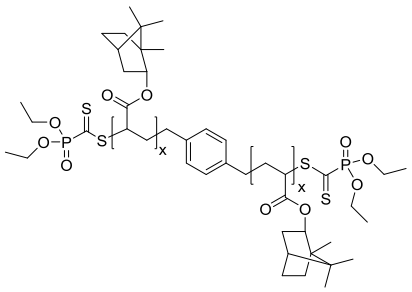

	M_n (g/mol)	M_w (g/mol)	$Đ_m$
PiBoA 4	18900	27000	1.45
PiBoA 6	37500	59000	1.57
PiBoA 7	59000	92700	1.57

(from SEC-SLS in THF at 25 °C)

Structure 8: **DA P^{i}BoA 4-Cp$_2$P(P^{i}BoA-^{n}BuA)**[69]

Structure 9: **DA P^{i}BoA 6-Cp$_2$P(P^{i}BoA-^{n}BuA)**[69]

Structure 10: **DA P^{i}BoA 7-Cp$_2$P(P^{i}BoA-^{n}BuA)**[69]

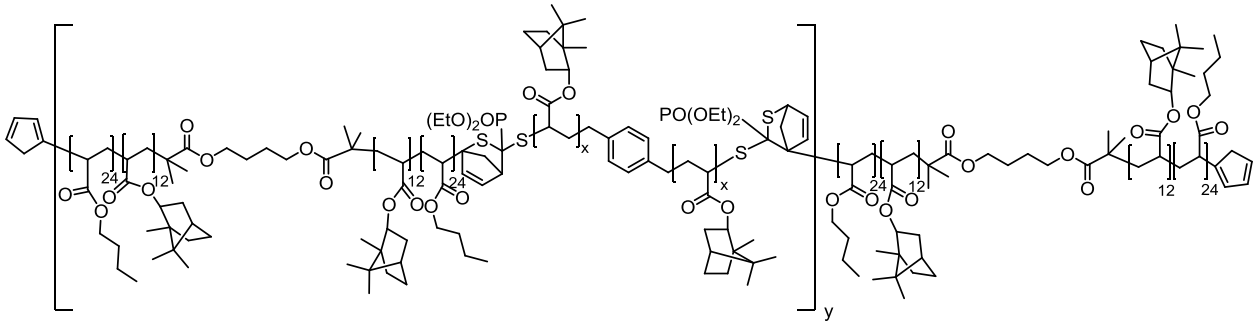

	M_n (g/mol)	M_w (g/mol)	$Đ_m$
DA-P^{i}BoA 4-Cp$_2$P(P^{i}BoA-^{n}BuA)	34100	96800	2.84
DA-P^{i}BoA 6-Cp$_2$P(P^{i}BoA-^{n}BuA)	88800	24300	2.74
DA-P^{i}BoA 7-Cp$_2$P(P^{i}BoA-^{n}BuA)	66000	177500	2.69

(from SEC-SLS in THF at 25 °C)

Structure 11: **Cp_2 P^{i}BoA**[71]

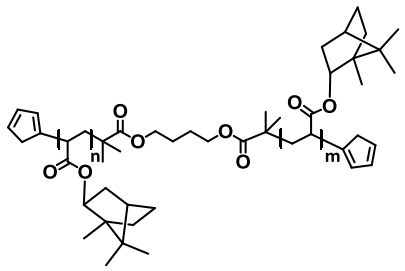

M_n = 10200 g/mol, M_w = 11400 g/mol, $Đ_m$ = 1.12 (n + m = approx. 50)

(from SEC in THF at 25 °C, using standard calibration with KMH coefficients)

Note: The polymer was also used with Br instead of Cp endgroups but otherwise identical properties.[71]

Structure 12: **Cp_2 PMA**[71]

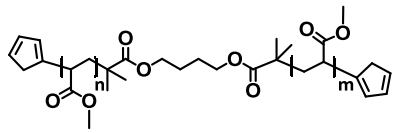

M_n = 4800 g/mol, M_w = 5200 g/mol, $Đ_m$ = 1.09 (n + m = approx. 50)

(from SEC in THF at 25 °C, using standard calibration with KMH coefficients)

Note: The polymer was also used with Br instead of Cp endgroups but otherwise identical properties.[71]

Structure 13: **Cp_2 P^{t}BuA**[71]

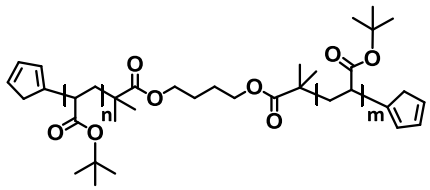

M_n = 6700 g/mol, M_w = 7200 g/mol, $Đ_m$ = 1.08 (n + m = approx. 50)

(from SEC in THF at 25 °C, using standard calibration with KMH coefficients)

Note: The polymer was also used with Br instead of Cp endgroups but otherwise identical properties.[71]

Structure 14: **Cp_2P^iBuA**[71]

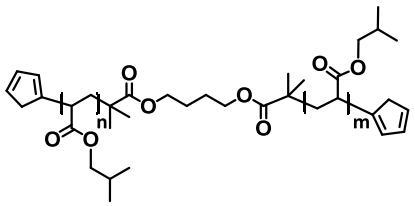

M_n = 7000 g/mol, M_w = 7500 g/mol, $Đ_m$ = 1.07 (*n* + *m* = approx. 50)

(from SEC in THF at 25 °C, using standard calibration with KMH coefficients)

Note: The polymer was also used with Br instead of Cp endgroups but otherwise identical properties. [71]

Structure 15: **Cp_2P^nBuA**[71]

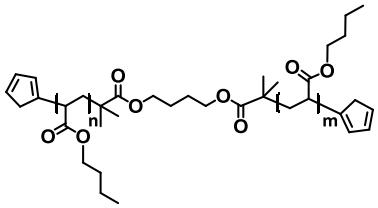

M_n = 6700 g/mol, M_w = 7200 g/mol, $Đ_m$ = 1.08 (*n* + *m* = approx. 50)

(from SEC in THF at 25 °C, using standard calibration with KMH coefficients)

Note: The polymer was also used with Br instead of Cp endgroups but otherwise identical properties. [71]

Structure 16: **Cp_2PS**[148]

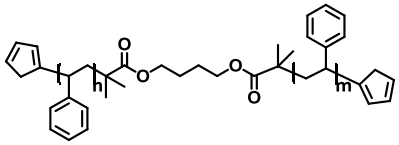

M_n = 5500 g/mol, M_w = 5900 g/mol, $Đ_m$ = 1.08 (*n* + *m* = approx. 50)

(from SEC in THF at 25 °C, using standard calibration with KMH coefficients)

Structure 17: **DA P^{i}BoA**[71]

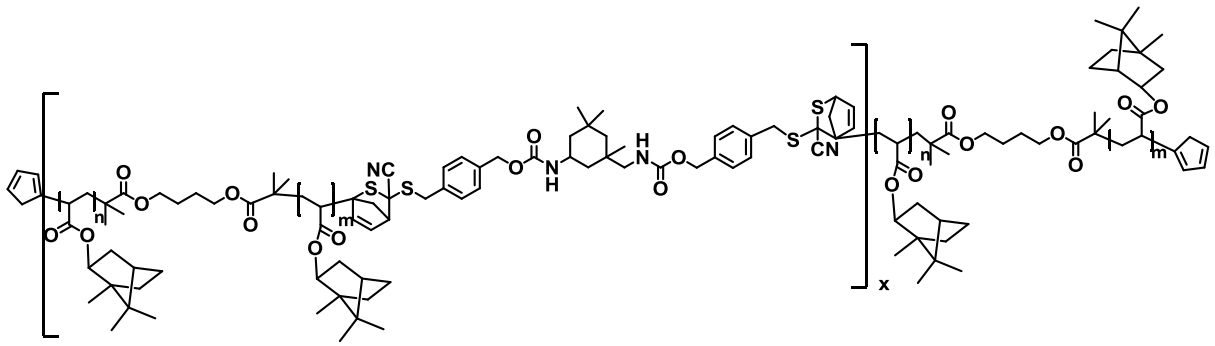

M_n = 34200 g/mol, M_w = 63600 g/mol, $Đ_m$ = 1.86

(*n* + *m* = approx. 50, x = approx. 3, molar masses from SEC in THF at 25 °C, using standard calibration with KMH coefficients)

Structure 18: **DA PMA**[71]

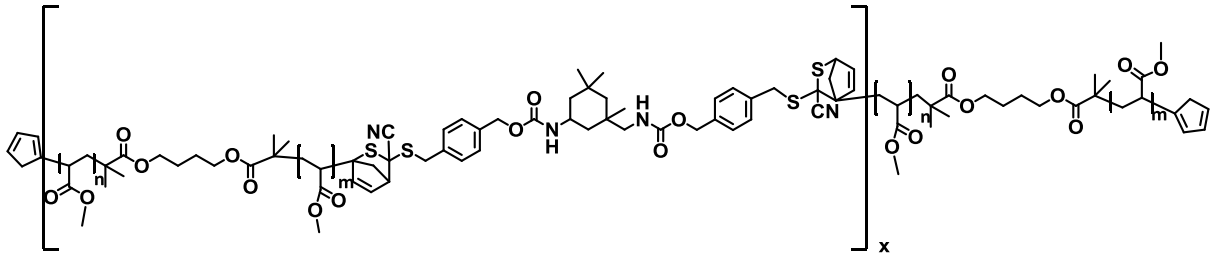

M_n = 17300 g/mol, M_w = 32200 g/mol, $Đ_m$ = 1.86

(*n* + *m* = approx. 50, x = approx. 3, molar masses from SEC in THF at 25 °C, using standard calibration with KMH coefficients)

Structure 19: **DA P^{t}BuA**[71]

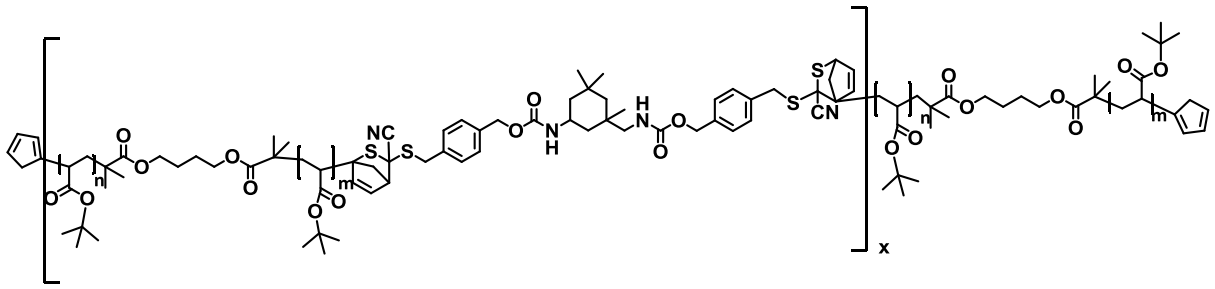

M_n = 22700 g/mol, M_w = 37900 g/mol, $Đ_m$ = 1.67

(*n* + *m* = approx. 50, x = approx. 3, molar masses from SEC in THF at 25 °C, using standard calibration with KMH coefficients)

Structure 20: **DA P^{i}BuA**[71]

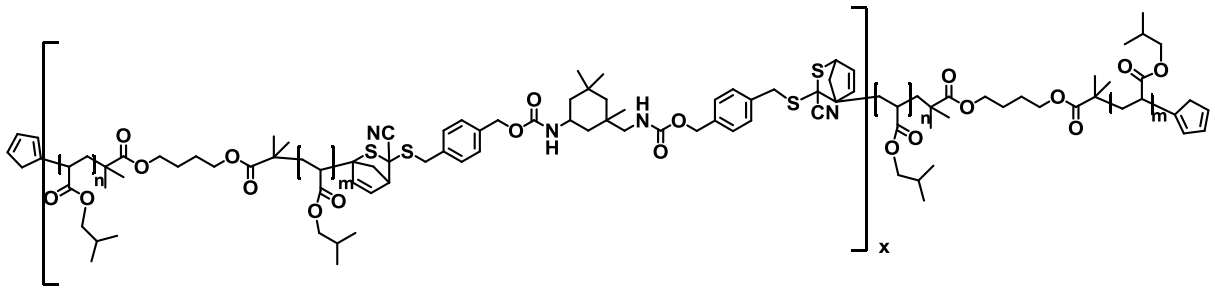

M_n = 22400 g/mol, M_w = 37400 g/mol, $Đ_m$ = 1.67

(*n* + *m* = approx. 50, x = approx. 3, molar masses from SEC in THF at 25 °C, using standard calibration with KMH coefficients)

Structure 21: **DA P^{n}BuA**[71]

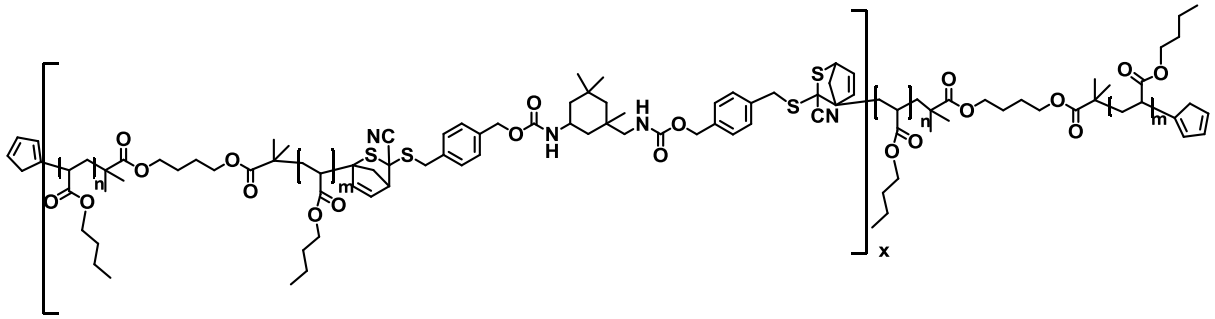

M_n = 20600 g/mol, M_w = 35600 g/mol, $Đ_m$ = 1.73

(*n* + *m* = approx. 50, x = approx. 3, molar masses from SEC in THF at 25 °C, using standard calibration with KMH coefficients)

Structure 22: **DA PS**[148]

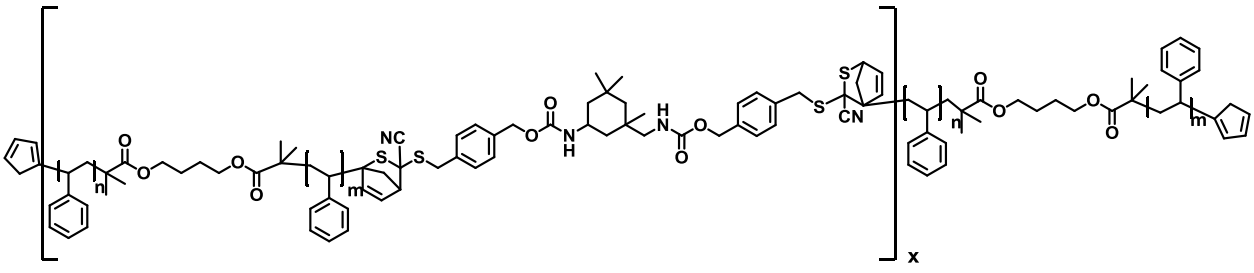

M_n = 21000 g/mol, M_w = 39900 g/mol, $Đ_m$ = 1.90

(*n* + *m* = approx. 50, x = approx. 3, molar masses from SEC in THF at 25 °C, using standard calibration with KMH coefficients)

Structure 23: **HDA Dilinker**[71,72]

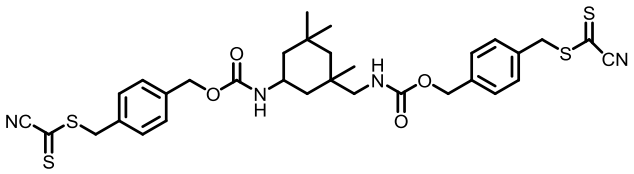

M = 668 g/mol

Structure 24: **HDA Tetralinker**[36]

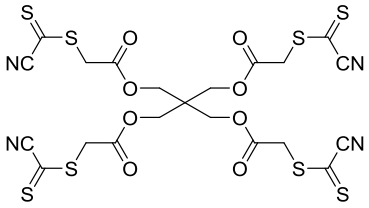

M = 709 g/mol

Structure 25: **DA P^{t}BuA network**

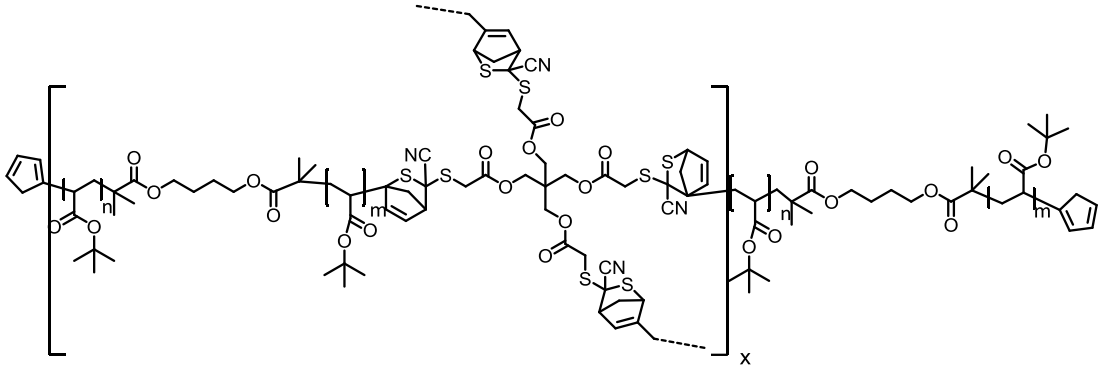

No detailed characterization available yet.

(*n* + *m* = approx. 50)

Structure 26: **PTEGA**[149]

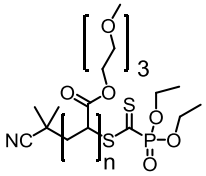

M_n = 6600 g/mol, M_w = 7400 g/mol, $Đ_m$ = 1.12

(from SEC in THF at 25 °C, using standard calibration relative to PMMA)

Structure 27: **P(S-*co*-I)**[149]

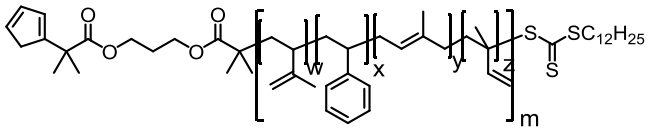

M_n = 9200 g/mol, M_w = 11200 g/mol, $Đ_m$ = 1.22

(from SEC in THF at 25 °C, using standard calibration relative to PS)

Structure 28: **DA PTEGA-P(S-co-I)**[149]

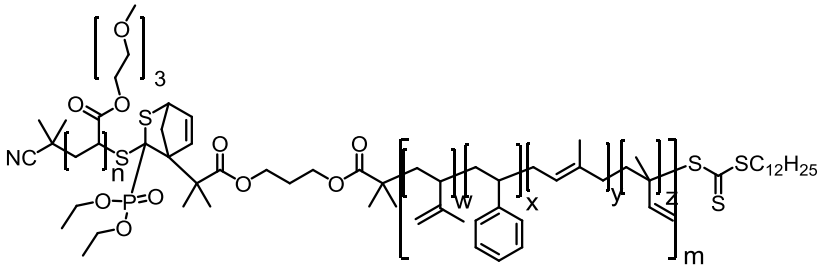

M_n = 16000 g/mol, M_w = 20800 g/mol, $Đ_m$ = 1.30

(from SEC in THF at 25 °C, using standard calibration relative to PS)

Structure 29: **DA Cp_2-P(^{i}BoA-^{n}BuA)**[72]

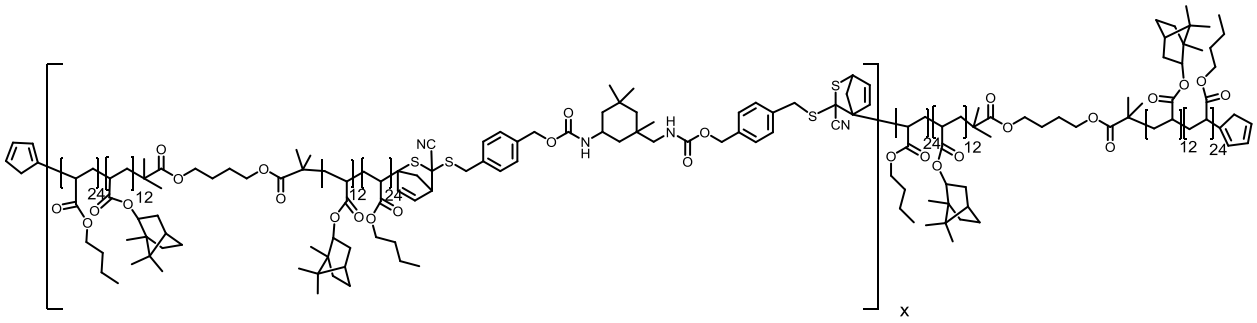

M_n = 34200 g/mol, M_w = 85500 g/mol, $Đ_m$ = 2.50

(x = approx. 3, molar masses from SEC in THF at 25 °C, using standard calibration with KMH coefficients)

The polymer building blocks (Structure 4, Structure 11 - Structure 15) were prepared by ATRP by using a symmetrical bifunctional initiator. That polymerization produces narrowly distributed polymers with bromine endgroups that can be converted in a nickelocene reaction into cyclopentadiene endgroups. The exact synthetic procedures are described in detail in literature.[69,71,72] The entire synthetic work of all investigated substances was carried out at the Karlsruhe Institute of Technology (KIT) by Nathalie

Guimard, Kim Öhlenschläger, Kai Pahnke and Marcel Langer. More details about the respective syntheses are given in the corresponding chapters. The DA reactions were obtained by reacting diene and dienophile at ambient temperature; in most cases without the need of a catalyst. If a catalyst was present it was removed during purification of the DA polymers so that all investigated samples were free of catalyst.

The main interest of the present work is to analyze the extent of debonding of a particular DA polymer at various conditions and to deduce reaction influencing parameters. Although the repolymerization (and the cyclabity of the DA reaction) is of major importance for the practical applicability of the system only the rDA reaction is investigated. The tendency of a DA polymer to debond at lower temperatures should be enough of an indicator for the reaction influencing parameters and focusing on the debonding reaction brings the advantage that diffusion as a limiting factor can be eliminated, as there is no need that reacting partners have to "find themselves". Controlling for concentration remains still important, as the reversible bonding reactions are effected by the absolute concentration of functional groups.[150]

3.2 Ambient temperature SEC with SLS

Ambient temperature SEC was performed on an Agilent Series 1200 instrument, equipped with a PLGel Mixed-C column (7.5 x 300 mm, 5 µm particles, Agilent Technologies, US), an ETA 2020 dRI- and viscosity detector (WGE Dr. Bures, Germany), a MiniDawn TriStar three-angle SLS detector (Wyatt Technology Corporation, US) and with THF (stabilized with 0.025 wt.-% BHT) as eluent at a flow rate of 1 mL/min. Data evaluation was cone with Astra 4.7.3 software (Wyatt Technology Corporation, US). Typical sample concentrations are about 2 mg/mL.

3.3 Temperature Dependent Size Exclusion Chromatography

3.3.1 Instrumentation

The general concept of SEC has already been explained in chapter 2.4. In this chapter some particularities that are associated with high temperature (HT) SEC shall be highlighted. HT SEC is mainly performed for analyzing crystalline polyolefins that need temperatures higher than their melting point in order to get dissolved.[151–154] To keep the samples in solution it is necessary to control the temperature of all relevant parts in the system. A further and so far unexplored application of a high temperature chromatograph is the in this dissertation developed **TD SEC**. The need for elevated temperatures does not come from solubility issues but from the motive to measure the outcome of debonding reactions as a function of different temperatures.

The setup of the instrument used for this work is shown schematically in Figure 19:

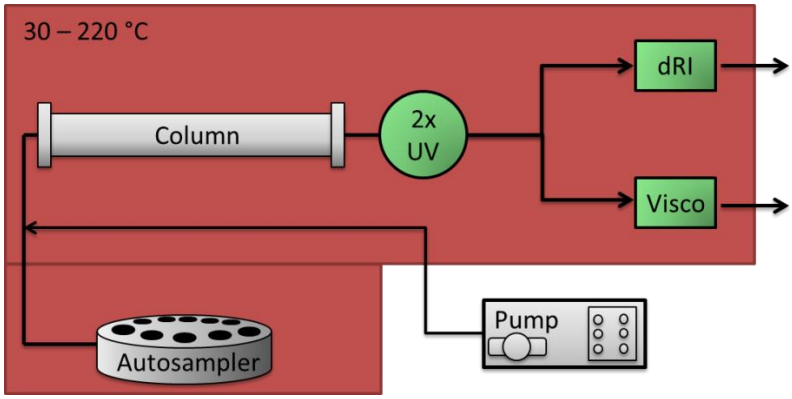

Figure 19: Schematic of the fully upgraded high temperature chromatograph. The autosampler, column(s) and detectors are temperature controlled up to 220 °C. UV is the UV/Vis absorption detector, dRI the differential refractive index detector and Visco the Viscometer.

All components except the pump and the solvent and the waste bottles are kept in the temperature controlled oven system. The autosampler carousel is controlled separately (although it is most feasible to have the same temperature as the main oven) and allows stirring. Upon injection the vial is lifted from the autosampler in the column oven and the entire separation and detection process is performed at the desired temperature. That setup requires particular temperature stability of all components, *i.e.* the columns and the detectors. In this work a PL GPC 220 instrument was used, which comes with a built in dRI-detector. It was later upgraded with a stock viscometer and a custom-made two-wavelength UV/Vis absorption detector. The detailed information can be found in Table 1:

Table 1: Specifications of the employed TD SEC setup.

Component	Details
HT SEC	PL GPC 220 (Agilent, US)
Pump	Agilent Infinity 1260 quaternary pump (Agilent, US)
Solvents	1,2,4-Trichloro benzene (TCB), stabilized with1 g/L BHT
	N,N-Dimethyl sulfoxide (DMSO), stabilized with1 g/L BHT
	N,N-Dimethylacetamide (DMAc), 3 g/L LiCl, stabilized with1 g/L BHT
	N,N-Dimethylformamide (DMF), stabilized with1 g/L BHT
Columns	ResiPore, 7.5 x 300 mm, 3 µm particles (Agilent, US)
	Mixed-D, 7.5 x 300 mm, 5 µm particles (Agilent, US)
	ABOA DMAc-Phil-P-300, 8 x 300 mm, 5 µm particles (Applichrom, Germany)
dRI detector	Integrated dRI detector, operating at 890 nm (Agilent, US)
Viscometer	220R Four capillary bridge differential viscometer (Agilent, US)
UV/Vis detector	Flow cell integrated into the column oven, two wavelengths simultaneously, Wavelength region: 200 – 700 nm (Testa Analytics, Germany)

The need for high temperatures limits the choice of the eluent. In polyolefin analytics it is most common to use 1,2,4-trichloro benzene (TCB) with a boiling point (b_p) of 213 °C and an octanol-water partition coefficient of 4.02. Further applicable solvents with high boiling points but different polarities are, for instance, *N,N*-dimethyl sulfoxide (DMSO, b_p = 189 °C, $log\ k_{OW}$ = -1.35), *N,N*-dimethylacetamide (DMAc, b_p = 165 °C, $log\ k_{OW}$ = -0.77), *N,N*-dimethylformamide (DMF, b_p = 154 °C, $log\ k_{OW}$ = -1.01) or ethyleneglycol monobutyl ether (EGMBE, b_p = 171 °C, $log\ k_{OW}$ = 0.8).[155] Mixing solvents is possible in principle but the effects of preferential solvation should be kept in mind.[99] If for a particular solvent temperatures close to or higher than the respective boiling point are required, a back pressure regulator can be used for artificially increasing the system's pressure and, thus, the boiling point.[151,156]

The high temperatures and especially significant changes in temperature are an extraordinary stress for the column materials. In SEC mostly highly crosslinked styrene-divinylbenzene-copolymers with a certain (usually concealed) surface modification are used for the packing materials.[88,157] Although polystyrene is not expected to undergo thermal depolymerization at temperatures lower than 250 °C[158] the columns are usually specified to be stable at temperatures lower than 120 °C. A reason for this is that the porous spherules that are used as a packing material are going to swell in the solvent. With significant changes in the temperature the particles will swell more or less, which could result in a mechanical stress that leads to reduction of their mechanical integrity. Furthermore, any kind of

oxidation processes of functional groups on the surfaces could be accelerated at higher temperatures. In order to assess the stability of the applied column materials a set of experiment was performed with readily packed ResiPore columns (3 µm particles) as well as loose column material. The performance of the columns before and after being used for several months in TD SEC was compared and in addition, the properties of the loose material were investigated before and after several heating cycles in air and swollen in solvent. Our studies showed no significant decrease of performance of the packed columns and no indicative degradation of the loose material, as observed by ATR-FTIR spectroscopy, SEM, TGA, DSC and physisorption measurements. Only when not contained in any solvent but in pure air signs of degradation have been found.[157] In the normal application the particles are, however, always encompassed by solvent so that no serious oxidation is to be expected. It shall be noted that over the entire time of this dissertation we observed that the packed column material is usually getting significantly darker over time. It is difficult to distinguish whether this is due to wearing of the column packing material or due to deposition of oxidized molecules from the solvents or their additives. In any case the separation efficiency did not seem to be impacted by the blackening of the column materials.

For the correct interpretation of the viscosity data a temperature dependent detector calibration was required. Therefore the viscosity of a narrowly distributed PS standard (usually 200 kDa) was determined at different temperatures in the SEC solvent in a temperature controlled capillary viscometer. For each viscosity determination a series of five standard solutions from 2 to 6 mg/mL was measured at identical conditions, together with the pure solvent. Then the data was processed according to a double fit in a Huggins and Kraemer plot as described in literature.[159] An exemplary plot is shown in Figure 20. The same standard sample was measured in the same solvent and at the same temperature in the TD SEC and the known intrinsic viscosity was used for calibrating the viscometer response.

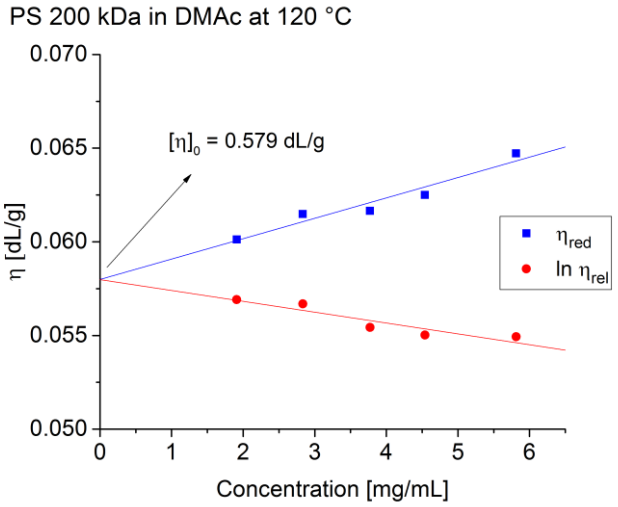

Figure 20: Determination of intrinsic viscosity according to fit to Huggins-Kraemer model.

3.3.2 Temperature effect on separation

Besides selecting appropriate components for the instrumentation it is evenly important to consider the effects of temperature on the separation mechanisms themselves. At first it shall be pointed out that temperature influences all enthalpic interactions and, thus, all separations that are due to enthalpic interactions.[154,156] The reported effects are not expected to play a significant role in SEC, since enthalpic interactions are sought to be insignificant. Significant effects can be observed, however, as shown in Figure 21:

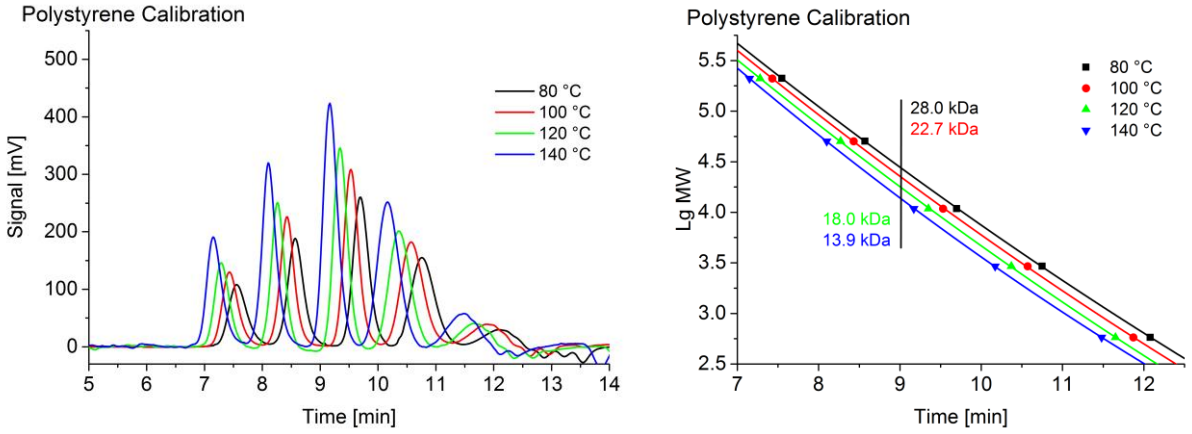

Figure 21: SEC Chromatograms of a polystyrene mix (210500 g/mol, 50400 g/mol, 10850 g/mol, 2930 g/mol and 580 g/mol), acquired at four different temperatures in DMSO (left) and the corresponding molar mass calibrations (right). The right graph demonstrates that, at a particular elution time (*e.g.*, 9 min) results in very different molar masses, if the calibration was done at a different temperature.

The figure shows clearly that at higher temperatures the chromatograms shift towards lower elution volumes and that the slope of the calibration curves increases with increasing temperatures. Calculating the molar masses at a particular elution time leads to very different molar masses, as can be seen in the right graph of Figure 21. Over a temperature difference from 80 to 140 °C the apparent molar masses differ about factor 2 if the elution time is set to 9 min! The shift of the chromatograms towards lower volumes can be explained by the thermal expansion of the solvent and is attributed to the fact that the pump is kept at ambient temperature. Consequently it delivers the set flow rate at ambient temperature but since the solvent is expanding when it is entering the oven, the effective flow rate is increasing and the analytes are reaching the detector more quickly.

A second effect is the increased rate of diffusion at elevated temperatures. Since the entire SEC mechanism is based on macromolecules diffusing in and out of the pores of the column material, the diffusion coefficients play an important role. Especially the separation of larger molecules can get less efficient if their diffusion is too slow to effectively exploit the theoretically accessible pore volume. At higher temperatures the mobility of the molecules is getting increased and, thus, the separation effectivity increases. This effect can be quantified by determining the theoretical plate height of the SEC setup as described in literature.[156,160] The plate height can be estimated by evaluating the peak width of eluting analytes, with respect to their elution time. Contributing parameters are for instance the peak broadening due to the different length of trajectories through the packing material (Eddy diffusion), the longitudinal diffusion of the analytes due to concentration changes or the intraparticle mass transfer.[161,162] A lower plate height indicates higher separation efficiency, as more theoretical (separation) plates fit into the length of the employed column. It is generally observed, that the plate height is dependent on both, temperature and flow rate. With higher temperature the plate height decreases and becomes less flow rate dependent. The practical consequence is that the peak resolution is increased and that higher flow rates can be applied without deteriorating the separation performance.[160]

One last effect has to be considered: the swelling of both, the analytes and the packing materials in the solvent. Following the basic laws of thermodynamics the solvent quality usually increases at higher temperatures and as a result the polymer coils and the column materials will attract more solvent molecules, eventually changing the effective hydrodynamic size of the analytes but also the pore size distribution of the column.[160]

The main practical implication of all the described effects is that chromatograms acquired at different temperatures cannot be compared directly. This means, that all calibration and reference

chromatograms have to be collected at identical conditions and, at best, at the same day. Otherwise, for instance the swelling of the column material had to be perfectly reversible, which is not easy to proof.

3.4 TD SEC analysis procedure

In this chapter, the procedures for the TD SEC experiments for investigating the rDA reactions shall be explained. As described in chapter 2.3 it is important to perform the rDA reactions and their analysis at as identical as possible conditions. Thus, it is most feasible to have the DA polymers readily dissolved in the SEC solvent and to have them in the heated autosampler for letting the reaction occur at a certain temperature (*e.g.*, 90 °C). After desired time intervals a sample can be automatically pulled and injected on the column and detected in the detectors, where all components are at the same temperature. Figure 22 shows the procedure schematically:

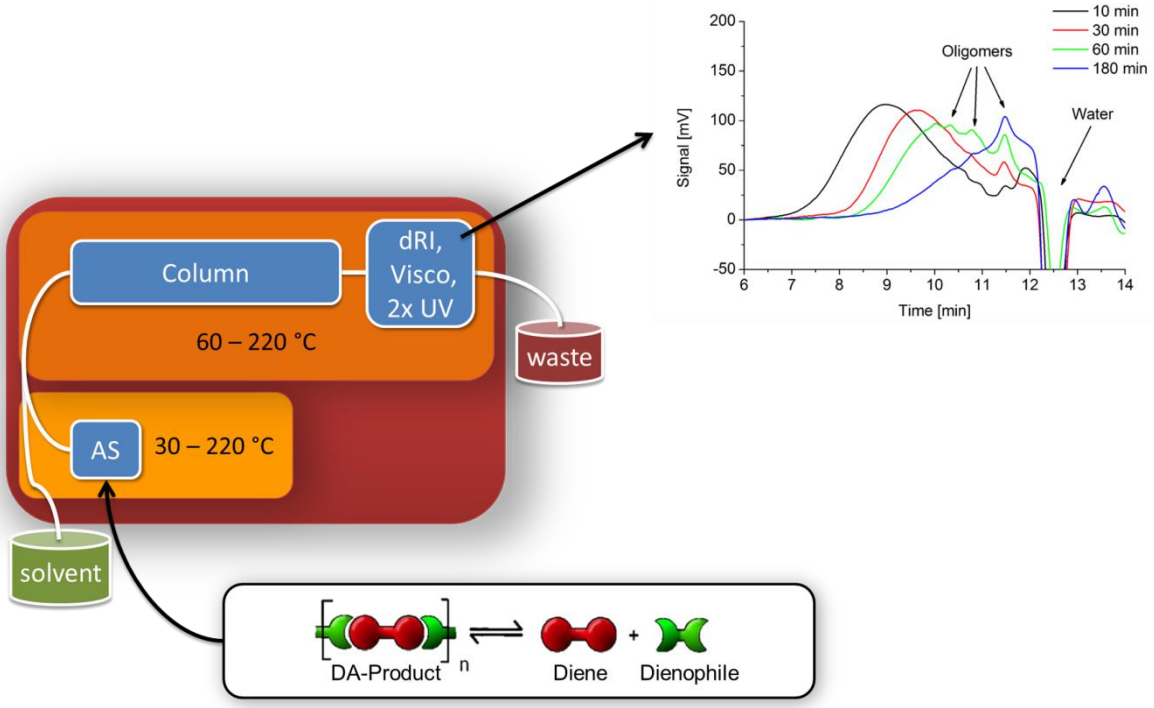

Figure 22: Analysis scheme for the investigation of rDA reactions via TD SEC.

Appropriate sample concentrations lie in the range of 3 – 5 mg/mL and the vial should be filled sufficiently to allow multiple injections from the same vial. By collecting chromatograms after various reaction times the kinetics of the reactions can be monitored, as shown in the graph in Figure 22.

An important question is how much of the rDA reactions is occurring in the columns during the analysis run. Or, more specific, what is the potential influence of the particular analysis conditions for

changing the reaction's outcome? To answer this question we have to compare all conditions in the vial with the respective conditions in the column: We know that the solvent composition and temperature are constant, but in the column the pressure and shear rates are significantly higher, as well as the dilution of the sample. Elevated pressures and shear rates should not impact the polymers or the rDA reactions, as the employed polymers are of rather low molar masses and degradation is not to be expected.[163] It shall be pointed out, however, that the depolymerization reactions or decay reactions in general are concentration dependent.[150] Keeping the initial sample concentrations as similar as possible (*e.g.*, 3.0 mg/mL) and analyzing peaks of comparable width should result in a similar magnitude of dilution for all measured sample, thus making the results comparable.

When the analysis time is short compared to the reaction time, information about the reaction kinetics can be obtained. The DA reaction usually follows second order, and the rDA reaction first order kinetics.[33] Deriving kinetic parameters from the obtained data was not the goal of this work and more focus was put on the evaluation of the equilibrium state.

3.4.1 Molar mass based evaluation

The most obvious way for evaluating the chromatogram is to calculate the molar mass (averages) and to correlate the molar mass with a degree of bonding or debonding. Connecting both is possible because of the step-growth-reaction type of the employed DA polymer systems. For step-growth reactions Carothers' equation can be employed that links the degree of polymerization (DP_n) with the conversion of the reaction, as shown in Equation 38. The conversion *X* can be interpreted as a degree of bonding and, consequently, an expression for the bonding decrease on a percentage basis can be derived, as shown in Equation 39.[69]

$$DP_n = \frac{1}{1 - X} \qquad \text{Equation 38}$$

$$\%BondingDecrease = \left(1 - \frac{1 - \frac{1}{DP_{n,rDA}}}{1 - \frac{1}{DP_{n,0}}} \right) \cdot 100\% \qquad \text{Equation 39}$$

In these equations DP_n is the degree of polymerization (*i.e.* M_n*(Polymer)/M(Monomer)*), the indices *rDA* and *0* denote the DP_n after a certain extent of rDA reaction and before any rDA reaction, respectively, and *X* is the conversion of the bonding reaction. The equation works best if the two monomers (or building blocks) are of approximately the same size. Then their molar mass can be

averaged and used for calculating the respective DP_ns. Imagine, however, a system where a large polymer building block is linked together by a small bifunctional linker. In such a system the molar mass of a DA polymer with two building blocks and only one linker (*i.e.,* block-linker-block) would be virtually identical to the same DA polymer with two additional linker molecules at the ends of the building blocks (*i.e.*, linker-block-linker-block-linker). Hence, distinguishing both is difficult and a "true" degree of bonding in terms of how many DA bonds have been formed is not directly possible. More than determining the number of linked building blocks and the minimum number of linker (= number of blocks – 1) is not possible.

3.4.2 Concentration based evaluation

Applying this approach implies the determination of precise molar masses in order to calculate with correct values of DP_n. As already discussed in chapter 2.4.3 the effective determination of molar masses is dependent on the absence of enthalpic interactions between analyte and column materials. If ideal SEC behavior cannot be assumed and absolute molar mass determination is not accessible another approach has to be found. In such cases the SEC can be used as an advanced concentration detector. A separation according to size is still required but we can tolerate a certain amount of enthalpic interactions, as long as entropy remains the dominant driving force for the separation. The concept is to define peaks or areas of the chromatogram and assign these to individual components, *i.e.* the DA polymer, the building block(s) and, if present, the linker molecule. In a second step the peak areas of the individual components can be calculated and converted into weight concentration by using appropriate calibrations. The concentrations can be monitored during the course of the rDA reaction and be used as an indicator for its progress.

That procedure requires two premises: At first it is necessary to define peaks for the DA polymer and the released building block(s). Both should be relatively different in their size so that we can use the elution time as a rough characteristic for distinguishing the components: At lowest elution volumes (highest molar masses) we expect the DA polymer, followed by the isolated building blocks and at highest elution volumes small linker molecules (if present). The corresponding elution volumes can be determined by measuring the individual components separately at identical conditions. At these positions we expect the rDA products of the DA polymer and additionally a high molar mass residue at lower elution volumes. In practice these peaks will not be separated well from each other so that a deconvolution step is required. Multiple assays can be found in literature explaining how to describe peaks by mathematical functions and to isolate contributions of overlapping signals.[164,165] The

procedure that has been used in this work shall be explained in general in the next paragraph. Details more specific to particular applications can be found in the respective sections.

Functions of the Gauss type have been used for the fitting process; their general form is shown in Equation 40

$$y = y_0 + \frac{A}{w\sqrt{\pi/2}} e^{-2\frac{(x-x_c)^2}{w^2}} \qquad \text{Equation 40}$$

, where y is the signal intensity, y_0 a base offset (usually $y_0=0$), A the peak area, w the peak width, x the corresponding position of the data point and x_c the position of the peak maximum. Per its definition the Gauss function describes perfectly symmetrical peaks. In order to make the model function applicable for non-symmetric peaks as well, linear combinations of two or three individual Gauss functions were used.

For analyzing the chromatogram of a DA polymer the following steps are performed:

1. Collect chromatogram(s) of individual reference sample(s) and determine peak parameters w and x_c and correlate peak area(s) A to concentration of the reference sample(s).
2. In the DA polymer chromatogram: Fit the peak(s) from step 1 in the new chromatogram but only use the peak area(s) A as variable. Add additional Gauss functions to fit the entire chromatogram.
3. The proper assignment of the individual peaks and the correlation of their peak area to their concentration has to be done carefully and specifically for each sample. More details about this procedure are explained in the respective chapter.

An example chromatogram of a DA polymer with the theoretically derived peaks is shown in Figure 23. All calculations were done in Microsoft® Excel® 2010 using the solver feature.

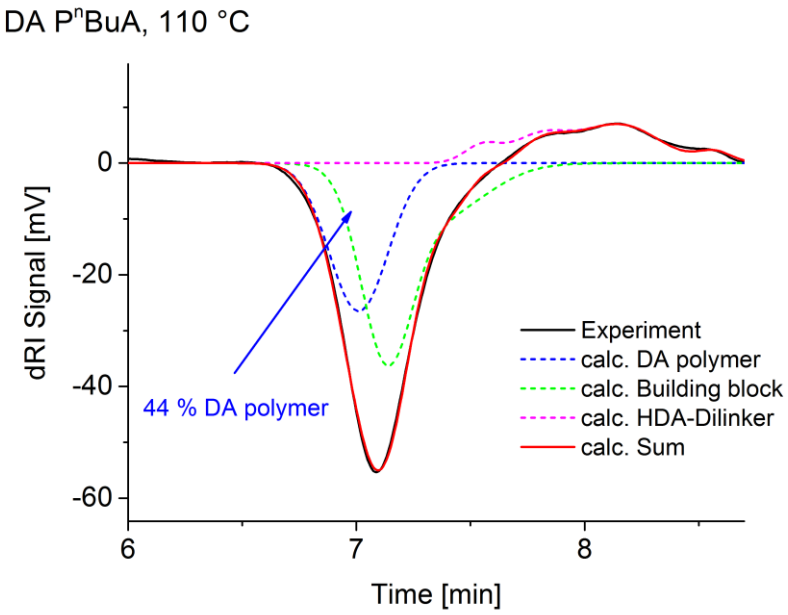

Figure 23: Deconvolution of a chromatogram of a DA polymer, acquired at 110 °C. The black solid line indicates the experimentally collected chromatogram, the dashed lines the calculated component contributions and the red solid line their sum that is in good agreement with the experimental curve.

3.5 DLS analysis procedure

The DLS experiments were carried out using a DynaPro NanoStar photospectrometer (WYATT Technology Corporation, US) in batch mode. 100 to 150 µL of sample solution are sufficient to be measured in a temperature range from -20 to 150 °C. The instrument works with a 658 nm laser and collects the light scattering intensity at 90 ° in intervals of 100 ns. A hardware correlator calculates the autocorrelation functions and the further data handling is done in the associated software (Dynamics 7.1.7). For each measurement 10 to 50 single autocorrelation functions are acquired (analysis time each 1 to 5 seconds) and averaged. It is possible to manually exclude poor correlation functions from this averaging. In the end the averaged correlation function is fitted by representative models, taking into account the temperature and the viscosity of the solvent (see chapter 2.6.2).

3.6 TD HPLC and 2D LC instrument setup

In Table 2 the instrumental details for the HPLC experiments that were conducted at the Universiteit van Amsterdam are summarized.

Table 2: Instrumental HPLC setup

Component	Details
HPLC integrated system	Waters Alliance 2695 HPLC system
Flow rate	0.5 mL/min
Solvents	ACN
	Ethyl acetate
	n-heptane
	THF
Columns	Inertsil ODS column, C_{18} surface, 3.0x150 mm, 5 µm particles (GL Sciences B.V., The Netherlands)
	Inertsil NH_2 column, 4.6x250 mm, 5 µm particles (GL Sciences B.V., The Netherlands)
Column oven	Chromapack column thermostat 3
Detection	Alltech 3300 Evaporative Light Scattering Detector (115 °C, 3 L/min N_2), (Grace, US)

In addition a two-dimensional setup was employed. Figure 24 depicts an exemplary 2D LC instrument setup. The working principle of the 10-port switching valve is depicted more in detail in Figure 25.

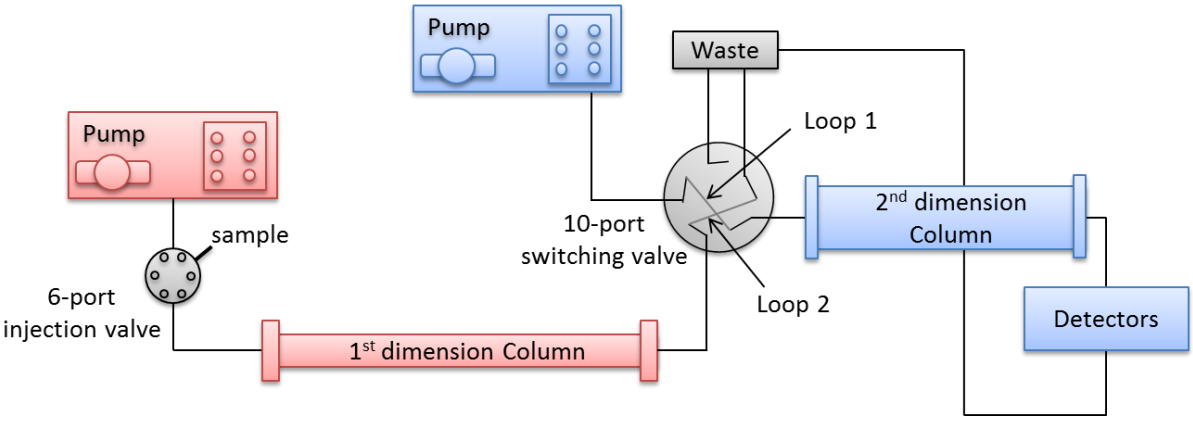

Figure 24: Schematic depiction of a 2D LC instrument setup. Adapted from Ref.[166]

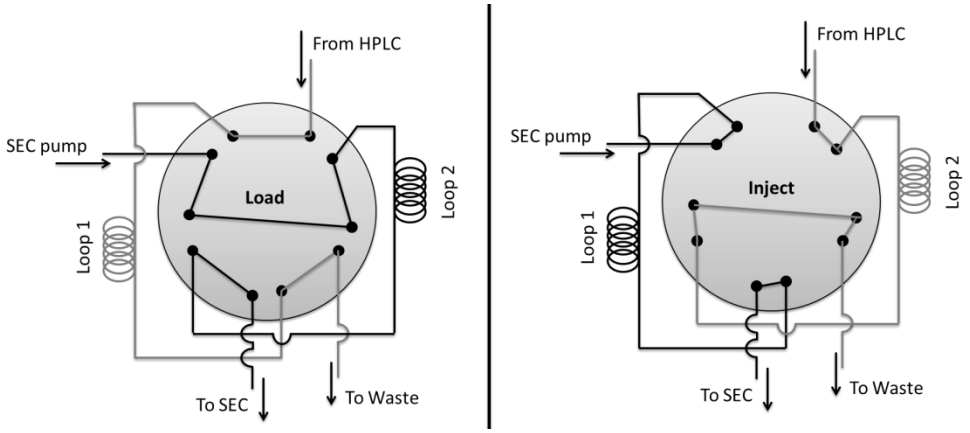

Figure 25: The two positions of the 10-port switching valve in an HPLC x SEC setup. Adapted from Ref.[166]

Both dimensions are connected through the 10-port valve and two sample loops that are connected to the valve. In order to be able to analyze each individual fraction coming from the 1st dimension in the 2nd dimension it is necessary to operate both dimensions at very different analysis speeds. The 1st dimension is usually performed at low flow rates (*e.g.*, 20 µL/min) and the second dimension at relatively high flow rates (*e.g.*, 1 mL/min). In that way the LC effluent can slowly fill one of the sample loops (loop 1), where, in the same time, the 2nd dimension completely acquires one chromatogram with the sample that was contained in the other sample loop (loop 2). Then, when dimension 1 is done filling loop 1 and dimension 2 has measured the content of loop 2 the valve switches and dimension 1 is now starting to fill loop 2, whereas the fraction in loop 1 is injected into the second dimension. By precise timing and continuous and quick switching of the air-actuated 10-port valve it is possible to fraction the entire 1st dimension chromatogram and to analyze it in the second dimension. In contrast to such a "comprehensive" 2D LC experiment it is also possible to fraction only a part of the 1st dimension in a so called "heart cut" experiment. The details of the herein employed 2D LC setup are compiled in Table 3:

Table 3: Instrumental NP HPLC x SEC setup

Component	Details
Controller	Shimadzu CMB-20 A (Shimadzu, Japan)
Pumps	2x Shimadzu LC-20 AD, 2x Shimadzu LC-10 AD (Shimadzu, Japan)
Solvents	*n*-hexane
	THF
Loops and valves	20 µL, manual injection port
	2x 60 µL transfer loop, controlled by 10 port pressure driven switch valve
Columns	1st dimension: Inertsil NH_2 column, 4.6x250 mm, 5 µm particles (GL Sciences B.V., The Netherlands), flow rate: 20 µL/min
	2nd dimension: Agilent Mixed-E, 7.5x100 mm, 3 µm particles (Agilent, US), flow rate: 1 mL/min
Detection	Alltech 3300 Evaporative Light Scattering Detector (115 °C, 3 L/min N_2), (Grace, US)

3.7 NMR instrument

The NMR measurements were performed on an Avance III 500 spectrometer (Bruker, Germany). ^1H spectra were acquired at a frequency of 500.13 MHz in $CDCl_3$.

3.8 SANS instrument setup

For the determination of the persistence length beam time at the *Institute Max von Laue – Paul Langevin* (ILL) at Grenoble, France, was granted. At ILL the currently most powerful High-Flux Reactor generates a continuous neutron flux of $1.5E^{15}$ neutrons per second and cm² at a thermal power of 58.3 MW. The neutrons are generated by the fission of enriched $Uranium^{235}$, where two or three neutrons are released per fission event (one of these neutrons is then consumed for triggering the next fission event).

Besides the challenging production of a steady neutron beam it is equally difficult to create elements that allow monochromation and collimation of the radiation. Tasks that can easily achieved by optical gratings and lenses require huge elements for neutron radiation. The layout of instrument D11 that was used for the investigations in this work is shown schematically in Figure 26. In the past decades the instrument was upgraded multiple times and offers now excellent conditions for SANS measurements of soft matter samples.[167,168]

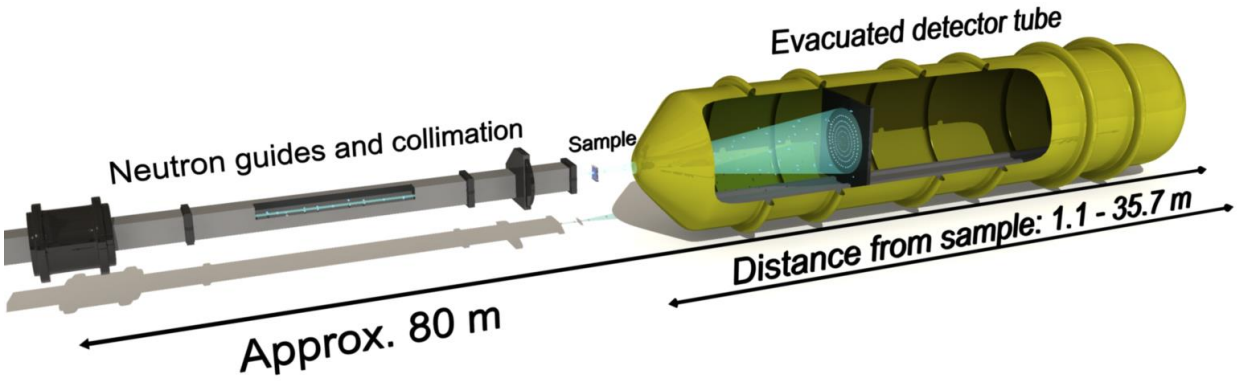

Figure 26: Simplified layout of the D11 experiment at the ILL, showing the collimation and detection components. In total the instrument requires approx. 80 m of space (state 1991).[167]

The experiments were performed at a neutron wavelength of 6 Å. Two detector distances, 8 m and 1.2 m, respectively, were used to cover a q-range from 0.0083 to 0.514 $Å^{-1}$. Samples of PMA, $P^{i}BoA$, $P^{n}BuA$, $P^{i}BuA$ and $P^{t}BuA$ were measured at concentrations of approx. 1, 2, 3, 4 and 5 wt% in toluene-d_8. The solvent was measured individually and its scattering curve was subtracted from the measurements of the polymer scattering curves.

The data treatment procedure is described in detail in chapter 2.6.3.

4 Molar Mass based data evaluation

One of the most intensively studied DA reactions is the reaction of furan with maleimide. It is known that both undergo DA reaction at ambient conditions in the presence of a catalyst (*i.e.*, a Lewis acid) while at elevated temperatures the rDA reaction is triggered.[169,170] A relatively simple DA polymer system was used for studying the basic rDA behavior by TD SEC; its structure and reaction scheme is shown in Figure 27:

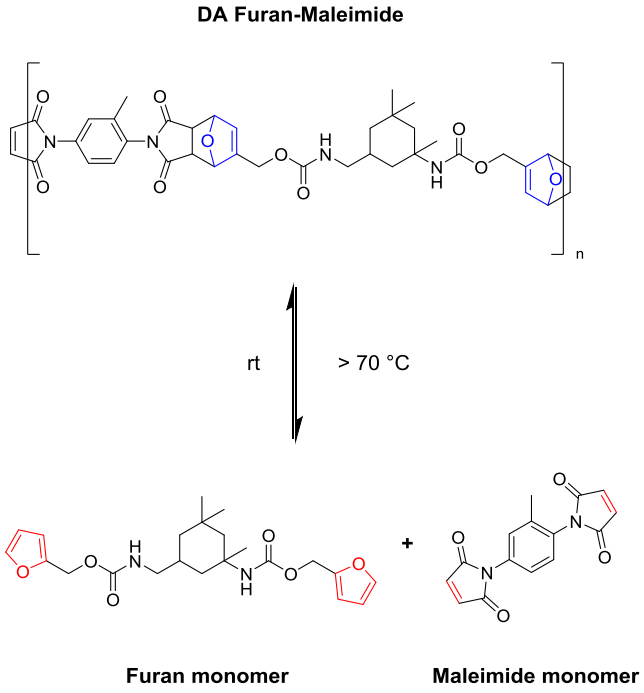

Figure 27: rDA reaction scheme of the investigated DA Furan-Maleimide system (Structure 3), yielding the furan (Structure 1) and the maleimide monomer (Structure 2).

The furan-maleimide system that was prepared by Kim Öhlenschläger (KIT) consists of a difuran (Structure 1) and a bismaleimide (Structure 2). Both molecules were reacted in 1:1 stoichiometric ratio in an AA-BB type step growth polymerization to give a polymer with an M_n of approx. 7000 g/mol (Structure 3).

When dealing with step growth polymer it is important to keep in mind that high monomer conversions are required to achieve high molar masses. Carothers equation (Equation 38 in chapter 3.4.1) allows linking the degree of polymerization to the reactions conversion but does not give information about the MMD. Since SEC allows determining the MMD it would be interesting to get a general idea of how the MMD would look like at different monomer conversions. Calculating the MMD for a given step

growth is possible by some simple statistical considerations. The scheme in Figure 28 shows a step growth polymer consisting of a certain number of BA monomers.

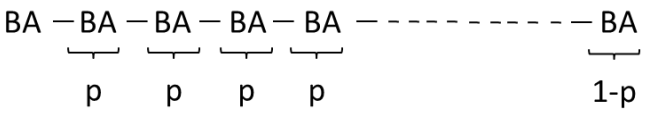

Figure 28: An AB step growth polymer of arbitrary degree of polymerization. The probability that a monomer is integrated into the polymer is given by *p*.

All BA monomers are identical and the only possible reaction is the reaction of A with B. Assuming that all bonding events are independent allows calculating the probability that a polymer with x monomers is formed by Equation 41:

$$p_x = p^{(x-1)} \cdot (1-p) = n(x) \qquad \text{Equation 41}$$

, where p_x is the probability that *x* monomers react together, *p* is the probability that one monomer unit is integrated into the polymer (*i.e.*, A and B have reacted). The probability for that particular polymer equals the number fraction *n(x)* of the respective *x*-mer in the mixture. With this equation it is possible to calculate *n(x)* for a desired range of values of *x*, where *p* can be considered to be the conversion of the reaction (fraction of reacted functional groups, *X*). As most concentration detectors in SEC yield weight distributions *w(x)* rather than number distributions a last step is required, where each number fraction *n(x)* is multiplied by the mass of the respective degree of polymerization.[171–173]

These considerations can be done for AA BB type reactions as well. They were done for monomers of the type AB out of a mathematical reason: For AB monomers only one orientation exists in which the monomer can be integrated into the polymer. In the case of symmetrical monomers (AA + BB) each monomer would have two possibilities to be integrated and, thus, the double probability to be incorporated. Both possibilities would give a chemically identical polymer and its fraction would have to be multiplied with 0.5 again so that in the end the same probability is obtained.

In Figure 29 the calculated weight distributions are calculated by using the averaged molar mass of the monomers shown in Figure 27 (= 350 g/mol) for conversions from 30 % (*p = 0.3*) to 98 % (*p = 0.93*). Furthermore the resulting values for the DP_n and the M_n are given.

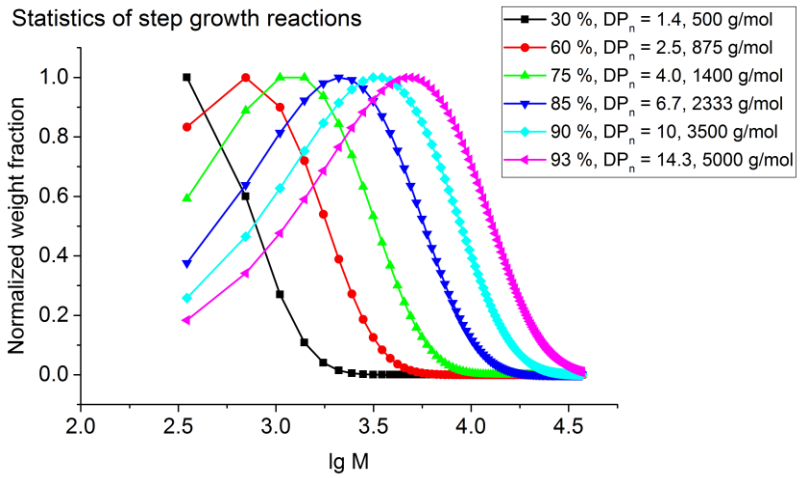

Figure 29: Calculated weight distribution of the furan-maleimide DA polymer system at conversions from 30 to 93 %.

These distributions demonstrate once more that high conversions are required for high molar masses. Portrayed the other way around the image shows that in the beginning of an rDA reaction the change in molar mass is relatively large, whereas at higher "rDA conversions" only minor changes in the MMD can be expected. By ambient temperature SEC-SLS an M_n of 7000 g/mol (see Figure 95 in appendix chapter 11.1) was obtained for the DA polymer, which corresponds to a conversion of 95 %.

Depolymerization of the DA polymer was observed at temperatures higher than 70 °C. Because of the relatively polar character of the DA polymer the TD SEC experiments were carried out in DMSO as the eluent. In Figure 30 the chromatograms of the DA Furan-Maleimide are shown after different heating times prior to injection at 80 °C. With increasing reaction time the molar mass distribution clearly shifts towards higher elution times (*i.e.*, lower molar masses). At 8 to 9 minutes distinct peaks develop, indicating the release of smaller oligomeric components. The dashed line represents the chromatogram of the furan monomer, which elutes very close to the solvent peak. Although the furan and the maleimide monomer are chemically different they were eluting at the same time and could not be distinguished by the SEC setup. Consequently the last positive peak in the chromatograms of the DA polymer can be assigned to the monomer peak but is occluded partially by the solvent peak. Due to the hygroscopic character of the eluent DMSO a solvent peak could never be avoided completely. Drying the samples prior to analysis *in vacuo* at 55 °C and dissolving it in DMSO that was taken directly from the SEC eluent reservoir and flushing the SEC vials with nitrogen before closing them served for minimizing the solvent peak, however.

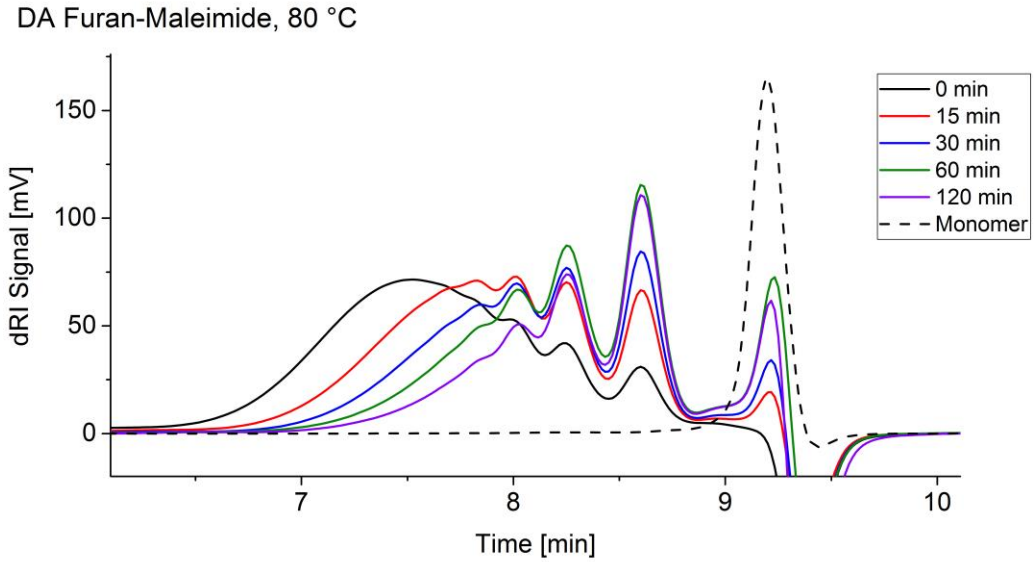

Figure 30: SEC chromatograms of DA Furan-Maleimide at 80 °C in DMSO after various reaction times prior to injection. The dashed line indicates the elution profile of the furan monomer. With increasing reaction time the peak shifts towards higher times that correspond to lower molar masses.

In order to calculate molar masses a suitable calibration method has to be found. A standard calibration with narrowly distributed Poly(2-vinyl pyridine) (PVP) standards was tested first because, similar to the investigated polymers, PVP contains nitrogen as well. No linear calibration curves were obtained (Figure 96 in appendix chapter 11.1), which indicates enthalpic interactions between the PVP and the column material. For calculating the desired *%Bonding Decrease* (Equation 29) the DP_n of the DA polymers during the rDA reaction has to be determined accurately. The DP_n may be calculated even with inaccurate calibration curves, since potential deviations cancel out when the obtained molar mass of the polymer is divided by the molar mass of the monomer, derived from the same calibration curve. Although this procedure can work for calculating the *%Bonding Decrease* of samples at one distinct temperature it is likely to fail if the results that were obtained across different temperatures. Applying the calibrations temperature dependently is more difficult, as the individual polymer types not only behave differently on the column but also are likely to show different thermodynamic swelling with temperature. Consequently the difference between the calibration curves of PVP and the DA Furan-Maleimide polymer is not the same at all temperatures. Furthermore, if enthalpic interactions are expected their effect would introduce an additional temperature dependency.

The suitability of the PVP calibration was assessed by two pathways. Firstly the molar mass of the monomer peak was determined according to the PVP calibrations at 80 °C, 90 °C, 100 °C and 120 °C. At the highest temperature a relatively realistic molar mass of 500 g/mol was obtained, but at the lower temperatures the apparent molar mass of the monomer increased to 800 g/mol, 1100 g/mol and at 80 °C finally 1500 g/mol. Thus, the obtained molar mass at 80 °C is three times higher than hat 120 °C, indicating that the calibration does not fit well. Nevertheless it was tested if reasonable *%Bonding Decrease* values can be calculated by using the obtained monomer mass for calibrating the respective DP_n values. It shall be noted that, for determining the M_n of the corresponding DA polymers the partially occluded monomer peak was not included in the calculations. Hence, the obtained M_n represents the average molar mass of the entire sample except the monomers. In Figure 31 the obtained values are plotted as a function of the reaction time.

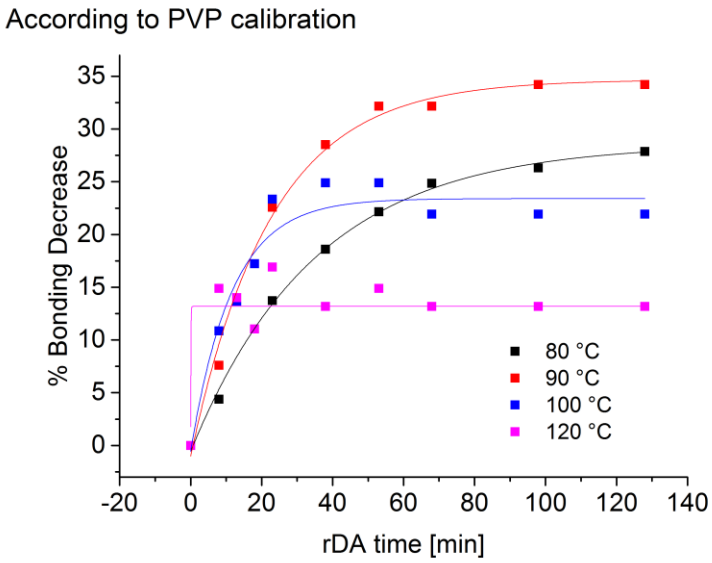

Figure 31: *%Bonding Decrease* obtained for DA Furan-Maleimide, calculated according to molar masses that were obtained from PVP calibrations at the respective temperatures. Clearly the trends do not agree with the expectations of more debonding at higher temperatures.

Focusing only at each temperature independently shows that with increasing reaction time a higher *%Bonding Decrease* is registered until a constant plateau is reached. Although this coincides with the expected behavior, comparing the individual *%Bonding Decrease* levels of the different temperatures does not show the expected trend of more debonding at higher temperatures. Instead, most debonding is obtained for 90 °C, followed by 80 °C, then 100 °C and eventually 120 °C.

Hence, a better method had to be found for establishing a calibration. In this case the best way for establishing a standard calibration could be performed, namely calibrating with the exact same polymer. When the chromatograms of the DA polymer were collected without any heating time prior to injection it was possible at all temperatures to capture a molar mass distribution with distinct oligomer peaks. Thus the corresponding molar masses can be calculated by simply counting the degree of polymerization and multiplying it with the average molar mass (=350 g/mol), where the chromatogram of the individual monomer served for determining the starting point. The left graph of Figure 32 shows the chromatogram of the DA polymer at 80 °C, together with its second derivation. Since a positive peak in the chromatogram leads to a sharp negative spike in the second derivation, the peak positions of the oligomers could be determined accurately.

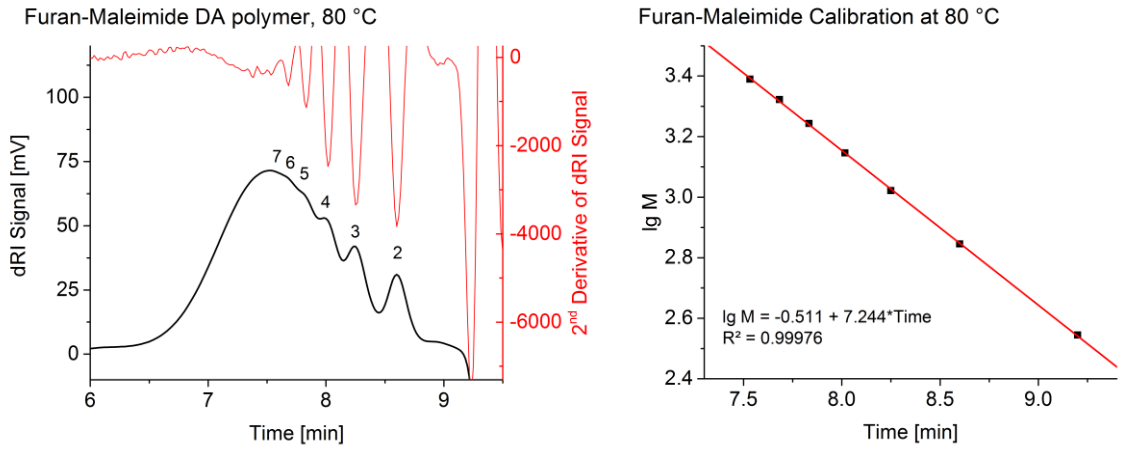

Figure 32: Left: SEC chromatogram of the DA polymer at 80 °C in DMSO and the 2nd derivative of the dRI signal. The numbers indicate the DP_n of the respective peaks. Right: Resulting calibration curve, indicating good SEC character of the separation.

The right graph of Figure 32 shows the resulting molar mass calibration, in which the determined oligomer positions fit the logarithm of their molar mass into a nearly perfect linear manner, thus indicating good SEC character of the separation. For calculating molar mass averages the calibration has to be extended towards higher molar masses. Extrapolating always implies the risk of not taking into account irregular effects but in this case it is unlikely that the calibration curve changes: Deviations from the expected SEC behavior can occur due to endgroup effects but such issues usually occur at the low molar mass end.[174] As no irregular behavior is observed until a DP_n of seven it appears save to perform the extrapolation towards higher molar masses.

Calculating the *%Bonding Decrease* according the furan-maleimide calibration yields the plots that are shown in Figure 33:

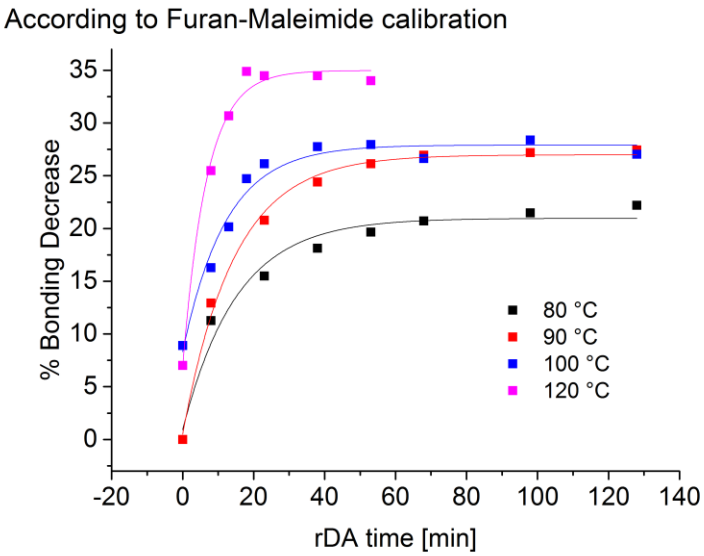

Figure 33: *%Bonding Decrease* as a function of the rDA time determined at different temperatures according to the respective molar mass calibrations that were established from the DA polymers themselves. Now the expected trend of more debonding at higher temperatures can be observed.

Now the obtained *%Bonding Decrease* values can be considered also across the different temperatures and reflect the trend that higher temperatures promote the rDA reaction. However, the data is biased towards lower *%Bonding Decrease* as practically achieved. Because the molar mass computations could not include the monomer peak (due to the overlap with the solvent peak) the resulting molar mass averages are actually too high, resulting in too small *%Bonding Decrease* values. Furthermore the results are strongly dependent on the DP_n that was calculated from the molar mass at ambient temperature in an SEC-SLS experiment. Although SLS usually yields reliable results it might be inaccurate due to the relatively low molar mass of the DA polymer.

At this point a second approach was tested for evaluating the acquired molar mass distributions without being sensitive to the missing monomer peak or to imprecisions in the ambient temperature DP_n. Therefore the acquired chromatograms were plotted as a function of molar mass and then the distribution was fitted by the above described procedure in order to find the conversion *X* of the step growth reaction that fits the experimentally acquired MMD best. In Figure 34 the results are shown for 80 °C and 90 °C, the corresponding figures for 100 °C and 120 °C can be found in Figure 97 in Appendix chapter 11.1.

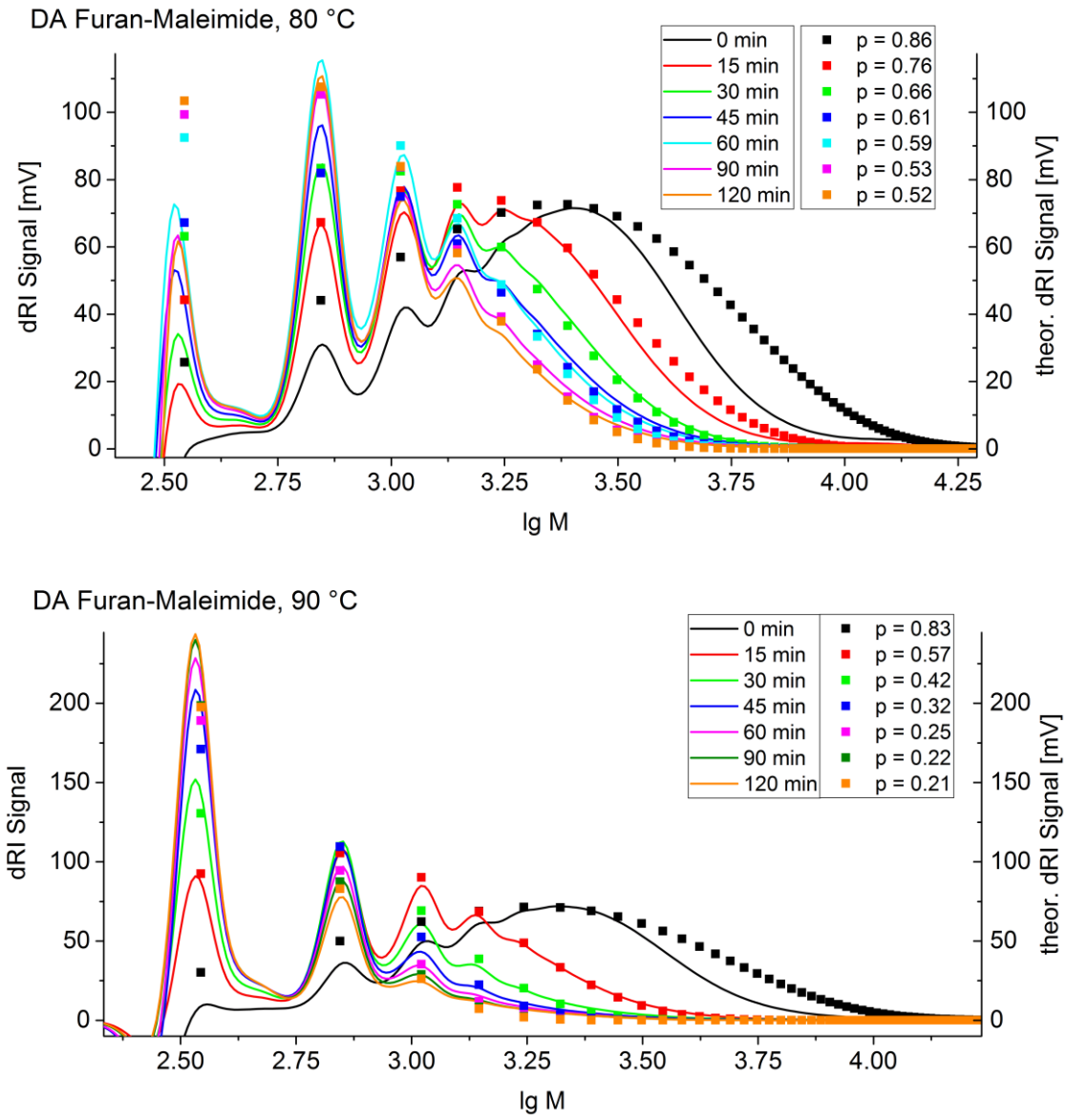

Figure 34: Through TD SEC in DMSO acquired MMDs of the DA polymers at 80 °C (top) and 90 °C (bottom). The left axis represents the dRI signal after different rDA reaction times, whereas the right axis gives the theoretically determined MMD at the indicated conversions (*p*). It was derived by multiplying the respective weight distributions with an arbitrary value in order to scale the distribution to the experimentally obtained dRI trace.

The agreement of the acquired MMDs and the statistically predicted MMDs is good except for the first measurements at each temperature. There the shape of the experimental MMDs cannot be represented well by the statistics because they are significantly less broad. Two explanations might contribute to the discrepancies at higher molar masses. One cause might be the extrapolation of the calibration from the oligomer range to higher molar masses as unforeseen inconsistencies would bias the results in the high MW range. A second explanation, however, might be that the step growth reaction

did not behave as perfectly as the statistics assume. Already formed polymers of higher molar mass diffuse more slowly and, thus, are less probable to react with other molecules; consequently the during synthesis produced polymers might not follow ideal step growth statistics. Therefore the obtained MMD does not necessarily represent the thermodynamic optimum. Furthermore, if the number of molecules is simply not high enough deviations from the "ideal" behavior have been found where the obtained distributions are less broad than predicted by Flory's considerations.[171] According to the work or Kricheldorf et al. another reason for lower DP_n can be cyclization reactions.[175–177] More in-depth investigations in that direction would require preparing new samples at different conditions, which was not possible at the time of these analyses.

The fitting procedure allowed assigning a DA conversion to each chromatogram, independent on the initial DP_n and less sensitive to the partially occluded monomer peak. The final values were converted into *% Bonding Decrease* by Equation 42:

$$\%\ Bonding\ Decrease = \frac{p_0 - p_{rDA}}{p_0} \cdot 100\ \% \qquad \text{Equation 42}$$

, where p_0 is the conversion prior to the rDA reaction and p_{rDA} the corresponding value after a certain particular reaction. X_0 was estimated by extrapolating the obtained p_{rDA} to 0 min. The thus obtained value of $p_0 = 0.90$ is slightly lower than the value of 0.95 that was calculated from the ambient temperature M_n. In the left graph of Figure 35 the *%Bonding Decrease* values that were calculated for the individual measurements are summarized as a function of the rDA reaction time and temperature. A consistent trend of more debonding at higher temperatures can be observed.

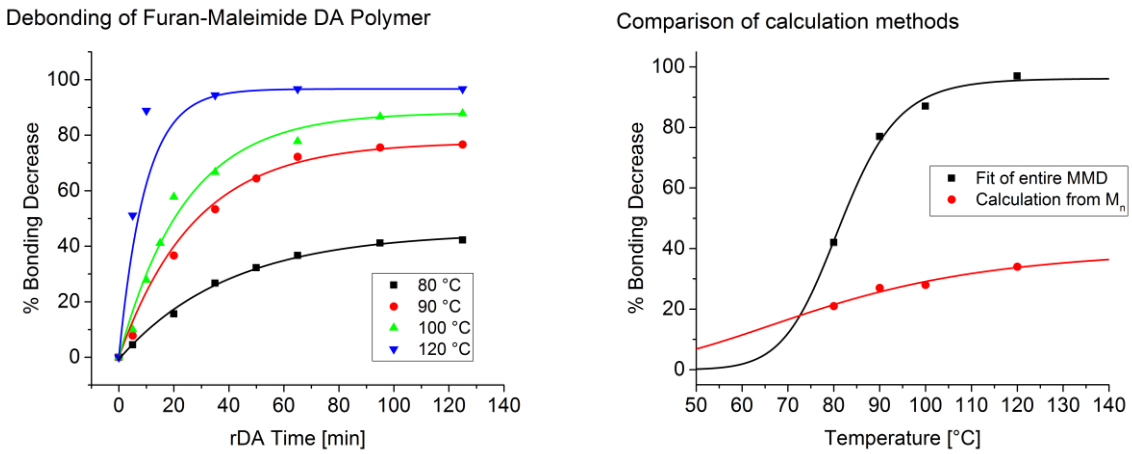

Figure 35: Time resolved *%Bonding Decrease* of the DA polymers calculated after fitting the entire MMD (left) and comparison of the equilibrium *%Bonding Decrease* determined from the M_n and the entire MMD (right). The lines represent a guide for the eye of the expected temperature dependency of the bonding decrease.

The right graph of Figure 35 compares the equilibrium values of each temperature from these calculations to the results of the procedure that derived the *%Bonding Decrease* from the M_n (Figure 33). At first sight the values obtained from fitting the entire MMD are significantly higher than the values calculated from the M_n. As already discussed previously the *%Bonding Decrease* results in too low values because the monomer peak was not included in the calculations. The fitting procedure is less sensitive to the partially occluded monomer and, thus, yields more realistic results. At 120 °C almost 100 % debonding is achieved which qualitatively agrees with the chromatograms that indicate a very high degree of debonding at 120 °C (see Figure 97 in Appendix chapter 11.1). In theory the *%Bonding Decrease* should show an *s-curve* like dependency on the temperature.[35,69,71] Predicting the temperature dependent bonding behavior requires extensive quantum mechanical calculations that could not be done for this system. Instead a simple Langmuir type function was employed for establishing a guide for the eye and for roughly estimating the debonding behavior at temperatures lower and higher than the experimental range. The fitted curves are included in the right graph of Figure 35. It is obvious that the data obtained from fitting the MMD can be described much more realistically by the used function. For instance, the data obtained from the M_n calculations would never reach 100 % debonding. On the other hand, at temperatures lower than 80 °C the *%Bonding Decrease* diminishes only gently. Keeping in mind that the DA polymer was synthesized at 70 °C this flat character of the curve seems contra intuitive. The much sharper form of the curve obtained from fitting the entire MMD describes much better that the synthesis of the DA polymer is possible at 70 °C whereas significant depolymerization can be observed at 80 °C. And in fact the curve predicts approx. 10 % debonding for 70 °C which agrees well with the initial

DA conversion of approx. 90 % that was estimated from the experiments. Thus the obtained results are consistent to each other.

The validity of the determined *p* values is supported further by more detailed kinetic considerations. It is known from theory that rDA reactions usually follow first order kinetics[33,34] and therefore the obtained *p* values were plotted accordingly. In the left graph of Figure 36 the logarithm of the rDA conversion of each temperature is plotted over the reaction time. The normalization is done by taking into account p_0 and p_{eq} of each temperature, where p_0 is the initial conversion before the rDA reaction (always 0.9) and p_{eq} the determined equilibrium conversion of each temperature. For 80, 90 and 100 °C an accurate linear correlation is obtained although it shall be noted that the last value of each temperature was not included into the fit. The last value is always practically identical to the respective equilibrium value and, hence, very sensitive to experimental error. In the case of the 120 °C all but the first two data points are close to the equilibrium value. Since all values are consequently prone to inaccuracies all of them were included into the fit in order to find a realistic average.

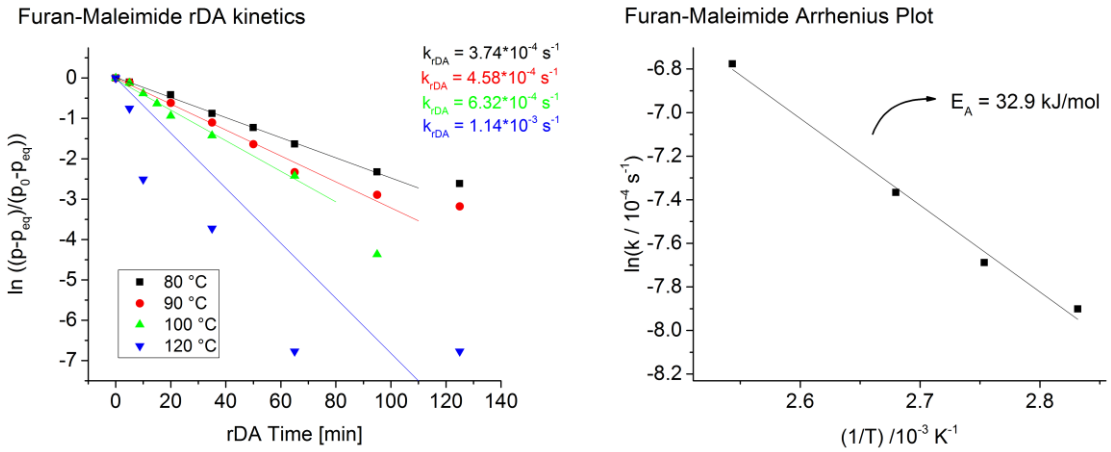

Figure 36: First order reaction plot of the Furan-Maleimide rDA reaction that allows determining the reaction rate constants (left) and the resulting Arrhenius plot that indicates the activation energy of the rDA reaction.

In the right graph the derived reaction rate constants were plotted logarithmically over 1/T to give the corresponding Arrhenius plot, which is based on Equation 43 and its logarithmic form in Equation 44.

$$k = A \cdot e^{-\frac{E_A}{RT}} \qquad \text{Equation 43}$$

$$\ln k = \ln A - \frac{E_A}{RT} \qquad \text{Equation 44}$$

In these equations k is the reaction rate constant (in s^{-1}), A a pre-exponential factor, E_A the activation energy, R the universal gas constant and T the absolute temperature. Hence, E_A can be calculated by multiplying the slope of the Arrhenius plot with $-R$. For the present example an activation energy of 32.9 kJ/mol is obtained. This value is in the order of magnitude of the result of Goiti et al. who performed spectroscopic based kinetic investigations on the rDA reaction of a furan-maleimide system where they obtained 21 kJ/mol.[34] The good linearity of the kinetic and the Arrhenius plot and the realistic activation energy once more underline the applicability of the fitting procedure.

In conclusion the fitting procedure appears to be the more elaborate but yet more robust evaluation procedure. Calculating the *%Bonding Decrease* according to the DP_n requires condensing the entire MMD into the single value of the M_n. In doing so a lot of information is lost and basing all further considerations on the determined M_n introduces the risk of errors in the final calculations.

The herein described experiments demonstrated that the progress of thermosensitive bonding reactions can be monitored and evaluated effectively with TD SEC. If molar masses cannot be calculated reliably by relative standard calibration and if light scattering or universal calibration is not accessible the polymer itself can be used as an internal standard. After acquiring the chromatograms and establishing the corresponding molar mass calibrations the data can be evaluated by simply calculating the molar mass average or by fitting the entire MMD according to the statistics of the underlying reaction principles. Although the latter procedure is more elaborative the obtained information are less sensitive to practical obstacles, such as overlapping peaks.

However, calculating molar masses is not possible in all cases. Then different evaluation approaches have to be employed in order to quantitatively monitor the progress of thermosensitive bonding reactions. In the following chapter the respective details are discussed.

5 Concentration based data evaluation

In this chapter examples are shown that demonstrate the details when working with the concentration based evaluation approach that was introduced in chapter 3.4.2. The examples are put into context with the investigations of rDA reactions for assessing experimentally the predicted entropy effects (see chapter 2.8).

5.1 The effect of polymer size on rDA reactions

The first effect that was investigated is the "size effect" that predicts a higher degree of debonding for larger polymer building blocks. Or, in other words, at the same temperature the larger building block leads to a higher degree of debonding. Therefore a set of DA polymers (Structure 8 - Structure 10) was synthesized by Nathalie Guimard at KIT for the experimental assessment of the proposed effects. A Cp endfunctionalized random copolymer of ^{i}BoA and *n*-butyl acrylate (^{n}BuA, Structure 4) reacts together with a building block of P^{i}BoA of different molar masses (P^{i}BoA X, Structure 5 - Structure 7). The P^{i}BoA blocks were synthesized with RAFT and carry dithioesther endgroups that can be used for the DA step growth reaction according to the scheme shown in Figure 37:

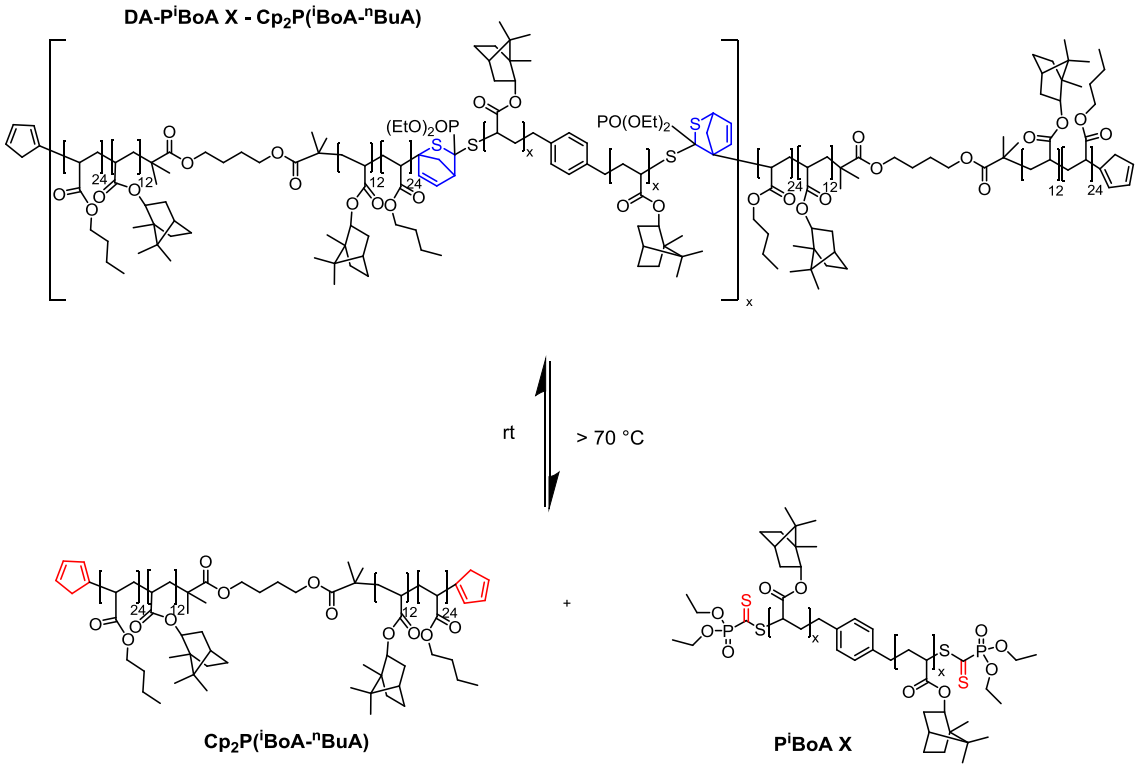

Figure 37: rDA reaction scheme of the DA P^{i}BoA-Cp$_2$(P^{i}BoA-^{n}BuA) (Structure 8 - Structure 10) for investigation of the size effect on the rDA reaction. P^{i}BoA X designates building blocks of different molar mass, ranging from 18900 Da (P^{i}BoA 4, Structure 5) to 55900 Da (P^{i}BoA 7, Structure 7).

For analyzing the polymers at ambient temperature and at elevated temperature the SEC instruments that are described in chapter 3.3.1 were used. At high temperatures two Agilent Mixed-D (5 µm, 300x7.5 mm) columns were used. The molar mass averages of all building blocks and the DA polymers were determined by static light scattering SEC in THF at ambient temperature. The DP_n values are obtained by dividing the molar mass of the DA polymers by the average molar mass of both building blocks. All results are summarized in Table 4:

Table 4: Molar masses of polymers for investigating the effect of size on the rDA behavior of the DA polymer. All molar masses were determined by SEC-SLS in THF at 25 °C. The DP_n of the DA polymers is obtained by dividing their M_n by the averaged the molar mass of both building blocks ($Cp_2P(^iBoA\text{-}^nBuA)$ and the respective P^iBoA).

Component	M_n (g/mol)	DP_n
$Cp_2P(^iBoA\text{-}^nBuA)$	12800	-
P^iBoA 4	18900	-
P^iBoA 6	36200	-
P^iBoA 7	55900	-
DA-P^iBoA 4-$Cp_2P(^iBoA\text{-}^nBuA)$	34100	2.2
DA-P^iBoA 6-$Cp_2P(^iBoA\text{-}^nBuA)$	88800	3.6
DA-P^iBoA 7-$Cp_2P(^iBoA\text{-}^nBuA)$	66000	1.9

The accuracy of the values for M_n and the DP_n of the DA polymers must not be overestimated. As can be seen in Figure 37 the DA polymer consists of a $Cp_2P(^iBoA\text{-}^nBuA)$ and a dithioesther endfunctionalized P^iBoA block. Both blocks are chemically different and contribute differently to the dRI signal due to their dissimilar d*n*/d*c* values. Calculating molar mass averages accurately requires a trustworthy concentration signal but dRI trace of a chromatogram is only proportional to concentration if the d*n*/d*c* of the analytes is constant. Unfortunately high accuracy of the results is required if the size effect is to be determined reliably.

Fortunately, the dRI signal can still be used as a concentration signal at certain positions in the chromatogram, for instance in the lowest molar mass regime: The $Cp_2P(^iBoA\text{-}^nBuA)$ building block is the component of lowest molar mass so that it can be safely assumed that the lowest molar mass region is represented by the $Cp_2P(^iBoA\text{-}^nBuA)$ building block. Hence, determining its concentration from the dRI signal is possible and monitoring the concentration of unbound Cp_2 building block should allow following the rDA progress. Because of the limited separation efficiency of the employed SEC setup the peak area of the $Cp_2P(^iBoA\text{-}^nBuA)$ peak cannot be directly read out of the chromatogram. Mathematical peak

deconvolution helps in this situation and allows deriving the peaks of the individual components. For demonstration the experimentally acquired chromatograms and the deconvolved peaks are displayed in Figure 38 for the DA P^{i}BoA 7-Cp$_2$P(^{i}BoA-^{n}BuA) polymer at ambient temperature in THF and at 100 °C in TCB:

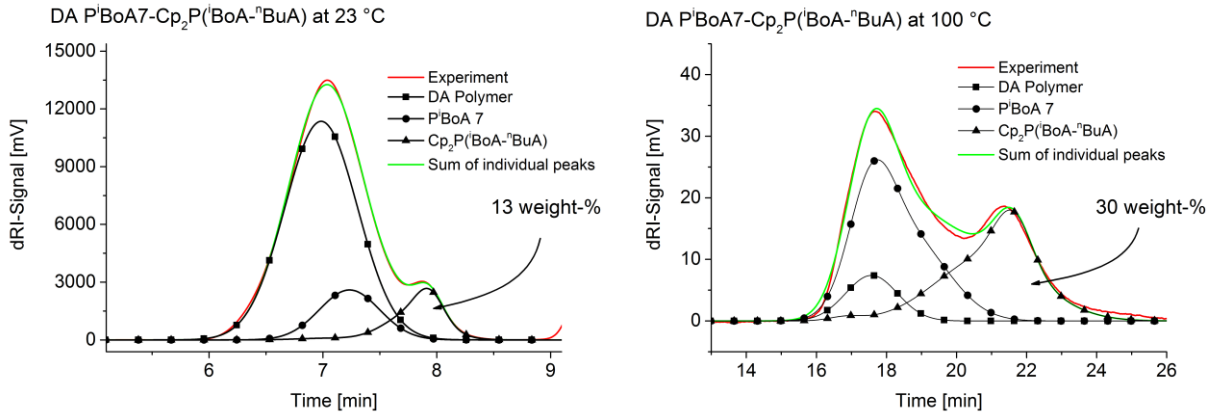

Figure 38: SEC chromatograms of DA P^{i}BoA-7-Cp$_2$P(^{i}BoA-^{n}BuA) acquired at ambient temperature in THF (left) and in TCB at 100 °C (right). The black lines indicate the deconvolved peaks of the individual components. Through a correlation of peak area to concentration the weight concentration of the released Cp$_2$P(^{i}BoA-^{n}BuA) building block can be calculated and is given in both pictures. The obtained values indicate an increase in released building block at 100 °C. (The 100 °C chromatogram was flipped vertically to have it visually better comparable to the ambient temperature measurement.)

The general deconvolution procedure that was described in chapter 3.4.2 works best if as many as possible of the required peak parameters can be determined by measuring reference samples. The procedure for determining the concentration of individual components was as follows:

(1) Collect the chromatograms of the individual building blocks P^{i}BoA and Cp$_2$P(^{i}BoA-^{n}BuA) of known polymer concentration at desired temperature, establish a correlation between peak area and concentration.

(2) Use Gauss functions to fit the chromatograms; multiple overlaying functions can be used if the peaks are asymmetrical. Fix the parameters for peak center and width and correlate the total peak area to the concentration.

(3) Acquire the chromatogram of a DA polymer at desired reaction time and temperature. In a second deconvolution procedure the building block peaks from step (2) and one or two additional Gauss peaks are fitted so that the experimental curve is described best. The center of the theoretical DA peak must be at lower elution volumes than the P^{i}BoA peak and can be varied freely in width.

(4) Calculate the concentration of the free $Cp_2P(^{i}BoA\text{-}^{n}BuA)$ out of the determined peak area and the correlation that was found in step (1).

The left graph of Figure 38 shows that most of the peak area is attributed to the DA polymer, although fractions of both building blocks are present. According to the concentration calibration 13 weight-% of unbound $Cp_2P(^{i}BoA\text{-}^{n}BuA)$ are present in the sample at ambient temperature. At 100 °C (Figure 38, right graph) the fraction of DA polymer is significantly decreased due to the rDA reaction and 30 weight-% of unbound $Cp_2P(^{i}BoA\text{-}^{n}BuA)$ are calculated. For assessing the accuracy of the deconvolution procedure test samples were prepared by mixing known amounts of both building blocks. After calculating the concentrations by acquiring the chromatograms and performing the described deconvolution procedure the results were confronted with the initially used masses of the polymers. Table 5 shows that the results are in good agreement, demonstrating that the procedure can be used for calculating the amount of unbound $Cp_2P(^{i}BoA\text{-}^{n}BuA)$ in DA polymer mixtures.

Table 5: For each $P^{i}BoA$ size a mixture of $P^{i}BoA$ X and $Cp_2P(^{i}BoA\text{-}^{n}BuA)$ of known concentrations was prepared for testing the accuracy of the deconvolution approach. The masses that were calculated by deconvolution of chromatograms of these mixtures (and applying the concentration calibrations) are very close to the true values, thus demonstrating the applicability of the proposed procedure.

	DA $P^{i}BoA$ 4-$Cp_2P(^{i}BoA\text{-}^{n}BuA)$		**DA $P^{i}BoA$ 6-$Cp_2P(^{i}BoA\text{-}^{n}BuA)$**		**DA $P^{i}BoA$ 4-$Cp_2P(^{i}BoA\text{-}^{n}BuA)$**	
	orig. mass (mg)	calc. mass (mg)	orig. mass (mg)	calc. mass (mg)	orig. mass (mg)	calc. mass (mg)
$P^{i}BoA$ X	1.12	1.15	0.83	0.81	1.01	1.04
$Cp_2P(^{i}BoA\text{-}^{n}BuA)$	1.39	1.35	1.03	1.05	1.05	1.06

In the next step the DA polymers of the differently sized $P^{i}BoA$ blocks were measured with TD SEC at temperatures from 80 to 100 °C in a time resolved manner in order to monitor the kinetics of the reaction. The chromatograms of the DA polymer with the smallest and the largest $P^{i}BoA$ block, collected at 80 °C after reaction times up to 120 min are shown in the panels A and B of Figure 39. Both pictures show the trend that during the rDA reaction the high molar mass part of the peaks vanish and that the peak of the $Cp_2P(^{i}BoA\text{-}^{n}BuA)$ at approx. 23 minutes increases in intensity, as more of the building block is released.

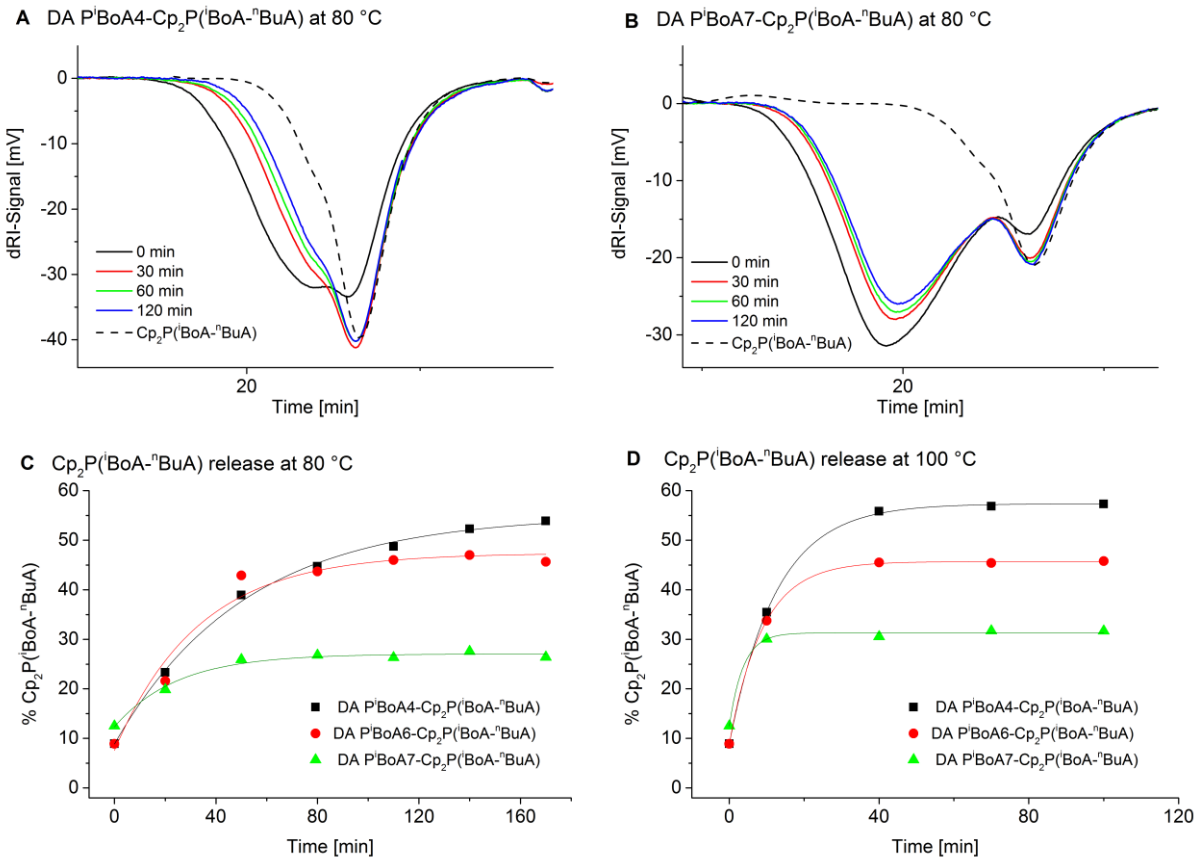

Figure 39: SEC chromatograms of the smallest (P^{i}BoA 4, panel **A**) and largest (P^{i}BoA 7, panel **B**) DA polymer at 80 °C in TCB after different reaction times prior to injection. For comparison the trace of the $Cp_2P(^{i}BoA\text{-}^{n}BuA)$ building block is included as a dashed line. The after deconvolution calculated concentrations of unbound $Cp_2P(^{i}BoA\text{-}^{n}BuA)$ at 80 °C and 100 °C are given in panel **C** and **D**, respectively.

The values for the fraction of unbound $Cp_2P(^{i}BoA\text{-}^{n}BuA)$ as a function of reaction time and building block size are compiled in the panels C (80 °C) and D (100 °C) of Figure 39. The plots show that the rDA reaction reaches equilibrium earlier at 100 °C than at 80 °C. In order to compare the obtained values of the different P^{i}BoA block sizes it is necessary to normalize the fraction of % $Cp_2P(^{i}BoA\text{-}^{n}BuA)$ for all samples according to Equation 45

$$normalized\ \%Cp_2 = \frac{[\%Cp_2(t) - \%Cp_2(t=0)] \cdot 100\%}{[\%Cp_2(max) - \%Cp_2(t=0)]} \qquad \text{Equation 45}$$

, where *%Cp_2(t)* is the weight concentration of the Cp_2 building block at the respective time, *%Cp_2(t=0)* the concentration of the building block before any rDA reaction (measured at ambient temperature in THF), and *%Cp_2(max)* the concentration after maximal conversion. The latter value was calculated by

heating each sample to 120 °C for five hours, where the chromatogram resembles the mixture of both building blocks and no DA polymer fraction is visible, so that 100 % debonding can be assumed.

In Figure 40 the normalized values are displayed as derived from the equilibrium points of the rDA reactions at the various temperatures.

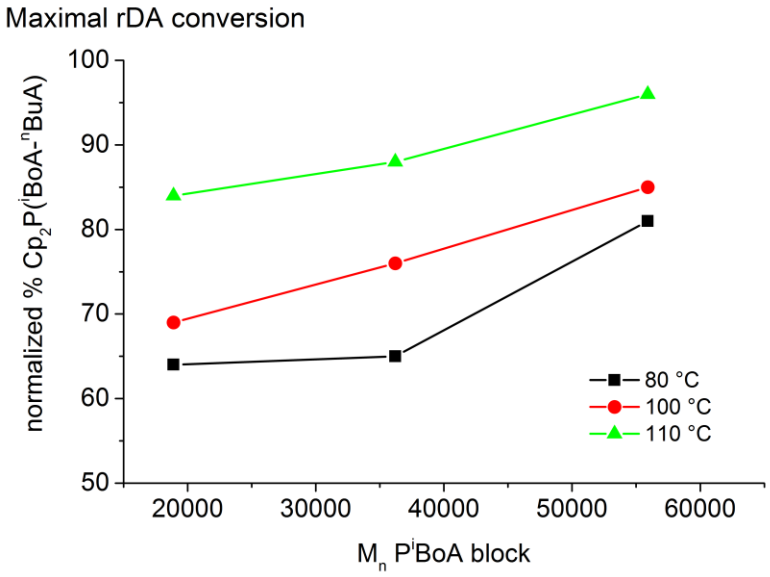

Figure 40: The rDA reaction of all DA P^{i}BoAX-$Cp_2P(^{i}$BoA-^{n}BuA) samples was evaluated at 80, 100 and 110 °C. The highest reached values of release of the $Cp_2P(^{i}$BoA-^{n}BuA) building block were normalized for the individual DA polymer systems in order to obtain values that are comparable to each other. It becomes evident that at each temperature a larger P^{i}BoA building block leads to a higher degree of debonding (more release of $Cp_2P(^{i}$BoA-^{n}BuA)).

The image clearly shows the presence of the proposed effect of the building block size on the rDA reaction, as higher molar masses lead to a higher release of the $Cp_2P(^{i}$BoA-^{n}BuA) building block and, thus, a higher rDA conversion. In other words, it is possible to tune the debonding properties of a thermoreversibly bonding polymer by adjusting the size of the employed components. It is important to keep this effect in mind when reaction concepts are transferred from small molecule studies to polymeric systems, as the size of the polymers is an important parameter for the overall performance of the reactions.

5.2 The effect of polymer flexibility on rDA reactions

After having demonstrated the effect of changing the building block size in a reversibly bonding polymer system the question about the influence of the nature of the polymer backbone came up. Theoretical studies were carried out by the group of Prof. Michelle Coote at Australian National University for estimating the bonding entropy contributions of different model oligomer systems. Methylacrylate (MA), *tert*-butyl acrylate (^{t}BuA), *iso*-butyl acrylate (^{i}BuA) and ^{i}BoA monomers were chosen as representative candidates with different monomer mass and geometry. The calculations treat the molecules as in solution phase and estimate gas-phase vibrational, translational and rotational entropy, as well as the solvation energy contributions. That concept proofed to be accurately enough for estimating qualitative trends.[69] In Figure 41 the results are shown for two different oligomer geometries, namely the lowest energy conformation and an optimized, rather extended conformation that is likely to be more representative for actual polymers.[71]

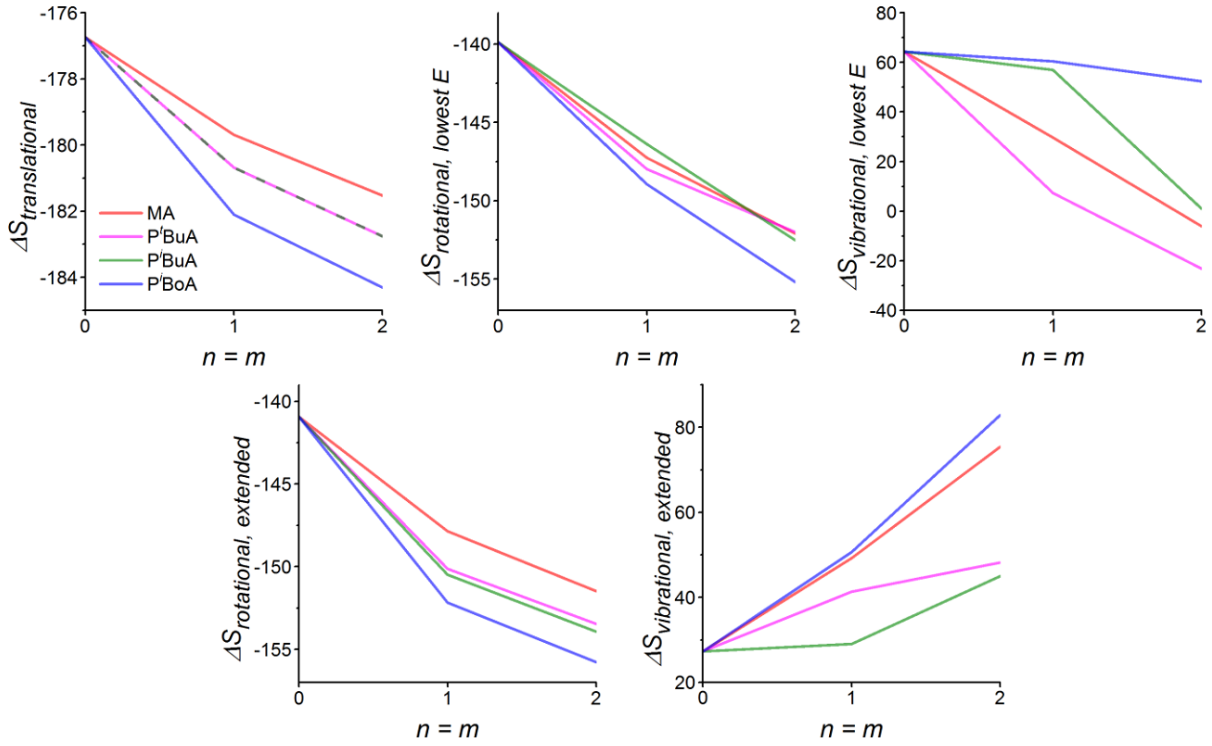

Figure 41: Calculated changes of the individual entropy contributions during a DA bonding reaction. The more negative the *ΔS,* the greater the free energy upon bonding will be. Or, the more negative the *ΔS,* the more debonding will occur at a given temperature. The values for *n* and *m* indicate the chain lengths of the different acrylate oligomers. (Reproduced from Ref.[71], Published by The Royal Society of Chemistry)

The translational entropy, being dependent only on the polymer's mass, indicates that heavier monomers debond easier (more negative ΔS). In that case more mass can be achieved through heavier monomers or increasing the degree of polymerization (m, n). The validity of the effect of the degree of polymerization of the building blocks was demonstrated in chapter 5.1. Both, the rotational and vibrational entropy contributions are sensitive to mass but also to its distribution in the oligomer, *i.e.* the oligomer geometry and, hence, effects of differently constituted monomers with otherwise identical mass can be expected. And in fact, different entropy contributions are calculated for the butyl acrylate isomers ^{t}BuA and ^{i}BuA. The differences are more consistent in the case of the extended conformation that is assumed to resemble larger polymers better. Furthermore the differences are most pronounced for the vibrational entropy contribution, which, in qualitative terms can be referred to the flexibility or chain stiffness of a polymer. The simulation shows a significant difference between the butyl acrylate isomers and makes the heavy ^{i}BoA less debonding than the MA. It seems that the bulky isobornyl substituent renders the molecule less flexible, thus countering its high mass that would otherwise favor the debonding.

For assessing the predicted trends experimentally the rDA reactions of DA polymers with chemically different building blocks but identical DA reaction pairings should be examined. Kai Pahnke prepared a library of DA polymers (Structure 17 - Structure 21), using the HDA-Dilinker (Structure 23) and polymer building blocks of different monomers, but same degree of polymerization of 50 (Structure 11 - Structure 15). The structures and the rDA reaction scheme are shown in Figure 42 and the molar masses are compiled in Table 6. All molar mass averages were determined at the KIT by ambient temperature SEC in THF by relative standard calibration, using KMH parameters. The DP_n was calculated as the quotient of the M_n of the DA polymer and the average molar mass of the Cp_2 building block and the HDA-Dilinker.[71] The P^{i}BoA and PMA backbones were chosen to represent a very stiff and a very flexible backbone, respectively. Unfortunately both are very different in their monomer mass, too, so that the stiffness effect cannot be studied isolated. For that purpose the three butyl acrylate monomers were added, as they have the same mass but different size of their side groups and, thus, different chain flexibility.

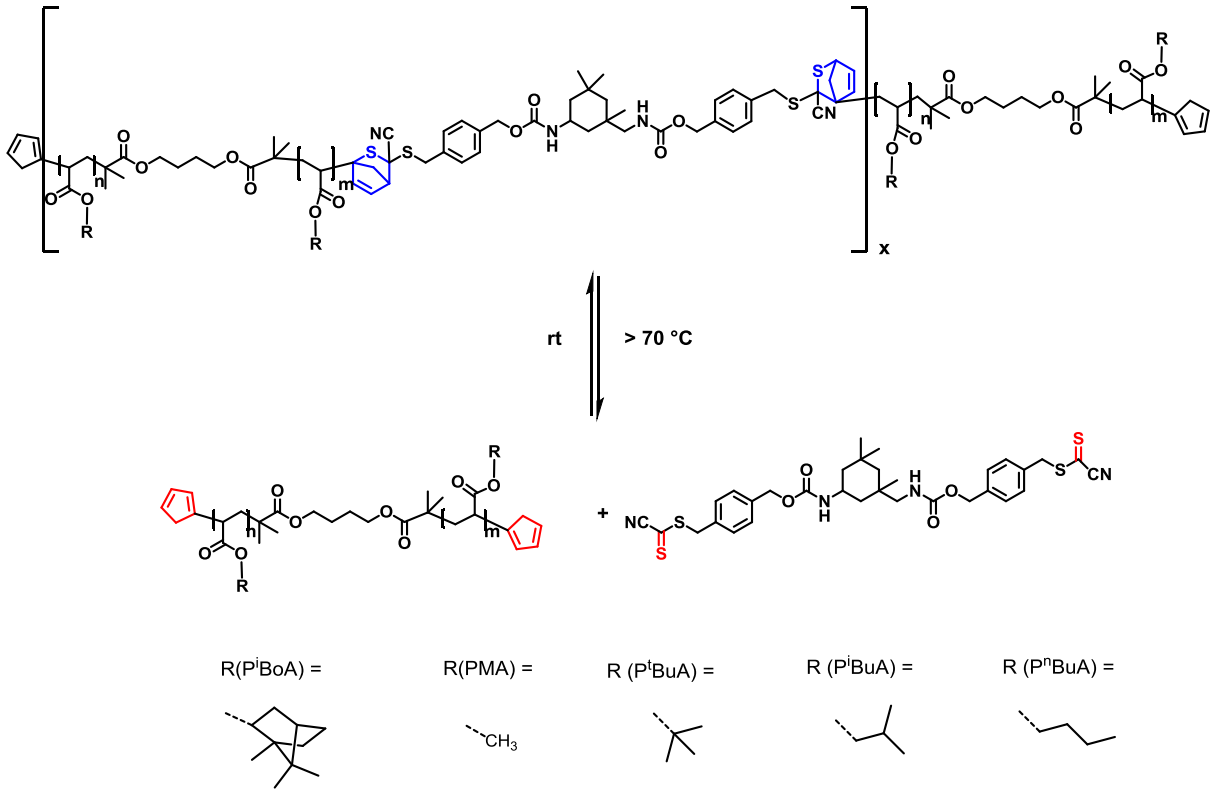

Figure 42: rDA reaction scheme of the DA polymer systems (Structure 17 - Structure 21) that were used as model systems for studying the effect of polymer flexibility on the rDA behavior. Therefore five different building blocks (P^{i}BoA, PMA, P^{t}BuA, P^{i}BuA and P^{n}BuA, Structure 11 - Structure 15) with different flexibilities but same size (DP_n = 50) were employed. In all cases the building blocks are connected by the HDA-Dilinker (Structure 23).

Table 6: Molar masses of the polymer building blocks and their corresponding DA polymers, as determined by SEC in THF and relative standard calibration (see chapter 3.1 for further details). The DP_n of the DA polymers is calculated by dividing the M_n of the DA polymer by the average molar mass of the HDA-Dilinker and the respective Cp_2 building block.

	M_n (Cp_2 building block)	M_n (DA polymer)	DP_n
PMA	4800 g/mol	17300 g/mol	6.3
P^{i}BoA	10200 g/mol	34200 g/mol	6.3
P^{n}BuA	6700 g/mol	20600 g/mol	5.6
P^{i}BuA	7000 g/mol	22400 g/mol	5.8
P^{t}BuA	6700 g/mol	22700 g/mol	6.2

The employed HDA-Dilinker is very reactive and allows the DA reaction with Cp at ambient temperature in the absence of catalysts within few minutes. Responsible for the high reactivity is the highly electron-withdrawing character of the cyano group neighboring the dithioester. It renders the C=S

double bond highly reactive but, on the other hand, makes the entire molecule prone to side reactions, such as dimerization.[72] Therefore the cyanodithioester (CDTE) is trapped with Cp during the synthesis and needs to be heated in order to release the Cp before any DA reaction with the actual building blocks can occur. The deprotection scheme is shown in Figure 43:

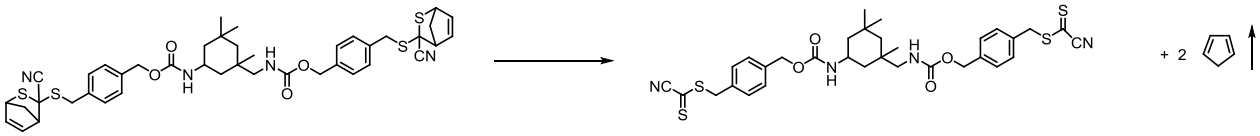

Figure 43: Deprotection scheme of the employed HDA-Dilinker (Structure 23). At ambient temperatures the CDTE is trapped with Cp, rendering it stable. If a DA reaction with another diene is desired the linker has to be heated to > 100 °C in order to release and evaporate the Cp. Upon cooling the CDTE can react with any other available diene.[72]

At this point it is important to address the question about the exact definition of a polymer's flexibility. For a very first impression about the flexibility of a polymer the glass transition temperature (T_g) was used. In theory, a more flexible polymer should reach the glass transition at lower temperatures. Table 7 summarizes the T_g values of the polymers under investigation, taken from literature. Although the T_g of a polymer is somehow connected to the flexibility of the polymer chains it is important to keep in mind that the T_g is a bulk material property, and does not necessarily describe well the circumstances of dissolved polymers.

Table 7: Glass transition temperatures of the investigated polymers as reported in literature (determined by mechanical tests). The values give a first idea about the trend of the flexibility of the polymers, assuming that a lower T_g corresponds to a less flexible backbone.

Polymer	T_g [°C]	Ref.
PMA	8	[178]
P^{n}BuA	-54	[178]
P^{i}BuA	-24	[179]
P^{t}BuA	43	[180]
P^{i}BoA	95	[180]

According to the T_g values P^{i}BoA is the least and P^{n}BuA the most flexible polymer in that set. Among the butyl acrylate isomers the stiffness seems to increase in the order ^{n}BuA, ^{i}BuA, ^{t}BuA, indicating that the increasingly bulky side group makes the polymer backbone less flexible.

As the rDA reactions are always performed in solution it was necessary to gain further insights about the polymer stiffness on a molecular level. The following chapter discusses supplementary experiments that were performed for that purpose.

5.2.1 Assessment of the polymer flexibility

Describing the flexibility of a polymer by the means of a simple parameter is difficult. One often used quantity for measuring a polymers flexibility on molecular scale (*e.g.*, in solution) is the persistence length l_p that can be determined from SANS measurements (see chapter 2.6.3). A set of polymers was measured by SANS at the ILL at Grenoble for determining the persistence length. In Figure 44 the scattering curves of $P^{i}BoA$ and $P^{n}BuA$ after subtraction of the solvent are displayed in a double logarithmic plot:

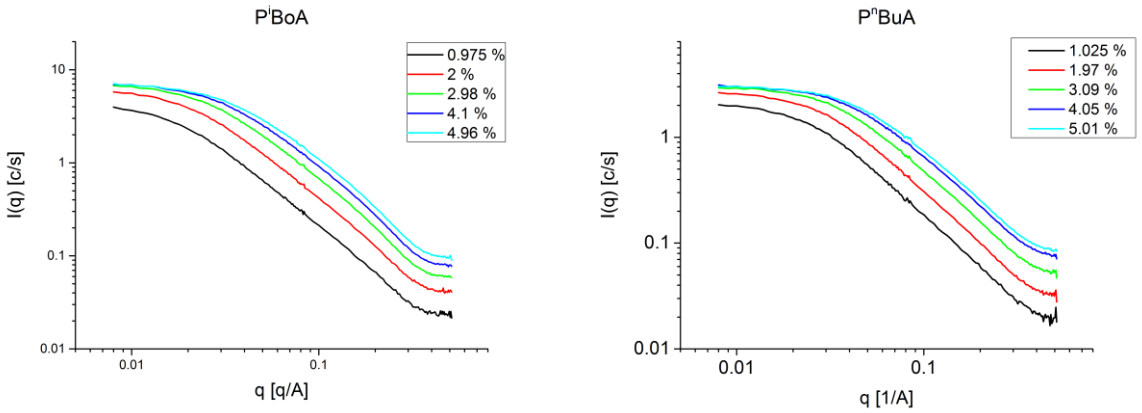

Figure 44: Raw scattering curves of $P^{i}BoA$ (left) and $P^{n}BuA$ (right) displayed double logarithmically. The SANS experiment was carried out in toluene-d_6 at a neutron wavelength of 6 Å. For each samples concentrations of approx. 1-5 wt.-% were used.

In Figure 45 the resulting form factors are displayed for $P^{n}BuA$, derived according the procedure described in chapter 2.6.3. For comparison the normalized scattering intensities are shown, too. The graph clearly shows that the form factors that were derived from the individual concentrations collapse well into one line, confirming the effectivity of the applied evaluation protocol.

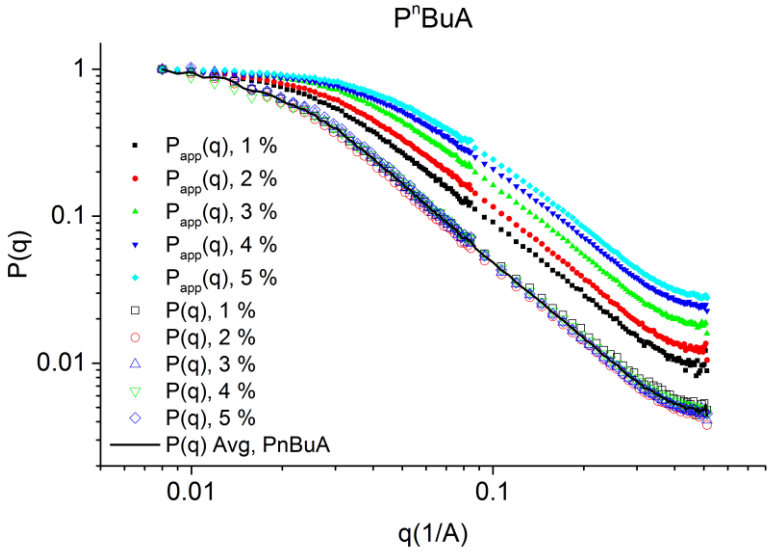

Figure 45: Apparent and true form factors of P^{n}BuA at different concentrations. The derived true form factors of the different concentrations collapse nicely into one line, demonstrating that the evaluation procedure reliably estimates the true form factor at finite concentrations.

For the final Casassa-Holtzer plots, the derived *P(q)* are multiplied with the M_w ($I_{norm}=P(q)*M_w$), then multiplied with q and finally divided by π. The M_w of the polymers was determined by SEC-SLS in THF (see chapter 3.2); the results are summarized in Table 8:

Table 8: Absolute molar masses of the in SANS investigated polymers as determined by SEC-SLS in THF (25 °C).

Polymer	M_n (g/mol)	M_w (g/mol)
PMA	36200	41300
P^{i}BoA	69500	89000
P^{n}BuA	34600	37400
P^{i}BuA	38300	41600
P^{t}BuA	39600	46500

Two exemplary Casassa-Holtzer plots are displayed in Figure 46 (A) and (B), together with the determination of q^* and, hence, l_p through performing linear regressions in the area of the coil-to-rod transitions. The plots of P^{i}BuA and P^{t}BuA can be found in Figure 99 (A) and (B) in chapter 11.2 of the appendix. The curves display the expected shape (see Figure 17 in chapter 2.6.3), except the upturn in the high q range that is visible in all of the curves. The upturn must not be overestimated, however, as the scattering curves are not corrected for incoherent scattering and the scattering contribution of the

monomers. Both phenomena can impact the scattering curves in the high *q* range. In the case of the PMA no good fit could be done because the data were noisier than for the other polymers, especially in the region of the coil-to-rod transition. For the other polymer samples reasonable fits could be established for identifying *q** and calculating l_p; the results are summarized in Table 9.

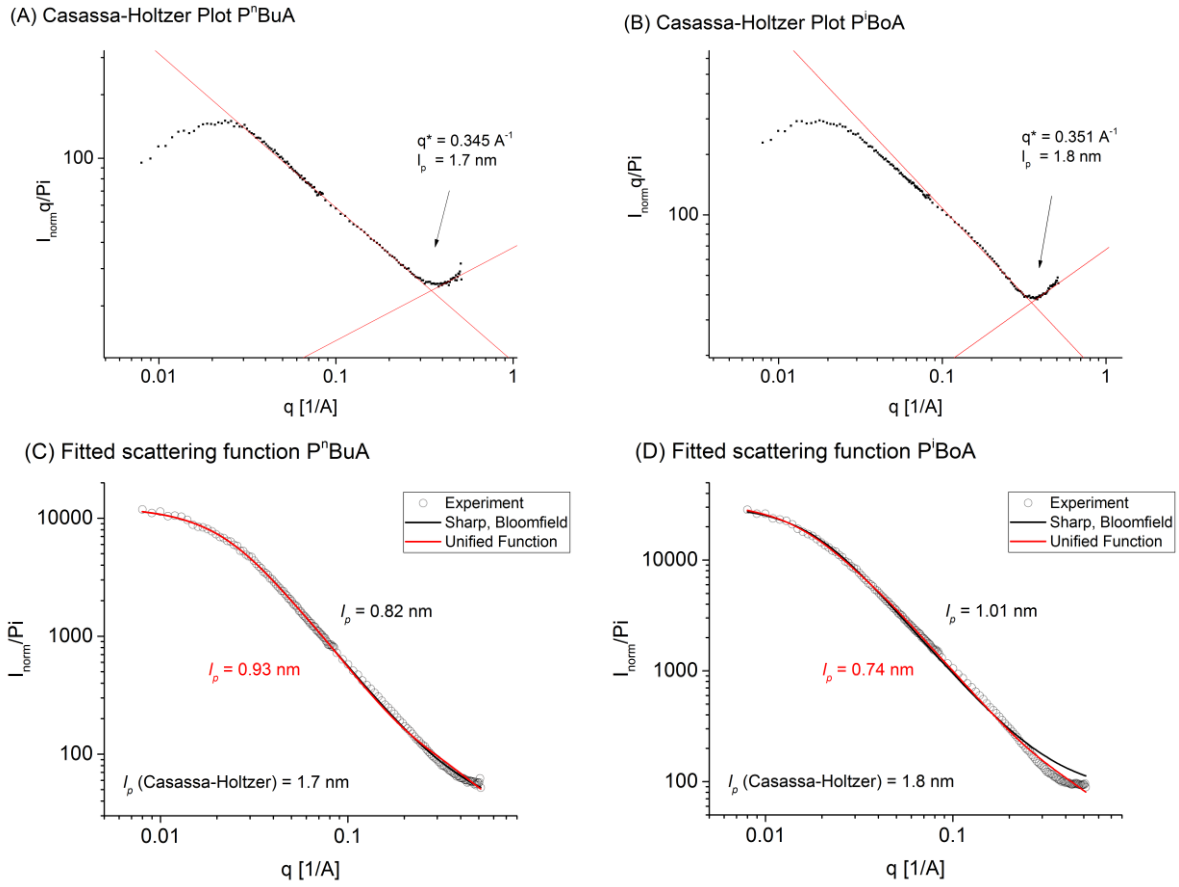

Figure 46: Casassa-Holtzer plots of P^{n}BuA and P^{i}BoA, including the persistence length determination (A, B). The crossover between coil- and rod-like behavior and, thus, l_p is determined purely graphically. In panel (C) and (D) the according to two different models fitted scattering intensities are displayed that yield l_p as an optimized parameter.

The graphical approach is easy to perform but suffers from inherent inaccuracies, as a gentle transition has to be identified as precisely as possible. In order to obtain more data for a more reliable evaluation the scattering curves were fitted by two individual model functions that were described by Beaucage et al.[143] The "Sharp-Bloomfield Global Function" and the "Unified Function" allow fitting the entire scattering curve with three and four parameters, respectively. One of these parameters is l_p, so that the persistence length is obtained through the fitting procedure. In the graphs (C) and (D) of Figure 46 the resulting fits for P^{n}BuA and P^{i}BoA are shown exemplary, the figures of the other polymers are

shown in Figure 99 (C), (D) and (E) in chapter 11.2 of the appendix. The fits work relatively well for describing the scattering functions but do not properly represent their shape at the high-*q* end. In Table 9 all results from the persistence length determination are summarized and confronted with the T_g values:

Table 9: Comparison of the different measures of polymer flexibility: Glass transition temperatures (T_g, from literature) confronted to persistence lengths (l_p, determined by SANS and obtained after graphical evaluation of the form factor (Casassa-Holtzer plot) and fitting the entire scattering curve according to the Sharp-Bloomfield model and the unified function):

Polymer	T_g (°C)	l_p (nm) Casassa-Holtzer	l_p (nm) Sharp-Bloomfield	l_p (nm) Unified Function
PMA	8	-	1.31	1.26
P^{i}BoA	95	1.8	1.01	0.74
P^{n}BuA	-54	1.7	0.82	0.91
P^{i}BuA	-24	1.8	0.85	0.85
P^{t}BuA	46	2.2	1.48	1.68

At first sight the values of l_p determined in the Casassa-Holtzer plot and by fitting the scattering curves differ significantly from each other. The values obtained from fitting the scattering curves are significantly lower than the graphically determined. Furthermore the results of both fit models differ from each other, too. Beaucage et al. found the results of the unified function to be more reasonable, as this model accounts more accurately for the persistence regime.[143] It is interesting, however, to observe that the differently determined persistence lengths represent the same trend: Among the isomers P^{n}BuA, P^{i}BuA and P^{t}BuA the persistence lengths support the trend that was expected by the T_g values and also the "bulkiness" of the side group. Where the l_p of P^{n}BuA and P^{i}BuA are relatively close together the l_p of P^{t}BuA is significantly higher, thus indicating a less flexible polymer backbone.

Putting P^{i}BoA and PMA into the picture is more difficult. The persistence length of the PMA indicates that it is less flexible than P^{t}BuA but more flexible than P^{i}BuA, P^{n}BuA and even P^{i}BoA. Hence, the trend agrees to the trend of the T_g values, except for the P^{i}BoA. The l_p of P^{i}BoA is surprisingly low, indicating it to be approximately as flexible as P^{i}BuA and P^{n}BuA, which does not coincide with the expectations. Looking again into figures (B) and (D) of Figure 46 shows that the scattering curve of P^{i}BoA features an unusual kink at *q = 0.2 Å* that might influence the evaluation in this region, which is close to the region of

*q**, unfortunately. As a consequence the determination of l_p might not be reliable in this particular example.

In Figure 47 the results from the SANS evaluation are confronted with the T_g values from literature. Both characteristics represent the flexibility of a polymer from different perspectives and it cannot be expected that a bulk state parameter (T_g) translates directly into a molecular dimension of dissolved polymers (l_p). The comparison was done anyways for testing if similar trends can be observed.

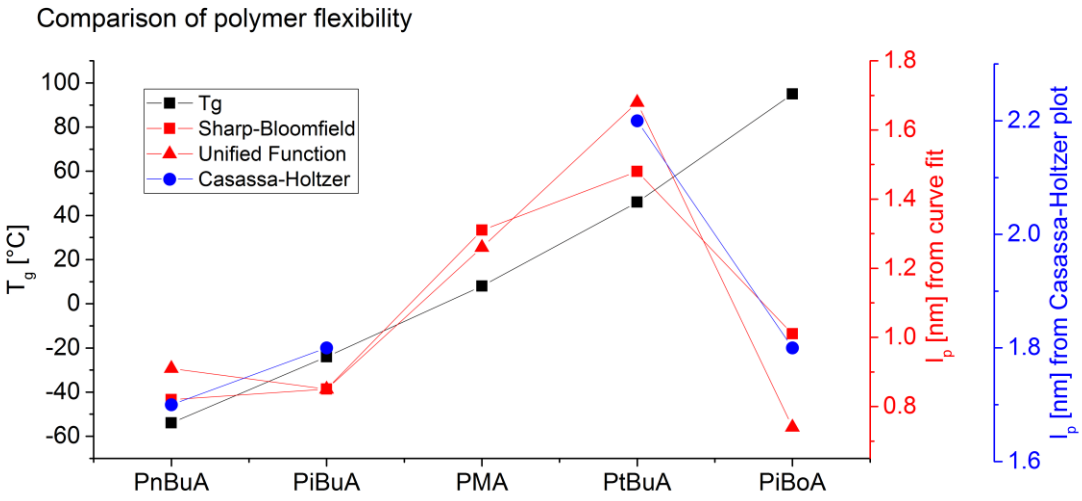

Figure 47: Measures of flexibility of the investigated polymer building blocks in graphical comparison. The T_g values are taken from literature, the l_p values were determined by SANS and obtained after graphical evaluation of the form factor (Casassa-Holtzer plot) and fitting the entire scattering curve according to the Sharp-Bloomfield model and the unified function. The l_p values of P^{i}BoA appear unrealistically low.

The graph shows that the trend of polymer flexibility that was indicated by the T_g values is represented relatively well by the determined persistence lengths, except for P^{i}BoA. This finding furthermore questions the reliability of the through SANS determined persistence length of P^{i}BoA. On the other hand the image supports the determined l_p of PMA as it appears to be in a reasonable dimension compared to the T_g values.

On further parameter that needs to be taken into account when discussing the persistence lengths of polymers is the thermodynamic quality of the applied solvent. In the case of a good solvent the polymer coil swells in the solvent and the incorporated solvent molecules lead to a stretching of the polymer backbone, thus increasing the persistence length. Vice versa, in a bad solvent the polymer minimizes solvent-polymer interactions by displacing the solvent molecules and coiling up tighter, resulting in an effectively decreased persistence length. Fortunately the thermodynamic quality can be determined out of the calculated form factors of the polymers. In the coil region (low *q*) the form factor decreases by a

power law of the negative fractal dimension (d_{frac}), as shown in Figure 48. Converting d_{frac} into the Flory exponent ($\nu = 1/d_{frac}$) allows evaluating the thermodynamic quality of the solvent and, thus, gives further insights. The Flory exponent ν ranges from 0.33 for very compact structures to 1 for rigid rods, with a value of 0.588 for random coils in a good solvent.[126]

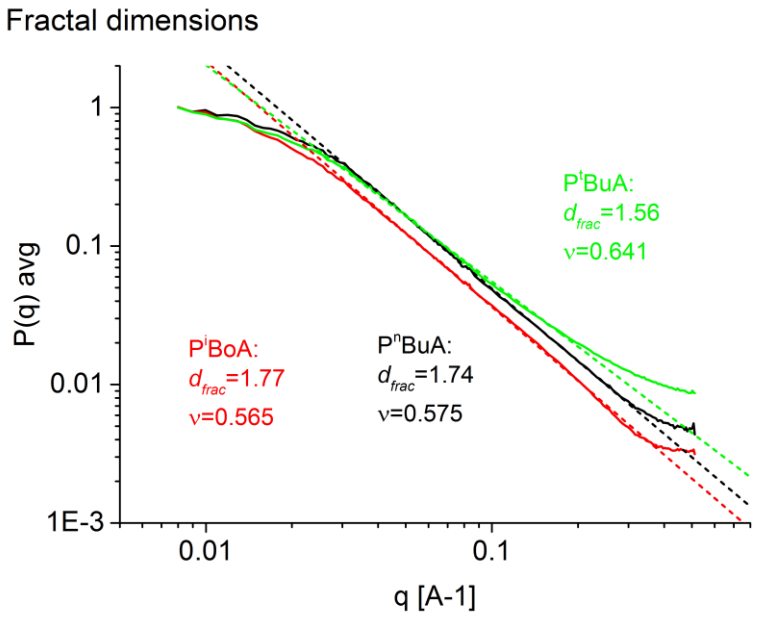

Figure 48: Averaged form factors of P^{i}BoA, P^{t}BuA and P^{n}BuA, respectively, indicating their fractal dimension (d_{frac}) and the corresponding Flory exponents (ν). P^{i}BoA and P^{n}BuA show the behavior of random coils in a good state of dissolution (ν = 0.588), whereas P^{t}BuA appears to be in a slightly worse state of dissolution.

The fractal dimension of P^{t}BuA is lower than of the other polymers (P^{i}BuA and PMA behave similarly, as displayed in Figure 100 in the appendix). The resulting ν is very close to the limit of a random coil in a good solvent in the case of P^{i}BoA, PMA, P^{i}BuA and P^{n}BuA, indicating that these polymers are swollen very well in toluene. Then the conformation of the backbone is mainly influenced by the presence of attached solvent molecules and the effect of the side groups is suppressed. In the case of the P^{t}BuA the ν is slightly higher (0.641). The higher ν hints towards a more elongated structure, which coincides with the finding of a higher persistence length.

The herein reported data show that assessing the flexibility of polymers is a difficult task. Interpreting the obtained results and evaluating their reliability is possible only with limitations. Further SANS experiments would be very valuable, especially in different solvents. Due to the different interactions between solvent and polymer segments different persistence lengths can be expected. Unfortunately the effect of the solvent on l_p could not be investigated with SANS further, as more experiments weren't

granted. The potential of viscosity measurements as a supplementary technique was tested but unfortunately the results did not appear in a completely consistent manner (see appendix chapter 11.3). Nevertheless the obtained results show that the polymers under investigation are characterized by different flexibilities and, thus, should be suitable for investigating the effect of polymer flexibility on the rDA reactions.

5.2.2 Investigating the stiffness effect by TD SEC

The evaluation of the in Figure 42 shown polymer systems has to be approached similarly to the DA polymer system that was investigated in chapter 5.1 for assessing the effect of polymer size. Again two different components react together to form the DA polymer and, vice versa, are released upon temperature increase. But instead of two different polymer building blocks one polymer building block and one small HDA-Dilinker are employed. In that case the chemical difference between both components is more pronounced than in the case of two building blocks with similar chemical constitution. As a consequence the detector responses of both substances have to be expected to be significantly different from each other, making the evaluation of the dRI signal difficult. Furthermore different interactions of the analytes with the column material can occur.

And in fact the first TD SEC experiments indicated enthalpic interactions between the HDA-Dilinker and the ResiPore column, when TCB was used as the solvent. In the absence of enthalpic interactions the HDA-Dilinker should elute slightly before the solvent peaks, as the molecule is relatively bulky (800 g/mol in its Cp protected form). The experiment showed, however, that the HDA-Dilinker elutes together with the solvent peaks. Irrational elution times were observed when measuring the DA polymers, too. In the left graph of Figure 49 chromatograms of DA PMA are shown at 90 °C after 0 min (black line) and 225 min (red line) heating prior to injection. A shift of the peak towards higher elution times is observed, as the rDA reaction splits the DA polymer and releases molecules of the building block and the HDA-Dilinker. Consequently the peak after 225 min (red) should correspond to the peak of the pure PMA building block, which is not the case as demonstrated by the respective reference chromatogram (dashed line). Polymer degradation as a cause for the higher elution time of the rDA product could not be evidenced because the position of the building block in the chromatogram did not change with different heating times. Heating the building block to high temperatures (> 150 °C) did not change the position of its peak either. Hence, it is more probable that the surprisingly high elution time of the DA PMA is associated with enthalpic interactions, rather than too low molar masses. The result could be explained if the building blocks after the rDA reaction were still connected to one or two HDA-Dilinker molecules that lead to additional retention.

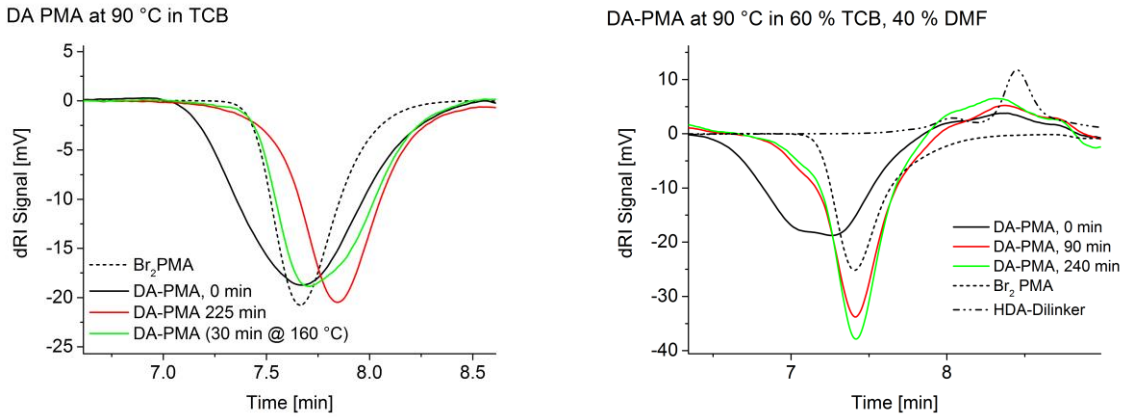

Figure 49: Left: SEC chromatograms of DA PMA at 90 °C in TCB after different times prior to injection. After 225 min at 90 °C the DA PMA elutes later than the Br_2PMA building block due to enthalpic interactions of the HDA-Dilinker with the column material. Only after additional heating to 160 °C the linker gets split off and the peaks of DA PMA and Br_2PMA converge. Right: The same situation when performing the TD SEC in a mixture of 60 % TCB and 40 % DMF at 90 °C. Due to the more polar solvent character the enthalpic interactions of the HDA-Dilinker are suppressed and the peak of DA PMA and Br_2PMA positions match.

For testing this hypothesis the very same DA polymer sample was heated for additional 30 minutes to 160 °C. The corresponding chromatogram is displayed as the green line in the left graph of Figure 49. A partial backshift of the peak towards lower elution times can be observed and the peak begins to converge to the shape of the building block. An additional experiment carried out at 140 °C showed that the peak position and shape of the building block is obtained after rDA reaction directly at this temperature (Figure 103 in appendix chapter 11.1), again disproving thermal degradation as a cause for the higher elution times of the rDA outcome and, thus, supporting the hypothesis that the rDA reaction yields block-linker combinations in the first instance and only at higher temperatures the pure building blocks are released. A more in-depth description and interpretation of this effect is discussed in chapter 5.3. At this point the practical implications for carrying out the TD SEC experiments are of higher relevance because it is necessary to be sure about the nature of the separation mechanism in order to interpret the obtained chromatograms correctly.

The cause of the different retention behavior of the acrylate building block and the HDA-Dilinker lies in their very different polarity. The building block is of average polarity, whereas the HDA-Dilinker appears to be significantly more polar. Consequently the HDA-Dilinker tries to minimize the interactions with the rather unpolar TCB eluent by favoring interactions with the column material. Conversely, increasing the polarity of the solvent should suppress the enthalpic interactions between column surface and the HDA-Dilinker. An incrementally increased polarity of the SEC eluent was achieved by mixing TCB

and *N,N*-Dimethyl formamide (DMF) in different volume ratios and carefully flushing the entire SEC with the new eluent at very low flor rates. At each ratio, the HDA-Dilinker, the PMA building block and the DA PMA were measured at 90 °C in order to watch out for the in the previous paragraph described effects of additional retention. As shown in the right graph of **Figure 49** at a eluent composition of 40 % DMF in 60 % TCB no further indications for enthalpic interactions are observed: the HDA-Dilinker elutes slightly prior the solvent peaks and the peak of the DA PMA after rDA reaction appears to elute according to size and corresponds well to the peak of the PMA building block.

Working with a mixed solvent was in this case the easiest accessible solution for controlling the enthalpic interactions and, thus, the separation mechanisms. However, one disadvantage of employing mixed solvents in LC is that preferential solvation can occur, where the polymers tend to accumulate one component of the solvent mixture preferentially in its proximity. As a consequence the local composition of the solvent mixture is effected by the presence of the polymers and each analyte can be present in slightly different solvent compositions.[99,181,182] In order to avoid preferential solvation it is better to work with pure solvents but in the present case no suitable solvent with a sufficiently high boiling point was found. Another strategy would be a modification of the column materials, but such means require decent knowledge and were not chosen to be practical for the purpose of the current analyses.

After having found convenient separation conditions the in chapter 3.4.2 described deconvolution procedure was applied for evaluating the chromatograms. In Figure 50 an exemplary chromatogram of DA P^{n}BuA, acquired at 110 °C is shown, including the calculated peaks for the DA polymer, the building block and the HDA-Dilinker. The latter one always appears as a set of peaks at the end of the chromatogram and it was not possible to fully elucidate the reason for that. Due to its high reactivity the HDA-Dilinker might react with the solvent or impurities. Especially the DMF with its hygroscopic character was suspected to lead to chemical degradation of the HDA-Dilinker. Acquiring ^{1}H spectra of the (protected) HDA-Dilinker before and after heating it to 120 °C in DMF for 120 min did not indicate significant changes in the chemical structure of the HDA-Dilinker, however (see Figure 104 in Appendix chapter 11.1).

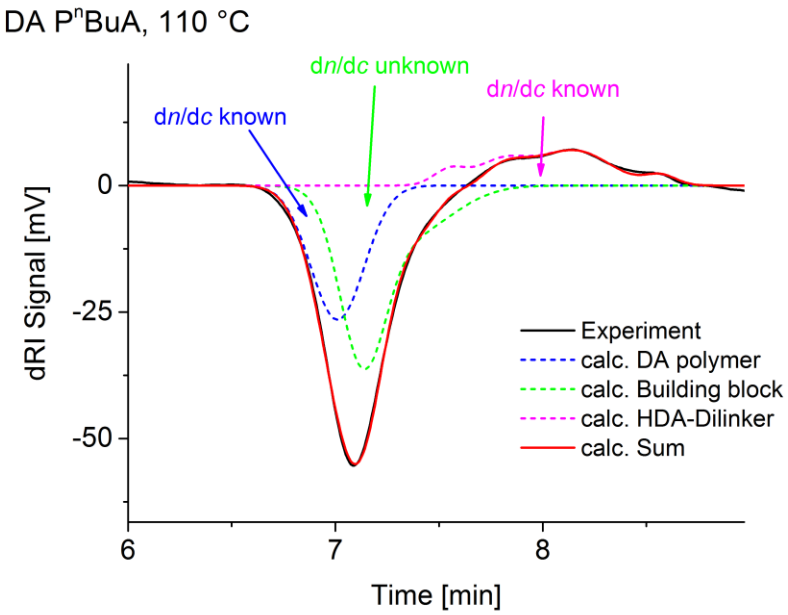

Figure 50: SEC chromatogram and deconvolved peaks of DA P^{n}BuA at 110 °C. Due to the unknown chemical composition (Building block plus x HDA-Dilinker with x = 0, 1, 2) and the thereby unknown d*n*/d*c* of the polymer in the middle of the peak the dRI signal cannot be used as a reliable concentration signal.

For the evaluation of the chromatogram it is important to be aware of the chemical nature of the individual peak areas, namely DA polymer, building block and HDA-Dilinker. A correlation of peak area to analyte concentration could be done for the pure HDA-Dilinker and the pure building block. But the latter one is not suitable for evaluating the peak area of the "building block" in the chromatograms of the DA polymers because in this setup it is not possible to distinguish by their retention times a building block from a building block with one or two HDA-Dilinker still attached. The detector response, however, changes significantly if a block is with or without a HDA-Dilinker because the block has a negative d*n*/d*c* and the HDA-Dilinker a positive one. Consequently the peak area of the building block cannot be converted into concentration in these experiments. It is, however, possible to evaluate the peak area of the DA polymer. Since building block and HDA-Dilinker are present in the DA polymer in a constant stoichiometric ratio of 1:1, the corresponding d*n*/d*c* can be estimated according to Equation 47, taking into account the weight-fraction of HDA-Dilinker (*FracLinker*) present in the DA polymer (Equation 46). Measuring the d*n*/d*c* directly at the given conditions is not possible because the rDA reaction would start immediately at the high temperatures.

$$FracLinker = \frac{M(Linker)}{M(Linker) + M_n(Building\ Block)}$$ Equation 46

$$\left(\frac{dn}{dc}\right)_{DA\ Polymer} = FracLinker \cdot \left(\frac{dn}{dc}\right)_{Linker} + (1 - FracLinker) \cdot \left(\frac{dn}{dc}\right)_{Building\ Block}$$ Equation 47

The corresponding d*n*/d*c* values were determined in terms of “contrast values” as the ratio of peak area to concentration of reference measurements of the individual components that were acquired under identical conditions at the same day to ensure best comparability of the obtained values. The term “contrast value” is used in order to avoid confusion with accurately determined d*n*/d*c* values. Those would require measuring samples of different dilution at each temperature. Because of low amounts of available samples it was chosen to measure only one concentration of each sample and to simply correlate the peak area to the concentration. After determining the contrast factors of the DA polymers their concentration in the rDA chromatograms can be determined and converted into *%DA Polymer Decrease* according to:

$$\%\ DA\ Polymer\ Decrease = 100\ \% - \frac{\left(\frac{c(DA\ Polymer)_{rDA,T}}{c(DA\ Polymer)_{0,T}}\right)}{FracDAPolymer_{RT}} \cdot 100\ \%$$ Equation 48

In this equation $c(DA\ Polymer)_{rDA,\ T}$ is the calculated concentration of the DA polymer at temperature *T* and after a certain extent of rDA reaction, $c(DA\ Polymer)_0$ the initial concentration of the DA polymer at the same temperature and $FracDAPolymer_{RT}$ the weight fraction of DA polymer in the respective sample, determined at ambient temperature in THF (prior to any rDA reaction). Calculating the *% DA Polymer Decrease* of samples of the different DA polymers allows comparing the extent of the rDA reactions. The value is insensitive to any rDA reactions that lead to the release of individual HDA-Dilinker molecules and, consequently, does not represent the entire rDA reaction process. It is basically possible to perform the same procedure with the peak area of the released HDA-Dilinker in order to calculate the amount of free HDA-Dilinker that was released during the rDA reaction. Evaluating the peak area of the HDA-Dilinker is less accurate because of its generally lower peak area and its proximity to the solvent peak that makes it more sensitive to baseline corrections. Hence, the area of the DA polymer was chosen for monitoring the progress of the rDA reactions.

In the left graph of Figure 51 chromatograms of DA P^{t}BuA after different rDA reaction times at 80 °C are shown.

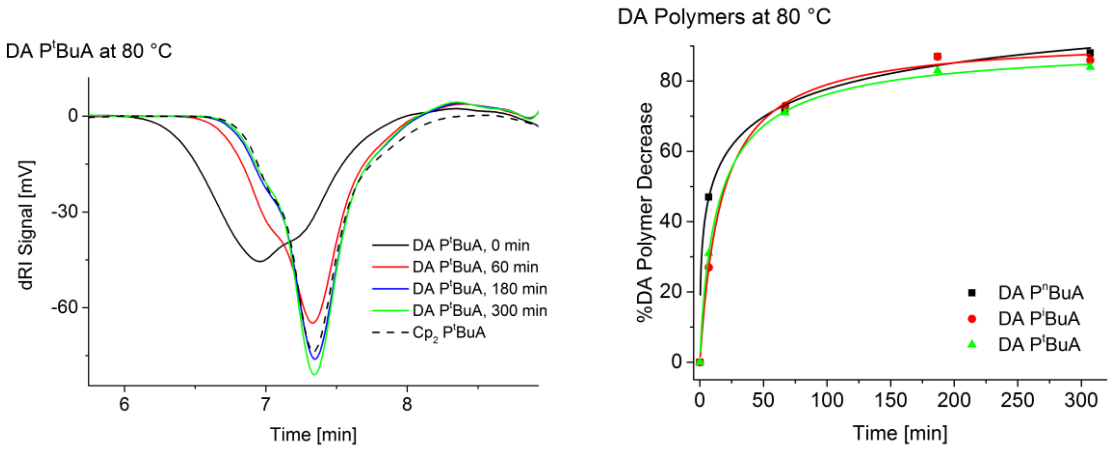

Figure 51: SEC chromatograms of DA P^{t}BuA at 80 °C in 60 % TCB, 40 % DMF after various rDA reaction times prior to injection (left) and the calculated *% DA Polymer Decrease* of the DA PBuA isomer samples at the same temperature (right).

Clearly the majority of decrease of the DA polymer happens in the first 60 minutes of the rDA reaction and then the change in DA polymer concentration levels off. The corresponding values of *%DA Polymer Decrease* of the PBuA isomer samples are displayed in the right graph of Figure 51. The plot shows that for all three PBuA samples relatively similar behavior is found, although a slight tendency for higher *%DA Polymer Decrease* is found for the DA P^{n}BuA, which is expected to be the most flexibly polymer. For each sample an equilibrium *%DA Polymer decrease* was calculated by averaging the last values of highest reaction time, were no further change in the DA polymer concentration could be observed. In the left graph of Figure 52 the equilibrium *%DA Polymer Decrease* is plotted for the PBuA samples.

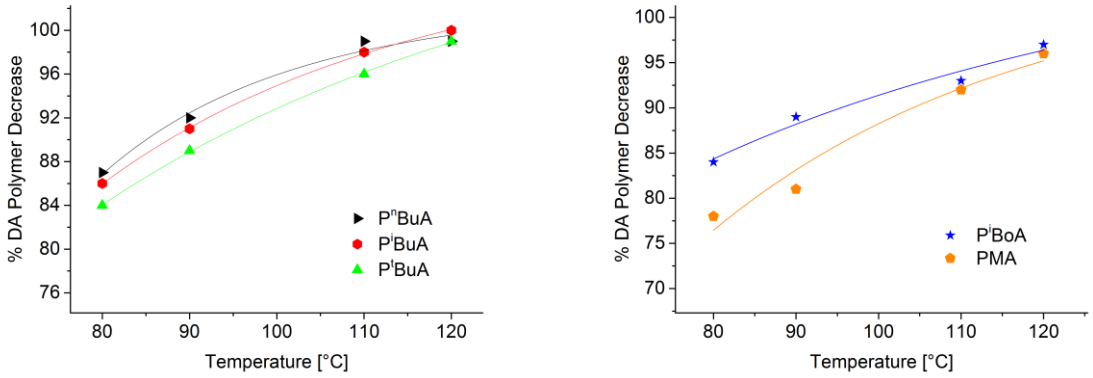

Figure 52: Equilbrium *%DA Polymer Decrease* values of the PBuA sample set (left) and P^{i}BoA and PMA (right) as a function of the rDA temperature.

The data compares the extent of the rDA reaction for three DA polymers consisting of building blocks of identical mass and degree of polymerization, yet different flexibility. At first sight the values are very close together, especially when taking into account an experimental error of 1-2 %. They display a continuous trend, however, in which the highest *%DA Polymer Decrease* is examined for P^{n}BuA, followed very closely by P^{i}BuA and eventually P^{t}BuA. Interestingly the trend of flexibility that was found in the previous chapter can be seen again in the SEC results: P^{n}BuA and P^{i}BuA are very close together, whereas P^{t}BuA was found to be significantly less flexible.

The magnitude of the stiffness effect appears to be smaller than of the size or mass effect, as demonstrated by the right image of Figure 52, where the *%DA Polymer Decrease* is compared for the P^{i}BoA and the PMA. Although the determination of the persistence lengths of PMA and P^{i}BoA showed some ambiguities it is most likely that the P^{i}BoA is significantly less flexible than the PMA. Hence, more *%DA Polymer Decrease* would be expected for the PMA, which is clearly not supported by the obtained data. The opposite finding can be explained by the already confirmed effect that a heavier polymer building block promotes more debonding, compared to a lighter one. Since P^{i}BoA is of significantly higher molar mass than PMA (7300 g/mol compared to 3100 g/mol) the mass effect overcompensates the stiffness effect.

Further experimental corroboration of the stiffness effect was achieved by Kai Pahnke at the KIT by temperature dependent NMR measurements of the same set of DA polymers. Following the *Degree of Debonding* through the signal ratio of protons of free Cp endgroups and the corresponding DA cycloadducts demonstrated the highest *Degree of Debonding* for the DA P^{i}BuA, closely followed by DA P^{n}BuA and finally DA P^{t}BuA.[71] The order of P^{i}BuA and P^{n}BuA is inversed to the trend found by TD SEC, which can be attributed to the different solvents that were employed: The TD SEC experiments were carried out in a mixture of 40 % DMF and 60 % TCB, whereas the TD NMR investigations were performed in toluene-d_8. As a consequence the thermodynamic quality of the solvents is most likely relatively different in both setups and, thus, can influence the phenomenon of flexibility of the dissolved polymers. The SANS experiments were carried out in toluene-d_8, too, and indicated highest flexibility for P^{n}BuA, followed by P^{i}BuA and P^{t}BuA as well. In that case the experiments were performed at ambient temperature, however, and consequently do not have to represent the situation at significantly higher temperatures.

The effect of polymer stiffness is, thus, a further possibility for fine tuning the behavior of a reversibly bonding polymer system. Its magnitude is more difficult to predict than the effect of polymer size or mass, though, because of its dependency on the employed solvent. How these systems behave in bulk state could not be assessed until now and still remains to be investigated. Varying the chemical nature of

a polymer backbone in order to access a different flexibility often coincides with modifying the mass of the backbone, too, which can lead to rather complicated interplay of the different entropy effects.

In the end the investigated effects shall allow predicting qualitative trends but also shall sensitize for the complexity of the topic and the consequential necessity for experimental proof in any specific case. The validity of the established concepts could be shown to be true for supramolecular associations as well and is considered to be universally applicable for all types of reversible ligation chemistry.[75,148]

5.3 Where macromolecules cleave

The observation of enthalpic interactions between the analytes and the column material in the previous chapter lead to more detailed insights about preferred positions for chain scission in polymer science. Having confirmed experimentally the effect of size and stiffness on the rDA behavior the question came up if the very same mechanisms also promote a certain selectivity towards cleaving a DA bond in the middle or in the end of a polymer chain, when multiple positions are possible. First theoretical considerations were carried out by the group of Prof. Michelle Coote (ANU) on a simplistic model of a linear chain polymer consisting of point masses with two distinct cleaving positions, as shown schematically in Figure 53.[148]

Figure 53: Polymer model for calculating entropy contributions for when the chain is cleaved in the middle or at the end. The masses for *A* and *B* and the bond lengths r_A and r_B are of arbitrary, but realistic dimensions. Adapted from Ref.[148]

The translational and rotational reaction entropy contributions for breaking the bond in the middle and in the end were calculated according to standard textbook equations. In contrast to the reaction enthalpy and the vibrational entropy the translational and rotational entropy contributions are sensitive to the distribution of the masses (*i.e.*, the architecture of the polymer) and less dependent on the chemical nature of the local ligation side.[71,148] The net ΔS_{trans} and ΔS_{rot} for the debonding reaction in the middle and at the end that were calculated for three different polymers: At first for the polymer shown in Figure 53 with the **initial** parameters $m_A = m_B = 10\ Da$ and $r_A = r_B = 10\ Å$, then for a **longer** version with $r_A = 150\ Å$ and finally for a **heavier** version with m_A increased to 1500 *Da*. In all three cases higher ΔS values were calculated for cleavage in the middle than for cleavage in the end, indicating that the latter

case is energetically less favored. Furthermore the preference for the cleavage in the middle becomes more pronounced if the model polymer was made longer or heavier.[148]

Verifying these predictions experimentally is not trivial, as many analytical techniques are reliable in detecting *how many* bonds are formed or cleaved but remain insensitive in detecting *where* these events occurred. The TD SEC experiment, however, enabled observing exactly this particularity, as discussed in the previous chapter and demonstrated in Figure 49 at the example of DA PMA. At 90 °C the chromatograms showed that mainly building block-linker combinations were released and significantly higher temperatures were necessary to release the HDA-Dilinker and to obtain the chromatogram of the isolated building block. Distinguishing an individual building block from a building block with a HDA-Dilinker attached was possible through the additional retention of the HDA-Dilinker molecules due to its enthalpic interactions with the column material.

Analyzing the selectivity for bonding or debonding sites in terms of the rDA reaction instead of the DA reaction comes with the advantage that, in contrast to the bonding reaction, the debonding reaction does not occur under diffusion control. Because in the DA reaction both reaction partners need to move towards each other for initiating the bonding event it would not be surprising to find higher reaction rates for the association of a smaller and a larger molecule, compared to two larger molecules because of their usually lower mobility. In the rDA case, however, the reaction can occur anytime and diffusion can be eliminated as an influencing parameter.

In Figure 54 the hypothesized course of the reaction is shown schematically:

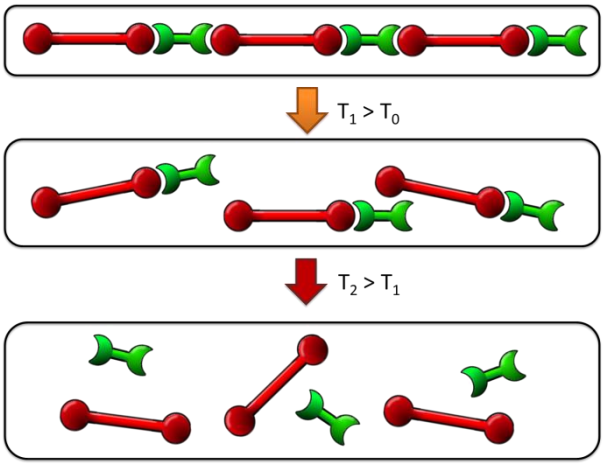

Figure 54: Schematic illustration of the DA PMA cleaving in the middle at T_1 and at a higher temperature T_2 at the end.

The upmost polymer shows the DA PMA as prior to any rDA reaction. Ambient temperature SEC experiments showed that, in average, each DA polymer consists of three building blocks and, consequently, at least two HDA-Dilinkers. In Table 10 all possible block-linker combinations are listed that are expected to be present during the rDA reaction. For each combination the number of bonds that lead to a decrease in molar mass and number of bonds that leads to the release of a free HDA-Dilinker molecule are indicated. Furthermore the average probability that a free HDA-Dilinker is released by a rDA event without significantly decreasing the molar mass is given for each "degree of polymerization" (*i.e.*, DA polymer with three, two or one building block).

Table 10: Possible combinations of building block and HDA-Dilinker and corresponding number of bonds that can be cleaved for releasing a HDA-Dilinker molecule or decreasing the MM. In the last column the probability that a random bond cleavage leads to the release of a HDA-Dilinker molecule is indicated.

N° Building Block	N° HDA-Dilinker	N° bonds releasing HDA-Dilinker	N° bonds decreasing MM	% bonds for HDA-Dilinker release	Avg. % bonds for HDA-Dilinker release
3	2	0	4	0	
3	3	1	4	20	**18**
3	4	2	4	33	
2	1	0	2	0	
2	2	1	2	33	**28**
2	3	2	2	50	
1	0	0	1	0	
1	1	1	1	50	**39**
1	2	2	1	67	

Assuming that the cleavage of the DA bonds occurs randomly without any preference would implicate that 18 % of rDA events would cause the release of a HDA-Dilinker, if DA polymers with three building blocks are present. For a higher rDA conversion the average size of the DA polymer decreases so that they contain only two or three building blocks. Therefore the probability that a random bond scission event releases a free HDA-Dilinker increases 28 % and 39 %, respectively.

These simple calculations show that, following the traditional concept of random chain scission, a significant amount of HDA-Dilinker should be released when the average DP_n of the DA polymers decreases. How much of the HDA-Dilinker is released in praxis was investigated in a second experiment after having upgraded the TD SEC instrument with an online UV detector. The HDA-Dilinker absorbs strongly at a wavelength of 386 nm and, consequently, can be detected very sensitively. The corresponding experiment was performed in TCB at the example of a DA PS polymer (Structure 22). PS is very well soluble in TCB and, in contrast to the HDA-Dilinker, does not experience any interactions with the column material. The DA PS was prepared by Kai Pahnke in analogy to the DA polymers shown in

Figure 42, resulting in an M_n of the building block and the DA polymer of 5500 g/mol and 21000 g/mol, respectively. At this molar mass three to four building blocks are present in the DA polymer and, hence, the considerations discussed above can be applied for this DA polymer, too. **Figure 55** shows the normalized dRI signal of the DA PS after 0 min (black line) and 60 min (red line) at 80 °C, superimposed to the chromatogram of the Cp_2 PS building block (dashed line). As in the case of the DA PMA higher retention times of the rDA products are obtained than for the isolated building block. Heating the sample for further 60 min at 140 °C (green line) leads to a narrower peak but only heating the sample to 160 and even 180 °C (blue line) makes the polymer elute earlier so that the peak maximum matches the position of the building block, thus demonstrating that the HDA-Dilinker molecules were split off the building blocks.

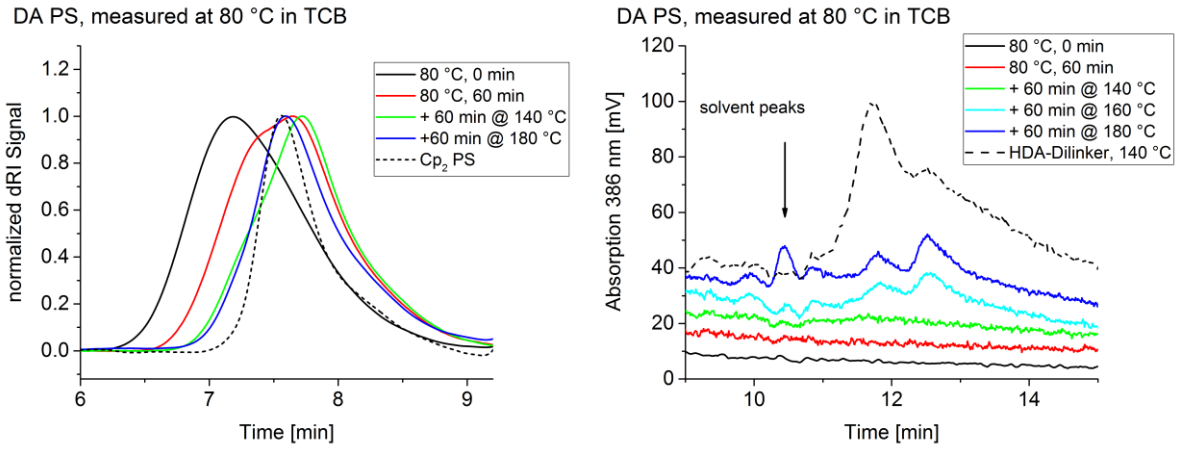

Figure 55: Normalized dRI signal (left) and stacked UV absorption traces (right) of the DA PS system, acquired by TD SEC at 80 °C in TCB. The left image indicates that high temperatures (>140 °C) are required for splitting of the HDA-Dilinker as the DA PS elutes later than the Cp_2PS at lower temperatures due to enthalpic interactions between HDA-Dilinker and column material. The right image corroborates this finding by demonstrating that only at temperatures higher than 140 °C the released HDA-Dilinker can be found.

More information can be extracted from the UV absorption traces, shown in the right graph of Figure 55. The black dashed line indicates the chromatogram of the pure HDA-Dilinker. It shows that the HDA-Dilinker absorbs nicely and results in intense peaks, also at low sample concentrations (approx. 0.5 mg/mL). Enthalpic interactions between HDA-Dilinker and column material are again indicated as the HDA-Dilinker elutes at very high elution times *after* the solvent peaks, despite its relatively large chemical structure. The chromatograms of the DA PS, however, do not exhibit any HDA-Dilinker peaks at 80 °C and only a very small peak at 140 °C. Only after having heated the sample to 160 and 180 °C the characteristic HDA-Dilinker peaks can be observed. But even at the high temperatures the HDA-Dilinker

peak area is significantly smaller than of the control sample, which is of approximately the concentration that corresponds to the concentration of HDA-Dilinker in the analyzed DA polymer.

That finding once more supports the hypothesis that the cleavage of the DA polymers occurs preferentially in the middle and that releasing small molecules at the end of a chain requires more energy. This effect means conversely that a bonding reaction where two large fragments are connected is less favored than a bonding reaction where a small molecule is being added to a larger one. Furthermore, the effect of molecule size and mass on the reaction's equilibrium constants should be less pronounced when a small molecule is added to a larger one (*i.e.,* in a chain growth polymerization) than when two larger molecules react together, as in a step growth polymerization. And in fact it was shown that propagation rate constants of radical polymerizations become chain length independent at relatively low molar masses (< 1000 g/mol)[183,184], whereas the in this work performed analyses showed measurable effects of polymer size, mass and stiffness on the characteristics of step growth reactions up to significantly higher molar masses of 60,000 Da.

In analogy to the previously described entropy effects, also the preferred chain cleavage in the middle is expected to be observable for any kind of bonding or debonding reactions, irrespective of its exact nature. And indeed, the preferred chain cleavage in the middle was observed for supramolecular assemblies, too.[148]

5.4 Demonstration of DA reversibility

Demonstrating the effect of different physicochemical properties of the polymers on their debonding behavior is an important aspect for the practical design of new materials. Another substantially important aspect is the reversibility of the DA reactions – especially in the case of self-healing materials.

For testing the reversibility of a DA reaction both pathways have to be investigated: the forward (DA) reaction at ambient temperatures and the reverse (rDA) reaction at high temperatures. For an effective *in situ* analysis the corresponding experiments would have to include measurements at low and high temperatures, too. What can be done easily with small batch instruments (as in the case of DLS, see chapter 8.1.2) is problematic in TD SEC. Quick changes in temperature are critical for the detectors and especially the columns. As a consequence it is not possible to directly monitor both, the DA *and* the rDA reactions of a given DA polymer without putting extreme stress to the entire SEC instrument. However, if the rDA reaction is not too quick the reversibility can be assessed by TD SEC in a rather indirect way:

1) A sample of the DA polymer is measured directly at high temperature and the progress of the rDA reaction is evaluated as discussed in the previous chapters.
2) After a certain time the sample is again measured at the same temperature and some progress in the rDA reaction should be visible.
3) The sample vial is taken out of the (heated) autosampler and cooled down to ambient temperature where the DA forward reaction is occurring to a certain extent.
4) After letting the DA reaction proceed until equilibrium the sample is again put into the TD SEC and step 1 to 3 are being repeated. The results of each cycle are compared to each other.

If the DA reaction is nicely reversible similar results will be obtained for multiple cycles in the first two steps, for instance 10 % debonding for step 1 and 50 % debonding for step 2.

That procedure was used to show the reversibility of an amphiphilic block copolymer (Structure 28) in which two polymer blocks (Structure 26 and Structure 27) are connected by a DA bond. In Figure 56 the corresponding reaction scheme is shown. All substances were synthesized by Marcel Langer at the KIT.

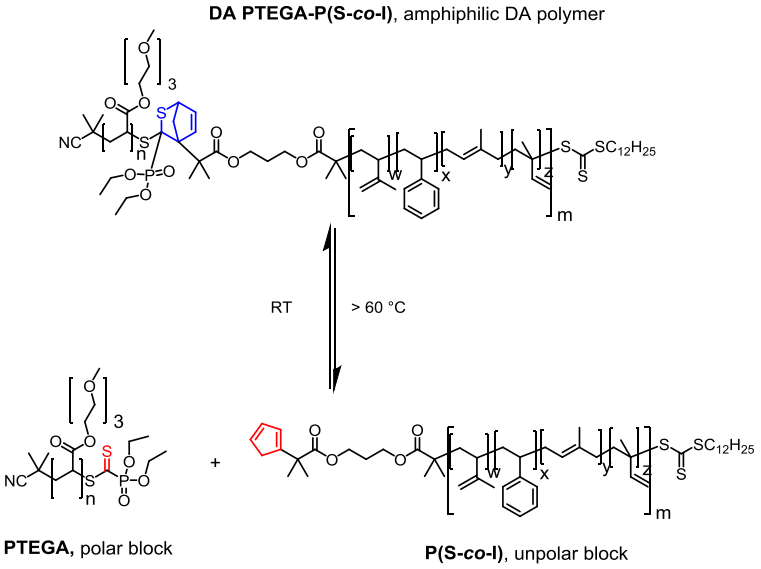

Figure 56: rDA scheme of the amphiphilic DA PTEGA-P(S-*co*-I) (Structure 28), giving the polar PTEGA block Structure 26) and the unpolar P(S-*co*-I) block (Structure 27)**.**[149]

For the nonpolar block an isoprene and styrene were copolymerized in an RAFT polymerization, so that the resulting polymer is terminated with Br at the one and with the RAFT function at the other side. In a post modification step the Br is transformed into a cyclopentadiene (cp) endgroup via a nickelocene reaction to give the P(S-*co*-I) polymer with a molar mass of approx. 9200 g/mol. Separately triethylene

glycol methyl ether acrylate (TEGA) is polymerized via RAFT to give the TEGA block with a molar mass of approx. 6600 g/mol. This time, however, the RAFT endgroup has an electron withdrawing phosphoric ester Z-group that renders it more reactive as a dienophile. Both polymer building blocks are ultimately reacted together at ambient conditions in presence of $ZnCl_2$ as a catalyst to give the DA polymer, for which an M_n of 16000 g/mol was determined.[149] The amphiphilic block copolymer can find application for the preparation of nanostructured materials, as it will undergo phase segregation on the scale of the size of the building blocks. Since the linkage between both blocks is thermoreversible interesting possibilities for controlled phase segregations can get accessible.[185]

The thermoreversible behavior of DA PTEGA-P(S-*co*-I) was assessed by TD SEC at 90 °C in TCB on a ResiPore column. Chromatograms of DA PTEGA-P(S-*co*-I) are shown in Figure 57; the left graph shows the situation when the sample is directly injected without any prior heating and the right graph after 30 minutes of prior heating. Again the rDA reaction is expected to be relatively quick so that we cannot expect to see 100 % bonding in the left image but a mixture of bonding and debonding products.

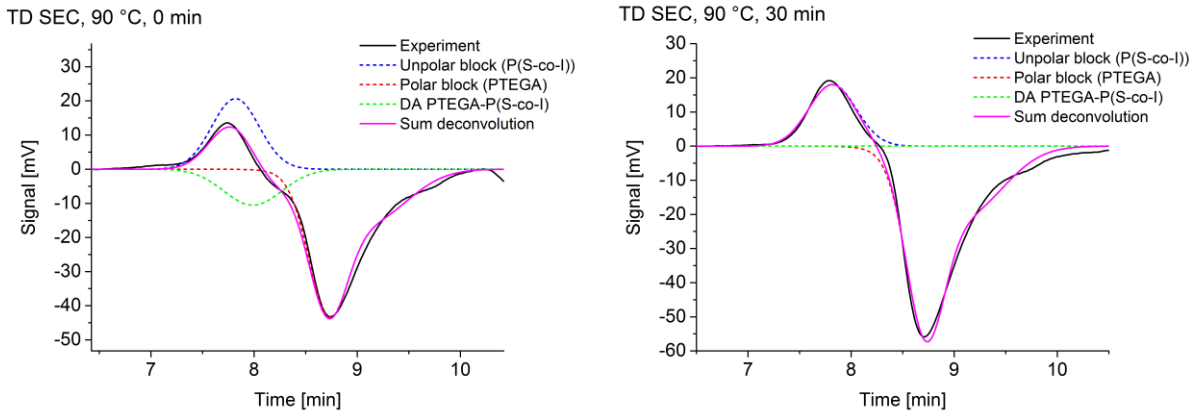

Figure 57: Chromatograms of DA PTEGA-P(S-*co*-I) at 90 °C in TCB, acquired after 0 min (left) and 30 min (right). The black line shows the experimentally obtained dRI signal, the blue, red and green dashed lines the calculated peaks for the unpolar block (P(S-*co*-I)), the polar block (PTEGA) and the DA PTEGA-P(S-*co*-I), respectively.

The left chromatogram shows a positive peak at approx. 7.8 min, a negative peak at approx. 8.6 min and a small negative shoulder between both. After 30 minutes (right chromatogram) we still see the positive and the negative peak but the small shoulder seems to have vanished. These observations do not really coincide with the expectation of a high molar mass polymer (low elution volumes) that turns into two smaller building blocks (higher elution volumes). For understanding the chromatograms we have to recapitulate two particularities of the present DA polymer:

1) The DA polymer consists of one 6.6 kDa and one 9.2 kDa building block and has an M_n of approx. 16 kDa (only one DA bond per molecule). The difference in molar mass from DA polymer to released building blocks is consequently relatively low and no large changes in elution volume can be expected (separation range of employed ResiPore column is 1000 g/mol up to 1-2 million g/mol).
2) Both building blocks are similar in molar mass but very different in their chemical composition. Different polarities can lead to enthalpic interactions with the column material. The present combination of ResiPore column with the unpolar TCB works well for unpolar polymers but can lead to non-ideal SEC behavior with polar analytes as we have seen already in chapter 5.2.2 and chapter 5.3.

With these facts in mind we can understand the chromatograms: The first peak can be assigned to the unpolar block and the last peak to the polar block that is retained more due to its high polarity. Both blocks are present in a 1:1 ratio in the DA polymer and are released simultaneously so that their concentration should be equal. Since we observe two peaks with different sign and peak area we can conclude that the d*n*/d*c* for the unpolar block is positive and for the polar block negative, but with a higher magnitude. Consequently the d*n*/d*c* for the DA polymer is expected to be slightly negative, and indeed we can see the small shoulder in the left chromatogram of Figure 57 that disappears in the right chromatogram as the rDA reaction proceeds further. Obviously the separation is driven by enthalpic interactions so that the peaks do not appear according their size but according their polarity: At first the unpolar P(S-*co*-I) block, than the averagely polar DA polymer and eventually the polar PTEGA block. Peak deconvolution was applied to derive the theoretical peaks for all three components and the results are displayed in Figure 57 as dashed lines.

The best test for these hypothesis would be to measure the individual building blocks, calculate their d*n*/d*c* and estimate the d*n*/d*c* for the DA polymer at given conditions. Unfortunately only the P(S-*co*-I) block was accessible as a reference substance. Its chromatogram is depicted in Figure 58 (grey dashed line) and it corresponds nicely to the first peak, thus supporting the indicated peak assignment. The other traces in the left graph of Figure 58 show the DA polymer in the course of three cycles: Each solid line represents a “0 min” sample; the black one the first one, the red one after the first and the green one after the second repolymerization at ambient temperature. The dashed lines show the corresponding traces after 30 minutes at 90 °C.

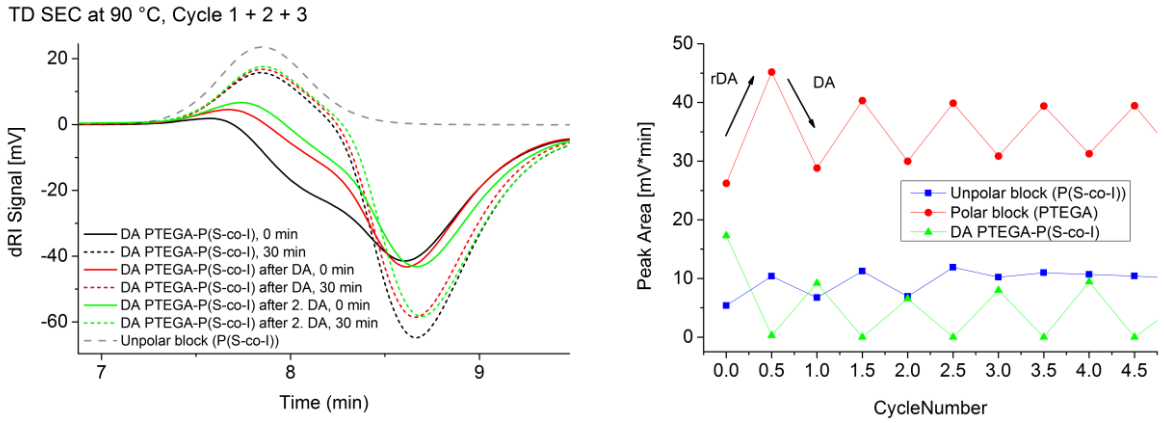

Figure 58: Left: SEC chromatograms of the DA PTEGA-P(S-*co*-I) in TCB at 90 °C during three heating/cooling cycles. The chromatogram acquired after 0 and 30 min are shown for each cycle. The sample was kept at ambient temperature for five days between each cycle. Right: Plot of the peak area of the individual components during multiple DA/rDA cycles, indicating good reversibility of the DA/rDA reaction.

We can see that in all three cycles the "0 min" sample exhibits the DA polymer shoulder at approx. 8 min retention time that vanishes in the "30 min" samples, whereas the peak of the unpolar block appears and the peak of the polar block increases in intensity. The individual peaks were calculated by peak deconvolution as mentioned above and the resulting peak areas are plotted as a function of cycle number in the right graph of Figure 58. The alternating appearing and disappearing of the DA polymer peak and the simultaneous increase and decrease of the peak areas of the polar and unpolar block demonstrate the reversibility of the DA polymer system, although the magnitude of the reaction seem to decrease with increasing cycle number. A peak area – concentration correlation could not be established, as the polar block was not available as an individual sample. Consequently the peak areas cannot be converted for calculating the degree of bonding, but the reversible pattern of the evolution of the peak areas indicates reversibility for at least four cycles.

The shown example demonstrates that the TD SEC concepts can be applied even if the enthalpic interactions of the analytes are becoming the main driving force for the separation. It shall be noted that the fact that only one DA reaction center is possible per DA polymer facilitates the interpretation of the data significantly.

6 TD HPLC of DA polymer systems

As demonstrated in the previous chapters it is not always possible to avoid enthalpic interactions of the analytes with the column material, especially if the investigated polymer system comprises chemically different substances. With certain assumptions the peaks can be assigned to distinct components and the peak areas can be calculated and correlated to concentrations but a proper evaluation of the retention times is not possible with trivial SEC interpretation. At this point it might be worth looking into the area of interaction chromatography, where enthalpic interactions are desired and can be properly assessed. The field of interaction chromatography is broad and applying the concepts to polymer analytics a particular challenge.[117]

6.1.1 Isocratic vs. gradient elution HPLC

At first it had to be tested what kind of HPLC was the most suitable for the present analytical task. Therefore two experiments were performed for demonstrating the in chapter 2.5 mentioned differences between isocratic and gradient elution in praxis. All HPLC experiments were performed in the laboratories of Prof. Peter Schoenmakers at Universiteit van Amsterdam (UvA). At first a mixture of narrowly distributed standards of PMMA, PBMA and PS with approx. 50 kDa was prepared and analyzed. At first the isocratic approach was tested by mixing ACN and THF in different ratios and testing the separation on a C_{18} functionalized HPLC column. The left graph in Figure 59 shows the resulting chromatogram when 48 % THF are mixed with 52 % ACN. All three polymers can be assigned to the three peaks and according to their elution order PMMA appears to be the most polar polymer, followed by PS and finally PBMA as the most unpolar. The separation power is not very good, however, as the peaks are not baseline separated and the PBMA peak is very broad. Increasing the fraction of strong solvent by just 1 % to 49 % makes the PBMA peak a lot sharper but PMMA and PS would coelute without any separation. On the other hand, decreasing the THF content by just 1 % to 47 % leads to a nice separation of PMMA and PS but no elution of PBMA, as the elution power of the solvent is too weak. That behavior demonstrates the extremely high sensitivity of an isocratic experiment with polymers – separating three different substances with sufficient separation efficiency can already be impossible. Little changes in the solvent composition can already have a significant effect and can lead to poorly reproducible results, as also shown by the fact that the peaks of the mixture do not completely coincide with the peaks of the reference samples.

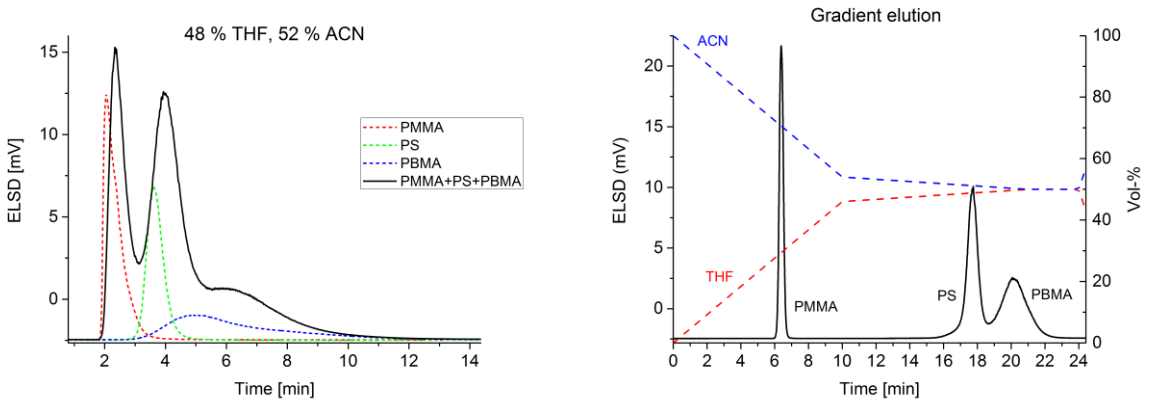

Figure 59: Left: Isocratic separation of PMMA, PS and PBMA. Right: Gradient elution separation of the same polymer mixture. The dashed lines show the programmed solvent gradient (*i.e.*, solvent composition at the pump).

At this example the advantage of gradient elution can be demonstrated, as shown in the right graph of Figure 59, where the dashed lines indicate the solvent composition at the pump. The same polymer mixture is injected in 100 % ACN where all three polymers precipitate. As the solvent's elution strength is steadily increased by increasing the THF fraction the most polar polymer (PMMA) elutes first, whereas the other two still remain precipitated. In the present experiment the slope of the solvent gradient was decreased at 46 % THF in order to avoid coelution of PS and PBMA as both appear to be relatively similar in polarity. Further optimization of the gradient in order to distribute the peaks more effectively in the chromatogram (*i.e.*, less space between PMMA and PS, more space between PS and PBMA) weren't done, as only a general impression about the advantages and disadvantages of the different approach should be gained.

Both, the isocratic and the gradient elution experiment can be evaluated following different criteria. Assessing the applicability of a separation technique is always specific for the respective analysis intentions and cannot be generalized. Table 11 summarizes the experiences from the test experiments with respect to criteria that are important for an effective *in situ* analysis:

Table 11: Comparison of isocratic and gradient elution chromatography. The individual characteristics are rated as bad (-), neither good nor bad (○), good (+) and very good (+++).

	Isocratic	**Gradient elution**
Analysis time	+	-
Method development	○	○
„Transferability“ to TD SEC instrument	+	○
Separation Performance	○	+++

An isocratic approach is favorable if analysis time and the “transferability” to the TD SEC instrument are of main relevance. The latter one means how easy it would be to perform the experiment on the TD SEC instrument with the present specifications (see chapter 3.3.1). In gradient elution neither the dRI detector nor the viscometer could be used further and a quaternary pump is required, together with dedicated control software that allows mixing solvents in a programmed time schedule. Putting into focus the necessary effort for developing the method and optimizing all parameters both techniques are more or less equal. The isocratic experiment seems simpler but usually it is best to perform a gradient experiment first, too, for getting a better overview over the elution behavior of the present analytes, which makes it more complicated again. The biggest difference between both techniques for separation of polymer mixtures is the actual separation performance: The gradient elution experiment offers substantially more separation power with more control over the entire process, which makes it the preferred approach for the scope of this thesis.

6.1.2 Gradient elution LC with DA polymers

After having fixed the gradient elution or HPLC approach for the analysis method of choice, further decisions have to be done as HPLC can be performed in different modes: In general one distinguishes normal phase (NP) from reversed phase (RP) HPLC. In NP HPLC a stationary phase with polar functionalities (*e.g.*, -OH, $-NH_2$) is used and a solvent gradient from less polar to more polar is applied. In RP HPLC the opposite is done; the solvent gradient goes from more polar to less polar and unpolar stationary phases ($-C_8$, C_{18}) are employed. In most analysis an RP HPLC setup is used, as it is the more robust variant. The quite reactive functional groups on the NP columns can react easily with the analytes, the solvents or present impurities and, thus, change their behavior for the separation. On the other hand, the NP setup offers potentially more selectivity through specific interactions with the functional groups, whereas in RP HPLC the main driving force is a precipitation/redissolution mechanism.

Both variations were tested for the DA Cp_2P^iBoA polymer system (Structure 17) that was introduced in chapter5.2; the structures are shown again in Figure 60:

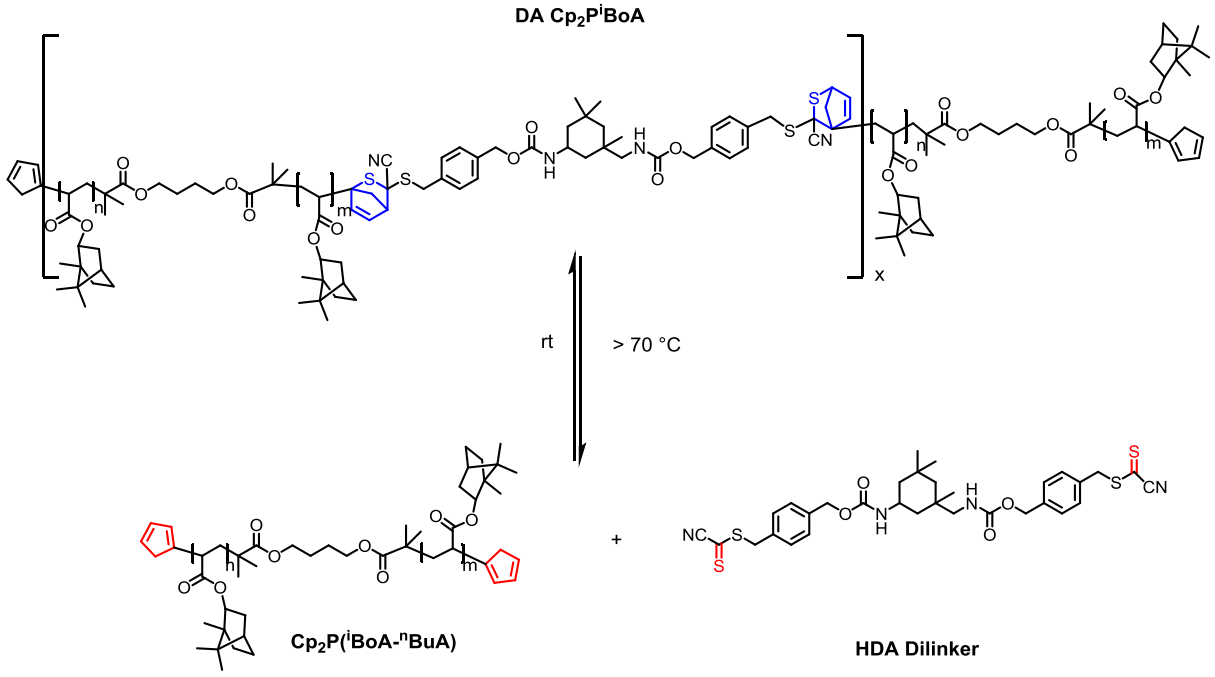

Figure 60: rDA scheme of DA P^iBoA (Structure 17), yielding Cp_2P^iBoA (Structure 11) and the HDA-Dilinker (Structure 23). The displayed system was employed as a model system for studying the applicability of TD HPLC for analyzing rDA reactions.

For the RP setup the above mentioned C_{18} column was used and the solvent composition was ramped from 50 to 85 % THF in ACN within 15 minutes; the chromatogram is shown in the left graph in Figure 61. As expected the HDA-Dilinker as the most polar substance elutes first, followed by the DA P^iBoA and finally the Cp_2P^iBoA (with high molar mass shoulder). The image shows that the quality of the separation is not really satisfying, because the DA polymer and the building block almost coelute and the HDA-Dilinker is not really retained at all, as it elutes right after the dead volume of the column.

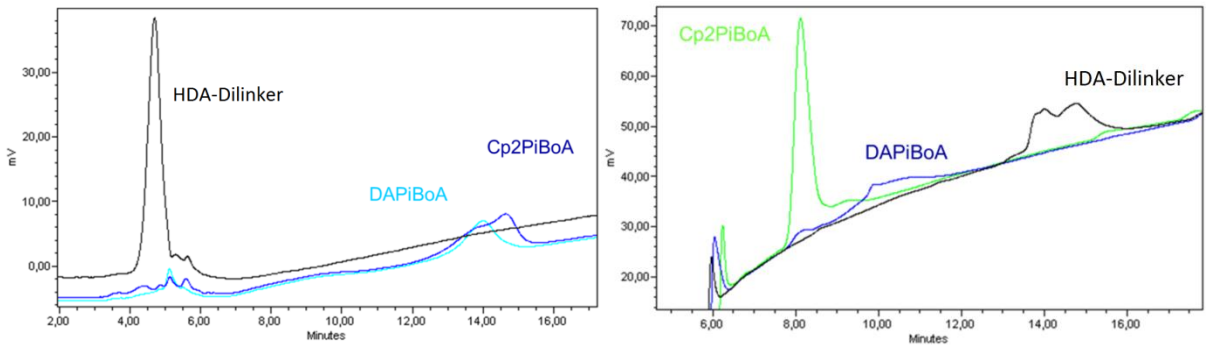

Figure 61: HPLC chromatograms (UV absorption at 347 nm) of the DA P^{i}BoA system at ambient temperature. In the left image an RP HPLC experiment is shown with a solvent gradient from 50 to 85 % THF in ACN within 15 min. In the right image an NP HPLC setup with a gradient from 0 to 100 % THF in heptane within 15 minutes is displayed.

The NP experiment, however, looks significantly better, as it can be seen in the right graph in Figure 61. In that case an Inertsil NP HPLC column (NH_2 surface modification) was used and a gradient from 0 to 100 % THF in heptane within 15 minutes was established at a flow rate of 1 mL/min. Now the least polar $Cp_2P^{i}BoA$ elutes first and the HDA-Dilinker last. The peaks are better defined and distributed in the chromatogram as for the RP experiment. Further understanding of the separation process was gained by determining the solvent compositions at which the individual components elute. Therefore it is necessary to calculate the time the gradient needs to travel from the pump through all capillaries and the column to the detector. That time can be determined by injecting a non-retained analyte (*e.g.*, toluene) and measuring the time it needs to flow through the entire instrument. This time has to be added to the programmed solvent gradient to obtain the composition of the solvent (and, thus, the solvent strength) at the detectors for a given position in the chromatogram. Following this scheme the solvent compositions at which the peak maxima of the individual components appear were determined and put into relation with the corresponding chemical composition. The chemical composition was chosen to be given in terms of the HDA-Dilinker content in the polymer. DA P^{t}BuA, together with the $Cp_2P^{t}BuA$ was added to the investigations to have more than just one example for testing the analytic strategy. Table 12 summarizes the weight fraction of the HDA-Dilinker for the DA polymer systems of P^{i}BoA and P^{t}BuA, their logarithms and the corresponding composition of the solvent at the point of elution in the NP HPLC experiment.

Table 12: Chemical composition of the DA polymers of P^{i}BoA and P^{t}BuA and the corresponding solvent composition (%THF in heptane) for eluting the respective substances. *In fact the HDA-Dilinker content in the Cp_2-polymers is of course 0 %. However, *lg(0)* is not defined and, thus, the very low value 1 % of HDA-Dilinker was taken, which is practically identical to 0 %.

	% HDA-Dilinker	lg % HDA-Dilinker	% THF (P^{i}BoA)	% THF (P^{t}BuA)
Cp_2-Polymer	1*	0	23	33
DA-P^{i}BoA	7.5	0.88	42	-
DA-P^{t}BuA	11.1	1.04	-	53
HDA-Dilinker	100	2	66	66

The HDA-Dilinker content can be calculated out of the molar masses of HDA-Dilinker and building block according to Equation 49:

$$\%\, HDA - Dilinker = \frac{M(HDA - Dilinker)}{M(HDA - Dilinker) + M(Building\ Block)} \cdot 100\ \% \qquad \text{Equation 49}$$

In Figure 62 the dependency of the composition of the solvent (% THF in ACN) on the HDA-Dilinker content is displayed graphically and we observe linear relations for both, P^{i}BoA and P^{t}BuA. Although the number of data points is very limited the plot indicates towards a separation that corresponds to the chemical composition. The logarithmic relationship is not unexpected: Imagine a hypothetical polymer made of units A and B but with just 1 % of A. If now the amount of A is increased by 1 % the total amount is doubled (increase of 100 %) because the content of A increases from 1 to 2 %. If, however we have a polymer with a content of A of 90 % and we increase the content of A by 1 % we end up with 91 % of A, which is just an increase of 1.1 %. In other words, increasing the content of one monomer in a copolymer linearly cannot be expected to change the general behavior of the resulting polymer in the same manner.

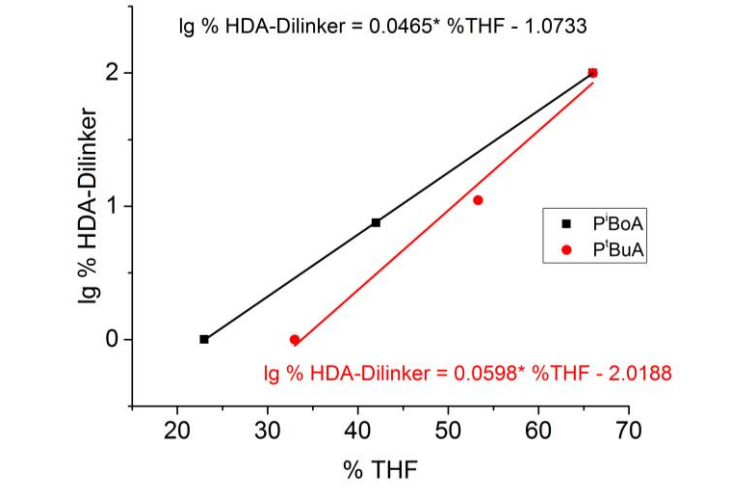

Figure 62: Correlation of solvent composition at elution with (weight) HDA-Dilinker content for DA P^{i}BoA and DA P^{t}BuA in NP HPLC at ambient temperature.

Insights into the nature of the separation mechanisms can be gained by complementary solubility tests. Samples of $Cp_2P^{i}BoA$, DA P^{i}BoA and the HDA-Dilinker were put into 100 % heptane and THF was added until dissolution. The simple experiment showed that $Cp_2P^{i}BoA$ was soluble already in 100 % heptane / 0 % THF, DA P^{i}BoA in approx. 70 % heptane / 30 % THF and the HDA-Dilinker in approx. 55 % heptane / 45 % THF. The THF fractions are consistently lower than the THF fraction at the point of elution in the HPLC experiment which means that besides a precipitation/redissolution mechanism further adsorption effects have to occur. Otherwise the fraction of THF at elution would be close to the solubility limit determined by the solubility tests.[115,186] The occurrence of adsorptive effects as a driving force is not surprising, because of the normal phase setup that normally promotes such behavior.[187]

In a next step the influence of the temperature on the separation was tested. If adsorption is expected to be responsible for the separation effect it cannot be assumed that temperature has no influence on these adsorptions and, thus, the outcome of the chromatograms. In general it should be expected that over a certain temperature the thermal energy (k_BT) overcomes the adsorption energy. As a consequence the adsorptions should break up and the driving force for the separation would be destroyed.

In order to test the present separation setup's temperature sensitivity chromatograms of $Cp_2P^{i}BoA$ and the HDA-Dilinker were acquired in a temperature range from 20 to 70 °C. A column oven was used to control the temperature of the HPLC column and an additional capillary of approx. 1.25 m was introduced before the column to ensure that the solvent has reached oven temperature when it enters

the column. Since THF is a too volatile solvent for the planned experiments it was substituted by ethyl acetate (EtOAc) with a boiling point of 77 °C. In a temperature range from 20 to 70 °C both samples were measured with two quick gradients of different speed. Both gradients went from 100 % heptane to 100 % EtOAc – the slow one in 45 minutes and the quick one in 25 minutes. The graphs A and B in Figure 63 depict the obtained elution times in the entire temperature range for both, the Cp_2P^iBoA and the HDA-Dilinker for the quick and the slow gradient, respectively. The graphs do not indicate a strong temperature dependency of the separations. The elution times of the Cp_2P^iBoA are slightly increasing and the times of the HDA-Dilinker are slightly decreasing with temperature, but the difference is only in the order of 0.5 to 1 %.

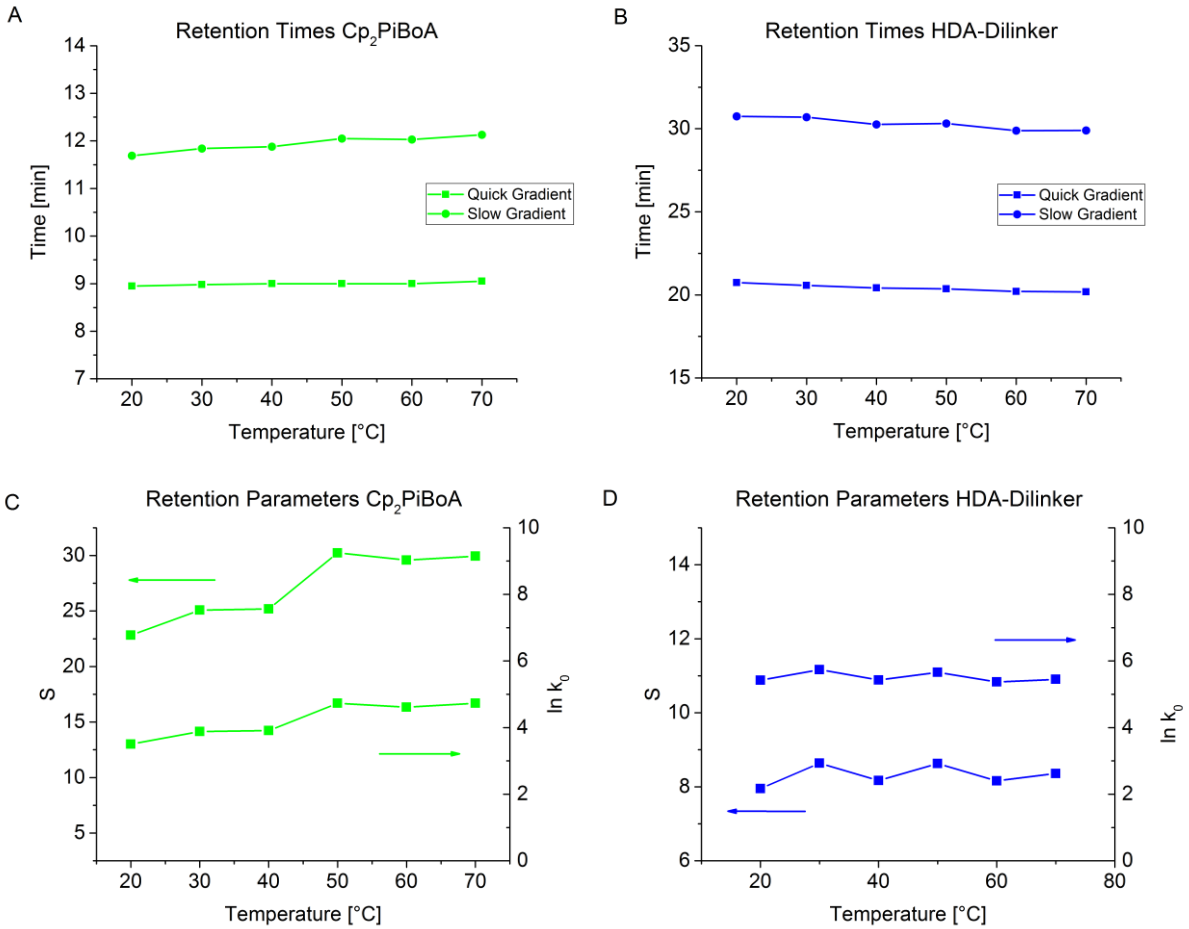

Figure 63: Temperature dependencies of retention times (A & B) and the corresponding parameters *S* and *ln* k_0 (C & D) for Cp_2P^iBoA (left) and the HDA-Dilinker (right). The retention parameters were determined according an RP HPLC model that takes into account the retention times of gradients from 100 % heptane to 100 % EtOAc within 25 minutes (quick gradient) and 25 minutes (slow gradient), respectively.

In order to derive further information from the experiments it was intended to determine *ln* k_0 and *S* for the analytes. These parameters were introduced in Equation 15 for characterizing the retention behavior as a function of the solvent composition in the case of HPLC separations. In a strict manner the linear relation of *ln k* and *φ* is only valid for reversed phase setups. In a normal phase setup the relation would be as given in Equation 50

$$\ln k = \ln k_1 - m \cdot ln\varphi \qquad \text{Equation 50}$$

, where k_1 is the retention factor at 100 % strong solvent and *m* the slope of the curve. According to this equation *ln k* is now linearly dependent on *ln φ*.[114] However, in the case of polymers the slope *S* (for RP) and the slope *m* (for NP) would be very steep anyways so that for practical considerations there is no real difference what model is applied. Treating the data according to the RP-HPLC theory allows for a rough estimation of the separation parameters that can be evaluated with respect to their temperature dependence: The values for *ln* k_0 and *S* of an analyte in a gradient experiment can be estimated by running two experiments with gradients of different velocity and performing a fitting procedure as described in detail in the literature.[114] That procedure was applied for the Cp_2P^iBoA and the HDA-Dilinker for all temperatures and the obtained values are plotted in the graphs C and D of Figure 63. A first observation gives us similar values of *ln* k_0 for both substances but significantly higher values for the slope *S* in the case of the Cp_2P^iBoA. As discussed earlier, the slope *S* is expected to be higher for increasing molar mass and since the Cp_2P^iBoA is a polymer and the HDA-Dilinker a relatively small molecule, the observed results agree to the expectations. In the case of the Cp_2P^iBoA we can observe a slight increase of both, *S* and *ln* k_0, whereas these parameters only fluctuate a bit for the HDA-Dilinker. Again no significant differences can be found, which demonstrates again that the separation does not seem to be very sensitive to temperature changes in the investigated temperature range.

Having in hand the *ln* k_0 and *S* values of different temperature allows calculating the actual retention parameter *k* at the solvent composition *φ* at elution according to Equation 15; in the present example this is $\varphi = 0.65$ for the HDA-Dilinker and $\varphi = 0.25$ for the Cp_2P^iBoA. The resulting values can be plotted logarithmically over *1/T* to give the so called Van't Hoff plot. It is based on the relation shown in Equation 51 and allows determining the entropy and enthalpy of adsorption in the chromatographic process.

$$\ln k = -\frac{\Delta H^0}{RT} + \frac{\Delta S^0}{R} + ln\Phi \qquad \text{Equation 51}$$

where ΔH^0 and ΔS^0 are the changes of the standard molar enthalpy and entropy, respectively, that are associated with the phase transfer of one mole of analyte from mobile to stationary phase, *R* is the

universal gas constant, *T* the absolute temperature and *ln Φ* the phase ratio of stationary to mobile phase.[188,189] The resulting plot is depicted in Figure 64:

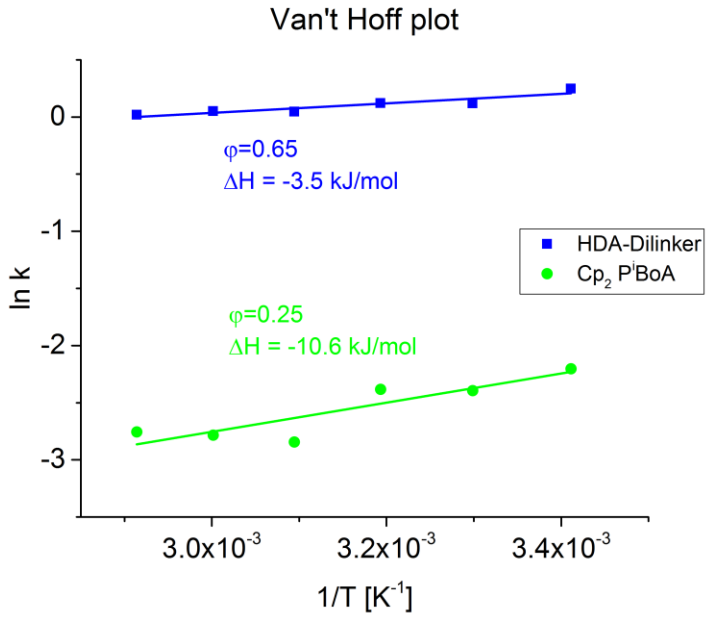

Figure 64: Van't Hoff plot for the HDA Dilinker and Cp_2P^iBoA. For each sample the indicated solvent composition at elution is used. The slope of the linear fit allows estimating the adsorption enthalpies.

The enthalpy of adsorption can now be derived from the slope of the linear fit (= $-\Delta H^0/R$) and values of -3.5 kJ/mol and -10.6 kJ/mol are obtained for the HDA-Dilinker and the Cp_2P^iBoA, respectively. The results demonstrate once again that adsorptive effects are responsible for the separation, as an energetic benefit is achieved by transferring the analytes from the mobile to the stationary phase.

6.1.3 2D LC with DA polymers

After heaving found that the separation of the DA polymer systems seems feasible with NP HPLC further experiments were performed for coupling the setup together with SEC in a two-dimensional (2D) LC experiment. The concept of 2D LC is to combine two different modes of chromatography for maximizing the amount of information that can be gained from a single experiment. One very common mode for the analysis of synthetic polymers is to couple HPLC with SEC.[166,190] In such a setup the fractions coming out of an HPLC experiment (1st dimension, ^{1}D) are reinjected into an SEC separation (2nd dimension, ^{2}D) so that the chemical composition distribution (CCD) and the molar mass distribution (MMD) can be determined simultaneously. In the beginnings of 2D LC fractions were collected and transferred manually but it did not take a long time until the first automated systems were developed.[191,192] The experimental setup of the herein described experiments is specified in chapter 3.6.

For the experimental implementation some considerations have to be taken, though. At first it is important to decide what kinds of separation are chosen to be the 1st and 2nd dimension. If the CCD and the MMD are to be measured it is feasible to establish a gradient elution (HPLC) separation in one dimension and an SEC in the other. In that case it is best to employ the HPLC as the 1st dimension and the SEC as the 2nd (HPLC x SEC). The reason for that is that HPLC can usually be performed more effectively at low flow rates than SEC and that in HPLC higher sample amounts can be injected without overloading the column. Remember that the polymer content in one fraction has to be high enough to give sufficiently strong detector signals when measured again in the second dimension. Furthermore it is important to keep in mind that both dimensions have to be "compatible". The HPLC dimension elutes the fractions in different solvent compositions, going from lowest to highest elution strength. The SEC dimension is, however, of course being run isocratically with a solvent of high elution strength in order to minimize enthalpic interactions. Ideally the strong solvent component of the 1st dimension is used as the SEC solvent. Problems can occur if one (or in the worst case both) solvent components coming from the HPLC cause problems in the SEC, as they are both injected into the SEC necessarily. If, for instance, water is used as a polar solvent in the HPLC dimension it should be ensured that the SEC columns are not harmed when water fractions are injected. There are few methods reported that allow for an automated solvent exchange in the sample loops by solvent evaporation or solid phase extraction, but their application is rare.[193] If, in the other case, the SEC would be performed as the 1st and the HPLC as the 2nd dimension problems can arise from overloading of the SEC and "breakthrough" in the HPLC. Breakthrough occurs if the samples for an HPLC experiment are injected in a solvent of too high elution strength (as it would be the case in an SEC x HPLC experiment). In that case the fractions of the samples move along in a "plug" of strong solvent and elute at the dead volume of the column, rather than coming in contact with the poor solvent that is needed for the separation mechanism.[194–196]

For the first dimension the in chapter 6.1.2 described NP HPLC approach with the Intertsil NH_2 column was used. A solvent gradient from 10 % THF to 75 % THF in *n*-hexane was performed. The second dimension SEC was performed in THF on a short Agilent Mixed-E column (7.5x100 mm). At a flow rate of 1 mL/min the separation could be completed within 3 minutes. Both sample transfer loops were chosen to be 58.9 µL in size, which means that the flow rate of the 1st dimension has to be 19.6 µL/min (= 58.9 µL/3 min). The hexane-THF gradient was optimized for a better distribution of the peaks; the final configuration can be found in Table 13:

Table 13: Solvent composition and flow rate conditions for 1st dimension NP HPLC (at ambient temperature) that allowed good separation and reasonable experiment times. During the first three minutes the dead volume of the column is compensated.

Time (min)	% THF in *n*-hexane	Flow rate (mL/min)
0	10	1
3	11	1
3.5	11.1	0.02
203	75	0.02
253	75	0.02
303	10	0.02

In the first three minutes the flow rate was set to 1 mL/min for overcoming the dead volume of the column more quickly (no decrease in separation performance was observed) so that both, the analysis time and the solvent consumption is kept in reasonable scales. With that setup the calibration for the chemical composition in terms of "lg % HDA-Dilinker" was investigated for DA polymers of P^{t}BuA and P^{i}BoA, analogously to the procedure in chapter 6.1.2. As shown in the left graph of Figure 65 the correlations are slightly worse than in the original 1D experiment but shall be sufficient for a "proof of concept".

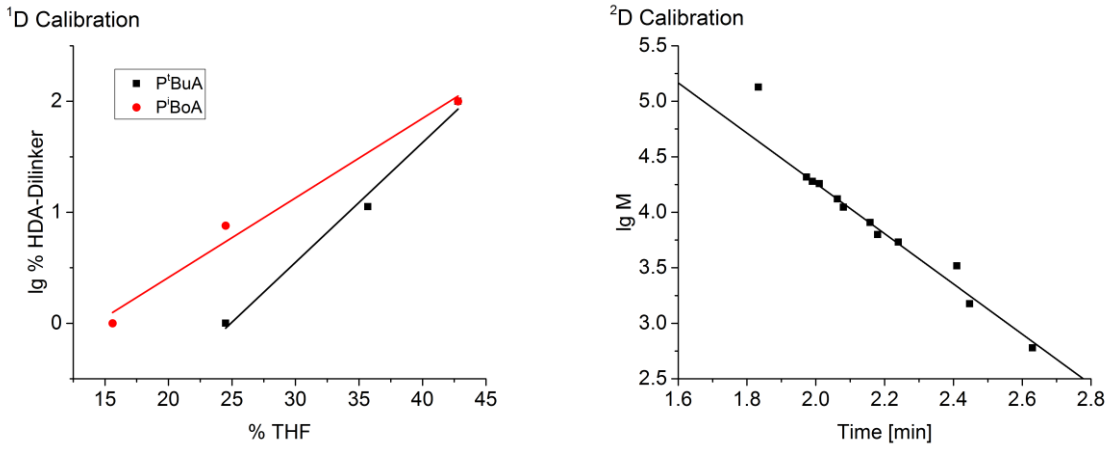

Figure 65: Left: Calibration of 1st dimension (NP HPLC, 10 % - 75 % THF in *n*-hexane) for determining the chemical composition of DA P^{t}BuA and DA P^{i}BoA. Right: Molar mass calibration in SEC (THF), established by collecting chromatograms of copolymers of methacrylic acid and methyl methacrylate in a molar mass range from 600 to 134000 g/mol. The experiments were carried out at ambient temperature.

The SEC calibration was performed with a set of narrowly distributed copolymers of methacrylic acid and methyl methacrylate in a molar mass range from 600 to 134000 g/mol. These polymers were available in the laboratory and should resemble the nature of the acrylate based polymers more closely than a polystyrene standard. The calibration curve can be seen in the right graph of Figure 65. The exclusion limit of the column appears at around 100,000 g/mol, which is an adequate molar mass range for the present polymers.

Investigating the rDA reactions of the DA polymers *in situ* was not possible, as the 2D instrument was not temperature controlled. Ginzburg et al. demonstrated that it is possible to set up a high temperature 2D instrument[197] but for the present scope of assessing the general applicability of 2D LC for investigating the DA polymers it is sufficient to perform the analysis offline after the actual rDA reactions. Therefore the DA polymers were dissolved in toluene and put into a crimp cap vial that can be closed relatively tightly. The vial was then put on a hot plate for letting the rDA reaction occur in the almost boiling toluene. After 30 – 45 min the solution was directly injected into the 2D LC instrument. It was not possible to set a particular temperature for the hot plate but the temperature of the solution can be assumed to have been at 110 – 120 °C, since the boiling point of toluene at ambient pressure is 111 °C and in the vial the pressure should have been slightly increased. According to the investigations of these DA polymers in chapter 5.2.2 these conditions should suffice to yield some rDA reaction. When the sample is cooled down to ambient temperature in the LC instrument there is a chance that some repolymerization occurs but due to the relatively high level of dilution the amount of repolymerization is not expected to be very high.

In Figure 66 the chromatogram of DA P^{i}BoA after rDA reaction is shown as acquired by the ELSD. The inset shows more in detail that the individual peaks appear every three minutes, which is the switching interval of the 10-port valve. It is now necessary to cut the chromatogram in slices, rearrange them and convert the elution times in solvent composition (1st dimension) and lg M (2nd dimension), respectively. The data processing was done with the program SciLab (www.scilab.org), the respective script can be found in the appendix (chapter 11.1).

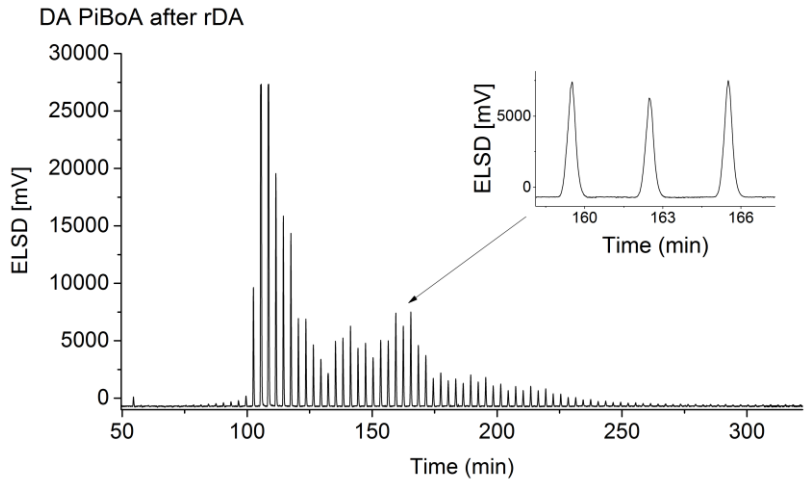

Figure 66: Raw chromatogram of the NP-HPLC x SEC experiment with the DA P^{i}BoA (after rDA), acquired at ambient temperature. The inset shows the individual SEC peaks, the times indicate the switching times of the 10-port valve.

The corresponding 3D plots of the DA P^{i}BoA before and after rDA reaction are shown in Figure 67:

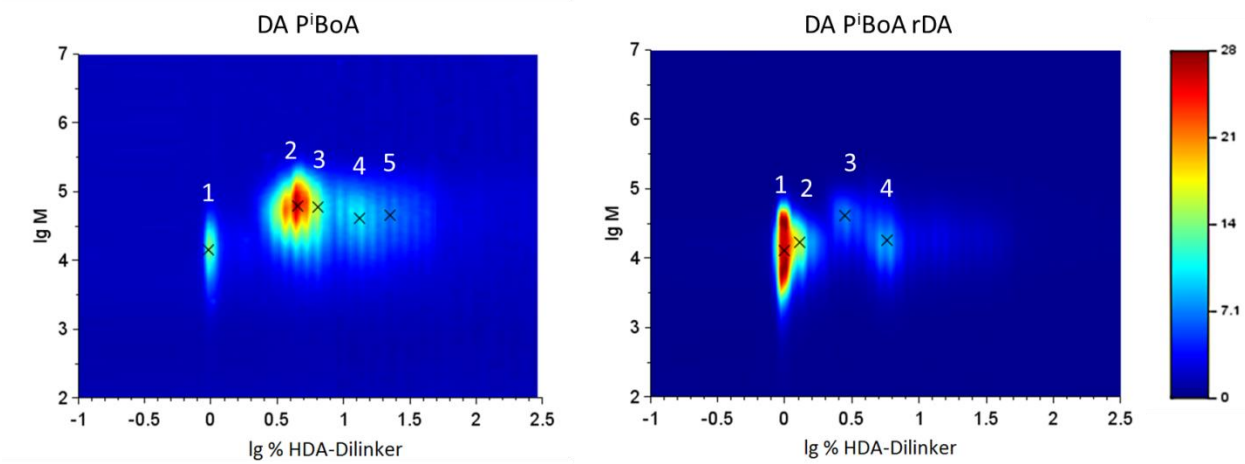

Figure 67: Processed 2D-chromatograms of DA P^{i}BoA before (left) and after (right) rDA reaction. The abscissa shows the CCD, the ordinate the MMD and the color the abundancy. Details to the peak numbers can be found in Table 14 and Table 15.

The left image of Figure 67 shows a rather complex distribution with multiple peaks of different chemical composition and molar mass. After the rDA reaction the peaks are shifted towards lower molar masses and lower HDA-Dilinker content. It is important to keep in mind that the results can only be evaluated qualitatively and not quantitatively, as the concentration of the injected sample solution has likely changed through the heating process on the hot plate (the used vials are not entirely gas tight). In

addition it shall be noted that in the case of peak 1 of the DA P^{i}BoA after the rDA reaction the detector limit was reached, which makes a quantitative interpretation of the detector response even less meaningful.

The results allow determining the chemical composition and molar mass of the individual peaks that are found in the plots. Because of their chemical nature (see Figure 60) the building block and HDA-Dilinker have to occur in a strictly alternating order in a DA polymer, which limits the possible combinations of building block and HDA-Dilinker. Table 14 and Table 15 list the measured molar masses and chemical compositions (in terms of % HDA-Dilinker) of the DA P^{i}BoA before and after rDA reaction, respectively, together with estimated combinations of numbers of block and HDA-Dilinker and the corresponding theoretical molar mass and % HDA-Dilinker values. For calculating the molar mass and the HDA-Dilinker content of the estimated compositions the respective molar masses of building block and HDA-Dilinker were used that were measured in the same setup. The last column gives a rough evaluation of the agreement of the assumed DA polymer composition and the measured values.

Table 14: Assignment of the peaks that were indicated in the 2D chromatogram of DA P^{i}BoA before rDA reaction. The according to the calibrations obtained molar mass and content of HDA-Dilinker are confronted to hypothetical values that result from combinations of $Cp_2P^{i}BoA$ and HDA-Dilinker. In the last column the quality of the accordance is evaluated taking into account the experimentally limited accuracy.

	Experiment		**Theoretical estimation**				
Peak ID	M (g/mol)	% HDA-Dilinker	N^{o} $Cp_2P^{i}BoA$	N^{o} HDA-Dilinker	M (g/mol)	% HDA-Dilinker	Quality
1	11500	1	1	0	14000	0	Good
2	51300	4	4	3	57800	4	Good
3	44800	6	3	3	43800	5	Good
4	31800	14	2	3	29800	8	Medium
5	30000	24	2	10	32000	24	Poor

Table 15: Assignment of the peaks that were indicated in the 2D chromatogram of DA P^{i}BoA after rDA reaction. The according to the calibrations obtained molar mass and content of HDA-Dilinker are confronted to hypothetical values that result from combinations of $Cp_2P^{i}BoA$ and HDA-Dilinker. In the last column the quality of the accordance is evaluated taking into account the experimentally limited accuracy.

	Experiment		**Theoretical estimation**				
Peak ID	M (g/mol)	% HDA-Dilinker	# $Cp_2P^{i}BoA$	# HDA-Dilinker	M (g/mol)	% HDA-Dilinker	Quality
1	14500	1	1	0	14000	0	Good
2	13500	2	1	1	14600	5	Medium
3	26000	3	2	1	28600	3	Good
4	14000	6	1	2	15200	11	Medium

The tables show that for most positions in the chromatograms feasible combinations of HDA-Dilinker and building block can be found. Only when calculating the composition of a point in the tailing of a peak as in the case of peak 5 in Table 14 the experiment yields unrealistically high HDA-Dilinker contents. In order to achieve 24 % HDA-Dilinker 10 HDA-Dilinker molecules would have to be connected with only two building blocks. Such inaccuracies can be caused by peak broadening effects and the not 100 % precise DA-Dilinker content calibration (see Figure 65). Especially the SEC dimension suffers from peak broadening because of the short column and, consequently, its low plate count. For a more precise calibration more substances with known HDA-Dilinker content would be required and for decreasing the peak broadening the separation conditions would have to be optimized further. During the short research stay it was not possible to optimize the analysis further but the so far obtained results seem at least feasible. It shall be noted that the targeted DP_n or, in other words, the number of DA cycloadducts per DA polymer was approx. 6.[71] The most dominant species in the chromatogram of the P^{i}BoA prior the rDA reaction was determined to consist of four blocks and three HDA-Dilinkers (Peak 2), which corresponds to six DA cycloadducts, which is in good agreement with the targeted DP_n. Furthermore, no "free HDA-Dilinker" was found in the chromatograms after the rDA reaction although it was visible in the chromatogram when measured individually (see Figure 105 in appendix chapter 11.1). That finding corresponds to the observations that releasing the free HDA-Dilinker requires relatively high temperatures (see chapter 5.3).

Further results were obtained by repeating the described procedure at identical conditions with a sample of the DA P^{t}BuA (Structure 19). According to the results shown in Figure 68 the distribution of the DA polymer prior to rDA reaction is much narrower than for the P^{i}BoA. The rDA reaction again leads to a shift of the peaks to lower molar mass and HDA-Dilinker content and the peaks can be assigned to feasible combinations of block and HDA-Dilinker, as listed in Table 16 and Table 17.

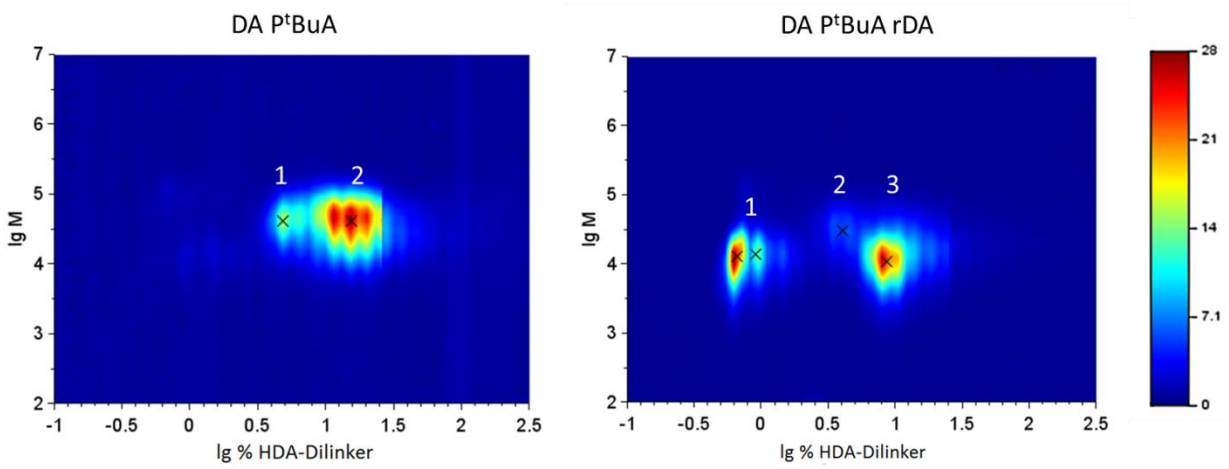

Figure 68: Processed 2D-chromatograms of DA P^{t}BuA before (left) and after (right) rDA reaction. The abscissa shows the CCD, the ordinate the MMD and the color the abundancy. Details to the peak numbers can be found in Table 16 and Table 17.

Table 16: Assignment of the peaks that were indicated in the 2D chromatogram of DA P^{t}BuA before rDA reaction. The according to the calibrations obtained molar mass and content of HDA-Dilinker are confronted to hypothetical values that result from feasible combinations of Cp_2P^iBoA and HDA-Dilinker. In the last column the quality of the accordance is evaluated taking into account the experimentally limited accuracy.

	Experiment		**Theoretical estimation**				
Peak ID	M (g/mol)	% HDA-Dilinker	N° Cp_2P^iBoA	N° HDA-Dilinker	M (g/mol)	% HDA-Dilinker	Quality
1	34100	5	3	3	34200	7	Good
2	34100	15	3	4	34800	9	Medium

Table 17: Assignment of the peaks that were indicated in the 2D chromatogram of DA P^{t}BuA after rDA reaction. The according to the calibrations obtained molar mass and content of HDA-Dilinker are confronted to hypothetical values that result from feasible combinations of Cp_2P^iBoA and HDA-Dilinker. In the last column the quality of the accordance is evaluated taking into account the experimentally limited accuracy.

	Experiment		**Theoretical estimation**				
Peak ID	M (g/mol)	% HDA-Dilinker	N° Cp_2P^iBoA	N° HDA-Dilinker	M (g/mol)	% HDA-Dilinker	Quality
1	11000	1	1	0	12500	0	Good
2	28800	4	2	1	25800	3	Good
3	10700	8	1	2	14100	11	Good

The 2D LC experiments with the DA P^{i}BoA and DA P^{t}BuA demonstrate the value of two-dimensional separations for detailed investigations of reactions where both, the chemical and the molar mass distribution are changing. The amount of information gained from these analyses is much higher than in

any 1D LC experiment, gained at the cost of a significantly higher experimental effort. Optimizing all the necessary parameters properly is an endeavor that must not be underestimated; especially when a temperature dependent *in situ* experiment is desired. The high analysis time of the 2D experiment is a further drawback. Interpreting the results presumes that the outcome of the rDA reactions is not influenced by the analysis experiment itself. In the case of an experiment that takes five hours and at least two changes in solvent composition this assumption is not easy to validate. Working at higher pressures (up to 1000 bar) with smaller columns with smaller packing materials as it is the concept of ultra-high pressure liquid chromatography (UHPLC) is a general concept for decreasing LC analysis time.[162] Such high pressures come with higher requirements for the instrumental setup, which limits the applicability of UHPLC in most laboratories, however.

Assessing the value of 2D LC for *in situ* investigations of dynamic bonding polymer systems once and for all requires further experiments. Complications from transferring the herein described procedure to significantly higher temperatures can only be elucidated by the actual experiment. This ultimate test was not possible in the context of this dissertation, unfortunately. However, the within this work presented results are promising and demonstrate that the concept of TD 2D LC is not inherently impossible. Ginzburg et al. demonstrated that HT 2D LC can be realized[197] and their experiences could be used as a starting point for developing a TD 2D LC setup. The stability of the individual components would have to be tested more in detail and it would be worth testing other detectors than the ELSD. Additional UV detection would be desirable because many telechelic polymers feature UV active groups. The effort would be rewarded by a very powerful analysis setup that allows performing the comprehensive 2D analysis for simultaneous molar mass and chemical composition determination or the individual analysis in just one of the dimensions. Thereby the instrument could be used in a very flexible manner for versatile analytical tasks.

7 Investigation of thermoreversible networks

As discussed in chapter 2.1 attractive applications of thermoreversibly bonding polymers lie in the fields of self-healing materials or printable polymer networks. These applications require that the thermoreversible groups are employed as multifunctional linkers so that reversibly crosslinked systems are obtained. Therefore the herein investigated linear HDA polymer systems were developed further. Kim Öhlenschläger synthesized a four-functional HDA-Tetralinker (Structure 24) that allows thermoreversible crosslinking of Cp endfunctionalized polymer building blocks.[36] In Figure 69 the synthesis of the HDA-Tetralinker is shown, together with the thermoreversible DA crosslinking reaction and photographs of the network that demonstrate its self-healing potential. Rheology investigations revealed that the material is brittle at ambient temperature but becomes an elastomeric rubber at temperatures higher than 70 °C that turns into a liquid like material at temperatures higher than 150 °C. Hence the material can be fractured at ambient temperature and remolded at elevated temperatures (*e.g.*, 120 °C). Further analyses of the material properties before and after the healing indicated that the original toughness of the material could be restored completely.[36]

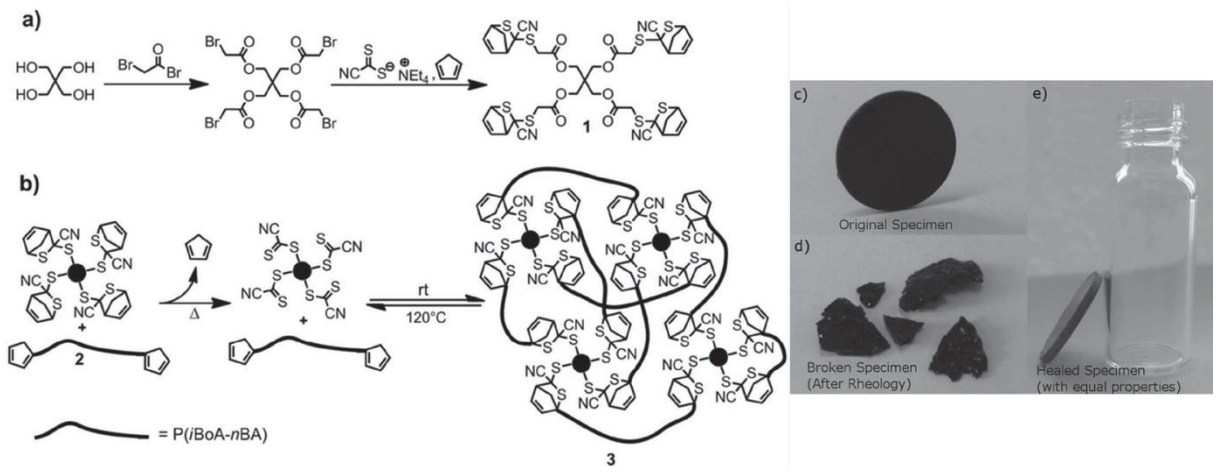

Figure 69: Synthetic pathway for the protected HDA-Tetralinker (Structure 24) (a), reaction scheme of the HDA-Tetralinker deprotection and the thermoreversible crosslinking reaction with the $Cp_2P(^{i}BoA\text{-}^{n}BuA)$ (Structure 4) (b). Photographs of the HDA network pressed into a tablet (c), the after rheology experiments destroyed sample (d) and the healed sample after heat treatment, showing identical mechanical properties (e). Reproduced with permission from Ref.[36], Copyright 2014, Wiley-VCH.

Mechanical analysis techniques are very effective for assessing the mechanical properties of such materials but do not reveal the progress of the underlying bonding reactions on a molecular scale. Investigating the bonding reactions in the crosslinked material itself is of high interest, though. For such analytical tasks one would first think about the use of spectroscopic techniques, such as IR, Raman or

solid-state NMR spectroscopy. The challenge of the herein described materials is, however, that they consider of a broad variety of different functional groups in relatively low concentrations. Thus, very high resolved spectra are necessary for effective spectroscopic investigations, which are difficult to obtain in solid state. Furthermore the obtained concentrations of functional groups do not necessarily have to correlate well with a degree of crosslinking, as reactions can also form "ineffective" products, such as loops or dangling ends.

At this point it might be worth heading into a different direction and, again, harness the potential of chromatographic techniques for the desired analyses. This chapter will discuss the potential of TD SEC for investigating thermoreversibly crosslinked polymers and illustrate the specific features on some basic examples.

7.1 Applicability of LC for analyzing polymer networks

Analyzing polymer networks by LC follows the concepts of an indirect analysis approach. The sample of interest is degraded in a controlled manner and the obtained (soluble) fractions are then being analyzed by LC. From the obtained distributions of degradation products characteristics of the starting network can be reconstructed. Popular methods for degrading polymer networks are pyrolysis[198,199] or chemical degradation[200–202], *e.g.*, hydrolysis.[203] These approaches are based on the quantitative cleavage of crosslink points in order to analyze the network building blocks individually.

A similar concept can be applied for the DA networks, as they naturally become soluble at high temperatures and, thus, can be analyzed by LC (see Figure 70). Degrading the networks completely would only yield the HDA-Tetralinker and the polymeric building block and hence does not lead to any valuable information. But the network can be degraded partially by controlling the rDA temperature and time, as illustrated by the previous investigations of the linear DA polymers.

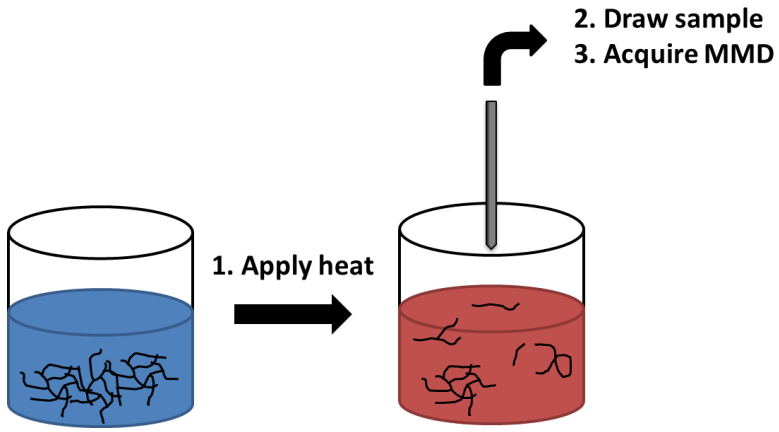

Figure 70: TD SEC scheme for analyzing the thermoreversibly crosslinked HDA networks. After heating the sample in the SEC vial in an appropriate solvent the dissolved fragments can be directly analyzed by SEC.

Most information about the DA polymers is obtained when LC and SEC are coupled in a two-dimensional experiment, as demonstrated in chapter 6.1.3 but it was not possible to establish a temperature dependent 2D LC setup at the time of this work. As a consequence only one of the general LC concepts, HPLC or SEC had to be chosen. For the present task SEC is more attractive, as the MMD is about to change significantly during the rDA reaction. Information about the chemical composition could still be derived *online* by a newly integrated UV/Vis detector that allows collecting the absorption at two wavelengths simultaneously and also to acquire entire spectra at desired positions of the chromatograms. Further information can be derived from the viscosity detection: Since the degree of branching of the DA networks is expected to decrease during the rDA reaction (see Figure 71) a different viscosity behavior should be found for early and late stages of the rDA reactions.

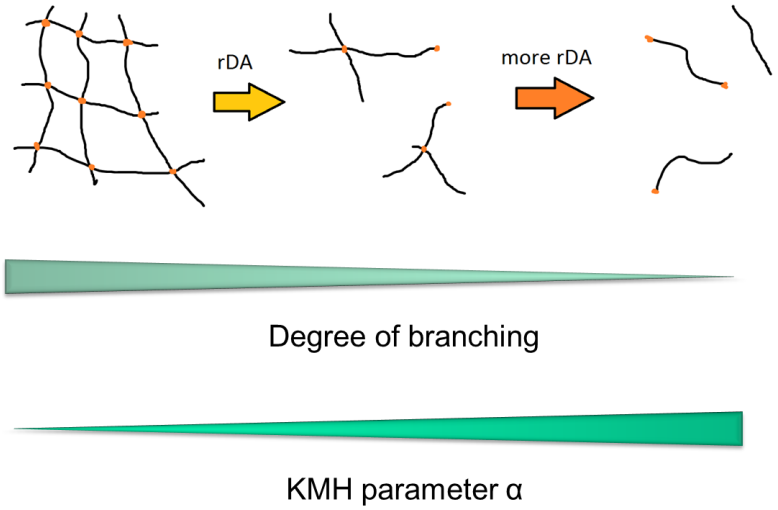

Figure 71: Decomposition of the DA networks displayed schematically. In the first stages of the rDA reactions relatively large networks fragments are expected that are characterized by a branched structure. At higher rDA conversions more linear structures have to be formed when the pure building blocks are released. A higher degree of branching is characterized by a lower α.

Deriving the viscosity and elucidating the viscosity scaling with molar mass through Kuhn-Mark-Houwink (KMH) plots requires an efficient molar mass determination. The difficulties of calculating molar masses for the rather complex DA polymer systems arise from potential enthalpic interactions of the analytes with the column material and mixed detector signals from the individual DA polymer components (see also chapter 5.2.2). The TD SEC setup was optimized for taking into account both issues: At first a new eluent-column pairing was developed for ensuring size based separations. Therefore different solvents were tested with regard to their potential in dissolving both, the moderately

polar acrylate building blocks and the relatively polar HDA-Tetralinker. *N,N*-Dimethylacetamide (DMAc) with 3 g/L LiCl was worked out as the new eluent. A particularly adapted SEC column was used for ensuring linear molar mass calibrations up to 400 kDa. Calculating reliable molar masses also for non-linear polymer fragments, too, is possible by performing universal calibration. The newly integrated UV/Vis detector allows collecting two concentration signals additionally to the dRI trace. Thereby more complex detector responses can be handled and the chemical composition can be derived at each position in the chromatogram.[101] In Figure 72 the employed TD SEC setup is displayed schematically:

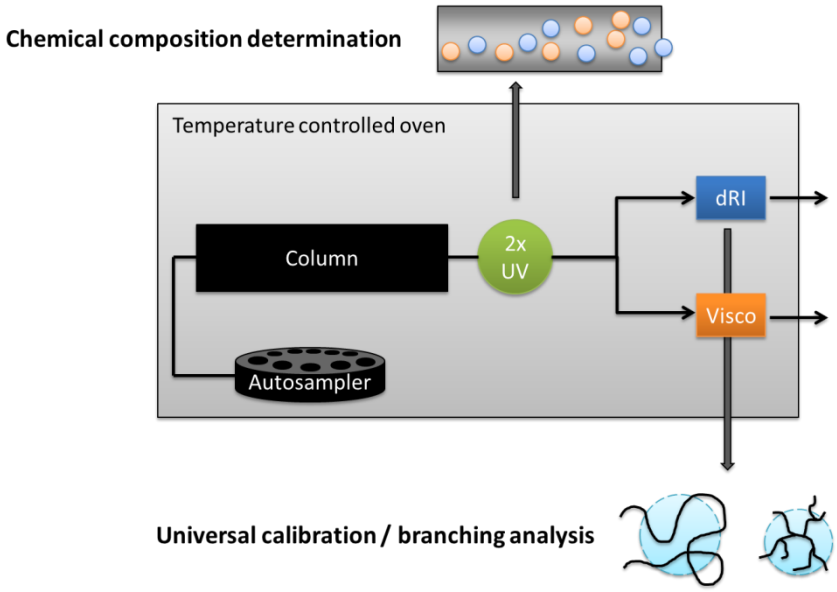

Figure 72: Schematic representation of the upgraded TD SEC setup for analyzing the crosslinked DA polymers. Being able to collect two UV traces gives detailed insights in the chemical composition and the combination of concentration and viscosity detection allows performing universal calibration and drawing conclusions about structural parameters, such as branching.

This setup should allow heating samples of the DA networks in the autosampler, thus cleaving a certain fraction of the DA bonds and releasing soluble components. Through the size based separation in the column and the comprehensive detection with three concentration detectors and the viscometer versatile information can be obtained.

7.2 Testing the upgraded TD SEC setup

The performance of the TD SEC setup was firstly tested at the example of the linear DA polymers which were discussed in chapter 5.2. In order to develop an evaluation procedure for more complex, branched or cross-linked structures, we have to start with simple, linear polymers. For this purpose the linear DA polymers are suitable: their evaluation is more straight-forward as no changes in polymer architecture can occur (they are linear at every stage of the rDA reaction), which makes the calibration

easier. Since they dissolve completely, the exact sample concentration is known and can be used for double checking the calculated concentrations. Another scope of the in this chapter explained analysis is to derive a trustworthy MMD that can be described according to step-growth statistics. The resulting bonding probabilities of the linear DA polymers are interesting for the evaluation of the MMD of the corresponding nonlinear (crosslinked) DA polymers.

A reliable molar mass determination requires, if absolute molar mass determination is not accessible, a purely entropic separation and a reliable concentration signal. The performance of the SEC column was tested by running samples of polystyrene standards, the butyl acrylate building blocks and the HDA-Dilinker. As demonstrated in Figure 73 the samples fall into the PS calibration, indicating the absence of enthalpic interactions between column material and analytes. The HDA-Dilinker yields trimodal peaks and the position of the peaks fit nicely the molar mass of a “monomer”, “dimer” and “trimer”. An exact structure of the multimers cannot be indicated but it is known that CDTE derivatives can undergo dimerizations and unwanted side reactions can occur when the CDTE is deprotected at elevated temperatures.[72]

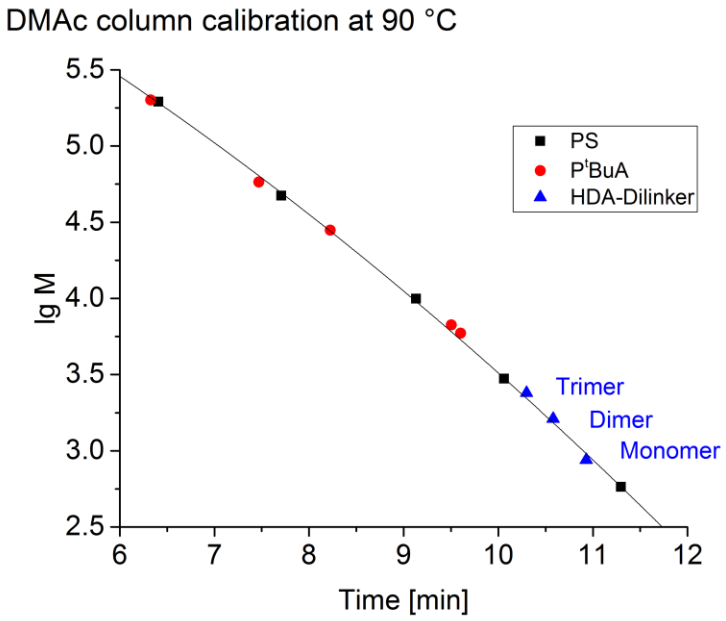

Figure 73: Molar mass calibration plot of PS and P^{t}BuA and the HDA-Dilinker, acquired at 90 °C in DMAc (3 g/L LiCl). PS and P^{t}BuA fall nicely into one calibration line and also the three peaks from the HDA-Dilinker agree well to the calibration. Thus, no enthalpic interactions between the different analytes and the column materials are evidenced and good SEC behavior of the separation can be assumed.

After having established good chromatographic conditions it is furthermore important to calculate the concentrations from the chromatograms reliably. For applying a regular column calibration the concentration would not be important. However, the goal is to establish a universal calibration in order to analyze the branched rDA polymers that are released from the DA networks. And for calculating the

intrinsic viscosity of the polymers at each position in the chromatogram the corresponding concentrations have to be known. As already discussed in chapter 5.2.2 in Figure 50 the chemical composition and, hence, the d*n*/d*c* of the DA polymers is not identical at all positions of the peaks. In the high molecular part of the peak a 1:1 stoichiometric ratio of building block to HDA-Dilinker can be assumed but deviations are expected at lower molar masses where a building block can be connected to zero, one or two HDA-Dilinkers.

The chemical composition at different positions in the chromatogram can be determined through the acquisition of multiple concentration signals. If at least as many signals are collected as there are individual components the chemical composition can be calculated (see chapter 2.4.4). For the practical realization of this concept it is important to exactly define the nature of the individual “components”. In the case of the DA PuA samples this is not trivial, unfortunately. In Figure 74 the structure of the DA PBuA system is shown and the parts that are relevant for the different detector types are highlighted. The dRI detector is responsive to the entirety of the molecule. Hence, the endgroups of the polymer building blocks are of less relevance as they are “diluted” by the polymer backbone. In the same manner also the HDA-Dilinker appears to give similar detector responses when being integrated in the DA polymer or when being released: Measuring samples of the Cp protected HDA-Dilinker after different heating times at 70 °C (*i.e.*, after different deprotection degrees) did not yield significantly different ratios of peak area to concentration.

For the UV/Vis detector, on the other hand, the PBuA backbone is virtually invisible at wavelengths higher than 300 nm (lower limit given by the absorption of DMAc) and only the Cp endgroups cause absorption (see Figure 109 in appendix chapter 11.6). Furthermore the cyanodithioesther group of the HDA-Dilinker should be visible and, of course, the DA cycloadduct of the DA polymer; both, due to their different electronic structure, with different absorption coefficients.

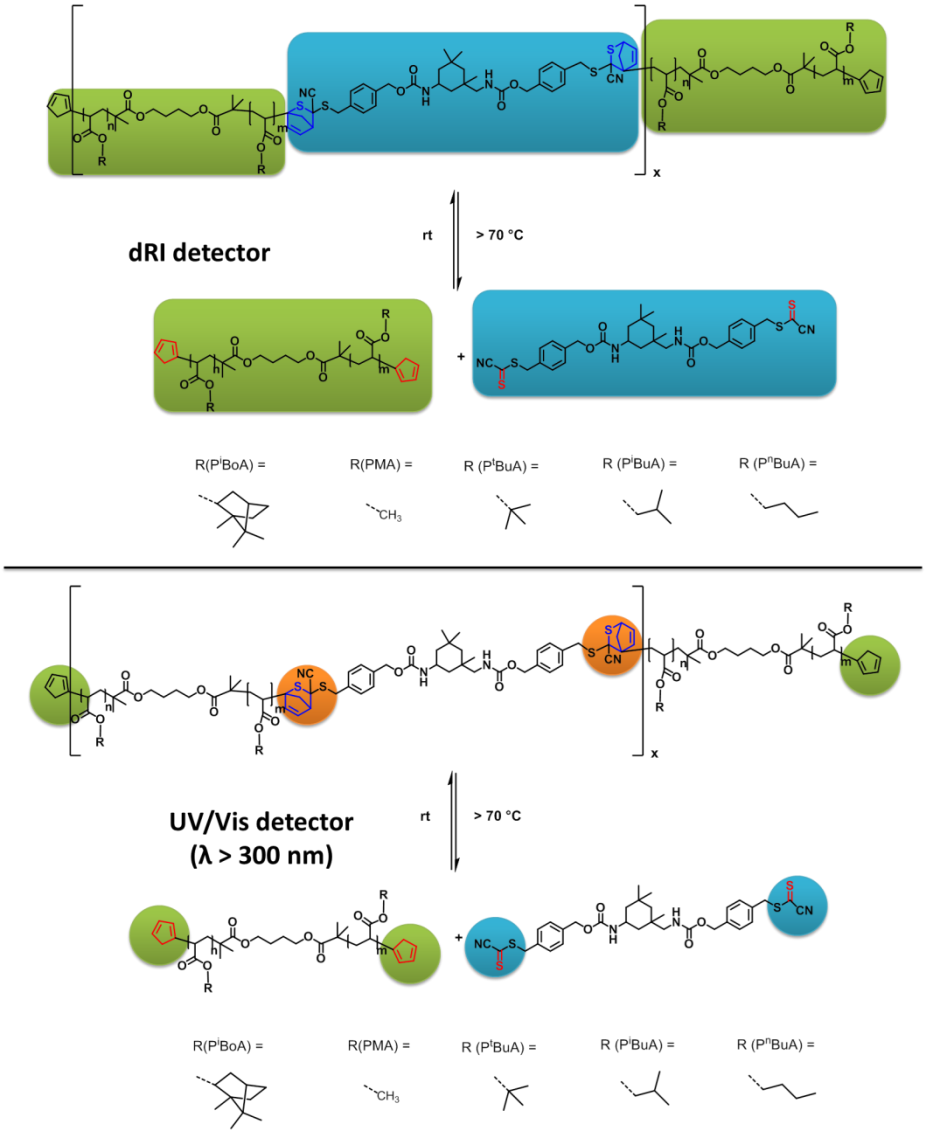

Figure 74: Structure of the DA PBuA samples, as seen by the dRI and UV/Vis detector, respectively. The highlighted areas point out the parts that are relevant for the respective detectors.

Hence, the question of how many components have to be considered is not easy to answer. The situation is more complicated because for an accurate evaluation the d*n*/d*c* and absorption coefficients ε of the highlighted elements would have to be determined. Estimating the d*n*/d*c* of the building block, HDA-Dilinker and the DA polymer can be done as described in chapter 5.2.2 (Equation 47) and in a similar way the ε of the Cp endgroups and the CDTE can be determined. However, the ε of the cycloadduct is not directly accessible because the exact ratio of reacted to unreacted building blocks and HDA-Dilinker in a DA polymer sample after a certain extent of rDA reaction is not known.

As a consequence simplifications have to be done. The goal of these analyses was to derive a reliable molar mass distribution and to calculate the KMH parameter α. Interpreting KMH plots requires a sufficiently high molar masses and a relatively broad distribution. Hence, the low molar mass regime,

where the pure building block (plus zero, one or two HDA-Dilinkers) and the released HDA-Dilinker appear, can be neglected for the current analytical purpose. Then the dRI signal can be evaluated easily by estimating the d*n*/d*c* of the DA polymer as the average of the d*n*/d*c* values of building block and HDA-Dilinker, weighted by their weight fractions. In Figure 75 the chromatograms of the DA polymer after 0 and 20 min of heating at 90 °C are displayed. The overlaid data show the intrinsic viscosities and the corresponding molar masses calculated for each slice of the chromatogram.

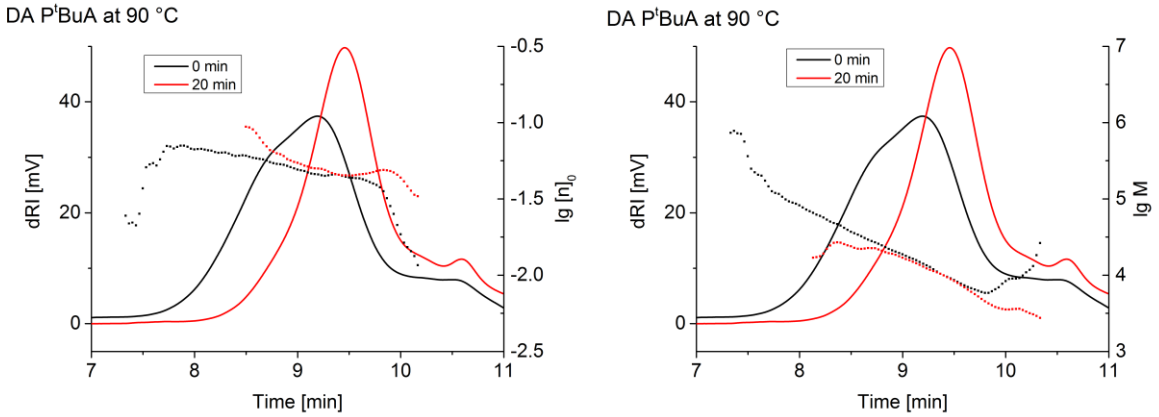

Figure 75: SEC chromatograms of DA P^{t}BuA after heating for 0 and 20 minutes at 90 °C in DMAc (3 g/L LiCl). The dRI traces are overlaid with the logarithm of the intrinsic viscosities (left) and the logarithm of the molar masses (right) that are obtained from the universal calibration.

Evidently the molar mass distribution shifts to lower molar masses. For both samples comparable intrinsic viscosities and molar masses are calculated throughout the distributions, indicating that the calculations work consistently. Closer to the borders of the peaks deviations occur due to the low signal intensities. A further indication for the validity of the procedure was that the integrated concentration of the peak correlated relatively well with the injected sample amount. An error of 10 % was found, however, that is to be attributed to the expected deviations at high elution volumes.

Having calculated the molar masses and concentrations allows fitting the molar mass distribution to step-growth statistics, as described in chapter 4. In the left graph of Figure 76 the results are shown for the linear DA P^{t}BuA at 90 °C. Each dot of the theoretical distribution depict the average abundancy of *n* building blocks with *n-1*, *n* or *n+1* HDA-Dilinkers, as the molar mass resolution of the SEC setup is too low to distinguish between the individual cases. Due to limited sample amount only few experiments could be performed. In the right graph of Figure 76 the highest achieved *p* values at 70, 80 and 90 °C are plotted. The equilibrium conversions at each temperature are interesting, as they allow for a more detailed understanding of the rDA reactions of the DA networks. The next chapter will deal with all necessary considerations.

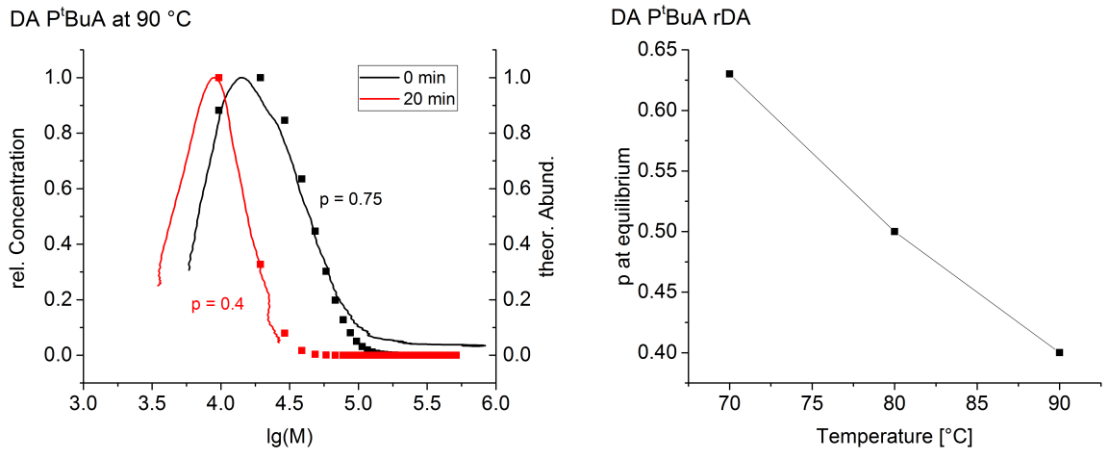

Figure 76: Left: Molar mass distributions of the linear DA P^{t}BuA after different reaction times at 90 °C. The dotted data indicates the molar mass distribution of a step-growth polymer with the indicated bonding probability (*i.e.*, conversion). Right: Determined conversions *p* of DA P^{t}BuA at different temperatures.

7.3 TD SEC investigations of DA networks

After having tested the reliability of the TD SEC setup the actual network analyses could be approached. In Figure 77 the scheme of the investigated DA polymer networks is shown. In contrast to the previously examined linear DA polymers the HDA-Dilinker is exchanged with a HDA-Tetralinker (Structure 24). The synthetic procedure for the network formation was worked out by Kim Öhlenschläger and can be found in the literature.[36] Although in theory each HDA-Tetralinker can react with four building blocks it is unlikely that in practice all four CDTEs on each HDA-Tetralinker are reacted. Because of the relatively compact structure the steric hindrance increases dramatically with every connected building block.

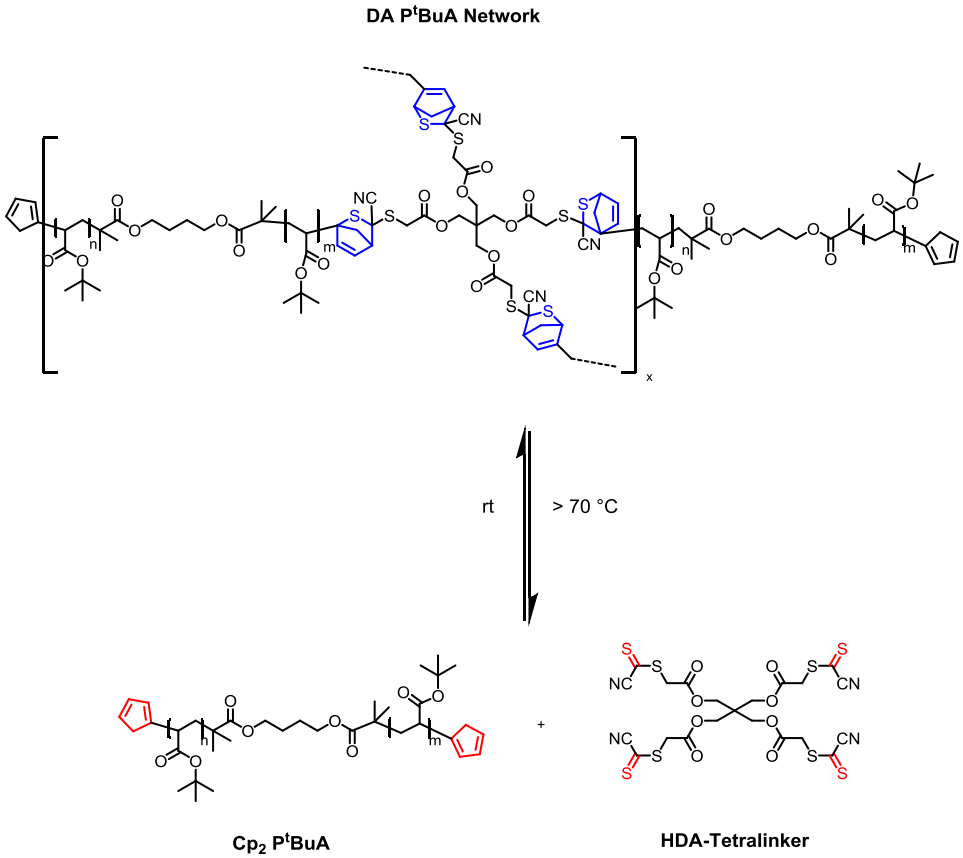

Figure 77: rDA reaction scheme of the DA P^{t}BuA network (Structure 25). The image displays the ideal case in which each HDA-Tetralinker (Structure 24) connects to four Cp_2P^tBuA building blocks (Structure 13). It is so far not known to what extent this is true.

The evaluation of the chromatograms is more difficult than in the case of the linear DA polymers. In fact the same approach as for the linear DA polymers could be tested. The d*n*/d*c* of the high molar mass region can be estimated from individual measurements of the respective building block and the HDA-Tetralinker. Whereas in the linear DA polymers there is a strictly alternating order of building block and HDA-Tetralinker in the network system there is a variety of different possibilities how the individual components can be connected with each other. Hence, the assumption that the d*n*/d*c* of the DA polymer should be represented accurately by the average d*n*/d*c* of the individual components (Equation 47) is not necessarily valid. Comparing the calculated total polymer concentration to the injected sample amount is not possible either, as the fraction of dissolved network is not known with certainty.

Therefore a second evaluation approach was derived for gaining a higher level of confidence in the results. It is based on the considerations about what parts of the linear DA polymers are relevant for the dRI and the UV/Vis detector (Figure 74). In the case of the HDA-Tetralinker the discussion is similar to the HDA-Dilinker. The CDTE groups should be visible nicely at wavelengths higher than 300 nm, whereas the

core of the molecule should be transparent for these wavelengths. More information about the UV spectra of the individual components were gained by acquiring UV/Vis spectra during the SEC run. The online UV/Vis detector can acquire an entire UV/Vis spectrum within few seconds so that individual spectra can be collected at arbitrary positions in the chromatograms without having to stop the flow. In Figure 78 the chromatogram of Cp_2P^tBuA is shown, together with the spectra that were acquired in a second run at the indicated positions.

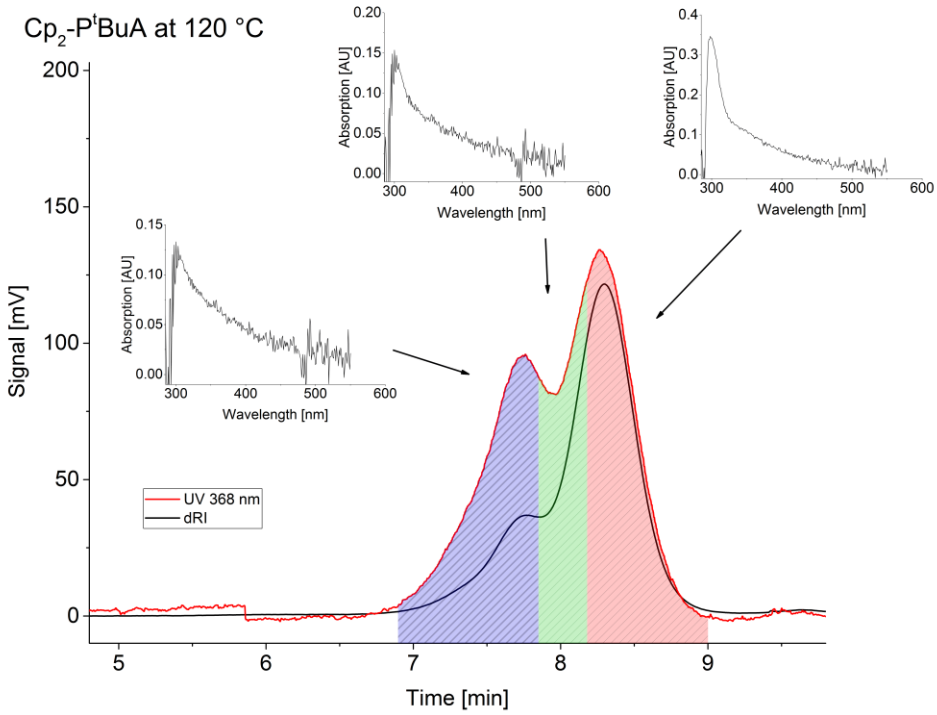

Figure 78: SEC chromatogram (dRI- and UV-trace (acquired at 386 nm)) of the Cp_2P^tBuA acquired at 120 °C in DMAc (3 g/L LiCl). The insets depict the corresponding spectra at the indicated positions.

The polymer building block is visible in both detectors. The UV/Vis spectra do not show particular features but a steadily decaying absorption up to 400-500 nm, irrespective of the position in the chromatogram. Again the building block features a dimer peak at approx. 7.7 min. Interestingly, the ratio of UV- to dRI-signal is higher at the dimer peak than at the monomer peak, indicating a higher absorption coefficient of the DA cycloadduct than for the free Cp endgroups.

In Figure 79 the chromatogram of the HDA-Tetralinker is depicted, together with the UV/Vis spectra of each peak. At first it shall be noted that the positions of the three peaks agree well with molar masses of monomer, dimer and trimer of the HDA-Tetralinker (see Figure 106 in appendix chapter 11.6). The spectra of the first two peak exhibit two overlapping absorption peaks; one at 365 and one at 386 nm. Only the last peak shows a single absorption peak at 386 nm. The CDTE is expected to cause an individual

absorption peak due to the π→π* transition in the C=S double bond.[72] Finding the pronounced absorption peak at the third peak in the chromatogram indicates that it represents the unprotected HDA-Tetralinker. If it would still be trapped with Cp the spectrum should look similar to the Cp building block spectrum (see SI of Ref.[72]). The second absorption in the first two peaks in the chromatogram has to arise from a different chemical construct. As already noted in the case of the HDA-Dilinker it is not yet fully clear what side reactions the CDTE undergoes but a multimerization of the molecule is possible in principle. A further indication towards multimerization is the peak shape of the HDA-Tetralinker after different heating times. If the HDA-Tetralinker is injected without any pre-heating time the last peak ("monomer") is dominant but with increasing time the second peak and eventually the third peak become largest (Figure 107 in appendix chapter 11.6). The total dRI peak area remains practically constant, however. The area of the UV signals, on the other hand, increases with heating time, indicating that the newly formed bonds feature higher absorption coefficients than the free C=S double bond.

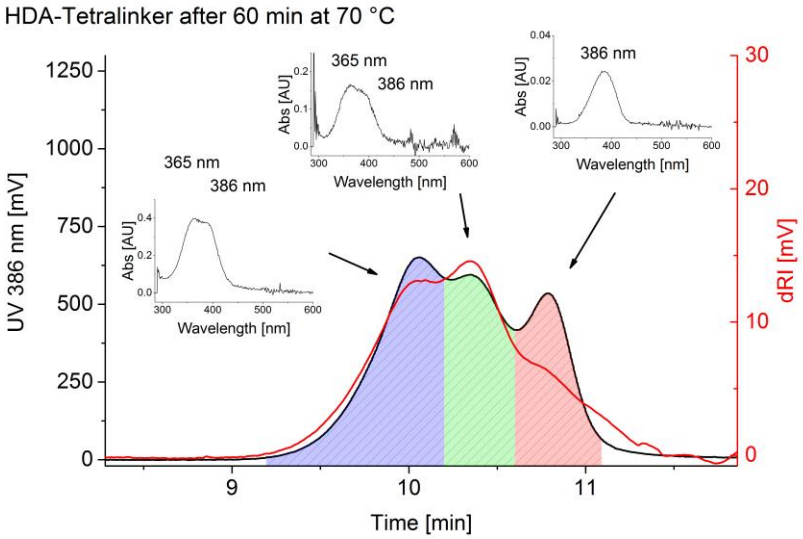

Figure 79: SEC chromatogram (dRI- and UV-trace (acquired at 386 nm)) of the HDA-Tetralinker, acquired after heating for 60 minutes at 70 °C in DMAc (3 g/L LiCl). The insets show the spectra of the individual peaks.

After having investigated the building block and the HDA-Tetralinker it is now time to look at a chromatogram of the DA P^{t}BuA network fragments. In Figure 80 the chromatogram of a DA P^{t}BuA network sample is shown that was drawn after 280 min at 70 °C. Spectra were again acquired for obtaining information about the chemical composition throughout the chromatogram. At low elution volumes the spectra show a broad peak around 340 to 386 nm. Up to 9.5 min the spectra are similar, although the absorption around 386 nm increases. At 10.4 min the absorption at 340 nm diminishes further and at 11 min only the absorption at 386 nm remains. Hence, the features of both, the Cp

building block and the HDA-Tetralinker can be found throughout the chromatogram of the DA polymer. In the high molar mass the spectra resemble the broad and continuous absorption of the Cp building blocks, overlaid with the distinct absorption of the C=S double bond at 386 nm. At higher elution times the absorption of the HDA-Dilinker becomes dominant. Interestingly two HDA-Tetralinker peaks can be identified in the chromatogram at 10.4 and at 11 min, which correlate to the elution times of the dimer and monomer of the HDA-Tetralinker, respectively.

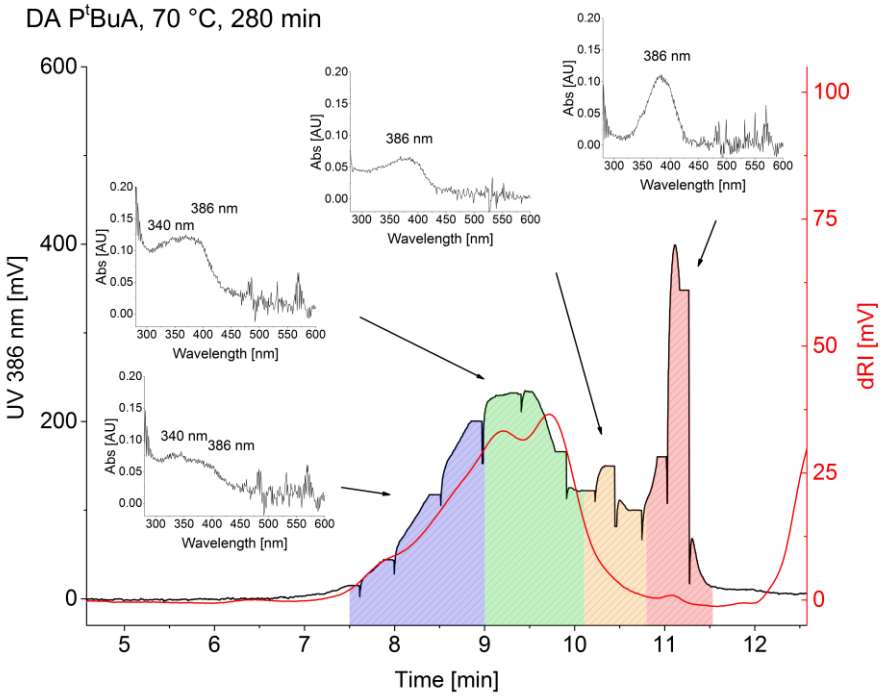

Figure 80: SEC chromatogram (dRI and UV-trace (acquired at 386 nm)) of the DA P^{t}BuA network after 280 min at 70 °C in DMAc (3 g/L LiCl). The insets depict the corresponding spectra at the indicated positions. The UV trace is interrupted because the spectra were acquired in the very same run.

The spectra indicate that in the main peak of the chromatogram both, the building block and the HDA-Tetralinker are present and that only at high elution volumes the pure HDA-Tetralinker can be found (presumably again in monomer and dimer form). Acquiring the spectra during the chromatography run serves for a general image of the chemical composition at different positions but is impractical when collecting a chromatogram that is supposed to be evaluated properly, as the UV traces are getting interrupted (dashed line in Figure 80). It is, however, possible to collect two UV traces simultaneously and to use their ratio as an indicator for the appearance of the respective spectrum. Therefore the UV/Vis absorption were acquired at 386 nm and 425 nm, hence at the absorption maximum of the C=S bond and at the descending part of the spectrum. When the pure HDA-Tetralinker dominates the spectrum this ratio should be high and when the HDA-Tetralinker is integrated in the DA

polymer the ratio should be lower. In Figure 81 the chromatograms of the HDA-Tetralinker and the DA P^{t}BuA are shown with the respective ratios of the UV absorption traces at 386 nm and 425 nm.

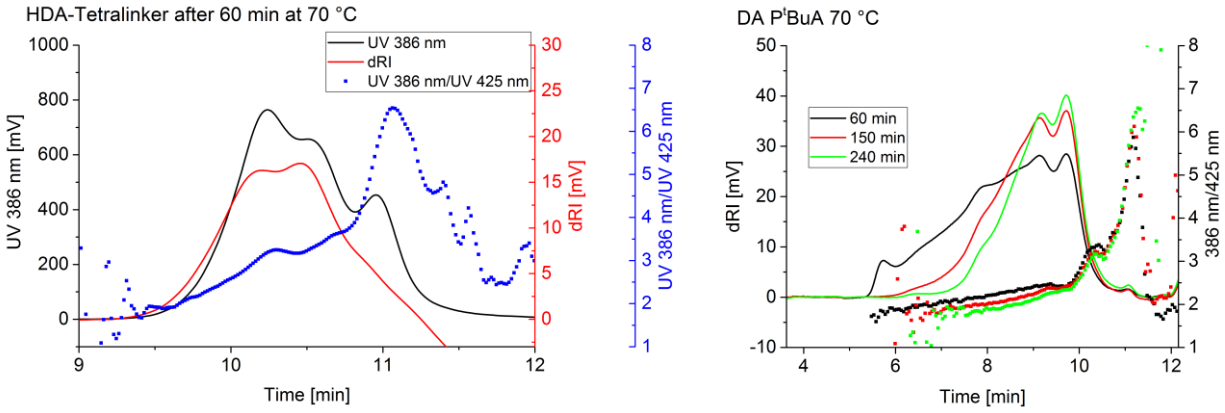

Figure 81: Left: UV- and dRI-trace of the HDA-Tetralinker at 70 °C with the overlaid ratio of the absorption at 386 nm to the absorption at 425 nm. Right: dRI traces of the DA P^{t}BuA after different heating times at 70 °C with the overlaid absorption ratio (386 nm/425 nm). The SEC chromatograms were acquired in DMAc (3 g/L LiCl).

In the case of the HDA-Tetralinker the image supports the already proposed hypothesis: The first two peaks are chemically different from the third one. Only at the third peak the sharp and distinct absorption at 386 nm is found that results in a high ratio of the absorption at 386 to 425 nm. At the other peaks the ratio is lower because of a second overlaid absorption that broadens the absorption peak. In the case of the DA polymer the image is relatively similar: In the high molar mass regime the absorption ratio is very low and only at high elution volumes, where the pure HDA-Tetralinker elutes, the ratio climbs up to similar values that were found for the monomer peak in the HDA-Tetralinker chromatogram. Hence, the ratio of the UV/Vis traces allows estimating if the HDA-Tetralinker is bound (by DA or dimerization reaction) or free.

With all these information the question of how to derive the chemical composition at all positions in the chromatogram can be faced again. As already demonstrated in Figure 74 the dRI and the UV/Vis detector respond to different features of the individual components of the DA polymer system. Furthermore the absorption coefficient of the DA adduct cannot be assessed directly, which makes the quantitative evaluation of the UV/Vis signals difficult. In Figure 82 a simplification of the situation is shown schematically that allows working with only two components, namely the building block (green) and the HDA-Tetralinker (blue). However, the HDA-Tetralinker is treated differently if it is present in bound (dark blue) or free (light blue) state. For all components the respective “contrast factors” (*i.e.*, dn/dc and ε) can be obtained from reference measurements of the building block and the HDA-Tetralinker. It is important to measure all samples at the same day and after identical heating times.

Especially the HDA-Tetralinker is sensitive as it undergoes unpredictable side reactions at elevated temperatures if heated too long.

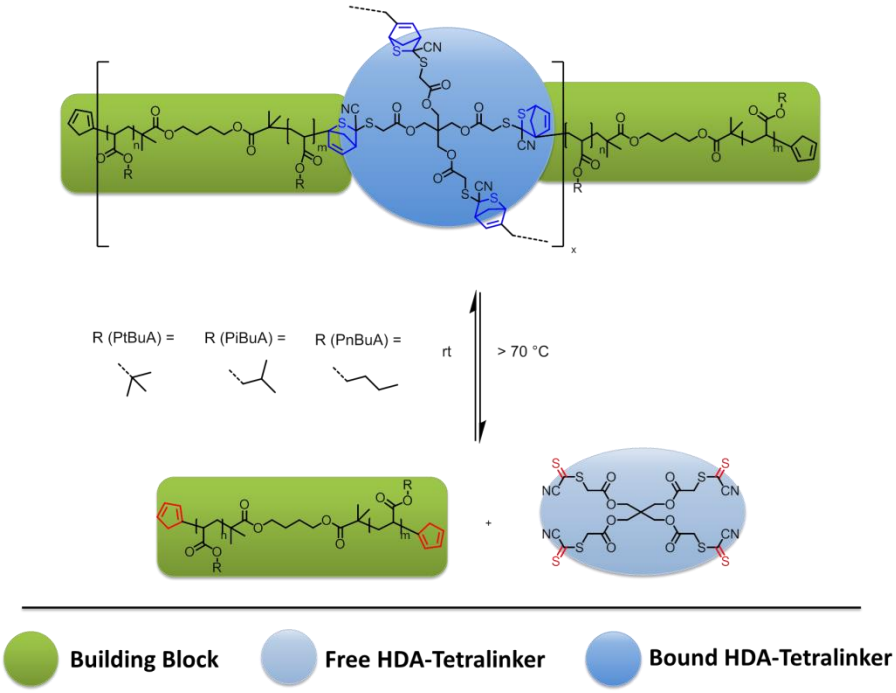

Figure 82: Simplification of the DA network system for calculating the chemical composition. In this way the concentrations of only two components, namely the building block and the HDA-Tetralinker, have to be determined.

A precise determination of the d*n*/d*c* values and the *ε* of the components was not possible due to very limited sample amount. Therefore the linearity of the individual detector responses with increasing sample concentrations were tested only once for each sample (see Figure 109 in appendix chapter 11.6). Because of the good linearity in the relevant concentration range only one reference sample of known concentration of the HDA-Tetralinker and respective building block was measured for deriving the correlation of peak area to sample concentration. The ratio of peak area to concentration will be called "contrast factor" in the following discussion for avoiding confusion with properly determined d*n*/d*c* and *ε* values. In addition it would be advisable to measure multiple concentrations of each reference sample to be able to determine also the intercept of each concentration calibration plot. It was shown in literature that taking into account the respective intercept improves the accuracy of the calculated concentrations, especially close to the peak borders.[101]

The contrast factors of the "free" and "bound" HDA-Tetralinker were determined from the chromatogram of the HDA-Tetralinker. There the concentration of monomer, dimer and trimer were calculated through deconvolution of the dRI trace because the d*n*/d*c* values of the three peaks appear to be very similar. Then the UV/Vis traces were deconvolved, too, and the ratio of UV/Vis peak area to concentration were calculated for the monomer and the sum of dimer and trimer (see Figure 107 and Figure 108 in appendix chapter 11.6). Having determined the contrast factors of building block, bound HDA-Tetralinker and free HDA-Tetralinker, the following set of equations has to be solved in order to calculate the total concentration of building block and HDA-Tetralinker at each position of the chromatogram:

$$dRI = Contrast_{dRI,Polymer} \cdot c_{Block} + Contrast_{dRI,Linker} \cdot c_{Linker} \quad \text{Equation 52}$$

$$UV1 = Contrast_{UV1,Polymer} \cdot c_{Block} + Contrast_{UV1,Linker} \cdot c_{Linker} \quad \text{Equation 53}$$

$$UV2 = Contrast_{UV2,Polymer} \cdot c_{Block} + Contrast_{UV2,Linker} \cdot c_{Linker} \quad \text{Equation 54}$$

In these equations, *dRI*, *UV1* and *UV2* are the individual detector signals, $c_{Polymer}$ and c_{Linker} the concentrations of building block and HDA-Tetralinker, respectively, and the six *Contrast* values of building block and HDA-Tetralinker in the corresponding detectors. The contrast factors of the HDA-Tetralinker were calculated for the bound and the free HDA-Tetralinker, as described above. In the calculations for each point of the chromatogram the values for the bound or free HDA-Tetralinker were used according to the ratio of the UV signals. If the ratio was higher than a set threshold (approx. 2.5 - 3) the values of the free HDA-Tetralinker, otherwise the values of the bound HDA-Tetralinker were applied.

Equation 52 to Equation 54 represent a set of three equations with only two unknowns, namely $c_{Polymer}$ and c_{Linker}. A least square error fit was performed for each point of the chromatogram in order to find the values of $c_{Polymer}$ and c_{Linker} that fit best to the experimentally acquired data. The calculations were done in Scilab 5.5.1, the script can be found in chapter 11.6 in the appendix. Having determined $c_{Polymer}$ and c_{Linker} then allows calculating the intrinsic viscosity from the viscosity signal and eventually applying the universal calibration for determining the molar masses.

In Figure 83 the results are shown for the DA P^{t}BuA after heating to 80 °C for 60 and 120 minutes. The calculated viscosities and molar masses are included, as well as the data of the linear DA P^{t}BuA (after 60 minutes at 80 °C).

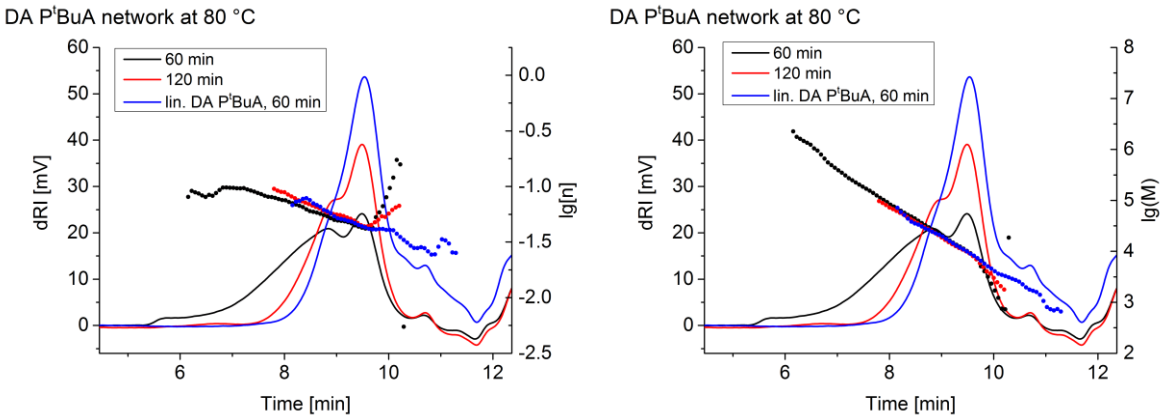

Figure 83: SEC chromatograms of the DA P^{t}BuA network after 60 and 120 min at 80 °C with the overlaid logarithm of the intrinsic viscosity (left) and molar mass (right). For comparison the data of the linear DA polymer are included. All chromatograms were acquired in DMAc (3 g/L LiCl).

The chromatograms show that, after only 60 minutes at 80 °C an extremely broad distribution is obtained that in fact covers the entire molar mass range of the employed SEC column. After additional 60 minutes, however, the distribution narrows significantly and the release of the building block becomes evident. The calculated viscosities and molar masses agree well with those of the linear DA polymer, indicating that the proposed calculation procedure yielded correct results. In Figure 84 the results obtained at 80 and 90 °C are plotted as KMH plots. For comparison the same DA P^{t}BuA network chromatograms were evaluated according to the procedure of estimating the d*n*/d*c* of the DA polymer as the average of the d*n*/d*c* of the building block and the HDA-Tetralinker (analogously to the procedure that was performed for the linear DA polymer) and the results are plotted, too. In both cases the results from averaging of the d*n*/d*c* (blue data points) results in higher viscosities than the results after calculating $c_{polymer}$ and c_{linker} (black data). Deciding which of the results is more realistic is facilitated by including further data into the plots. At first the viscosities of narrowly distributed linear P^{t}BuA samples were determined under identical TD SEC conditions (red data). Then the results from the linear DA P^{t}BuA samples were added (green data). The data from the linear DA P^{t}BuA and from the P^{t}BuA building blocks can be considered relatively trustworthy as the calculation of the results is straight-forward as described in the previous chapter.

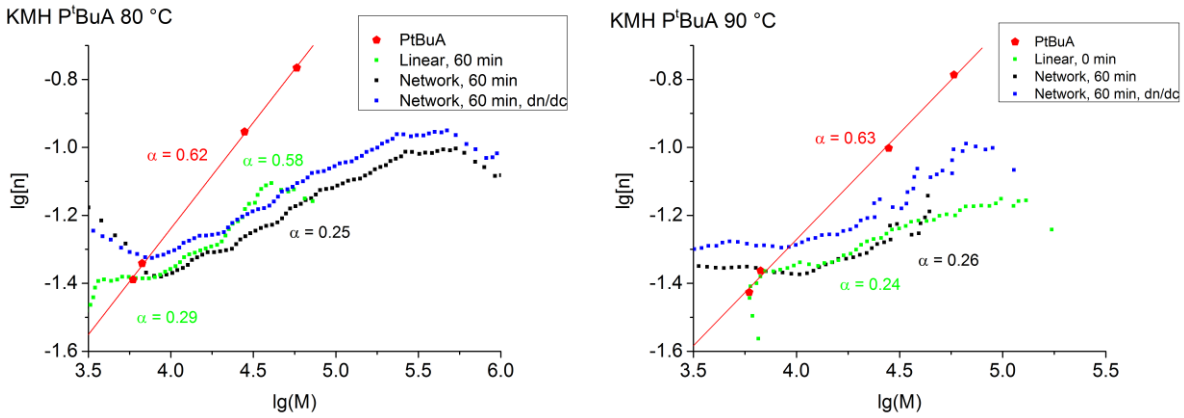

Figure 84: KMH plots of the DA P^{t}BuA networks calculated after the calculating the concentrations according to the chemical composition (black data) and according to the averaged d*n*/d*c* of the DA polymer (blue data). For comparison the bulk intrinsic viscosities of linear P^{t}BuA samples are included, as well as the data from the linear DA P^{t}BuA.

Comparing the different results shows that the data from the chemical composition determination (black data) fits more nicely into the image, as the viscosities at *lg M ≈ 3.8* (molar mass of the building block) are very similar to the viscosities that are obtained for the linear P^{t}BuA at this molar mass. The calculation according to the averaged d*n*/d*c* (blue data points) appears to yield too high viscosities. Therefore the herein proposed procedure of calculating the chemical composition appears better suited for the calculation of the concentrations and, thus, intrinsic viscosity and eventually molar mass.

An unexpected message from Figure 84 is that the *α* of the linear DA P^{t}BuA is significantly lower than expected from the *α* of the P^{t}BuA of different molar masses. At 80 °C a kink in the KMH plot of the linear DA polymer can be observed, where the *α* increases from 0.29 to 0.58. This kink could not be reproduced and is most likely an artifact. The *α* of the linear DA P^{t}BuA was found to be 0.25 – 0.30, which is substantially lower than the 0.62 of the linear P^{t}BuA building blocks. The logic consequence is that a DA P^{t}BuA is more compact than a P^{t}BuA of similar molar mass. One explanation for this finding could be the structure of the employed HDA-Dilinker. An MM2 geometry optimization of both, the HDA-Dilinker and the HDA-Tetralinker was done with Chem3D Pro 14.0.0.117 (PerkinElmer, US) and the result is shown in Figure 85:

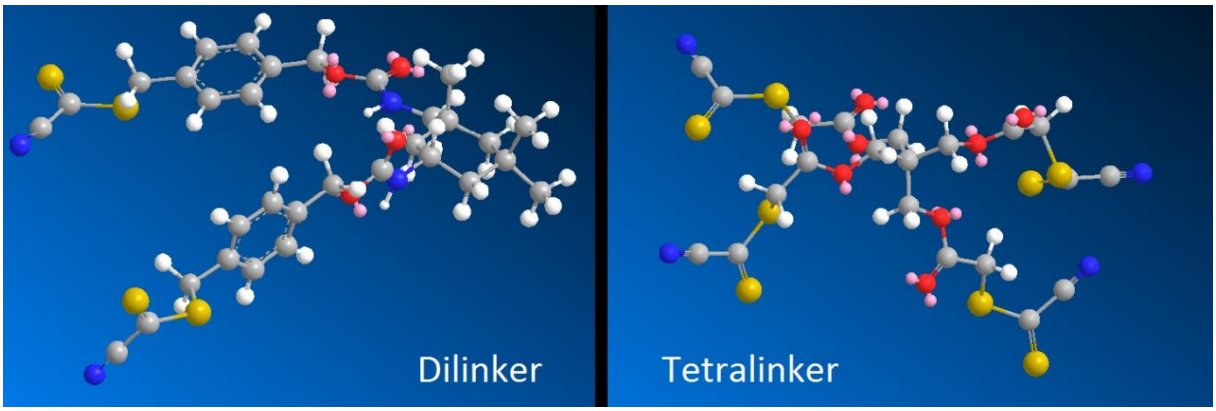

Figure 85: Optimized geometrical structure of the HDA-Dilinker (left) and HDA-Tetralinker (right).

The structure shows that the HDA-Dilinker does not adapt a very "rod like" structure. In contrast both CDTE groups are relatively close together and, consequently, the reacting building blocks are connected relatively close together, too. Although the structure might be different when the HDA-Dilinker is integrated into a DA polymer it appears convenient that the DA polymers adapt a more compact structure than a building block of similar molar mass but without any HDA-Dilinker. Hence, the low α of the DA polymers might be a consequence of the HDA-Dilinker structure but further structural investigations (*e.g.*, by light scattering) could not be done in the time frame of this work.

Interestingly the α values of the DA networks are slightly lower than of the linear DA polymers if the samples are drawn before the reaction reaches equilibrium and approach the values of the linear DA polymers after longer rDA reaction times (Figure 110 to Figure 112 in appendix chapter 11.6). The direct interpretation of the KMH is difficult, though, as all structures appear relatively compact and, consequently, the resulting α values are close together.

More information can be derived from the calculated molar mass distributions. Fitting the entire molar mass distribution according to simple statistics as it was done for the linear polymers (see chapter 4) is not as easily possible for non-linear polymers. However, Macosko and Miller developed a relatively easy model for predicting the M_n and M_w of non-linear polymers at a certain bonding probability p (= conversion), assuming that all HDA-Tetralinkers have the functionality f.[204] Or, vice versa, if M_n, M_w and p of a non-linear polymer sample are known it is possible to determine the degree of functionalization f that fits best the experimentally obtained molar mass averages by a simple optimization procedure. This was done for the rDA reaction of DA P^{t}BuA at 70, 80 and 90 °C. The molar mass averages were calculated out of the obtained molar mass distributions and the p was taken from the reference measurements of the linear DA polymers (right graph of Figure 76). The experimentally derived molar mass averages could be fitted well, as shown in Table 20 in appendix chapter 11.6. At this

point it has to be questioned if the conversion can be assumed to be similar in the case of a linear and a non-linear DA polymer. The in chapter 5.1 demonstrated effect of polymer size on the rDA reactions could potentially be important in this discussion. If there is an effect could not be tested in this work and similar behavior of the linear and non-linear polymers was assumed.

In Figure 86 the average functionality of the HDA-Tetralinker *f* that was obtained for DA P^{t}BuA at 70, 80 and 90 °C is shown, together with the *p* that was obtained from fitting the molar mass distributions of the linear DA polymers. At 70 °C *f* is approx. 3.1 and decreases to approx. 2.4 at 80 and 90 °C. The values indicate that, on average, only every second HDA-Tetralinker molecule leads to a branch. Therefore the degree of branching is significantly lower than if every HDA-Tetralinker would have reacted with four building blocks. A functionality of only 2.4 furthermore explains why the differences in the KMH plots between the linear and the non-linear DA polymers are minor.

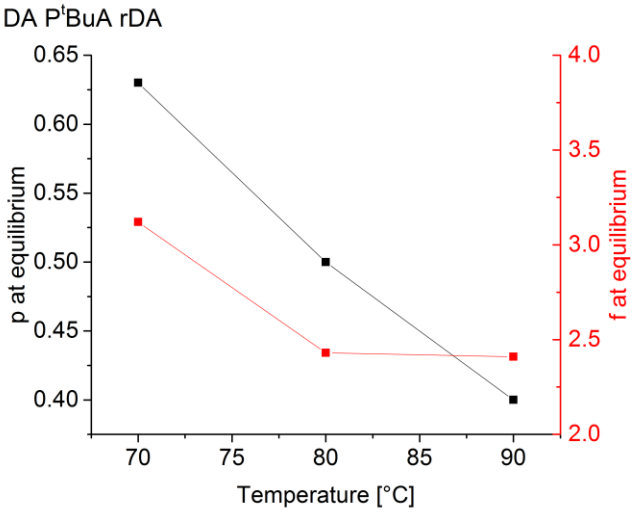

Figure 86: Obtained values for conversion *p* and HDA-Tetralinker functionality *f* as a function of temperature for DA P^{t}BuA.

These observations appear logical. The structure of the HDA-Dilinker is rather compact (right image of Figure 85) and, thus, the probability four building block connect is accordingly low due to the steric hindrance. Furthermore the herein obtained values represent the situation after a certain degree of debonding. In the initial state the functionality of the linker is of course expected to be higher.

The herein reported evaluation scheme enables drawing detailed conclusions about the rDA reaction of crosslinked polymer systems. Although the results appear reasonable more samples have to be measured at different temperatures for the ratification of the procedure. When the evaluation protocol is supported by more data different DA polymer networks could be compared to each other in order to study how the previously described entropy effects can be observed in the corresponding network structures.

8 Dynamic Light Scattering as supporting technique

The considerations that were discussed in the previous chapters are based on the observation of changing size distributions in the course of thermoresponsive bonding/debonding reactions. SEC was shown to be an effective tool for the *in situ* investigation of the respective reactions and that quantitative conclusions can be drawn. The experimental effort is a fact that must not be underestimated. Tuning and optimizing the relevant parameters takes time and the evaluation of the data can be rather complicated. In this chapter Dynamic Light Scattering (DLS) shall be portrayed as an alternative technique that is potentially easier to handle than SEC at the cost of fewer information that are gained.

The general concept of DLS was introduced in chapter 2.6.2. DLS allows determining the hydrodynamic size of a dissolved sample simply by irradiating it with a laser and analyzing the scattered light. In that way the experiment can be easily performed in a cuvette and for temperature dependent measurements it is only necessary to control the temperature of a small cuvette instead of an entire SEC instrument. As a consequence it is much easier to apply steep temperature gradients (*e.g.,* 15 K/min) and to run more complex temperature programs with multiple heating/cooling cycles. Similarly to SEC the size of the molecules is the main parameter that is being observed; but instead of obtaining size distributions by SEC only averaged values are determined by DLS. It is technically possible to resolve differently sized species from the correlation functions by applying the corresponding mathematical treatment (*e.g.*, regularization fit) but it must be kept in mind that the difference in size of two species should be at least of factor 5 for being recognized by the algorithms as two different species. Translating changes in “size” (given by the hydrodynamic radius or the radius of gyration) to changes in mass is possible through a conformation plot, as shown exemplary in Figure 87. Its slope for linear polymers in a good thermodynamic solvent is usually around 0.5-0.6.[88]

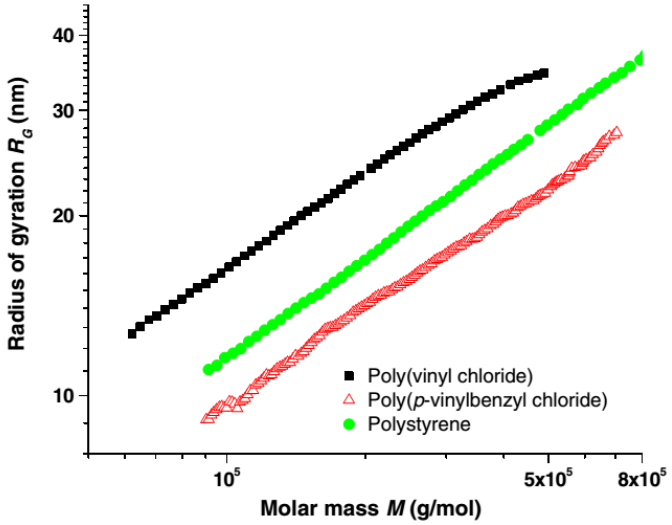

Figure 87: Conformation plot of different linear polymers in a good thermodynamic solvent.[126]

An exemplary scaling parameter of 0.55 would consequently mean that the molar mass scales to 1/0.55 = 1.81 with the size. Or, in other words, increasing the size by a factor of five would mean that the molar mass increases by a factor of $5^{1.81}$ = 18.7 in the same moment. This simple estimation shall demonstrate that the ability of DLS evaluation algorithms for displaying size distributions is comparably weak and should not be overestimated. The DA polymers described in the previous chapters consist of approx. 3 building blocks and the change of mass during rDA reaction is, consequently, of around 3, or in terms of size only of factor $3^{0.55}$ = 1.83. Hence the DLS experiment will only show an average value of the entire size distribution.

A further difficulty is the interpretation of the hydrodynamic size, as the R_h itself depends strongly on the thermodynamic quality of the solvent (see chapter 2.7) and cannot be directly related to a degree of bonding. Therefore the conclusions that can be drawn from a DLS experiment are of rather qualitative nature. More than stating that a polymer is growing or shrinking in reasonable scales is hardly possible.

8.1 Kinetics and reversibility

In this chapter the potential of TD DLS for examining DA reactions is discussed. The high analysis speed should be very useful for monitoring changes in polymer size due to temperature changes, which makes TD DLS interesting for studying the kinetics and reversibility of DA reactions.

8.1.1 Real time analysis of reaction kinetics

Another very quickly reacting DA polymer system was prepared by Kim Öhlenschläger (Structure 29). It is based on the reaction of a Cp endfunctionalized polymer building block (Structure 4) with the HDA-Dilinker (Structure 23) as shown in Figure 88:

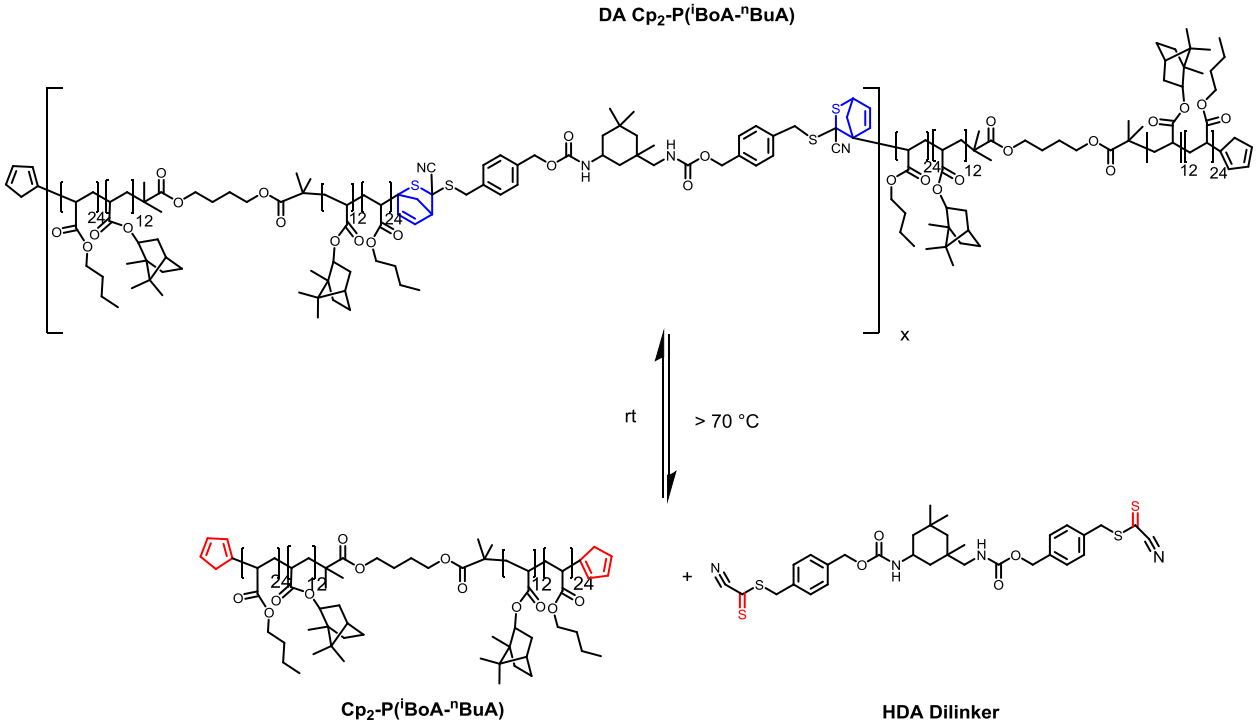

Figure 88: rDA reaction scheme of the DA $Cp_2P(^{i}BoA\text{-}^{n}BuA)$ (Structure 29), releasing the $Cp_2P(^{i}BoA\text{-}^{n}BuA)$ (Structure 4) and the HDA-Dilinker (Structure 23).[72] At high temperatures a significant decrease in molecular size should be observable by DLS.

The molar mass of the $Cp_2\text{-}P(^{i}BoA\text{-}^{n}BuA)$ building block is approx. 13 kDa and the DP_n of the DA polymer is of about 6, or, in other words each DA polymer contains about 3 building blocks and 3 HDA-Dilinkers, resulting in a molar mass of approx. 34 kDa.[72]

First investigations of the performance of the DA reaction were made by UV/Vis spectroscopy at the KIT, as the C=S double bond absorbs strongly at a wavelength of 347 nm (π→π* transition). The measurements demonstrated that both, the bonding and the debonding reactions occur in the time scale of few minutes.[72] Monitoring the progress of reactions that fast would be impossible with SEC but seems to be an interesting challenge for testing the capabilities of DLS.

The most important prerequisite for obtaining good DLS results is to ensure good dissolution of the polymers. In the present case the polymer backbone consisting of $P^{i}BoA$ and $P^{n}BuA$ should be soluble in rather unpolar solvents, whereas the HDA-Dilinker would be insoluble in very unpolar solvents. 1,2,4-

Trichlorobenzene (TCB) was chosen as an appropriate solvent with a sufficiently high boiling point (214 °C). The disadvantage of TCB is that its refractive index (1.571) is relatively close to the refractive index of many polymers and, thus, the resulting specific d*n*/d*c* values are relatively low. Hence, high polymer concentrations are required in order to obtain sufficiently strong light scattering intensity signals. In the present example a concentration of 17 mg/mL was used. Going to high concentration increases the chance of unwanted secondary scattering events and the risk of promoting polymer aggregation, so that higher concentrations for even better signals were avoided. Conclusions about the quality of dissolution can be drawn already from the obtained autocorrelation functions. Two exemplary autocorrelations are shown in Figure 89:

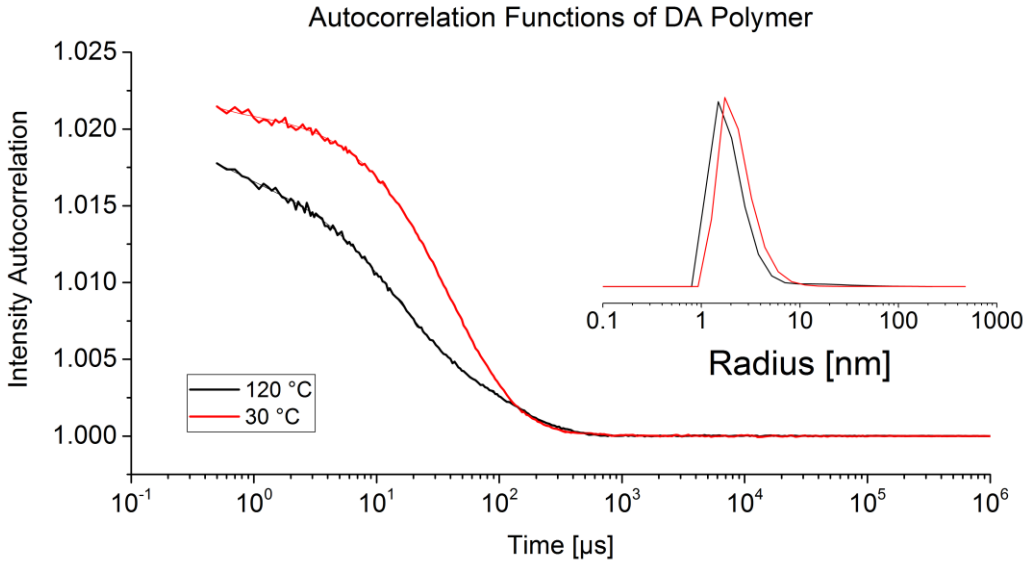

Figure 89: Acquired autocorrelation functions of the DA $Cp_2P(^{i}BoA\text{-}^{n}BuA)$ at 120 °C (black) and 30 °C (red) in TCB. The thin lines represent the corresponding fits. The inset shows the regularization graph (abundancy in weight-%). A good state of dissolution of the DA polymer (*i.e.*, the absence of aggregation) is indicated by the early decay of the autocorrelation function and the results of the regularization graph that displays a monomodal size distribution.

Both functions show a clean decay of the autocorrelation in less than 1 ms, which indicates a good state of dissolution. In the case of aggregation the correlation functions are usually much broader. The software (Dynamics 7.1.7, Wyatt Technology, US) uses a regularization fitting procedure that allows calculating size distributions of the measured samples. The inset in Figure 89 shows the resulting size distributions and, again, indicates the absence of aggregates. The low amplitude of the autocorrelation function and the relatively noisy beginning at low times indicate that the light scattering intensity was still relatively weak. In order to increase the accuracy of the experiment 15-25 acquisitions (2 s

acquisition time) were collected for each measurement. The individual correlation functions are averaged and finally fitted.

In the next step the behavior of the DA polymer during temperature changes was investigated. Therefore the temperature of the cuvette was increased from 30 to 120 °C with the highest achievable temperature ramp of 15 °C/min. The effect of decreasing polymer size as the consequence of the rDA reaction can be seen in the left graph of Figure 90.

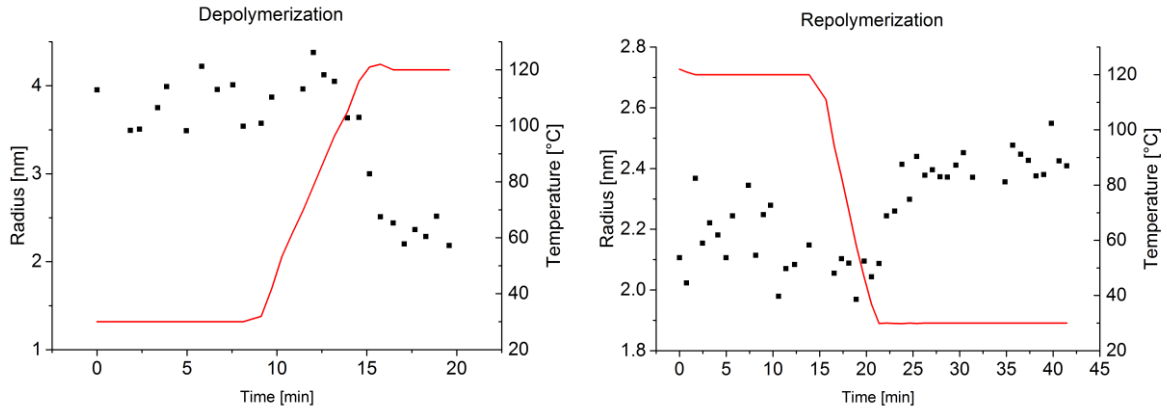

Figure 90: Changes of the hydrodynamic radius of the DA $Cp_2P(^{i}BoA\text{-}^{n}BuA)$ during heating (30 – 120 °C, left graph) and cooling (120 – 30 °C right graph). The measurements were performed in TCB and every data point is obtained from averaging 15 – 25 individual autocorrelation functions of 2 s acquisition time. Although the obtained results are relatively noisy the expected trends of depolymerization (left) and repolymerization (right) can be observed.

A decrease of the hydrodynamic radius from 3.75 to 2.2 nm within 3 minutes can be observed when the temperature rises higher than 80 °C. The decrease of factor 1.7 is within reasonable scale: The molar mass is expected to decrease by a factor of approx. 3, which would translate into a change in size of 1.8 (assuming a scaling parameter of 0.55). Unfortunately it is not possible to draw more detailed conclusion from the measured value, as they would require precise knowledge about the scaling behavior and the magnitude of thermodynamic swelling of the polymer coils.

The second step of the experiment was, of course, to decrease the temperature and investigate if an increase of the radius due to repolymerization can be observed. In the right graph of Figure 90 the corresponding data are displayed, showing a slight increase of the radius from 2.2 to 2.4 nm when the temperature approaches 30 °C. An increase in size of factor 1.1 would correspond to an increase in mass of 1.2, again assuming a scaling parameter of 0.55 and neglecting the thermodynamic contraction during cooling, which is expected to be significant in that temperature range. The much less pronounced increase in size during repolymerization indicates that only a fraction of the originally present DA cycloadditions is restored. This finding has to be interpreted considering that, in contrast to the

depolymerization, the repolymerization is dependent on building blocks and HDA-Dilinkers finding themselves by diffusion and, consequently, on the concentration of the solution. For achieving high conversions the "initial" DA polymerization was carried out in the polymer bulk rather than in solution. The concentration in the experiment can be evaluated by simple theoretical considerations. According to literature, the overlap concentration of a polymer solution, *i.e.*, the concentration where the polymer coils can come in contact, can be estimated by Equation 55

$$c^* \cong \frac{3M}{4\pi N_A R_g^3} \qquad \text{Equation 55}$$

, where c^* is the overlap concentration, M the molar mass of the polymers, N_A Avogadro's number and R_g the radius of gyration.[205] With a molar mass of the polymer building block of 13 kDa and a radius of 2.2 nm one obtains an overlap concentration of 484 mg/mL, which is far above the employed concentration of 17 mg/mL. Consequently it cannot be expected to observe a conversion of functional groups in the relatively dilute DLS solution similar to the conversion that was achieved in bulk. Furthermore the previous work indicated that the unprotected HDA-Dilinker undergoes side reactions at elevated temperatures and, therefore, is not anymore fully accessible for repolymerization reactions at lower temperatures.

The experiments demonstrate that DLS is powerful for following fast rDA/DA reactions, even if they do not proceed in very high conversions. The measured time scales agree well to the times that were found by UV/Vis spectroscopy[72]. Furthermore the events responsible for the size changes have to be of chemical nature, as they overcompensate the thermodynamic swelling/collapsing of polymer coils. In the following chapter the question about the DA reaction's reversibility is investigated.

8.1.2 Assessing the reversibility of DA reactions by TD DLS

In the next step the DA $Cp_2P(^{i}BoA\text{-}^{n}BuA)$ polymer was subjected to a more complex temperature program, consisting of seven heating and cooling cycles. For a better understanding of the results the temperature program was performed identically with the $Cp_2P(^{i}BoA\text{-}^{n}BuA)$ building block. In Figure 91 the results are compiled in one graph.

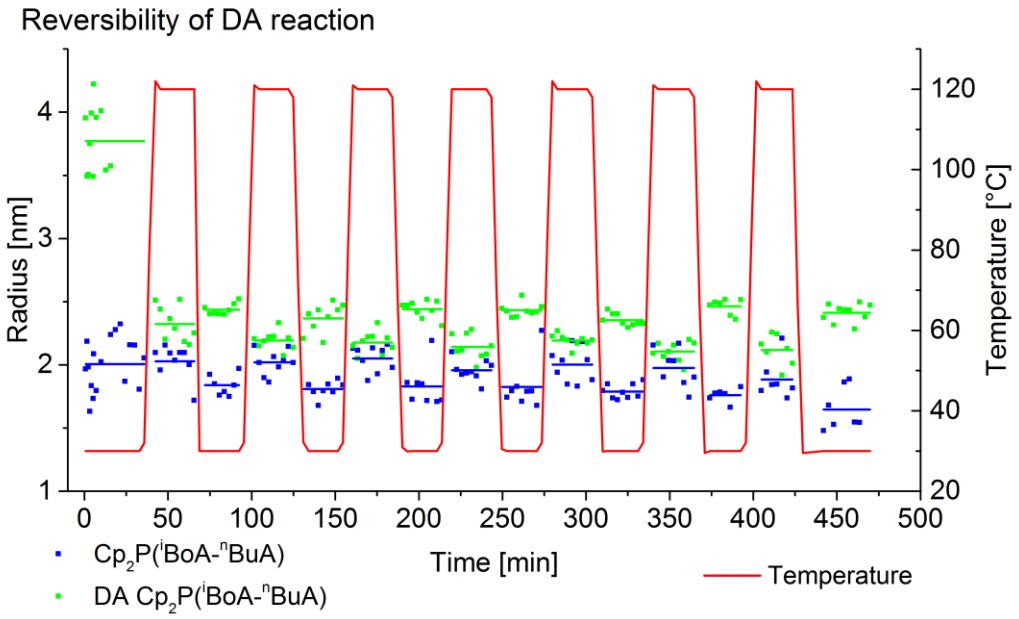

Figure 91: Results of the TD DLS experiments with the DA $Cp_2P(^{i}BoA\text{-}^{n}BuA)$ and its building block ($Cp_2P(^{i}BoA\text{-}^{n}BuA)$) during seven heating/cooling cycles between 30 and 120 °C (in TCB). The dots depict individual measurements (average of each 15-25 single acquisitions) and the lines the averaged values for each temperature step. As expected the radius of the DA $Cp_2P(^{i}BoA\text{-}^{n}BuA)$ decreases during heating (rDA reaction) and increases during cooling (DA reaction).

The green data show the radii of the DA polymer, whereas the blue data represent the radii of the $Cp_2P(^{i}BoA\text{-}^{n}BuA)$ building block at the respective temperatures that are indicated by the red line. Let us first discuss the data from the DA polymer (green data). The beginning of the graph again shows the rDA and DA behavior that was discussed in the previous chapter. Interestingly, over the following heating/cooling cycles, the temperature induced changes in size are nicely reproducible. That finding supports the previously made hypothesis that after the first rDA reaction the solution is too dilute to repolymerize up to the initial conversion that was achieved through the original DA reaction in bulk. Since the concentration remains essentially constant throughout the experiment the extent of DA and rDA reaction and, thus, the change in size, stays constant.

The behavior of the individual $Cp_2P(^{i}BoA\text{-}^{n}BuA)$ building block is interesting, too, and reveals further insights: Since it is not able to undergo temperature dependent reactions with itself (the self-dimerization of cyclopentadiene can be neglected), the building block will show the physicochemical swelling/collapsing of a polymer that was described already in chapter 2.7. According to theory the polymer coil should swell to larger dimensions when the thermodynamic quality of the solvent increases, as it is usually the case upon heating. The blue data in Figure 91 show exactly this behavior, again in a

very reproducible manner. An equal effect of temperature dependent swelling should occur for the DA polymer too, as its physicochemical properties should be dominated by the properties of the polymer building block rather than by the relatively small HDA-Dilinker. The effect is not visible in the case of the DA polymer, however, because it is overcompensated by the DA/rDA reactions.

As a second example the amphiphilic DA PTEGA-P(S-*co*-I) (Structure 28), which was already studied by TD SEC in chapter 5.4, was analyzed similarly. Its structure is displayed again in Figure 92:

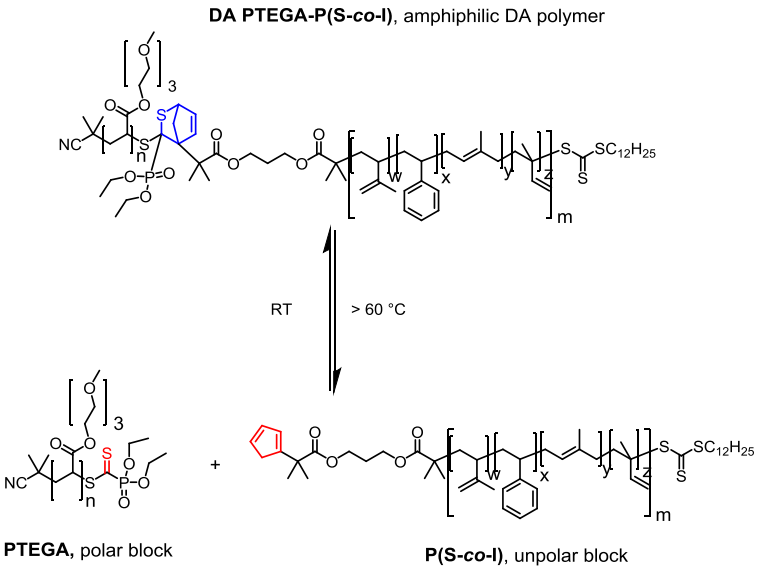

Figure 92: rDA scheme of the amphiphilic DA PTEGA-P(S-*co*-I) (Structure 28), giving the polar PTEGA block (Structure 26) and the unpolar P(S-*co*-I) block (Structure 27)**.**[149]

The number averaged molar masses are 9200 g/mol for the unpolar block (P(S-*co*-I)), 6600 g/mol for the polar block (PTEGA), and 16000 g/mol for the DA copolymer (DA PTEGA-P(S-*co*-I)), respectively.[149] As a consequence the scattered light intensity will be rather weak and the expected difference in molar mass and, hence, size is small. Aggregation must be avoided very carefully if trustworthy results are desired. Establishing a good state of dissolution for the different components requires particular care when selecting the solvent and employed polymer concentrations, which renders the analysis of the present DA by DLS system a particular challenge.

Different solvents, such as TCB, toluene or DMAc were tested but they all lead to aggregation at some point of the experiment. Finally a mixture of 80 % DMAc and 20 % toluene was found to work well for the amphiphilic copolymer. Because of the need of the present DA system for a catalyst, 2.75 mg/mL $ZnCl_2$ were added to the mixture. Polymer concentrations of 25 mg/mL were employed and for each

measurement 25 single acquisitions (2 s acquisition time) were collected. Under these conditions it was possible to obtain clean correlation functions, as shown in Figure 93:

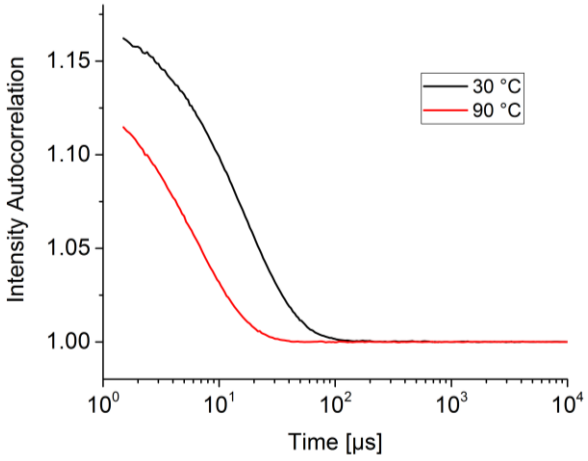

Figure 93: Autocorrelation functions of the DA PTEGA-P(S-*co*-I), acquired at 30 and at 90 °C in a mixture of 80 % DMAc and 20 % toluene. A good state of dissolution is indicated by the quick decay of the autocorrelation functions to baseline in less than 1 ms.

For the evaluation of the data it is important to know the viscosity of the solution (see chapter 2.6.2). Usually the viscosity of the solution is approximated by the viscosity of the solvent. In the present experiments the viscosity of the actual polymer solution was determined separately in order to increase the accuracy of the calculations. By measuring the solvent mixture and the solvent mixture including 25 mg/mL at 30 and 90 °C significantly higher viscosity values for the viscosity were found (approx. 25 % higher for the solution). For all following calculations the solution viscosity values were used.

The TD SEC measurements (chapter 5.4) already showed that the rDA reaction is expected to be rather quick, whereas the repolymerization is expected to be significantly slower. The TD DLS experiments, too, showed that the rDA reaction occurs within less than one hour, whereas the repolymerization took several hours, even in the presence of the $ZnCl_2$ catalyst. The temperature cycling experiment was done by heating at 90 °C and measuring the radius continuously for one hour after which the temperature was decreased to 30 °C and measurements were done every hour for one day. Two different solutions of the DA PTEGA-P(S-*co*-I) of the same batch and a sample of the unpolar P(S-*co*-I) building block were subjected to that procedure. Unfortunately the polar PTEGA block was not available as an individual sample. In Figure 94 the results of the three experiments are shown, whereas each data point is the average of each at least 5 single measurements.

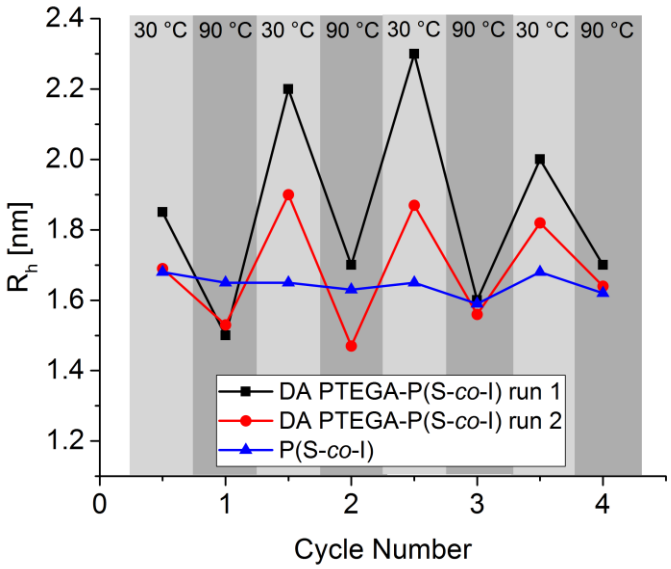

Figure 94: Results of the TD DLS experiment of the amphiphilic DA PTEGA-P(S-*co*-I) in 80 % DMAc and 20 % toluene. The temperature cycling (30 – 90 °C) with the DA PTEGA-P(S-*co*-I) was done twice in order to increase the confidence in the obtained R_h values. Both runs are displayed in the figure ("DA PTEGA-P(S-*co*-I) run 1" and "DA PTEGA-P(S-*co*-I) run 2", respectively). In addition the R_h of the unpolar P(S-*co*-I) building block was determined at identical conditions and included in the figure.

The experiment shows that the DA polymers exhibit a strong temperature dependence of their size, although the radii from the individual experiments only show the same trend but do not agree well in their magnitude. The size difference between 30 and 90 °C ranges from 1.1 to 1.4, which is roughly in a reasonable scale: Assuming a scaling parameter of 1/3, as it would be the case for rather poor solvents, would mean that for a molar mass increase from 8 kDa (average of both building blocks) to 16 kDa the size should increase by a factor of 1.26.

The size of the building block, however, seems to be independent of the temperature. In contrast to the previous experiment with the $Cp_2P(^{i}BoA\text{-}^{n}BuA)$ building block (Figure 91) the unpolar building block of this DA system does not seem to swell at higher temperatures. A possible interpretation of this finding is that the relatively polar solvent mixture (80 % DMAc, 20 % toluene) is too poor for the unpolar building block so that the polymer coil is in a collapsed state. Deriving more details from this experiment is not possible, as it would require more in-depth light scattering experiments for deducing the conformation of the polymer in the present solvent mixture.

In general the quality of the measurement is worse than for the previous example, where a good state of dissolution for all components of the DA polymer system could be found. Nevertheless it was possible to show that the amphiphilic DA copolymer is able to connect and disconnect both blocks

reversibly in dependency of the temperature. The TD DLS results corroborate the TD SEC results in a qualitative manner.

9 Conclusions and Outlook

The main objective of this work was to develop and establish a temperature dependent SEC methodology for the quantitative *in situ* analysis of thermoreversibly bonding polymer systems. The in depth understanding of stimuli responsive bonding reactions is key for the development of novel advanced functional materials. The benefits of SEC for analyzing dynamic bonding reactions are evident: the molar mass distribution of a reversibly bonding polymer system gives detailed insights into the progress of the respective bonding reactions. Monitoring the MMD during a bonding or debonding event is consequently a promising approach.

Setting up the chromatograph and working out the analysis protocols was accompanied by several challenges. SEC is usually done at a constant temperature, as especially the employed columns are sensitive to temperature changes. Therefore the integrity of the column materials was analyzed with respect to changes in chemical structure, pore size distribution and separation characteristics.[157] The results indicated that the columns are relatively stable if gentle heating rates (0.5 °C/min) are applied. Nevertheless it appears advisable to perform drastic temperature changes (*e.g.*, from 120 °C to ambient temperature) only when it is absolutely necessary.

Besides the column materials also the SEC separation itself is sensitive to temperature changes, which implies further complications. Although temperature does not have a direct influence due to the (in the ideal case) absence of enthalpic interactions there are secondary phenomena that impact the outcome of an SEC experiment (swelling of the column packing particles and increasing diffusion of molecules at higher temperatures). A direct consequence is that all chromatograms that have to be referenced to each other (*e.g.*, calibration standards) have to be collected at the same temperature and, at best, at the same day. Then it is possible to obtain robust and reproducible results.

The TD SEC concept was developed, tested and improved on the example of a variety of DA polymers that undergo rDA reaction at temperatures higher than 70 °C. At first sight the interpretation of the obtained SEC chromatograms is straight-forward: The peaks shift towards higher elution times with increasing heating times of the samples (*i.e.*, rDA reaction times), indicating an MMD that shifts towards lower molar masses. In order to quantify this qualitative observation correctly requires careful calibrations, however. The main reason for the complexity of the data interpretation is the chemical heterogeneity of the employed DA polymer systems. In each case at least two molecules react together that are different in their chemical structure and molar mass. The individual components but also their different combinations can interact differently with the column materials and contribute differently to

the detector signals. As a consequence the separation mechanisms and the concentration dependency of the obtained chromatograms are difficult to assess.

It could be shown that, if a purely size based separation could be evidenced, the MMD in fact can be evaluated relatively easily: Either by calculating molar mass averages or by exploiting statistical models that allow fitting the entire MMD. In either way the MMD can be correlated to a conversion of the underlying DA/rDA reactions that allow comparing the extent of a debonding reaction across different polymer systems (chapter 4). If enthalpic interactions cannot be excluded and/or if the chemical composition distribution throughout the chromatogram is unknown a different approach proved to work for all so far investigated examples: The chromatograms can be deconvolved with the information that are obtained by measuring reference samples and the individual peaks can be treated individually. In particular the deconvolution approach allows determining the concentration of individual components of the DA polymer system. Monitoring these concentrations during an rDA reaction again allows quantifying the extent of bonding or debonding. Therefore the quantitative analysis of rDA reactions with TD SEC was possible in all tested cases, although it has to be noted that no universal evaluation protocol could be given. On the contrary it is necessary to assess each DA system individually in order to deduce the most reliable evaluation procedure (chapter 5). As a further possibility for analyzing reversibly bonding systems TD HPLC was tested. In a proof-of-concept the feasibility of interaction based chromatography and also two-dimensional chromatography was confirmed (chapter 6).

The development of the TD SEC methodology was done in the context of the experimental corroboration of entropy effects that were predicted to influence the extent of debonding in a reversibly bonding polymer system. It was predicted that the physicochemical properties of polymers in between the reversibly bonding moieties do have an effect on the thermodynamics of the actual bonding reactions. So, in contrast to conventional approaches not only the chemical constitution of the actual reaction centers but also the nature of the polymer building blocks can be used for fine-tuning the bonding reactions.[69,71] For the experimental proof of the hypotheses adequate model polymers were prepared by Nathalie Guimard and Kai Pahnke at KIT that vary either in building block size (chapter 5.1) or building block flexibility (chapter 5.2). The herein described analyses by TD SEC support the proposed trends and indicate that at a given temperature a higher degree of debonding is achieved, when the building blocks are made larger or more flexible. On the one hand these novel insights open new pathways for the synthesis of tailor-made responsive materials that match the precise requirements of versatile applications. But on the other hand these insights demonstrate that from small molecule studies obtained results cannot be transferred directly to polymer systems, because of entropy effects that will become significant when polymers are introduced.

A second objective of this work was to investigate the reversibility of the DA/rDA reactions. Although TD SEC proved to be an effective tool for this purpose, too, it was especially TD DLS that could be used for obtaining valuable insights. With TD DLS the R_h of the DA polymers can be monitored in real time during multiple heating/cooling cycles. Even though the R_h cannot be related directly to a degree of debonding it allows following the bonding/debonding events qualitatively. The methodology was sensitive enough to follow DA/rDA reactions with less than factor 2 between the molar mass of DA adduct and the respective building blocks (chapter 8).

In conclusion TD SEC and TD DLS proved to be valuable analytical tools for versatile investigations of thermoresponsive bonding reactions. Both methodologies can reliably assess the progress of reversible bonding reactions and allow for a better understanding of the fundamental mechanisms that can be used for tuning their performance. However, the described analysis concepts are still in their infancy and carry potential for improvement. They need further experimental applications for corroboration of the proposed analysis protocols on the basis of more comprehensive experiences. A few precise options for future investigations shall be mentioned at this point.

At first the determination of the chemical composition distribution by UV/Vis detection should be exploited and optimized more. Upgrading the flow cell with a second inlet capillary that bypasses the column and can be accessed via a syringe would allow doing time resolved UV/Vis spectroscopy with reference substances independently at identical conditions as in the actual TD SEC experiment. The results of a more detailed determination of the chemical composition could be correlated to *offline* spectroscopy experiments (*e.g.*, NMR, Raman) in order to verify them.

Further potential lies in the improvement of the TD HPLC approach. The herein reported results can be understood as a “proof of concept” that needs to be verified on more and diverse samples. Assessing the applicability of the 2D LC approach is a future goal, too. If the long analyses times do not appear to bias the outcome of the reactions this approach offers tremendously detailed results. Deducing both, the MMD and the CCD simultaneously yields an otherwise unreached level of detail in insights in the formed reaction products. The work of Ginzburg et al. demonstrated the practical feasibility of 2D LC at elevated temperatures[197] and can serve as a general guide for setting up a TD 2D LC approach. Another advantage of a 2D LC setup would be that the single LC dimensions can be used independently so that the operator can always choose between TD SEC, TD HPLC and TD 2D LC.

Besides consolidating the herein described techniques and promoting the development of more advanced LC methodologies it would be worth improving the TD DLS investigations. Particular value of DLS can be found in the real time analysis of the crosslinking reactions. Although DLS is a classical

solution technique it is occasionally employed for investigating gelation reactions.[127,128,206–212] First tests on the present DA networks revealed promising results, but further optimization is required for better reproducibility (see appendix chapter 11.7). The effort would be rewarded by the possibility of following the reversible crosslinking reactions in real time and drawing conclusions about the mesh size of the formed networks.

The concept of size-based *in situ* analyses could be widened by taking into account separation techniques other than SEC. Hydrodynamic chromatography and field flow fractionation are suitable for the separation of very large polymers or even supramolecular associates because of substantially lower shear rates during the experiments.[89,106,107,129,213] Especially asymmetrical flow field-flow fractionation (AF4) has gained increasing attention in the analyses of biopolymers and bioparticles because of the possibility to work under physiological conditions.[91,93,94] Changing solvents is easier in AF4 than in LC so that additionally to temperature dependent also pH dependent measurements could be realized. Hence, biologically relevant dynamic bonding systems could be investigated more in detail than with SEC.

In summary there are still many pathways for optimizing and extending the herein introduced methodologies further. With the help of more advanced analytical tools the development of tailor-made functional material will be facilitated as the important influencing parameters can be deduced more effectively. Simultaneously detailed information about the occurring reactions are obtained that support the general knowledge of the fundamental processes.

10 Bibliography

[1] J.-M. Lehn, *Prog. Polym. Sci.* **2005**, *30*, 814.

[2] W. Knoben, N. A. M. Besseling, L. Bouteiller, M. A. C. Stuart, *Phys. Chem. Chem. Phys.* **2005**, *7*, 2390.

[3] T. Maeda, H. Otsuka, A. Takahara, *Prog. Polym. Sci.* **2009**, *34*, 581.

[4] S. J. Rowan, S. J. Cantrill, G. R. L. Cousins, J. K. M. Sanders, J. F. Stoddart, *Angew. Chemie Int. Ed.* **2002**, *41*, 898.

[5] Y. Jin, C. Yu, R. J. Denman, W. Zhang, *Chem. Soc. Rev.* **2013**, *42*, 6634.

[6] R. P. Wool, *Soft Matter* **2008**, *4*, 400.

[7] N. K. Guimard, K. K. Oehlenschlaeger, J. Zhou, S. Hilf, F. G. Schmidt, C. Barner-Kowollik, *Macromol. Chem. Phys.* **2012**, *213*, 131.

[8] M. D. Hager, P. Greil, C. Leyens, S. van der Zwaag, U. S. Schubert, *Adv. Mater.* **2010**, *22*, 5424.

[9] C. Wang, G. Wang, Z. Wang, X. Zhang, *Chem. Eur. J.* **2011**, *17*, 3322.

[10] H. Lee, W. Wu, J. K. Oh, L. Mueller, G. Sherwood, L. Peteanu, T. Kowalewski, K. Matyjaszewski, *Angew. Chemie Int. Ed.* **2007**, *46*, 2453.

[11] E. R. Gillies, J. M. J. Fréchet, *Chem. Commun.* **2003**, 1640.

[12] C. J. Kloxin, T. F. Scott, B. J. Adzima, C. N. Bowman, *Macromolecules* **2010**, *43*, 2643.

[13] S. J. Kalista, Dissertation: Self-Healing of Thermoplastic Poly(Ethylene-Co-Methacrylic Acid) Copolymers Following Projectile Puncture, Virginia Polytechnic Institute and State University, **2003**.

[14] S. J. Kalista, T. C. Ward, *J. R. Soc. Interface* **2007**, *4*, 405.

[15] S. J. Kalista, J. R. Pflug, R. J. Varley, *Polym. Chem.* **2013**, *4*, 4910.

[16] A. Bapat, J. Ray, D. Savin, B. Sumerlin, *Macromolecules* **2013**, *46*, 2188.

[17] H. Otsuka, S. Nagano, Y. Kobashi, T. Maeda, A. Takahara, *Chem. Commun.* **2010**, *46*, 1150.

[18] A. P. Vogt, B. S. Sumerlin, *Soft Matter* **2009**, *5*, 2347.

[19] J. Brandt, K. K. Oehlenschlaeger, F. G. Schmidt, C. Barner-Kowollik, A. Lederer, *Adv. Mater.* **2014**, *26*, 5758.

[20] H. Barth, F. C. Jr, *J. Liq. Chromatogr.* **1984**, *7*, 1717.

[21] I. Roy, M. N. Gupta, *Chem. Biol.* **2003**, *10*, 1161.

[22] M. A. C. Stuart, W. T. S. Huck, J. Genzer, M. Müller, C. Ober, M. Stamm, G. B. Sukhorukov, I. Szleifer, V. V Tsukruk, M. Urban, F. Winnik, S. Zauscher, I. Luzinov, S. Minko, *Nat. Mater.* **2010**, *9*, 101.

[23] M. R. Islam, Z. Lu, X. Li, A. K. Sarker, L. Hu, P. Choi, X. Li, N. Hakobyan, M. J. Serpe, *Anal. Chim. Acta* **2013**, *789*, 17.

[24] E. S. Gil, S. Hudson, *Prog. Polym. Sci.* **2004**, *29*, 1173.

[25] C. Dry, *J. Intell. Mater. Syst. Struct.* **1993**, *4*, 420.

[26] J. W. Kamplain, C. W. Bielawski, *Chem. Commun.* **2006**, *16*, 1727.

[27] F. Tournilhac, P. Cordier, D. Montarnal, C. Soulié-Ziakovic, L. Leibler, *Macromol. Symp.* **2010**, *291-292*, 84.

[28] O. Ikkala, G. ten Brinke, *Science* **2002**, *295*, 2407.

[29] Y. Amamoto, M. Kikuchi, H. Masunaga, S. Sasaki, H. Otsuka, A. Takahara, *Macromolecules* **2010**, *43*, 1785.

[30] H. Otsuka, K. Aotani, Y. Higaki, Y. Amamoto, A. Takahara, *Macromolecules* **2007**, *40*, 1429.

[31] J. Canadell, H. Goossens, B. Klumperman, *Macromolecules* **2011**, *44*, 2536.

[32] J. Li, J. M. a Carnall, M. C. a Stuart, S. Otto, *Angew. Chemie - Int. Ed.* **2011**, *50*, 8384.

[33] H. Kwart, K. King, *Chem. Rev.* **1968**, *68*, 415.

[34] E. Goiti, M. B. Huglin, J. M. Rego, *Macromol. Rapid Commun.* **2003**, *24*, 692.

[35] J. Zhou, N. K. Guimard, A. J. Inglis, M. Namazian, C. Y. Lin, M. L. Coote, E. Spyrou, S. Hilf, F. G. Schmidt, C. Barner-Kowollik, *Polym. Chem.* **2012**, *3*, 628.

[36] K. K. Oehlenschlaeger, J. O. Mueller, J. Brandt, S. Hilf, A. Lederer, M. Wilhelm, R. Graf, M. L. Coote, F. G. Schmidt, C. Barner-Kowollik, *Adv. Mater.* **2014**, *26*, 3561.

[37] P. Reutenauer, E. Buhler, P. J. Boul, S. J. Candau, J.-M. Lehn, *Chem. Eur. J.* **2009**, *15*, 1893.

[38] M. A. Tasdelen, *Polym. Chem.* **2011**, *2*, 2133.

[39] P. Froimowicz, H. Frey, K. Landfester, *Macromol. Rapid Commun.* **2011**, *32*, 468.

[40] J.-M. Lehn, *Chem. Eur. J.* **1999**, *5*, 2455.

[41] A. B. W. Brochu, S. L. Craig, W. M. Reichert, *J. Biomed. Mater. Res. A* **2011**, *96*, 492.

[42] M. J. Harrington, O. Speck, T. Speck, S. Wagner, R. Weinkamer, in *Adv. Polym. Sci.*, **2015**, pp. 1–38.

[43] J. P. Brockes, *Science.* **1997**, *276*, 81.

[44] Y. C. Yuan, *eXPRESS Polym. Lett.* **2008**, *2*, 238.

[45] D. Y. Wu, S. Meure, D. Solomon, *Prog. Polym. Sci.* **2008**, *33*, 479.

[46] S. Chen, N. Mahmood, M. Beiner, W. H. Binder, *Angew. Chemie Int. Ed.* **2015**, n/a.

[47] Y. Higaki, H. Otsuka, A. Takahara, *Macromolecules* **2006**, *39*, 2121.

[48] J. M. Craven, *Cross-Linked Thermally Reversible Polymers Produced From Condensation Polymers With Pendant Furan Groups Cross-Linked With Maleimides*, **1969**.

[49] C. Toncelli, D. C. De Reus, F. Picchioni, A. a. Broekhuis, *Macromol. Chem. Phys.* **2012**, *213*, 157.

[50] D. Kowalski, M. Ueda, T. Ohtsuka, *J. Mater. Chem.* **2010**, *20*, 7630.

[51] O. Diels, K. Alder, *Justus Liebigs Ann. Chem.* **1928**, *31*, 98.

[52] G. Franc, A. K. Kakkar, *Chem. Eur. J.* **2009**, *15*, 5630.

[53] A. A. Kavitha, N. K. Singha, *ACS Appl. Mater. Interfaces* **2009**, *1*, 1427.

[54] K. C. Nicolaou, S. Snyder, T. Montagnon, G. Vassilikogiannakis, *Angew. Chemie Int. Ed.* **2002**, *41*, 1668.

[55] G. W. Goodall, W. Hayes, *Chem. Soc. Rev.* **2006**, *35*, 280.

[56] S. Sinnwell, C. V Synatschke, T. Junkers, M. H. Stenzel, C. Barner-Kowollik, *Macromolecules* **2008**, *41*, 7904.

[57] A. A. Kavitha, N. K. Singha, *Macromolecules* **2010**, *43*, 3193.

[58] A. a. Kavitha, N. K. Singha, *Macromol. Chem. Phys.* **2007**, *208*, 2569.

[59] A. Sanyal, *Macromol. Chem. Phys.* **2010**, *211*, 1417.

[60] J. R. McElhanon, D. R. Wheeler, *Org. Lett.* **2001**, *3*, 2681.

[61] M. L. Szalai, D. V. McGrath, D. R. Wheeler, T. Zifer, J. R. McElhanon, *Macromolecules* **2007**, *40*, 818.

[62] R. Pipkorn, W. Waldeck, B. Didinger, M. Koch, G. Mueller, M. Wiessler, K. Braun, *J. Pept. Sci.* **2009**, *15*, 235.

[63] J. Schoch, M. Wiessler, A. Jäschke, *J. Am. Chem. Soc.* **2010**, *132*, 8846.

[64] N. K. Devaraj, R. Weissleder, S. a Hilderbrand, *Bioconjug. Chem.* **2008**, *19*, 2297.

[65] M. L. Blackman, M. Royzen, J. M. Fox, *J. Am. Chem. Soc.* **2008**, *130*, 13518.

[66] K. W. Hill, J. Taunton-Rigby, J. D. Carter, E. Kropp, K. Vagle, W. Pieken, D. P. C. McGee, G. M. Husar, M. Leuck, D. J. Anziano, D. P. Sebesta, *J. Org. Chem.* **2001**, *66*, 5352.

[67] B. Seelig, A. Jäschke, *Tetrahedron Lett.* **1997**, *38*, 7729.

[68] A. J. Inglis, C. Barner-Kowollik, *Macromol. Rapid Commun.* **2010**, *31*, 1247.

[69] N. K. Guimard, J. Ho, J. Brandt, C. Y. Lin, M. Namazian, J. O. Mueller, K. K. Oehlenschlaeger, S. Hilf, A. Lederer, F. G. Schmidt, M. L. Coote, C. Barner-Kowollik, *Chem. Sci.* **2013**, *4*, 2752.

[70] J. A. Syrett, G. Mantovani, W. R. S. Barton, D. Price, D. M. Haddleton, *Polym. Chem.* **2010**, *1*, 102.

[71] K. Pahnke, J. Brandt, G. Gryn'ova, P. Lindner, R. Schweins, F. G. Schmidt, A. Lederer, M. L. Coote, C. Barner-Kowollik, *Chem. Sci.* **2015**, *6*, 1061.

[72] K. K. Oehlenschlaeger, N. K. Guimard, J. Brandt, J. O. Mueller, C. Y. Lin, S. Hilf, A. Lederer, M. L. Coote, F. G. Schmidt, C. Barner-Kowollik, *Polym. Chem.* **2013**, *4*, 4348.

[73] H. Kawai, T. Umehara, K. Fujiwara, T. Tsuji, T. Suzuki, *Angew. Chemie Int. Ed.* **2006**, *45*, 4281.

[74] S. Yu, R. Zhang, Q. Wu, T. Chen, P. Sun, *Adv. Mater.* **2013**, *25*, 4912.

[75] K. Pahnke, O. Altintas, F. G. Schmidt, C. Barner-Kowollik, *ACS Macro Lett.* **2015**, *4*, 774.

[76] E. Altuntaş, U. S. Schubert, *Anal. Chim. Acta* **2014**, *808*, 56.

[77] H. Lee, J. H. Jeong, T. G. Park, *J. Control. Release* **2001**, *76*, 183.

[78] T. Gruendling, M. Guilhaus, C. Barner-Kowollik, *Macromolecules* **2009**, *42*, 6366.

[79] F. Günzler, E. H. H. Wong, S. P. S. Koo, T. Junkers, C. Barner-Kowollik, *Macromolecules* **2009**, *42*,

1488.

[80] S. K. Chowdhury, M. Doleman, D. Johnston, *J. Am. Soc. Mass Spectrom.* **1995**, *6*, 478.

[81] Z. Takáts, J. M. Wiseman, B. Gologan, R. G. Cooks, *Science* **2004**, *306*, 471.

[82] Z. Takáts, J. M. Wiseman, R. G. Cooks, *J. Mass Spectrom.* **2005**, *40*, 1261.

[83] J. M. Wiseman, D. R. Ifa, Q. Song, R. G. Cooks, *Angew. Chemie Int. Ed.* **2006**, *45*, 7188.

[84] D. Cornett, M. Reyzer, P. Chaurand, R. Caprioli, *Nat. Methods* **2007**, *4*, 828.

[85] L. H. Cazares, D. a Troyer, B. Wang, R. R. Drake, O. J. Semmes, *Anal. Bioanal. Chem.* **2011**, *401*, 17.

[86] L. A. Mcdonnell, R. M. A. Heeren, *Mass Spectrom. Rev.* **2007**, *26*, 606.

[87] T. Gruendling, M. Guilhaus, C. Barner-Kowollik, *Anal. Chem.* **2008**, *80*, 6915.

[88] A. M. Striegel, W. W. Yau, J. J. Kirkland, D. D. Bly, *Modern Size-Exclusion Liquid Chromatography*, John Wiley & Sons, Hoboken, New Jersey, **2009**.

[89] S. Podzimek, *Light Scattering, Size Exclusion Chromatography and Asymmetric Flow Field Flow Fractionation*, WILEY, Hoboken, New Jersey, **2011**.

[90] L. K. Kostanski, D. M. Keller, A. E. Hamielec, *J. Biochem. Biophys. Methods* **2004**, *58*, 159.

[91] S. Boye, N. Polikarpov, D. Appelhans, A. Lederer, *J. Chromatogr. A* **2010**, *1217*, 4841.

[92] S. K. Ratanathanawongs Williams, D. Lee, *J. Sep. Sci.* **2006**, *29*, 1720.

[93] K. Rebolj, D. Pahovnik, E. Zagar, *Anal. Chem.* **2012**, *84*, 7374.

[94] G. Yohannes, M. Jussila, K. Hartonen, M. L. Riekkola, *J. Chromatogr. A* **2011**, *1218*, 4104.

[95] B. Roda, A. Zattoni, P. Reschiglian, M. H. Moon, M. Mirasoli, E. Michelini, A. Roda, *Anal. Chim. Acta* **2009**, *635*, 132.

[96] W. Burchard, *Adv. Polym. Sci.* **1999**, 113.

[97] H. J. A. Philipsen, *J. Chromatogr. A* **2004**, *1037*, 329.

[98] S. J. Kok, C. A. Wold, T. Hankemeier, P. J. Schoenmakers, *J. Chromatogr. A* **2003**, *1017*, 83.

[99] M. Malanin, K.-J. Eichhorn, A. Lederer, P. Treppe, G. Adam, D. Fischer, D. Voigt, *J. Chromatogr. A* **2009**, *1216*, 8939.

[100] T. F. Beskers, T. Hofe, M. Wilhelm, *Polym. Chem.* **2015**, *6*, 128.

[101] W. Hiller, M. Hehn, *Anal. Chem.* **2014**, *86*, 10900.

[102] W. Hiller, M. Hehn, T. Hofe, K. Oleschko, P. Montag, *J. Chromatogr. A* **2012**, *1240*, 77.

[103] W. Hiller, P. Sinha, M. Hehn, H. Pasch, *Prog. Polym. Sci.* **2014**, *39*, 979.

[104] W. Hiller, M. Hehn, T. Hofe, K. Oleschko, *Anal. Chem.* **2010**, *82*, 8244.

[105] M. Hehn, T. Wagner, W. Hiller, *Anal. Chem.* **2014**, *86*, 490.

[106] A. M. Striegel, *Anal. Bioanal. Chem.* **2012**, *402*, 77.

[107] A. M. Striegel, A. K. Brewer, *Annu. Rev. Anal. Chem.* **2012**, *5*, 15.

[108] Z. Grubisic, P. Rempp, H. Benoit, *Polym. Lett.* **1967**, *5*, 753.

[109] T. Chang, *Adv. Polym. Sci.* **2003**, *163*, 1.

[110] H. Pasch, B. Trathnigg, *HPLC of Polymers*, Springer-Verlag Berline Heidelberg New York, **1997**.

[111] M. Al Samman, W. Radke, A. Khalyavina, A. Lederer, *Macromolecules* **2010**, *43*, 3215.

[112] S. Park, T. Chang, *Macromolecules* **2006**, *39*, 3466.

[113] Y. Brun, P. Alden, *J. Chromatogr. A* **2002**, *966*, 25.

[114] P. Schoenmakers, F. Fitzpatrick, R. Grothey, *J. Chromatogr. A* **2002**, *965*, 93.

[115] P. J. C. H. Cools, Dissertation: Characterization of Copolymers by Gradient Polymer Elution Chromatography, **1999**.

[116] F. P. B. van der Maeden, M. E. F. Biemond, P. C. G. M. Janssen, *J. Chromatogr. A* **1978**, *149*, 539.

[117] E. Uliyanchenko, S. van der Wal, P. J. Schoenmakers, *Polym. Chem.* **2012**, *3*, 2313.

[118] F. Fitzpatrick, R. Edam, P. Schoenmakers, *J. Chromatogr. A* **2003**, *988*, 53.

[119] P. J. C. H. Cools, A. M. Van Herk, A. L. German, W. Staal, *J. Liq. Chromatogr.* **1994**, *17*, 3133.

[120] G. Glöckner, D. Wolf, H. Engelhardt, *Chromatographia* **1994**, *38*, 559.

[121] A. Albrecht, L. C. Heinz, D. Lilge, H. Pasch, *Macromol. Symp.* **2007**, *257*, 46.

[122] C. S. Young, S. Scientific, *LC Troubl.* **2003**, 1.

[123] K. F. Arndt, *Polymercharakterisierung*, Hanser Fachbuch, München, Wien, **1996**.

[124] P. J. Wyatt, *Anal. Chim. Acta* **1993**, *272*, 1.

[125] B. H. Zimm, *J. Chem. Phys.* **1948**, *16*, 1099.

[126] I. a Haidar Ahmad, A. M. Striegel, *Anal. Bioanal. Chem.* **2011**, *399*, 1515.

[127] J. Nie, B. Du, W. Oppermann, *J. Phys. Chem. B* **2006**, *110*, 11167.

[128] B. Ferse, S. Richter, K.-F. Arndt, A. Richter, *Macromol. Symp.* **2007**, *254*, 378.

[129] J. Ehrhart, A.-F. Mingotaud, F. Violleau, *J. Chromatogr. A* **2011**, *1218*, 4249.

[130] G. Bryant, J. C. Thomas, *Langmuir* **1995**, *11*, 2480.

[131] X. Liu, J. Shen, J. C. Thomas, L. A. Clementi, X. Sun, *J. Quant. Spectrosc. Radiat. Transf.* **2012**, *113*, 489.

[132] D. J. Pine, D. a. Weitz, J. X. Zhu, E. Herbolzheimer, *J. Phys.* **1990**, *51*, 2101.

[133] K. Schätzel, M. Drewel, J. Ahrens, *J. Phys. Condens. Matter* **1990**, *2*, 393.

[134] P. Zakharov, S. Bhat, P. Schurtenberger, F. Scheffold, *Appl. Opt.* **2006**, *45*, 1756.

[135] S. W. Provencher, *Die Makromol. Chemie* **1979**, *180*, 201.

[136] M. Kaszuba, M. T. Connah, F. K. McNeil-Watson, U. Nobbmann, *Part. Part. Syst. Charact.* **2007**, *24*, 159.

[137] B. a. Miller-Chou, J. L. Koenig, *Prog. Polym. Sci.* **2003**, *28*, 1223.

[138] G. Madras, V. Karmore, *Polym. Int.* **2001**, *50*, 683.

[139] G. J. Price, P. F. Smith, *Polym. Int.* **1991**, *24*, 159.

[140] S. M. King, *Mod. Tech. Polym. Charaterisation* **1999**, *1999*.

[141] H. Yamakawa, *Modern Theory of Polymer Solutions*, Harper & Row, Kyoto, Japan, **1971**.

[142] W. Burchard, *Macromol. Symp.* **2010**, *295*, 49.

[143] G. Beaucage, S. Rane, S. Sukumaran, M. M. Satkowski, L. a. Schechtman, Y. Doi, *Macromolecules* **1997**, *30*, 4158.

[144] J. S. Pedersen, M. C. Simulations, *Macromolecules* **1996**, *9297*, 7602.

[145] W. Burchard, A. Khalyavina, P. Lindner, R. Schweins, P. Friedel, M. Wiemann, A. Lederer, *Macromolecules* **2012**, *45*, 3177.

[146] M. Rubinstein, R. H. Colby, *Polymer Physics*, OUP Oxford, **2003**.

[147] S. Gupta, Q. Zhang, T. Emrick, A. C. Balazs, T. P. Russell, *Nat. Mater.* **2006**, *5*, 229.

[148] K. Pahnke, J. Brandt, G. Gryn'ova, C. Y. Lin, O. Altintas, F. G. Schmidt, A. Lederer, M. L. Coote, C. Barner-Kowollik, *Angew. Chemie Int. Ed.* **2016**, *55*, 1514.

[149] M. Langer, J. Brandt, A. Lederer, A. S. Goldmann, F. H. Schacher, C. Barner-Kowollik, *Polym. Chem.* **2014**, *5*, 5330.

[150] E. B. Stukalin, L.-H. Cai, N. A. Kumar, L. Leibler, M. Rubinstein, *Macromolecules* **2013**, *46*, 7525.

[151] H. Cho, S. Park, M. Ree, T. Chang, J. C. Jung, W. C. Zin, *Macromol. Res.* **2006**, *14*, 383.

[152] B. Monrabal, J. Sancho-Tello, in *Appl. B. North Am.*, **2009**, pp. 58–59.

[153] L. D'Agnillo, J. B. P. Soares, A. Penlidis, *J. Polym. Sci. Part B Polym. Phys.* **2002**, *40*, 905.

[154] T. Greibrokk, T. Andersen, *J. Chromatogr. A* **2003**, *1000*, 743.

[155] "GESTIS-Stoffdatenbank, Institut für Arbeitsschutz der Deutschen Gesetzlichen Unfallversicherung (IFA)," can be found under http://gestis.itrust.de/, accessed: 2015-07-28.

[156] C. Zhu, M. David, a C. Stephen, *LCGC Asia Pacific* **2005**, *8*, 48.

[157] J. Brandt, N. K. Guimard, C. Barner-Kowollik, F. G. Schmidt, A. Lederer, *Anal. Bioanal. Chem.* **2013**, *405*, 8981.

[158] N. Grassie, W. W. Kerr, *Trans. Faraday Soc.* **1957**, *53*, 234.

[159] R. Pamies, J. G. Hernández Cifre, M. del Carmen López Martínez, J. García de la Torre, *Colloid Polym. Sci.* **2008**, *286*, 1223.

[160] S. Park, H. Cho, Y. Kim, S. Ahn, T. Chang, *J. Chromatogr. A* **2007**, *1157*, 96.

[161] F. D. Antia, C. Horvath, *J. Chromatogr. A* **1988**, *435*, 1.

[162] A. de Villiers, F. Lestremau, R. Szucs, S. Gélébart, F. David, P. Sandra, *J. Chromatogr. A* **2006**, *1127*, 60.

[163] N. Aust, *J. Biochem. Biophys. Methods* **2003**, *56*, 323.

[164] C. O. Ingamells, J. J. Fox, *X Ray Spectrom* **1979**, *8*, 79.

[165] J. Li, *J. Chromatogr. A* **2002**, *952*, 63.

[166] A. van der Horst, P. J. Schoenmakers, *J. Chromatogr. A* **2003**, *1000*, 693.

[167] P. Lindner, R. P. May, P. A. Timmins, *Phys. B* **1992**, *180*, 967.

[168] P. Lindner, R. Schweins, *Neutron News* **2010**, *21*, 15.

[169] A. Gandini, *Polímeros* **2005**, *15*, 95.

[170] S. D. Bergman, F. Wudl, *J. Mater. Chem.* **2008**, *18*, 41.

[171] S. Kéki, M. Zsuga, Á. Kuki, *J. Phys. Chem. B* **2013**, *117*, 4151.

[172] P. J. Flory, *J. Am. Chem. Soc.* **1936**, *58*, 1877.

[173] W. H. Carothers, *J. Am. Chem. Soc.* **1929**, *51*, 2548.

[174] A. M. Striegel, *Anal. Bioanal. Chem.* **2013**, *405*, 8959.

[175] H. R. Kricheldorf, G. Schwarz, *Macromol. Rapid Commun.* **2003**, *24*, 359.

[176] H. R. Kricheldorf, *Acc. Chem. Res.* **2009**, *42*, 981.

[177] H. R. Kricheldorf, *Macromol. Rapid Commun.* **2009**, *30*, 1371.

[178] L. J. Hughes, G. L. Brown, *J. Appl. Polym. Sci.* **1961**, *5*, 580.

[179] C. E. Rehberg, W. A. Faucette, C. H. Fisher, *J. Am. Chem. Soc.* **1944**, *66*, 1723.

[180] J. E. Mark, *Physical Properties of Polymers Handbook*, Springer, New York, **2007**.

[181] D. Berek, T. Bleha, Z. Pevná, *J. Polym. Sci. Polym. Lett. Ed.* **1976**, *14*, 323.

[182] D. Berek, T. Bleha, Z. Pevna, *J. Chromatogr. Sci.* **1976**, *14*, 560.

[183] J. P. A. Heuts, G. T. Russell, *Eur. Polym. J.* **2006**, *42*, 3.

[184] B. B. Noble, M. L. Coote, *Int. Rev. Phys. Chem.* **2013**, *32*, 467.

[185] C. J. Hawker, T. P. Russell, *MRS Bull.* **2005**, *30*, 952.

[186] M. A. Quarry, M. A. Stadalius, … *Chromatogr. A* **1986**, *358*, 1.

[187] P. Jandera, M. Holčapek, L. Kolářová, *J. Chromatogr. A* **2000**, *869*, 65.

[188] L. A. Cole, J. G. Dorsey, *Anal. Chem.* **1992**, *64*, 1317.

[189] W. Lee, H. C. Lee, T. Park, T. Chang, K. H. Chae, *Macromol. Chem. Phys.* **2000**, *201*, 320.

[190] M. Van Hulst, A. Van Der Horst, W. T. Kok, P. J. Schoenmakers, *J. Sep. Sci.* **2010**, *33*, 1414.

[191] F. Erni, R.W. Frei, *J. Chromatogr.* **1978**, *149*, 561.

[192] M. M. Bushey, J. W. Jorgenson, *Anal. Chem.* **1990**, *62*, 161.

[193] H. Tian, J. Xu, Y. Xu, Y. Guan, *J. Chromatogr. A* **2006**, *1137*, 42.

[194] E. Reingruber, F. Bedani, W. Buchberger, P. Schoenmakers, *J. Chromatogr. A* **2010**, *1217*, 6595.

[195] E. Reingruber, J. J. Jansen, W. Buchberger, P. Schoenmakers, *J. Chromatogr. A* **2011**, *1218*, 1147.

[196] X. Jiang, A. Van Der Horst, P. J. Schoenmakers, *J. Chromatogr. A* **2002**, *982*, 55.

[197] A. Ginzburg, T. Macko, V. Dolle, R. Brüll, *Eur. Polym. J.* **2011**, *47*, 319.

[198] D. A. Smith, J. W. Youren, *Br. Polym. J.* **1976**, *8*, 101.

[199] H. Matsubara, A. Yoshida, Y. Kondo, S. Tsuge, H. Ohtani, *Macromolecules* **2003**, *36*, 4750.

[200] P. Waszeciak, H. G. Nadeau, *Anal. Chem.* **1964**, *36*, 764.

[201] V. W. Funke, W. Gebhardt, H. Roth, K. Hamann, *Die Makromol. Chemie* **1958**, *28*, 17.

[202] G. G. Esposito, M. H. Swann, *Anal. Chem.* **1962**, *34*, 1048.

[203] R. Peters, Dissertation: Characterisation of Polymeric Network Structures Characterisation of Polymeric Network Structures, University of Amsterdam, **2009**.

[204] C. W. Macosko, D. R. Miller, *Macromolecules* **1976**, *9*, 199.

[205] Q. Ying, B. Chu, *Macromolecules* **1987**, *20*, 362.

[206] M. Shibayama, T. Norisuye, *Bull. Chem. Soc. Jpn.* **2002**, *75*, 641.

[207] M. Shibayama, *Bull. Chem. Soc. Jpn.* **2006**, *79*, 1799.

[208] M. Shibayama, *Macromol. Chem. Phys.* **1998**, *199*, 1.

[209] J. G. H. Joosten, E. T. F. Geladé, P. N. Pusey, *Phys. Rev. A* **1990**, *42*, 2161.

[210] M. J. P. Orkisz, Dissertation: Dynamic Light Scattering Studies of Phase Transitions in Polymers and Gels., Computer Science, Massachusetts Institute of Technology, **1994**.

[211] T. Coviello, W. Burchard, E. Geissler, D. Maier, *Macromolecules* **1997**, *30*, 2008.

[212] P. N. Pusey, W. Van Megen, *Physica A* **1989**, *157*, 705.

[213] S. L. Brimhall, M. N. Myers, K. D. Caldwell, J. C. Giddings, *Sep. Sci. Technol.* **1981**, *16*, 671.

[214] J. W. Qian, M. Wang, D. L. Han, R. S. Cheng, *Eur. Polym. J.* **2001**, *37*, 1403.

[215] K. Terao, Y. Terao, A. Teramoto, N. Nakamura, M. Fujiki, T. Sato, *Macromolecules* **2001**, *34*, 4519.

11 Appendix

11.1 TD SEC - molar mass based approach

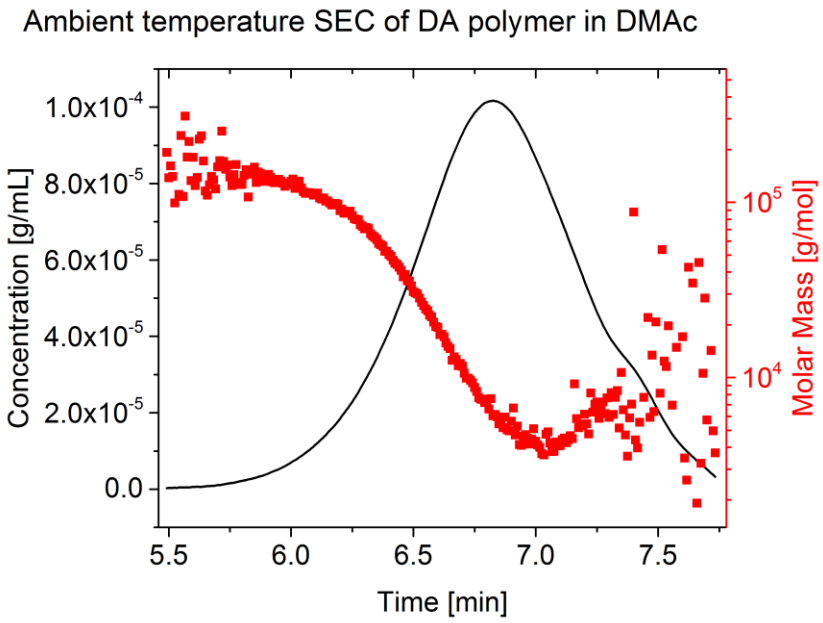

Figure 95: SEC chromatogram of DA Furan-Maleimide, acquired with SEC-SLS in DMAc at ambient temperature. The black line shows the dRI signal that was converted into concentration by estimating the d*n*/d*c*. Good SEC behavior of the separation is indicated by the steadily decreasing molar mass (red data).

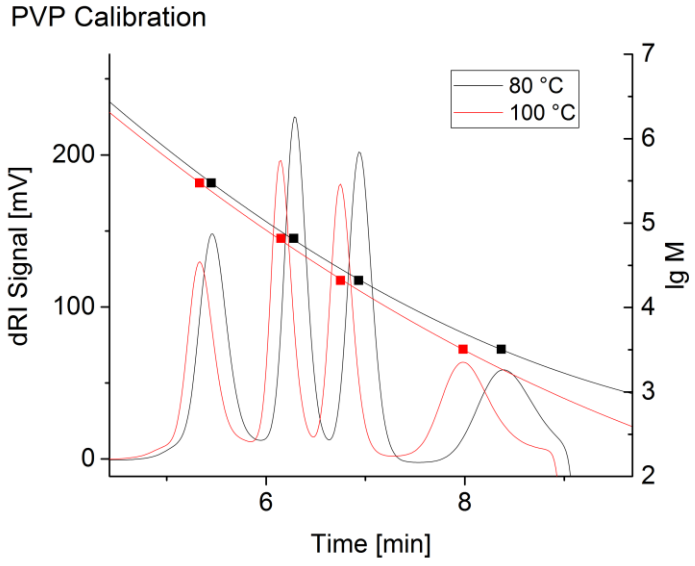

Figure 96: SEC chromatograms of PVP standards (297000, 65700, 20900, 3200 g/mol), acquired at 80 and 100 °C in DMSO. A second order polynomial was used as a calibration function.

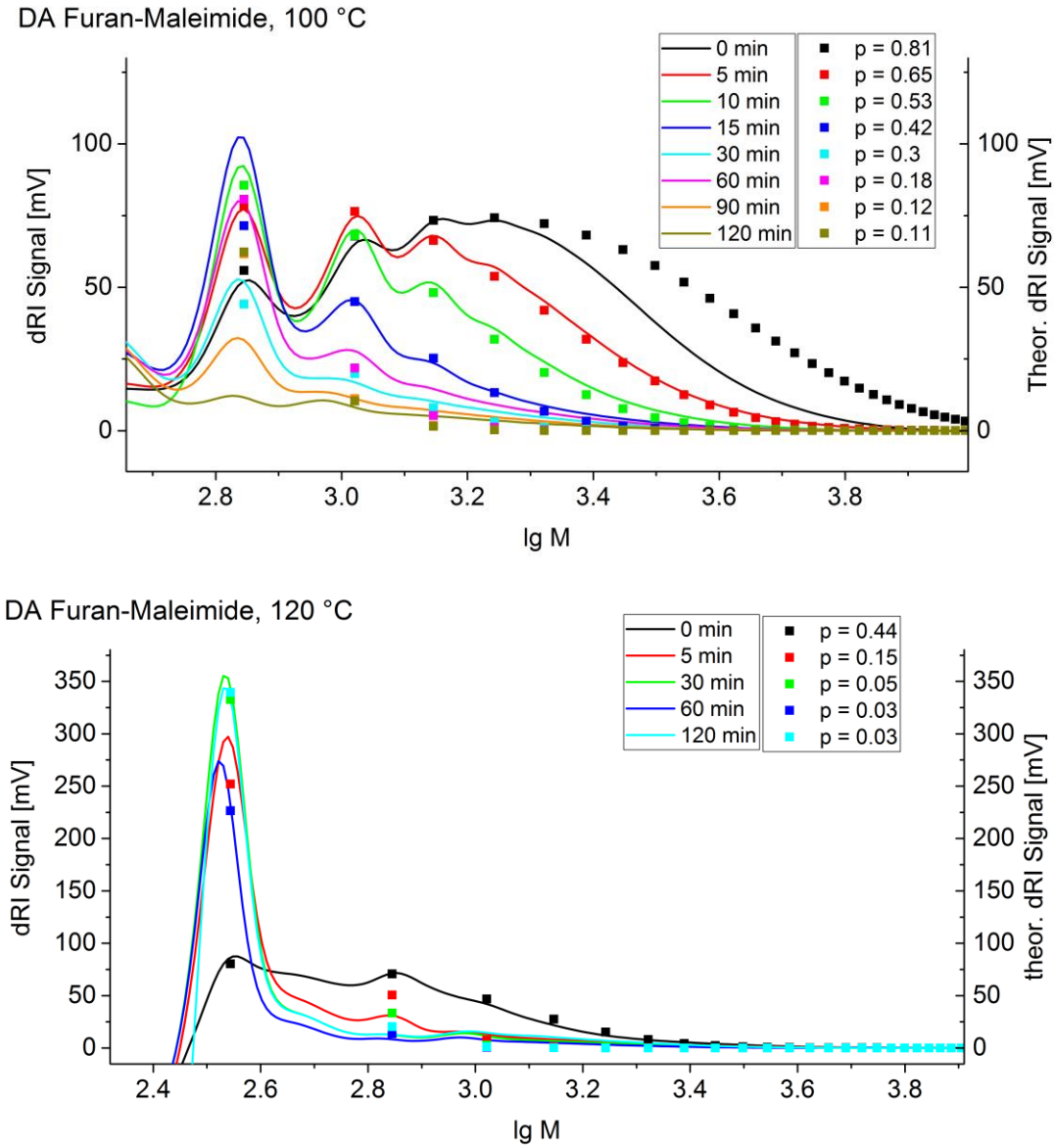

Figure 97: Through TD SEC in DMSO acquired MMDs of the DA Furan-Maleimide at 100 °C (top) and 120 °C (bottom). The left axis represents the dRI signal after different rDA reaction times, whereas the right axis gives the theoretically determined MMD at the indicated conversions (*p*). It was derived by multiplying the respective weight distributions with an arbitrary value in order to scale the distribution to the experimentally obtained dRI trace.

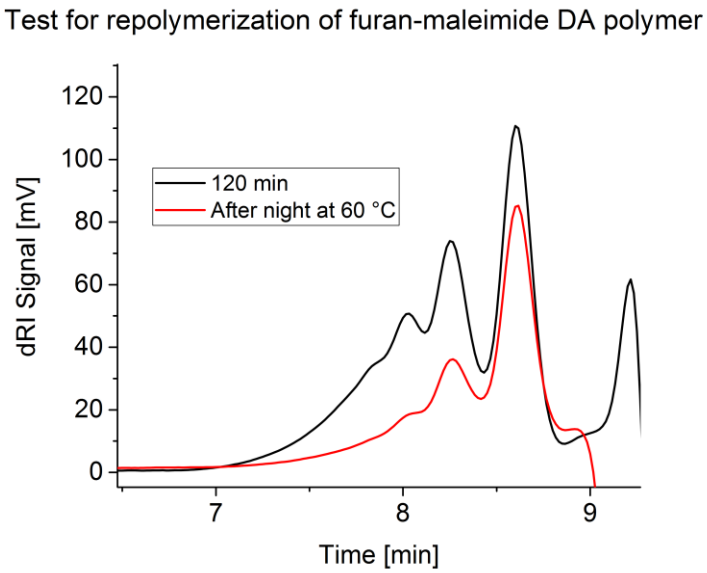

Figure 98: SEC chromatograms of the DA polymer after 120 min at 80 °C (black). The same sample was kept at 60 °C (DA temperature) over night and was measured again at 80 °C without any preheating (red line). No repolymerization can be seen for this polymer, which is not surprising as even with $ZnCl_2$ as catalyst five days were required in synthesis for obtaining the DA polymer.

11.2 SANS data

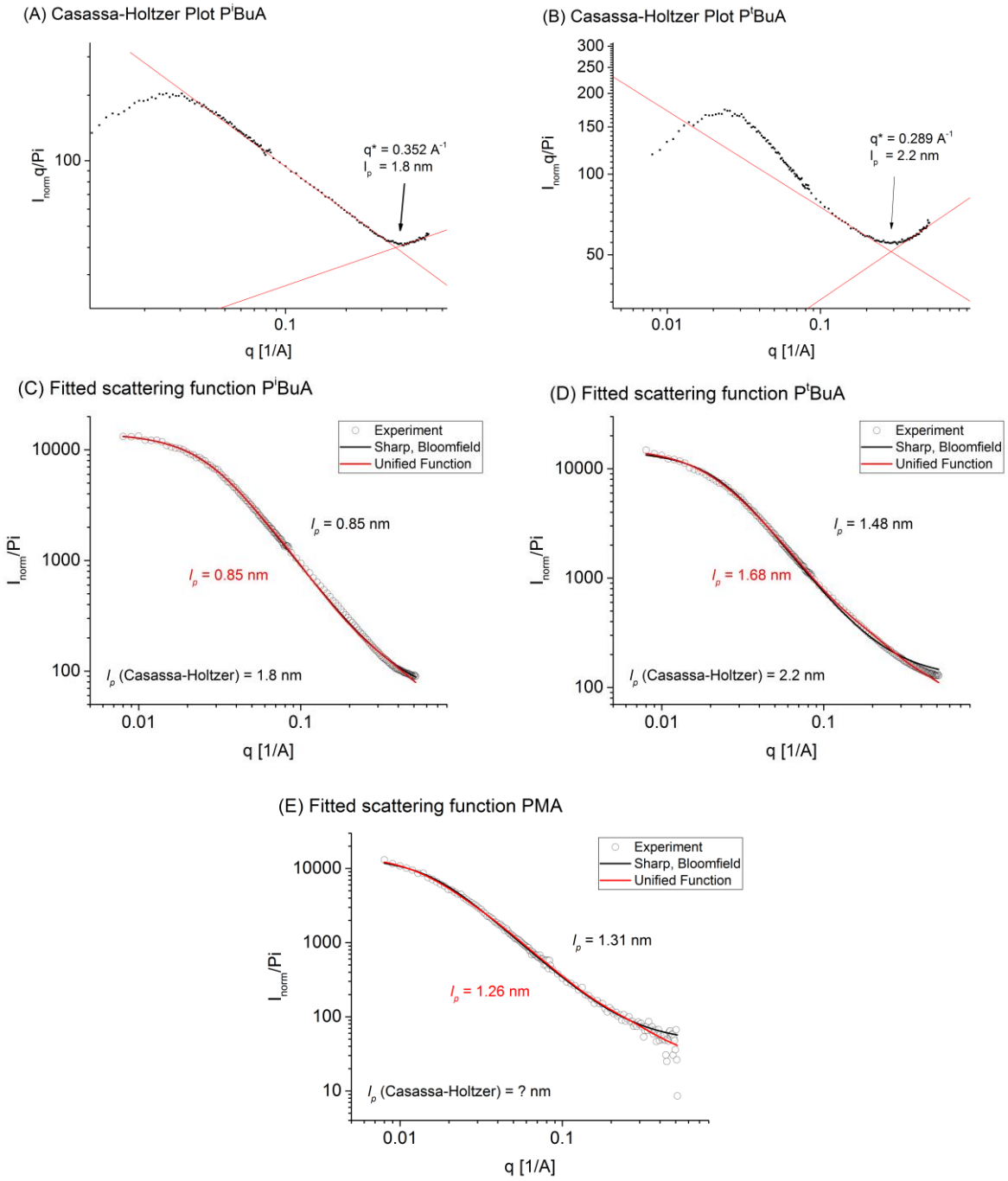

Figure 99: Casassa-Holtzer plot and fitted scattering functions of P^{t}BuA (A, C), P^{i}BuA (B, D) and PMA (E). In panels A and B l_p is determined graphically from the coil-to-rod transition at q^*. In panels C, D and E l_p is obtained after fitting the entire scattering function to two different models ("Sharp, Bloomfield model" and "unified function") that were described in literature[143].

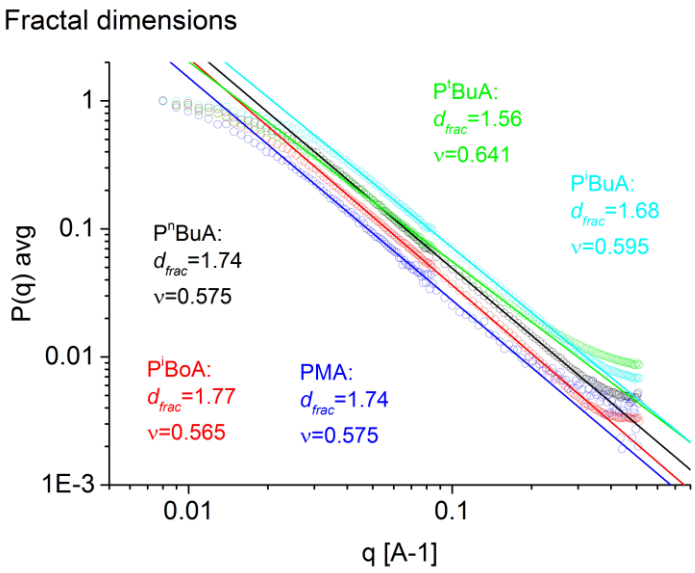

Figure 100: Fractal dimensions of all investigated polymers as determined by a linear fit of the coil region of the true form factor.

11.3 Temperature dependent viscosity measurements

The molar mass scaling of the viscosity of polymers is an additional parameter that reflects the thermodynamic quality of the solvent and the polymer flexibility, similar to the scaling of the radius of gyration with molar mass in the conformation plot.[88,126] In Table 18 the values that are expected for different polymer conformations are summarized:

Table 18: Comparison of scaling parameters based on radius of gyration and intrinsic viscosity for different polymer conformations as described in literature.[88]

	R_g **Conformation plot slope** α	**Mark-Houwink plot slope** α
Hard sphere	0.33	0
Random coil (good solvent)	0.5 – 0.6	0.7 – 0.8
Rigid rod	1	2

The interpretation of the R_g conformation plot slope a and the α obtained from a Mark-Houwink plot with respect to polymer flexibility is difficult, however, as the influence of the solvent is very pronounced. In general a more rod like structure is expected to correspond to a larger persistence length than a more compact structure. Hence an increasing α could be interpreted as an increasing l_p, although the precise interpretation of viscosity data is substantially more complex.

The used TD SEC instrument allowed the easy determination of the intrinsic viscosity of measured polymers and, thus, Mark-Houwink plots could be constructed with little effort. Therefore narrowly

distributed polymer samples (prepared by Kai Pahnke via ATRP) were measured individually, which allowed the independent determination of the intrinsic viscosities of all samples. Their molar masses (determined by SEC-SLS in THF) are summarized in Table 19:

Table 19: Molar masses of the investigated polyacrylate building blocks (obtained from SEC-SLS in THF at ambient temperature).

Polymer	M_n (g/mol)	M_w (g/mol)	$Đ_m$
PMA	4950	5350	1.08
	21800	23600	1.09
	36200	41300	1.14
	46000	51000	1.11
P^{i}BoA	2500	3200	1.28
	7700	8200	1.06
	13850	18000	1.30
	69500	89000	1.28
	139500	190000	1.36
P^{n}BuA	2800	5250	1.88
	18700	19700	1.05
	34600	37400	4.09
	46500	190000	1.08
P^{i}BuA	2950	3750	1.27
	11350	37100	3.27
	23450	24300	1.04
	36300	127500	3.51
	38300	41600	1.08
P^{t}BuA	2700	3100	1.15
	31600	36600	1.16
	39600	46500	1.17
	73000	118000	1.62
	63350	71600	1.13

Kuhn-Mark-Houwink plots were constructed for the five polymer types in TCB and in the 60:40 mixture of TCB and DMF, respectively. In both cases the measurements were done in an extended range of temperatures. The obtained α values (slope of linear fit in KMH plot) are shown in Figure 101:

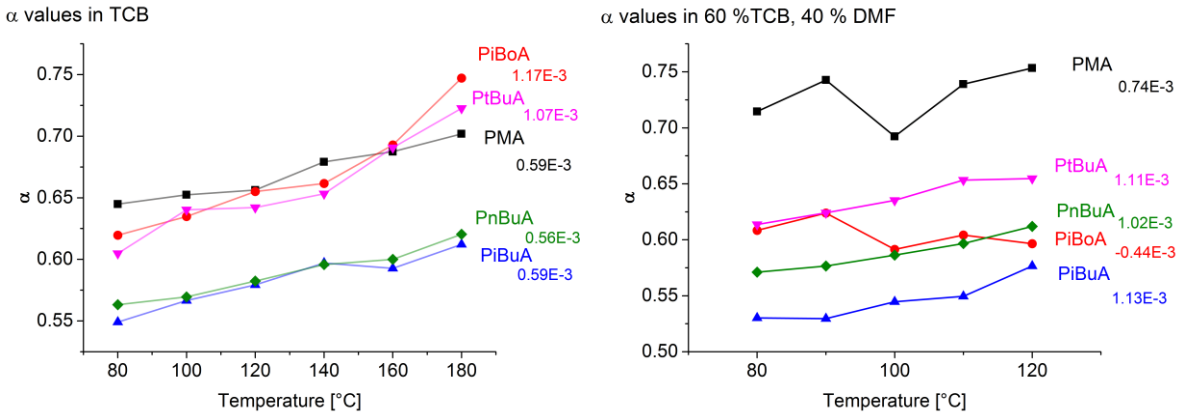

Figure 101: α values of the investigated polymers in TCB (left) and 60 % TCB and 40 % DMF (right). The numbers on each plot give the slope of a linear fit of the respective data points. Each α value was determined by measuring samples of different molar mass of the respective polymer type (see Table 19) with TD SEC. KMH plots for each sample at each temperature were constructed by determining the bulk viscosity of each measured polymer. The slope of a linear fit was taken as the α value of the respective sample.

At first sight the determined values are between 0.5 and 0.75, indicating random coil behavior in a relatively good state of dissolution for all samples (*α(Θ conditions) = 0.5*[214]). Interpreting the data with regard to the polymer's flexibility is, as already mentioned, not trivial.[215] Let us focus on the TCB data first. There P^{i}BuA and P^{n}BuA show the lowest *α*, indicating the most compact structures. PMA, P^{t}BuA and P^{i}BoA appear to be more swollen in the solvent, however. Furthermore the temperature dependency of *α* is interesting: For PMA, P^{n}BuA and P^{i}BuA *α* increases about approx. 0.6E^{-3} K^{-1}, whereas the *α* of P^{t}BuA and P^{i}BoA increases about approx. 1.1E^{-3} K^{-1} and 1.2E^{-3} K^{-1}, respectively. The temperature dependency of the *α* parameter is not yet well investigated. Interpreting *α* as a measure of conformation or dissolution quality, however, allows applying known concepts. The temperature scaling of the excluded volume, for instance, was discussed in chapter 2.7. Its consequence is that polymers swell to larger dimensions at elevated temperatures because they incorporate more and more solvent molecules. Hence, a random coil polymer that is close to *Θ* conditions (*α = 0.5*) should become less compact upon temperature increase and therefore the *α* should increase to the characteristic values of a random coil in a good solvent (*α = 0.7 - 0.8*). In this regard the data shown in the left graph of Figure 101 can be explained qualitatively by simple thermodynamic considerations. The magnitude of the increase of *α* needs further discussion, however. Interpreting the data that a more compact structure close to *α = 0.5* incorporates less solvent molecules than a more swollen structure at, for instance, *α = 0.65*. Accordingly the effect of increasing solvent quality should appear more pronounced in the case of a more swollen polymer structure. And in fact we observe that the *α* of P^{i}BoA and P^{t}BuA (both at a higher *α* than P^{n}BuA and P^{i}BuA) increases more noticeably than in the case of P^{n}BuA and P^{i}BuA. Only PMA does not fit into this image. In that simple consideration a more swollen structure would correspond to a higher persistence

length than a more compact one. Hence, the temperature effect on α should be more pronounced for less flexible structures. Following that interpretation PMA, P^{n}BuA and P^{i}BuA would be of comparable flexibility and P^{t}BuA and finally P^{i}BoA would be less flexible. Confronting these results with the T_g values and the persistence lengths gives the image in Figure 102. The viscosity results of the PBuA isomers appear consistent with the SANS and T_g data. In the case of PMA the viscosity result displays PMA more flexible as indicated by T_g and SANS and in the case of P^{i}BoA the resulting value agrees with the expected trend from the T_g but disagrees with the SANS results. The SANS results of P^{i}BoA, however, are not free of doubts, as discussed in chapter 5.2.1. In the general picture the viscosity data appear feasible, however.

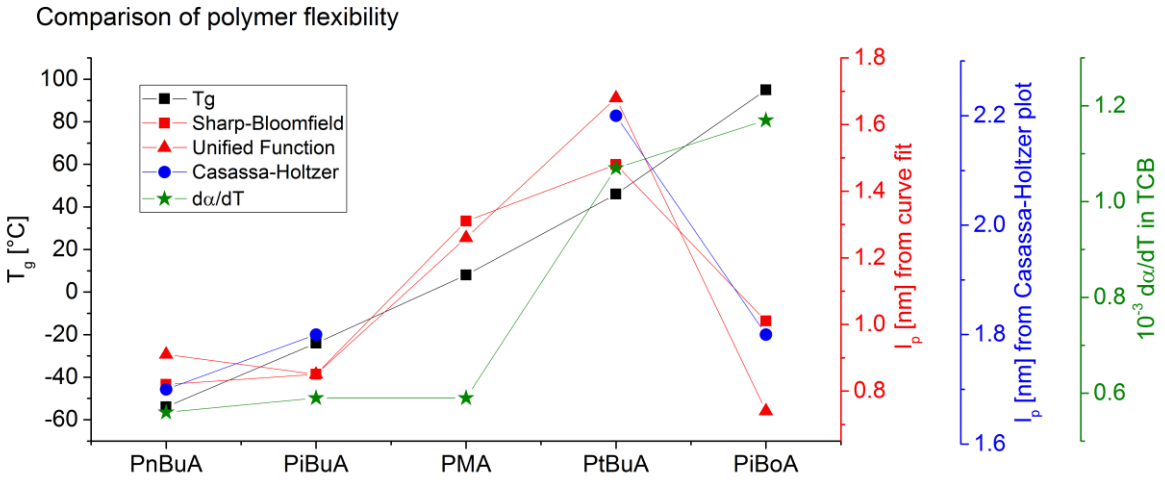

Figure 102: Comparison of the measure of flexibility through the glass transition temperature T_g (taken from literature), the persistence length l_p (determined by SANS) and the temperature dependency of the Mark-Houwink parameter α (dα/dT, determined by TD SEC).

When the solvent was changed to the substantially more polar mixture of 40 % DMF and 60 % DMF the picture changed, as depicted in the right graph of Figure 101. Whereas the α of the three PBuA isomers are relatively close to the α values in TCB the α values of PMA are significantly higher than in TCB and the values of P^{i}BoA are significantly lower than in TCB. This is expected because of the different polarities of the polymers. In the case of PMA the relatively polar acrylate backbone is shielded less by the methyl side group than in the case of the butyl and isobornyl-acrylate. Evaluating the temperature dependency of the α values is more difficult in this case because of the smaller temperature range that was probed and because of the more noisy data. Nevertheless, according to the above described interpretation, the data indicate PMA as the most flexible structure, followed by P^{n}BuA and then P^{i}BuA

and P^{t}BuA. The α of P^{i}BoA decreases with temperature, which appears unexpected. This trend could not yet be explained and further experiments would be required for a deeper understanding of the mechanisms.

Unfortunately, more experiments could not be performed as the employed solvent mixture appeared to corrode the stainless steel capillaries of the SEC instrument at temperatures higher than 100 °C. In addition it would be necessary to validate the obtained trends of polymer flexibility with independent measurements of flexibility. Proposals for further SANS investigations were not accepted, however, so that no experiments could be done in this direction either. If the herein proposed discussion could be confirmed and supported by further experiments a very easy accessible way for assessing polymer flexibilities would be found. Viscosity experiments do not require expensive equipment and, in contrast to SLS, can also be done with relatively small polymers.

11.4 TD SEC for assessing the stiffness effect on rDA reactions

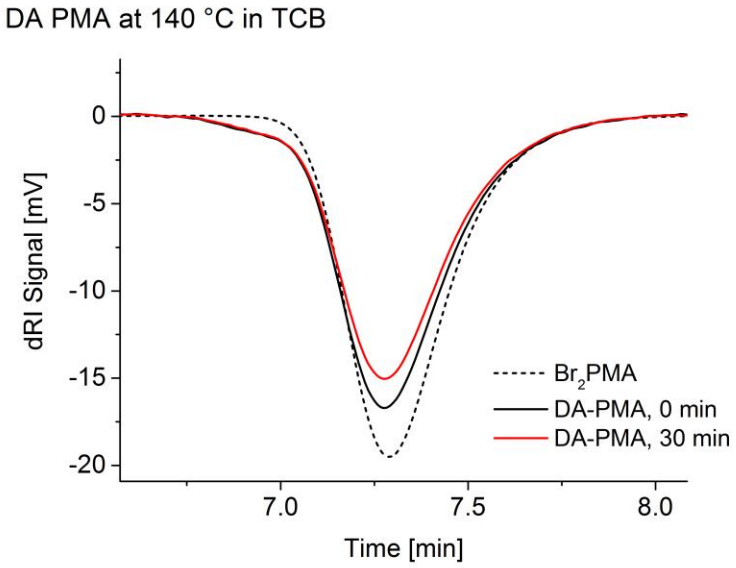

Figure 103: SEC chromatograms of DA PMA, directly acquired at 140 °C (black line) and after 30 minutes (red line). The dashed line shows the PMA building block that now corresponds well to the outcome of the rDA reaction. At 140 °C the rDA reaction proceeds very quick, so that already without any preheating of the sample only a very low amount remains DA polymer present in the mixture (small high-MM shoulder at approx. 7 min).

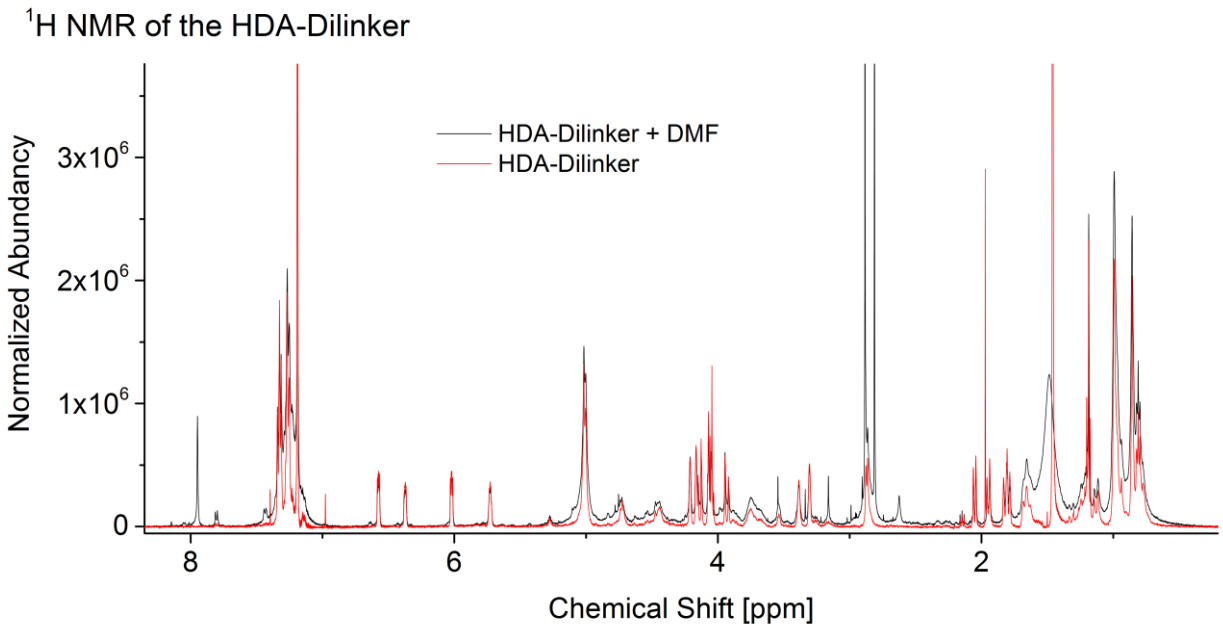

Figure 104: ^{1}H NMR spectra of the HDA-Dilinker before (red) and after heating to 120 °C in DMF for 120 minutes. After heating some of the signals got broadened but the overall structure appears to be stable under these conditions.

11.5 2D LC Evaluation

The following script was used in Scilab 5.5.1 for processing the data from the 2D LC experiments. The ELSD detector trace was imported from an ASCII file were the slice index is in the first and the corresponding ELSD signal in the second column. As the chromatograms were acquired at 10 Hz each slice corresponds to 0.1 seconds elution time.

```
Data = 0;
Data = fscanfMat(‘FILENAME.asc', "%lg")/2; //read the data

// For the Plot Formattings:
Title = "DAPtBuA rDA";
XTitle = "lg % Linker";
YTitle = "lg M";
minM = 2;
maxM = 7;
minLinker = -1;
maxLinker = 2.25;
FontSize = 4;

// Calibration Data:
//HPLC Calibration
Slope1 = 0.1079;
```

```
Interc1 = -2.6879;

// SEC Calibration
Slope2 = -2.26;
Interc2 = 8.78;

// Reset Variables
ELSD = 0;
Time1 = 0;
Time2 = 0;
Vol1 = 0;
THF = 0;
MM = 0;
Linker = 0;

UVSize = length(Data)/2;
FirstCut = (4*600)+UVSize;
CutInt = 3*600;
NumberCol = ceil((UVSize-4*600)/CutInt)-1;

i=1
while i<=NumberCol;
   j=1;
   while j<=CutInt;
      ELSD(j,i)=Data(((i-1)*CutInt)+FirstCut+j);
      j = j+1;
   end;
   i = i+1;
end;

//Recalculate 1D Time:
Time1 = linspace(0, UVSize/600, NumberCol)'; //Time in Minutes
i =1;
for i=1:NumberCol;                          //Time to Volume (correct for different flow rates)
   if Time1(i) <= 3 then
      Vol1(i) = Time1(i);
      elseif Time1(i) <= 3.5 then
           Vol1(i) = (3-1.96/2*(Time1(i)^2-9)+6.88*(Time1(i)-3));
           else Vol1(i) = 3.255 + (Time1(i)-3.5)*0.02;
      end;
end;

Vol1 = Vol1-3.68-0.25;

i=1;
for i=1:NumberCol                           //Volume to % THF (according to HPLC calibration)
   if Vol1(i) <= 0 then
      THF(i) = 0;
      elseif Vol1(i) <= 3 then
         THF(i) = (38-10)/3*(Vol1(i)-0)+10;
         elseif Vol1(i) <= 3.225 then
         THF(i) = 38;
            elseif Vol1(i) <= 7.455 then
            THF(i) = (75-38)/(7.455-3.225)*(Vol1(i)-3.225)+38;
               else THF(i) =75;
               end;
end;
```

```
Linker = Slope1*THF + Interc1;                    //%THF to lg Linker

//Recalculate 2D Time:
Time2 = linspace(0, CutInt/600, CutInt)';       //Time in Minutes

MM  = Slope2*Time2+Interc2;

//Plot Setup
xdel(winsid())
ELSD = ELSD';
xset("colormap",jetcolormap(256));
Sgrayplot(Linker,MM,ELSD);
colorbar(0, max(ELSD)/100);

a = get("current_axes");
a.font_size = FontSize;
a.data_bounds = [minLinker,minM;maxLinker,maxM];

xtitle(Title, XTitle, YTitle);
a.title.font_size = FontSize+1;
a.x_label.font_size = FontSize;
a.y_label.font_size = FontSize;

//Get points from Graph:
Locations = 0;
Locations = locate(-1,1)';
Locations = 10^Locations;

Comp = 0;
i=1;
for i=1:length(Locations)/2;
   M = Locations(i,2);
   LinkerContent = Locations(i,1);

   Comp(i,1) = M;
   Comp(i,2) = LinkerContent;
end;

disp(Comp, " Exp M (g/mol), Exp % Linker");

clear i M;
```

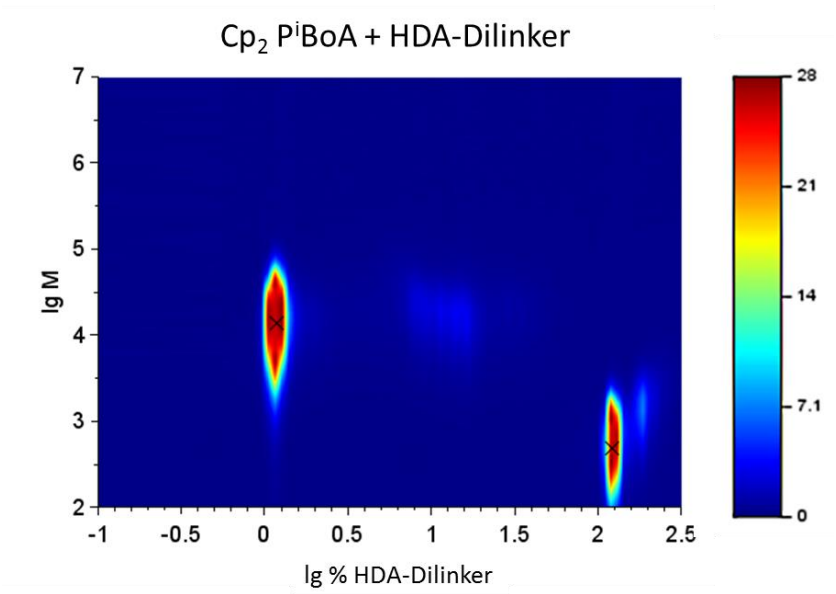

Figure 105: Processed 2D-chromatogram (NP-HPLC x SEC, acquired at ambient temperature) of a mixture of Cp_2P^iBoA (left peak) and the HDA-Dilinker (right peak).

11.6 SEC-UV/Vis with HDA-Networks

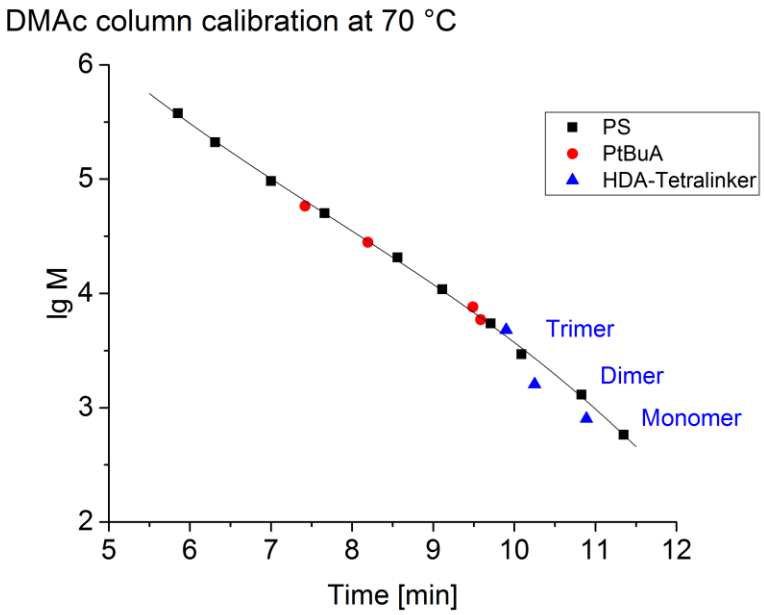

Figure 106: SEC column calibration at 70 °C in DMSO. The individual peaks of the HDA-Tetralinker fit relatively well into the calibration line if molar masses corresponding to monomer, dimer and trimer are assumed.

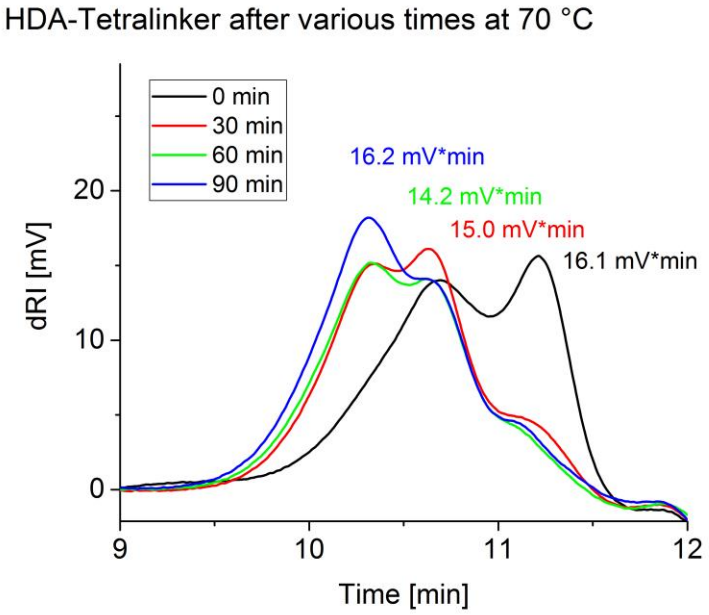

Figure 107: dRI trace of SEC chromatogram of the HDA-tetralinker (concentration: 0.305 mg/mL) after various heating times at 70 °C. The image demonstrates that after short reaction times the last peak is dominating. With increasing heating time, however, the area of the first two peaks is increasing. This finding supports the hypothesis of successive multimerization at elevated temperatures. The overall peak area of the dRI signal does not change significantly, indicating that the d*n*/d*c* vales of monomer, dimer and trimer are similar.

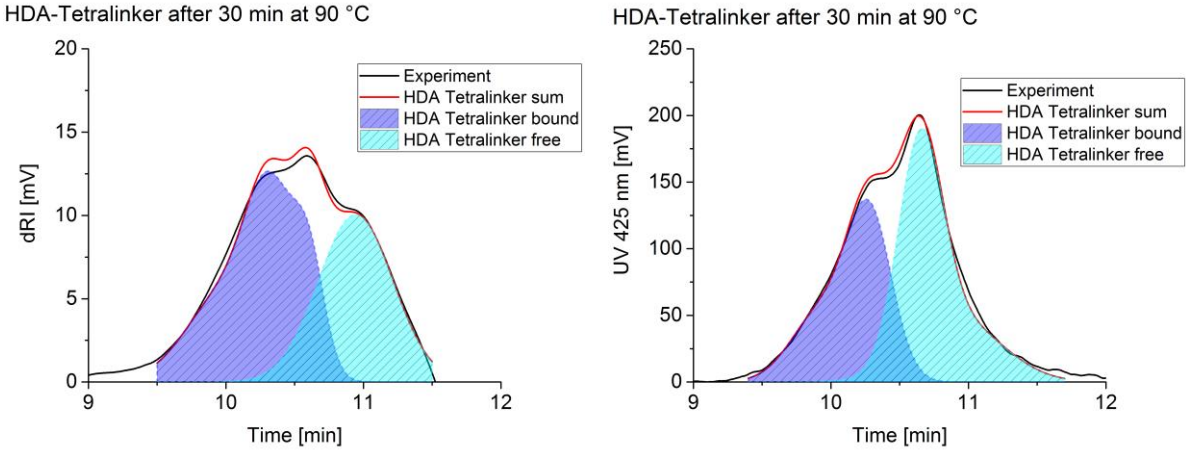

Figure 108: dRI- (left) and UV-trace (right) of SEC chromatograms of the HDA-Tetralinker after heating to 90 °C for 30 min in DMAc (3 g/L LiCl). The black line indicates the experimentally acquired data and the dashed peaks demonstrate the deconvolved peaks for the bound and free HDA-Tetralinker. The first two peaks are added and denoted “bound linker”, whereas the last peak is identified as the “free liner”. Multiple Gauss peaks were used for describing the antisymmetric peaks.

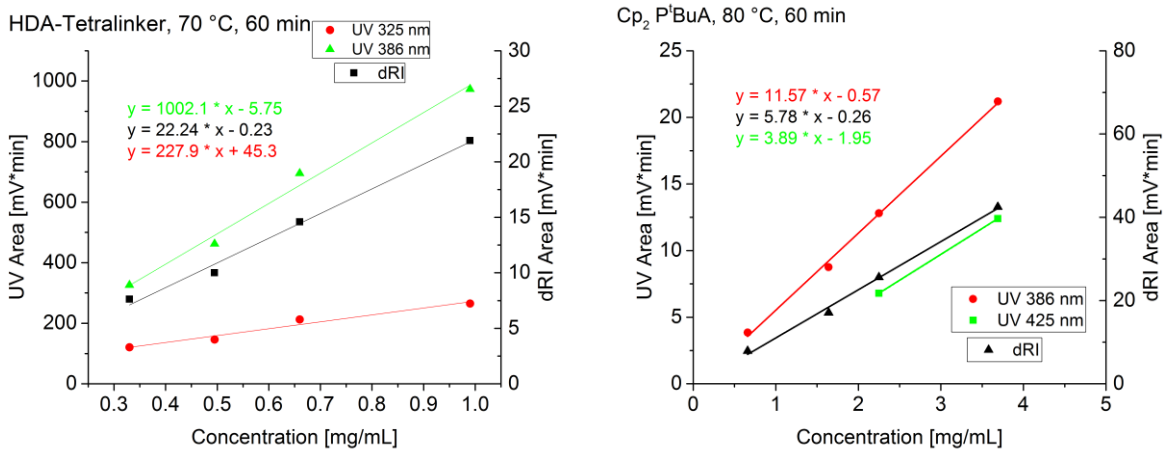

Figure 109: Calibration of HDA-Tetralinker concentration after heating to 70 °C for 60 min (left) and of the Cp_2P^tBuA after heating to 80 °C for 60 min (right).

Scilab script for calculating $c_{polymer}$ and c_{linker} of the chromatograms:

```
Data = fscanfMat('ptbua-0151.txt', "%lg");      //read in data

Frequence = 5;      //Data points/s

kDP = 9.032535522;
IP = 31400;         //Inlet Pressure in Pa

clear MM;
clear Results;

Data(:,5) = abs(Data(:,5));

//Concentration Calibrations:

dRIPolymerSlope = 12.23180339;
dRIPolymerInterc = 0;

UV1PolymerSlope = 2.476166102;
UV1PolymerInterc = 0;

UV2PolymerSlope = 1.835820339;
UV2PolymerInterc = 0;

dRILinkerSlope = 50.02507407;
dRILinkerInterc = 0.0;

UV1LinkerInterc = 0;
UV2LinkerInterc = 0;

UV1LinkerSlope1 = 2859.05;  //bound linker
UV1LinkerInterc1 = 0;

UV2LinkerSlope1 = 4797.12;
UV2LinkerInterc1 = 0;

UV1LinkerSlope2 = 1132.91;  //free linker
UV1LinkerInterc2 = 0;

UV2LinkerSlope2 = 851.13;
UV2LinkerInterc2 = 0;

//Determine Peak Borders

FontSize = 4;
clf();
plot(Data(:,1), Data(:,3),"b");
plot(Data(:,1), Data(:,2),"b");
xlabel("Time (min)");
ylabel("UV1 (mV)");
title("Chromatogramm");
a = gca();                  //Get Current Axes (gca)
a.font_size = FontSize;         //Schriftgröße Achsenbeschriftung
a.title.font_size = FontSize+1;
a.x_label.font_size = FontSize;
```

```
a.y_label.font_size = FontSize;
a.data_bounds(1,1) = 4;
a.data_bounds(1,2) = -10;
a.data_bounds(2,1) = 14;

Borders = locate(2,1)';        //Get Peak Borders Points

Index0 = round(Borders(1,1)*60*Frequence);
Index1 = round(Borders(2,1)*60*Frequence);

//Determine Concentrations

slice = Index0;
counter = 1;

Results = zeros((Index1 - Index0), 7);

function f=Error(x)
      cPolymer = x(1);
      cLinker = x(2);

   dRICalc = dRIPolymerSlope * cPolymer + dRIPolymerInterc + dRILinkerSlope * cLinker + dRILinkerInterc;
   UV1Calc = UV1PolymerSlope * cPolymer + UV1PolymerInterc + UV1LinkerSlope * cLinker +
UV1LinkerInterc;
   UV2Calc = UV2PolymerSlope * cPolymer + UV2PolymerInterc + UV2LinkerSlope * cLinker +
UV2LinkerInterc;

      f = abs(dRICalc-dRI)^4 + abs(UV1Calc-UV1)^4 + abs(UV2Calc-UV2)^4;
endfunction

for counter = 1:(Index1-Index0)


   dRI = Data(slice, 2);
   UV1 = Data(slice, 3);
   UV2 = Data(slice, 4);

   if UV1/UV2 > 2.8 then
      UV1LinkerSlope = UV1LinkerSlope2;
      UV2LinkerSlope = UV2LinkerSlope2;
   else
      UV1LinkerSlope = UV1LinkerSlope1;
      UV2LinkerSlope = UV2LinkerSlope1;
   end


   c0Polymer = dRI/dRIPolymerSlope;
   c0Linker = UV2/UV2LinkerSlope;

   x = [c0Polymer, c0Linker]

   [f, xopt, gopt] = leastsq(Error, x);                    //Optimization
   g = Error(x);
   cPolymer = xopt(1);
   cLinker = xopt(2);

   if cPolymer <=0 then
```

```
    cPolymer = 1E-6;
  end

  if cLinker <=0 then
    cLinker = 1E-6;
  end

  Results(slice, 1) = cPolymer;
  Results(slice, 2) = cLinker;
  Results(slice, 3) = cLinker + cPolymer;
  Results(slice, 4) = log10(4*Data(slice,5)/(IP - 2*Data(slice,5)) * kDP*10 / Results(slice,3)); // =  lg(4*DP/(IP -
2*DP) * kVisco / ctotal) = lg[n]0
  Results(slice, 5) =  -0.78642*Data(slice,1) +  10.09731 - Results(slice,4);   //Universal calibration
  Results(slice, 6) = slice/300;                                  //Time (min)
  Results(slice, 7) = Results(slice, 3) + Results((slice - 1), 7);       // summed mass
  Results(slice, 8) = f^0.5;                                      //Error of fit
  Results(slice, 9) = (f^0.5)/(dRI + UV1 + UV2)*100;                    //Percent Error of fit
  Results(slice, 10) = cLinker/(cLinker + cPolymer)*100;
  MM(slice, 1) = Results(slice, 2)/10^Results(slice, 5);              // Concentration
  MM(slice, 2) = Results(slice, 2);                                 // Concentration * Molar Mass
  MM(slice, 3) = Results(slice, 2)*10^Results(slice, 5);              // Concentration * Molar Mass²

 slice = slice + 1;
end

Results(:,7) = Results(:,7)/max(Results(:,7))*100;      // Normalize summed mass to 100 %

MPolymer = inttrap(Results(:,6), Results(:,1));
MLinker = inttrap(Results(:,6), Results(:,2));
MTotal = inttrap(Results(:,6), Results(:,3));

LinkerContent = MLinker/MTotal;

Mn = sum(MM(:,2))/sum(MM(:,1));
Mw = sum(MM(:,3))/sum(MM(:,2));
Dm = Mw/Mn;

disp(Mn, "Mn (g/mol) =");
disp(Mw, "Mw (g/mol) =");
disp(Dm, "Dm =");
disp(MPolymer, "Masse Polymer (mg) =");
disp(MLinker, "Masse Linker (mg) =");
disp(MTotal, "Gesamtmasse (mg) =");
disp(LinkerContent, "Linker content=");
```

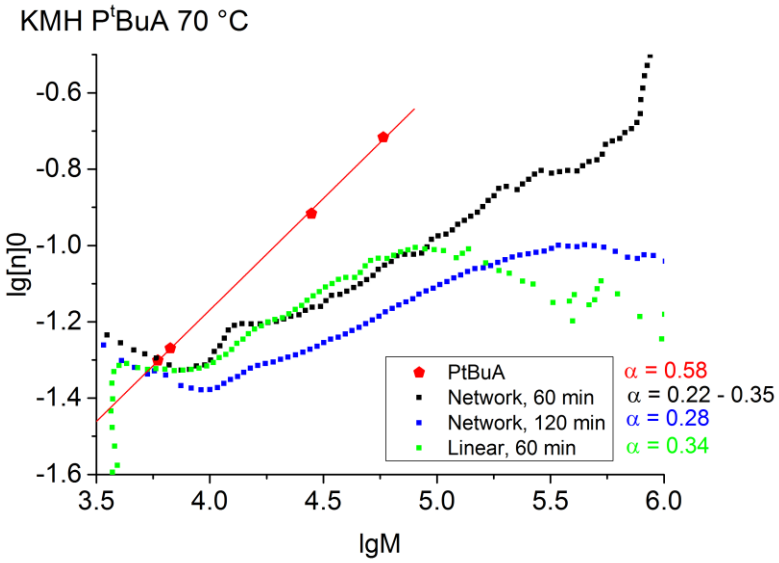

Figure 110: KMH plot of DA P^{t}BuA at 70 °C in DMAc (3 g/L LiCl). The red data indicate the viscosity of linear and narrowly distributed P^{t}BuA samples. The viscosity of the network after 120 min appears underestimated but the slope of the plot should be unaffected by the offset.

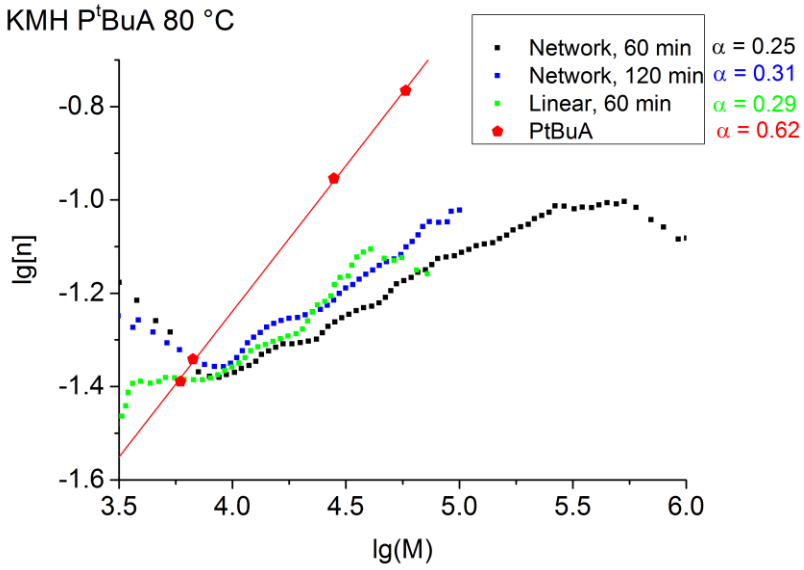

Figure 111: KMH plot of DA P^{t}BuA at 80 °C in DMAc (3 g/L LiCl). The red data indicate the viscosity of linear and narrowly distributed P^{t}BuA samples.

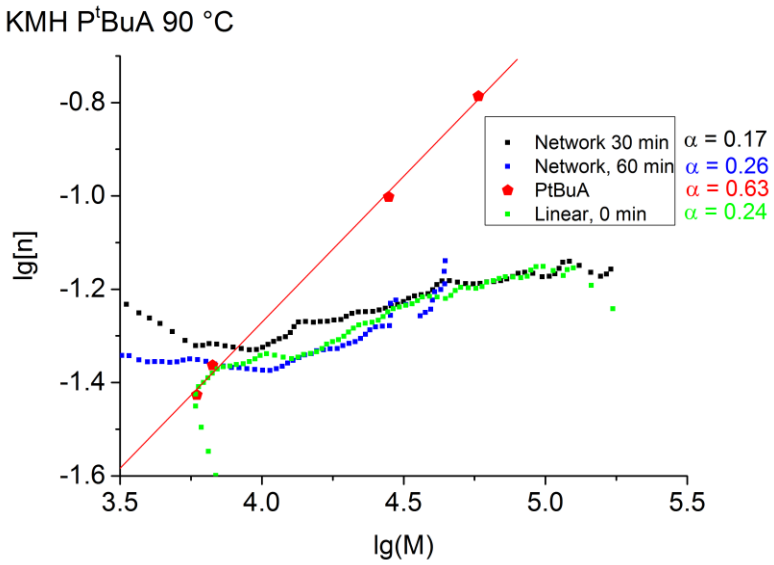

Figure 112: KMH plot of DA PtBuA at 90 °C in DMAc (3 g/L LiCl). The red data indicate the viscosity of linear and narrowly distributed P^{t}BuA samples.

Table 20: Molar masses of the dissolved DA P^{t}BuA fractions as determined by TD SEC in DMAc, determined after 120 minutes (70 °C and 80 °C) and after 60 min (90 °C). The bonding probabilities (*i.e.*, monomer conversions) *p* were determined by TD SEC experiments of linear DA P^{t}BuA samples at identical conditions. The effective functionality of the HDA-Tetralinker *f* was determined by a best fit optimization of the experimentally determined molar mass averages. The used equations are described in literature.[204]

	M_n (g/mol) experiment	M_w (g/mol) experiment	*p*	*f*	M_n (g/mol) calculation	M_w (g/mol) calculation
70 °C	15200	110000	0.63	3.12	110000	17799
80 °C	10500	19700	0.50	2.43	10294	19700
90 °C	8670	14500	0.40	2.41	9004	14500

11.7 TD DLS of DA networks

Investigating polymer networks and gelling reactions through DLS is described in detail in the literature.[127,128,206–212] The experiments are based on the difference in light scattering behavior between *ergodic* (solution state) and *non-ergodic* (network state) media. An *ergodic* polymer solution is spatially homogeneous and, thus, the (average) intensity of the scattered light is constant over time and independent of the position of the scattering volume. In contrast to that, a *non-ergodic* polymer network is characterized by spatial inhomogeneities that lead to position dependent scattering. But also the time averaged scattering intensity starts fluctuating much more pronounced than it is observed in

homogeneous polymer solutions. In Figure 113 the light scattering intensity is shown during the progress of a gelation reaction. The characteristic “speckle pattern” can be observed after crossing the gel point. [206]

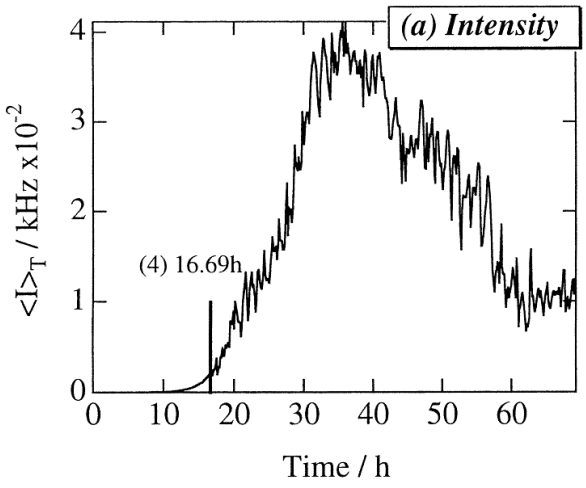

Figure 113: Example from literature: Light scattering intensity during the gelation of tetramethyoxysilane in DMF. The gelation was initiated by adding HCl. After 16.69 hours at 58 °C the gel point at 16.69 hours with its typical speckle pattern appears. Reproduced with permission from the Chemical Society of Japan from Ref.[206]

Besides collecting the scattered light intensity as a function of time DLS allows more detailed characterizations, as described in the above cited publications. The intensity approach is the approach that could be realized easiest on the available equipment (Wyatt DynaPro Nanostar). Therefore 5.3 mg of Cp_2P^tBuA and 0.3 mg of the (protected) HDA-Tetralinker were dissolved in approx. 75 µL anisole (resembling the typical conditions of the network formation[36]). The mixture was then transferred into the DLS cuvette and the light scattering intensity was acquired during three heating/cooling cycles, as shown in Figure 114.

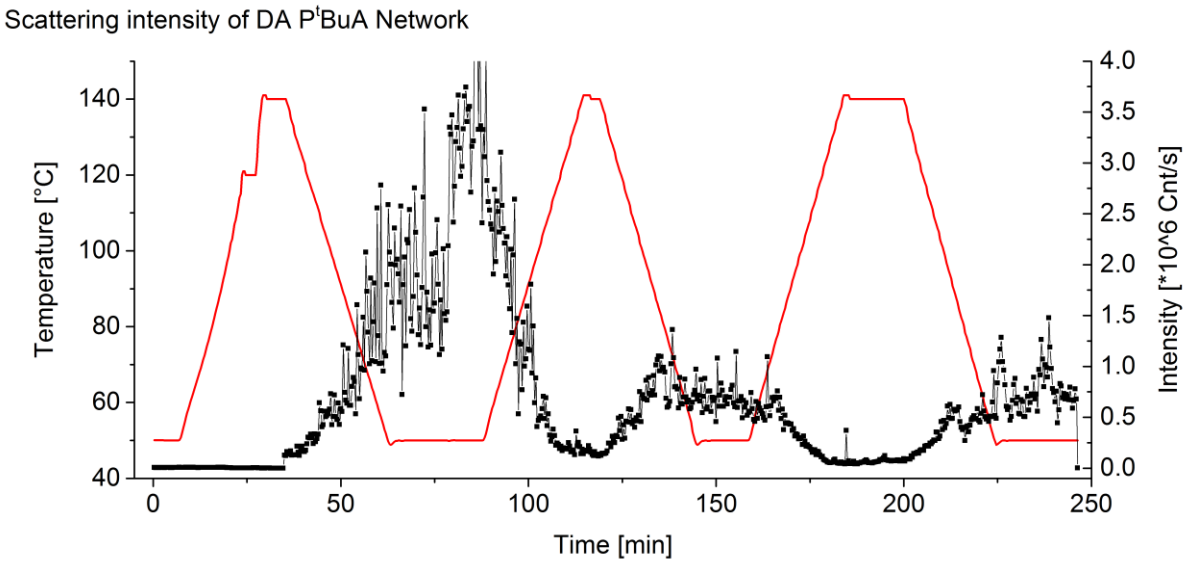

Figure 114: Light scattering intensity during three heating/cooling cycles of the DA P^{t}BuA network in anisol ($c_{polymer}$ = approx. 75 mg/mL). At low temperatures the speckle pattern appears (network) and at high temperatures the scattering intensity is constant (solution). Although the effects are visible the experiments showed poor reproducibility.

At the beginning of the experiment building block and HDA-Tetralinker are dissolved but cannot react because the HDA-Tetralinker is still protected with Cp. Upon the first heating the HDA-Tetralinker gets deprotected and the Cp can evaporate. Then, at the first cooling process, HDA-Tetralinker and building block can react to form a network. And in fact the expected speckle pattern appears. When the sample is heated again the speckle pattern disappears and reappears during the subsequent cooling. Those observations support the reversible formation of the DA network. It was, unfortunately, very difficult to reproduce these experiments. Only in few cases the result was as clear as in Figure 114. In addition even in this relatively good experiment the temperatures at which the speckle pattern appears and vanishes are not consistent.

Issues arise from the high polymer concentration (approx. 75 mg/mL) that is not ideal for DLS measurements. The correlation functions themselves could not be evaluated directly due to their poor quality (Figure 115). At lower concentrations no networks were obtained, however. Due to the evaporation of the solvent it was possible to occasionally add a few drops of fresh anisol, which makes it difficult to control the concentration over multiple heating/cooling cycles. Furthermore the solution turns to a very dark brown color after some time at elevated temperature and the light scattering intensity can be influenced by this behavior, too.

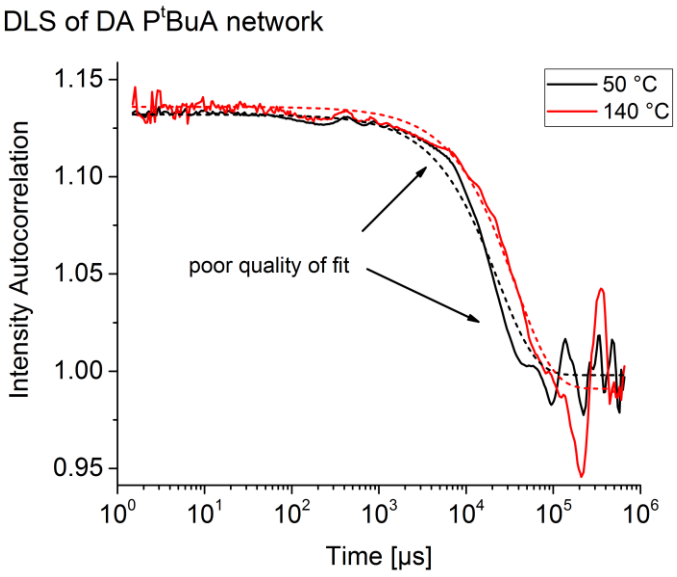

Figure 115: Autocorrelation functions of the DA P^{t}BuA network, acquired in anisol ($c_{polymer}$ = approx. 75 mg/mL) at 50 and 140 °C, respectively. The dashed lines show the corresponding cumulant fits that do not always agree well with the experiment. Furthermore the decay of the correlation function is at very high times, indicating very low mobility of the polymers (most likely due to the very high concentration).

In order to get more reliable and better reproducible data it would be advisable to prepare networks that can be formed at lower concentrations and with higher mesh sizes. Most DLS analyses are performed on hydrogels with comparably very high mesh sizes at substantially lower polymer concentrations. The precise detection of the gel point and the characterization of the formed network would require a more dedicated DLS instrument that allows measurements at different angles and sample positions (*i.e.*, by rotating a cylindrical cuvette). Then the cooperative diffusion coefficients can be determined that allow drawing conclusions about the mesh size of the network.

The here shown results demonstrate that DLS should be a powerful technique for monitoring and evaluating the process of thermoreversible bonding reactions in real time but from the current point on a lot of optimization is still required.

Versicherung

Hiermit versichere ich, dass ich die vorliegende Arbeit ohne unzulässige Hilfe Dritter und ohne Benutzung anderer als der angegebenen Hilfsmittel angefertigt habe; die aus fremden Quellen direkt oder indirekt übernommenen Gedanken sind als solche kenntlich gemacht. Die Arbeit wurde bisher weder im Inland noch im Ausland in gleicher oder ähnlicher Form einer anderen Prüfungsbehörde vorgelegt.

Die vorliegende Arbeit wurde unter der wissenschaftlichen Betreuung von Frau Prof. Brigitte Voit und Frau PD Albena Lederer in der Zeit von Januar 2013 bis Februar 2016 an der TU Dresden und am Leibniz-Institut für Polymerforschung Dresden e.V. angefertigt.

Bislang haben keine weiteren Promotionsverfahren stattgefunden.

Hiermit erkenne ich die Promotionsordnung der Fakultät Mathematik und Naturwissenschaften der Technischen Universität Dresden in geänderter Fassung vom 19.03.2003 an.

Josef Brandt, Dresden, den 12. Februar 2016

Danksagung

Diese Arbeit wäre ohne die Hilfe und Unterstützung zahlreicher Menschen in dieser Form nicht möglich gewesen. Zuerst möchte ich Prof. Brigitte Voit für die Gelegenheit danken, meine Dissertation am Leibniz-Institut für Polymerforschung Dresden e.V. durchführen zu können. Ganz besonderer Dank geht an PD Albena Lederer, die mich schon seit meiner Masterarbeit kontinuierlich wissenschaftlich betreut und unterstützt hat und immer für einen guten Rat da war – auch während der langen (und oft sehr frühen) Fahrten zu den Projekttreffen. Während meiner gesamten Promotionszeit hat sie viel möglich gemacht und mir viele Wege geöffnet!

Für die Finanzierung meiner Arbeit danke ich Evonik Industries AG. Besonderer Dank geht dabei an Dr. Friedrich Georg Schmidt, der bei den Projekttreffen stets für sehr konstruktive Gespräche sorgte.

Außerdem möchte ich der gesamten Arbeitsgruppe Polymerseparation und darüber hinaus der Abteilung Analytik danken, die mir am IPF stets mit Rat und Tat zur Hand stand. Insbesondere zu nennen sind dabei Petra Treppe und Christina Harnisch (vielen Dank für das unerschöpfliche Wissen über die technischen Spirenzien der GPC und die stetige Hilfsbereitschaft) und Susanne Boye (gute Ratschläge in allen Situationen). Weiterer Dank geht an Johannes Lenz, der mich in meiner Abschlussphase sehr tatkräftig unterstützt hat. Wertvolle Diskussionen gab es außerdem mit Dr. Michel Lang, dessen theoretisches Wissen über Stufenwachstumsreaktionen sehr richtungsweisend war. Aber ich möchte auch Mikhail Malanin, Kristina Eichhorn, Eileen Schierz, Andrea Käppler, Martin Geisler, Laura Schlechte und Kerstin Arnhold erwähnen, weil sie einfach für ein angenehmes Arbeitsklima gesorgt und sichergestellt haben, dass die Kaffeepausen auch pünktlichst eingehalten werden!

Weiterhin möchte ich der Gruppe um Prof. Christopher Barner-Kowollik mit Kim Öhlenschläger, Kai Pahnke, Nathalie Guimard und Marcel Langer am Karlsruher Institut für Technologie danken. Ohne deren unermüdlichen Synthesearbeiten wäre diese Arbeit natürlich gar nicht erst möglich gewesen. Durch die gute Kommunikation und die immer auch unterhaltsamen Projekttreffen war das Zusammenarbeiten wirklich angenehm. Gleiches gilt für die Arbeitsgruppe um Prof. Michelle Coote an der Australian National University. Trotz nicht zu unterschätzender Zeitverschiebung gab es stets eine gute Kommunikation zu unseren Experten der theoretischen Chemie.

Für die gute Zeit und die vielen schönen Eindrücke und neuen Erkenntnissen möchte ich außerdem der PolymerAnalysisGroup um Prof. Peter Schoenmakers an der Universiteit van Amsterdam danken. Mein dreimonatiger Forschungsaufenthalt war in vielerlei Hinsicht ein sehr schönes Erlebnis. Nicht

unerwähnt lassen möchte außerdem ich Prof. Walther Burchard von der Universität Freiburg, der mir bei der Auswertung der Neutronenstreumessungen sehr tatkräftig zur Seite stand.

Nicht zu vergessen ist auch der Dank an meine Familie, meine Freundin Sandra und meine Freunde, die mich privat unterstützt haben und es mir nicht übel genommen haben, wenn ich mich in stressigen Phasen doch einmal für längere Zeiten im Labor vergraben musste. Danke, dass ihr mich während meiner Zeit treu begleitet habt!